Design, Modeling and Optimization of Hybridized Automated Manual Transmission for Electrified Vehicles

by

Guang Wu
B.Eng, Hunan University, China, 2007
M.Sc, Hunan University, China, 2010

A Dissertation Submitted in Partial Fulfillment of the
Requirements for the Degree of

DOCTOR OF PHILOSOPHY

in the Department of Mechanical Engineering

Design, Modeling and Optimization of Hybridized Automated Manual Transmission for Electrified Vehicles

by

Guang Wu

B.Eng, Hunan University, China, 2007

M.Sc, Hunan University, China, 2010

Supervisory Committee

Dr. Zuomin Dong, Supervisor
(Department of Mechanical Engineering)

Dr. Curran Crawford, Departmental Member
(Department of Mechanical Engineering)

Dr. Panajotis Agathoklis, Outside Member
(Department of Electrical and Computer Engineering)

Supervisory Committee

Dr. Zuomin Dong, Supervisor
(Department of Mechanical Engineering)

Dr. Curran Crawford, Departmental Member
(Department of Mechanical Engineering)

Dr. Panajotis Agathoklis, Outside Member
(Department of Electrical and Computer Engineering)

Abstract

This research systematically compares various electrified vehicles based upon electrification levels and powertrain configurations. A series of novel hybrid electric powertrain systems based on the newly proposed Hybridized Automated Manual Transmission (HAMT) concept are introduced. One representative hybrid powertrain system is selected to illustrate their operation principle. The new HAMT-based hybrid powertrain system overcomes the bottleneck problem of mainstream power-split hybrid systems with relatively low torque capacity and the constraint for utility vehicle electrification, and presents advantages over other hybrid powertrain systems in efficiency and costs. In addition, the new hybrid powertrain system can deliver continuous output torque by filling torque hole during gearshift, through coordinated control of engine, motor, and transmission, improving the driveability of regular Automated Manual Transmission (AMT), whose applications have been hampered by torque hole over the past years. The proposed HAMT-based hybrid systems with improved torque capacity, efficiency, costs, and driveability come with a compact design and more flexible operation through the amount of gearwheels equivalent to a 5-speed AMT to achieve 8 variable gear ratios for the Hybrid Electric Vehicle (HEV) mode and Electric Vehicle (EV) mode operations of a Plug-in Hybrid Electric Vehicle (PHEV).

Model-based optimization, dynamics analysis, and powertrain control strategies have been introduced for a PHEV with a representative 8-speed HAMT. Vehicle simulations have been made to study and verify the capability and advantages of the new electrified powertrain system.

Firstly, the operation principles of various HAMTs are discussed through detailed power flows at each gear. The fundamental principles of typical HAMT variations are explained using a new power-flow triangle with three ports. Based on the concept of Torque Gap Filler (TGF), a set of HAMT system designs have been introduced and closely studied to provide continuous and stable output torque. The selected hybrid powertrain system equipped with a representative HAMT system supports both HEV mode and EV mode with eight variable gear ratios for each mode. Among the eight forward gear ratios, six are independent and two are dependent on the

other gears. Combinations of dog clutches at all gears are designed to eliminate torque holes. Gear ratios and gearshift schedule of the 8-speed HAMT are designed to support the new design. Torque paths at each gear are illustrated and transient scenarios including gearshifts and mode transitions are investigated. The gear ratio of each gear is determined by considering the unique clutch combination of this HAMT, using the classical gear ratio design method - Progressive Ratio Steps. Due to the broader high efficiency operation region of electric motors, a model-based optimization method is used to determine the two gear ratios for the EV mode to achieve better fuel economy and avoid unnecessary gearshifts. Dynamic Programming (DP) is used to identify the optimal gear ratios, considering vehicle fuel economy for the EPA75 and Highway Fuel Economy Fuel Test (HWFET) driving cycles. The 4^{th} and 6^{th} gears among the eight gear ratios in the EV mode of PHEV are based on 2-speed gearbox design for an EV, and their gearshift schedules are determined by optimization. Combining the considerations for the hybrid and EV modes of a PHEV, key elements of the proposed HAMT system, including gearshift schedule, clutch combination, and gear ratios for highly efficient operation are determined.

The more challenging driveability issues during mode transition from EV to HEV and power-on gearshift with TGF during acceleration are addressed. Both of these two operations require relatively high power/torque outputs and involve multiple powertrain components, including engine, motor, main clutch and gearbox, within a period of two seconds. A lumped-mass model (LMM) of the HAMT-based hybrid vehicle is built to analyze the driveline dynamics in two steady states and four transient states. Each of these states is analyzed independently, according to states of main clutch and gear selectors, considering different phases of the TGF operation and EV-HEV mode transition. The methods for modeling the discontinuity of clutch torque and dog clutch inside the HAMT are discussed to support the subsequent powertrain system modeling and control development. To identify the optimal control schemes for model transition and gearshift, the model-based optimization method for a post-transmission parallel PHEV is developed. The vehicle powertrain model was initially built using AUTONOMIE and MATLAB/Simulink with primary parameters from a prototype PHEV and its dSPACE ASM model developed at University of Victoria. System dynamics in EV mode and hybrid mode are described as a group of state-space equations, which are further discretized into matrix form to simplify the optimization search. A DP-based global optimization method is used to identify the optimal control inputs, including engine torque, motor torque, and main clutch torque. Four principles for desirable EV-HEV mode transitions are extracted based on the results of the optimization.

To model different operation modes and complex power flows, the initial baseline powertrain system model is then replaced by a customized MATLAB/SimDriveline model. In this new physics-based powertrain model, gearshift actuators and controller are added to model the gearshift and mode transition processes. To achieve good driveability, the TGF feature of the HAMT design is split into five transient and two steady phases, each corresponding to a fundamental operating mode. Control logics of upshift and downshift, as well as EV-HEV mode

transition are introduced. Four principles of mode transition derived from global optimization results are introduced for powertrain system control.

Simulations of the HAMT-based hybrid powertrain operations have been carried out to verify the functionality and advantages of the proposed HAMT design in achieving excellent driveability during mode transition and gearshifts. Through controlled coordination of engine, motor and main clutch, EV-HEV mode transition can be achieved smoothly within a period of 2-3 seconds. Even slight driveline fluctuation can be eliminated by dedicated anti-shuffle control with the motors as actuators. The same simulation model also demonstrates excellent driveability during power-on gearshift. Comparing simulation results with and without TGF shows that this new hybrid powertrain system can effectively eliminate torque holes during gearshift. With the demonstrated advantages of this new system in efficiency, torque capacity, simplicity in design and manufacturing costs over its existing rivals, the research provides a promising alternative to mainstream power-split hybrid electric powertrain system design.

Contents

List of Figures

List of Tables

List of Abbreviations

AMT	Automated Manual Transmission
AT	Automated Transmission
AWD	All Wheel Drive
CAFÉ	Corporate Average Fuel Economy
CVT	Continuously Variable Transmission
D	Differential
DCT	Dual Clutch Transmission
DOF	Degree of Freedom
DP	Dynamic Programming
e-CVT	Electronically-Controlled Continuously Variable Transmission
ECU	Engine Control Unit
EM	Electric Machine
E-REV	Extended Range Electric Vehicle
ESS	Energy Storage System
EV	Electric Vehicle
FD	Final Drive
FWD	Front Wheel Drive
HEV	Hybrid Electric Vehicle
HAMT	Hybridized Automated Manual Transmission
HAT	Hybridized Automatic Transmission
HCVT	Hybridized Continuously Variable Transmission
HDCT	Hybridized Dual Clutch Transmission
HIL	Hardware-in-the-loop
HT	Hybridized Transmission
ICE-V	ICE-Powered Vehicle
IMA	Integrated Motor Assist
ICE	Internal Combustion Engine
IM	Induction Motor
LMM	Lumped-mass Model
MT	Manual Transmission
PEV	Pure Electric Vehicle
PHEV	Plug-in hybrid electric vehicle
PMC	Physical Modeling Connecting
PMSM	Permanent magnet synchronized machine
PSAT	Powertrain Simulation Toolkit
PSD	Power-Split Device
PGSs	Planetary Gear Sets
SOC	State of Charge
SPPHEV	Series-Parallel Plug-in Hybrid Electric Vehicle
TC	Torque Converter
TCU	Transmission Control Unit
TGF	Torque Gap Filler
Trans	Transmission
VCC	Vehicle Central Controller

Acknowledgements

I appreciate my PhD supervisor, Prof. Zuomin Dong, very much for bringing me to the field of electrified vehicle and powertrain simulation. It would be impossible to complete this work without his long-time mentorship and funding support. In addition to academic instruction, I have been benefiting a lot from your research methods, way of thinking and life philosophy. I would like to acknowledge my parents, Aimin and Baolin, whose hard-working manner and persistence fundamentally determined my attitude to life and research. I also wish to express my deep appreciation to my wife, Cheng Zhang, for her continuous support throughout this long journey. Her full commitment and love to our small family created a peaceful environment for me to focus on my research work. Her accompany during every tough period is always the most touching part. Finally yet importantly I wish to acknowledge my grandpa, Kong, whose encouraging life experience and determination below surface greatly influence my vision and decision.

1 Introduction

1.1 Background

Today the automotive industry is experiencing the fastest changing and challenging period of time with many new and emerging technologies. Powertrain electrification is one of most significant developments. Different and often conflicting factors are influencing how vehicle electrification has evolved and where it will proceed. Tightened regulations for fuel economy and emissions drive automotive manufacturers and suppliers to increase the level of vehicle electrification, while customers, on the other hand, pursuit higher vehicle driveability and performance with higher fuel economy. In addition, automotive manufacturers have to seek the balance between the benefits of various electrification technologies and the impacts of these new technologies on vehicle costs.

Fuel consumption and tailpipe emissions have been critical topics in transportation sustainability. It is projected that world petroleum and other liquids supply through 2040 will further increase by 30% on the basis of 2011 due to expected energy demand [2]. As part of response to the energy and environment crisis in transportation section, researchers around the world are working on a wide range of strategies and techniques to reduce petroleum consumption and cut tailpipe emissions [3]. One influential action is the 2017 and Later Model Year Light-Duty Vehicle Greenhouse Gas Emissions and Corporate Average Fuel Economy Standards that will take effect in U.S. from 2017 model year [4]. As shown in Figure 1-1, fuel economy requirements for passenger cars and light-duty trucks will be enhanced by about 50% and 35%, respectively [2].

There are different advanced technologies that help to enhance powertrain efficiency, reduce petroleum consumption and tailpipe emissions. One straightforward approach is to enhance powertrain efficiency and lower vehicle resistance forces. This technical path can be further divided into four major technical categories: engine, transmission, vehicle techniques and hybrid techniques. A comprehensive survey of those techniques can be found in [5]. Hybridization of powertrain is widely considered as a practical and effective solution to improve ICE efficiency and emissions in near future [2][4]. Hybrid Vehicle (HV) is defined as a vehicle with two or more energy storage system (ESS), both of which must provide propulsion power–either together or independently [6]. Specifically, in addition to conventional fuel tank, the secondary ESS could be flywheel, compressed air tank, battery, ultracapacitor as well as combination of battery-ultracapacitor, as summarized in right-bottom block of Figure 1-2 [7] [8] [9]. These types of HVs differ from each other greatly from operation principle, performance and FE benefits as well as costs. Those HVs equipped with battery as ESS are in a monopoly position from aspects of both count and type, in comparison with other competitors. Therefore, in this review hybrid vehicle refers only to HVs with battery as ESS.

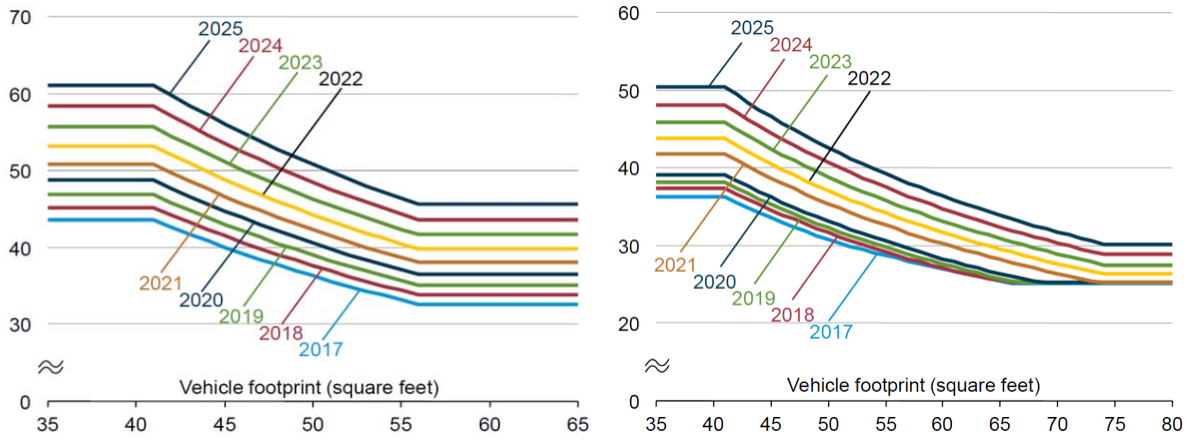

(a) passenger car (b) light-duty truck

Figure 1-1 Projected average CAFE compliance targets between 2017 and 2025

The second strategy of reducing petroleum consumption is to shift use of petroleum to other energy sources. Various alternative fuel and powertrain solutions are summarized in left-bottom block of Figure 1-2, according to energy sources, on-board energy and propulsion systems. Among various choices, hybrid electric vehicle (HEV) and plug-in hybrid electric vehicle (PHEV) are the most practical and promising powertrain solution for reducing petroleum consumption and lessening environmental crisis in the short- to middle-term for 3 reasons:

a) Electric energy is pivotal element for diversification of energy sources, beneficial for energy security. Different types of regenerative energy and nuclear energy can provide rich energy sources [10].

b) Petroleum will continue to be primary fuel of on-land vehicles in decades, so hybridization of vehicle will play a critical role in improving mass-production vehicle efficiency and reducing emission;

c) HEV and PHEV belong to both electrification and hybridization approaches, provide a wide range of technical solutions [2] [5] [11]. Pure Electric Vehicle (PEV) is a promising solution in long term, but concern of driving distance is one apparent shortcoming. As a compromise of various factors, PHEV with even more capable battery and improved overall efficiency have apparently solved the concern of driving distance of EV, and led to much less petroleum fuel use and lower emissions.

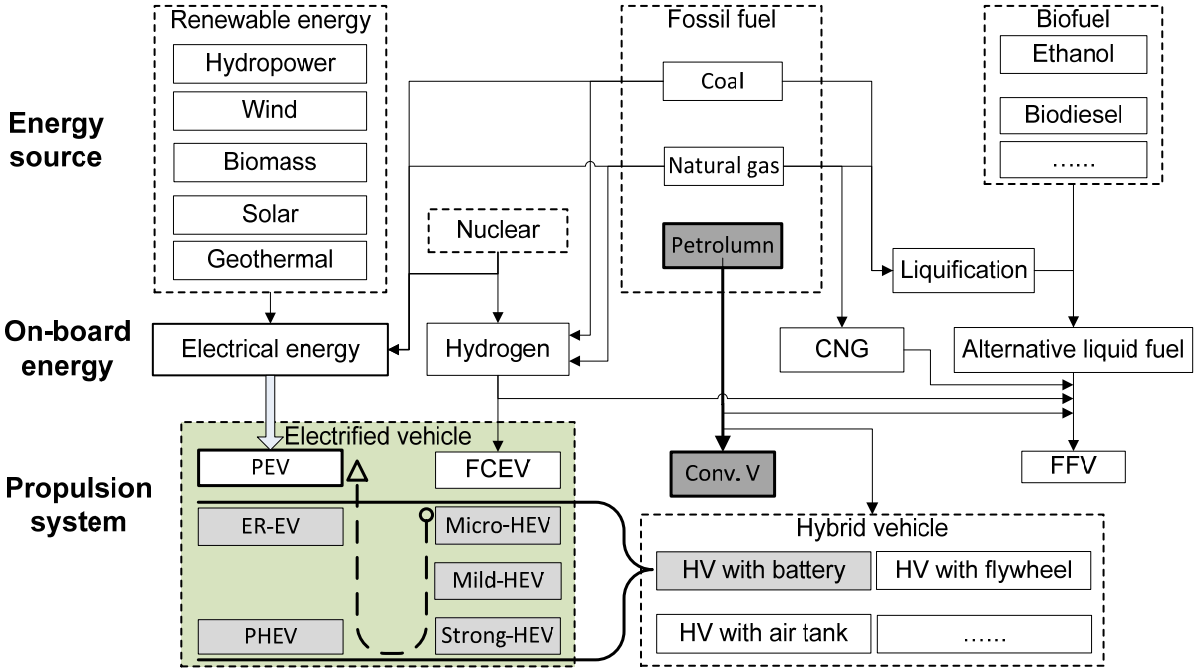

Figure 1-2 Alternative fuel and powertrain solutions

Electrification level determines energy-saving "tools" of each xEV. Electrification level, which can be evaluated by battery power and size, breaks up xEVs into five categories of hybrid vehicle (Micro-HEV, Mild-HEV and Strong-HEV, PHEV, ER-EV), PEV and FCEV, as shown in Table 1-1. Micro-HEV is the simplest HEV, with only the ability to stop engine, as vehicle is static and restart it immediately after Vehicle Central Controller (VCC) detects driver's intention to launch vehicle; Mild-HEV has additional but limited power assist capability and regenerative braking (RB) capability, where the recovered energy over Federal Test Procedure is at least 15% but less than 65%. Representative Mild-HEVs include GM Chevrolet Malibu with eAssist and HONDA Insight with Integrated Motor Assist (IMA) system. Strong-HEV can run like a PEV at low speed and has more powerful power-assist capability and RB capability, where the recovered energy over the Federal Test Procedure is at least 65% [4] (p534). Toyota Prius and Ford Escape are two well-known Strong-HEV passenger car and SUV, respectively. All the three HEVs above can improve efficiency along the first strategy [12]. PHEV, ER-EV and PEV have big battery size to store electric energy from grid system via an on-vehicle charger. PHEV generally supports PEV driving at least 20 Km, like Honda Accord Hybrid and Plug-in version of Toyota Prius. ER-EV was invented by GM for its Chevrolet Volt to emphasize its full-performance, all-electric capability. According to analysis from GM, ER-EV can further enhance fuel economy and reduces engine-launch times [12]. HEVs are intermediate steps and PEV is ultimate target from aspect of electrification. PEV is exclusively by EM(s) that is powered by electric energy in battery.

Table 1-1 Comparison among EVs based on electrification level

	Micro-HEV	Mild-HEV	Strong-HEV	PHEV	ER-EV	PEV
Idle-stop	◎	◎	◎	◎	◎	-
Power assist		○	◎	◎	◎	-
RB		○	◎	◎	◎	◎
PEV driving			○	◎	◎	◎
Charger				◎	◎	◎
Voltage	12	48+	300+	300+	300+	300+
Effectiveness	2-4%	8-11%	20-35%	50-60%	>60%	>60%
◎: full capacity; ○:partial capacity; -: inapplicable						

PHEV and HEV are two closely related but quite different powertrain concepts. On one side, PHEV and HEV of the same powertrain architecture share similar operation modes as well as most of energy-saving abilities; On the other hand, PHEVs that are equipped with larger EMs and battery package have extra ability to store electric energy extract from grid in carry-on large battery package and to support EV drive without start-up of ICE in the first dozens of kilometers (EV range depending on battery size, power, usage and other factors), hugely reducing oil consumption. PHEV can be considered as a combination of PEV and HEV. Advantage of PHEV over HEV can be explained by people's driving habits. According to 2009 national household travel survey conducted by US Department of Transportation and Federal Highway Administration, 68% of vehicles drive not over 65km daily, mean driving length and mean trip length are 62km and 15km, respectively [13] [14]. Therefore, a PHEV with capacity of 20 plus EV drive range and top speed of 60 plus km/h (for city driving) can achieve obviously higher FE than HEV.

1.2 Overview of HEV/PHEV Architectures

Powertrain architecture, which refers to layout and energy flow paths among powertrain components, is another important aspect of xEV powertrain. Architecture design and selection prior to development of an EV is a critical procedure since powertrain architecture will cast significant influence on future design, control and optimization. However, identifying a desirable architecture in the early stage is a very challenging task. Unlike conventional powertrain, which has only one operation mode and limited layout choices, architecture of xEV powertrain refers to more variables (e.g. number of electric machines (EMs), type and count of coupling/switching devices, transmission selection and topological relationship of components). In addition, a specific architecture could operate in different mode by changing states of coupling devices, transmission and EMs. As powertrain architecture interacts with powertrain management strategies and sizing of components, selection of an appropriate architecture from almost

numerous possible choices becomes more difficult. Furthermore, electrification level has great impact on architecture design and selection.

Three big categories of hybrid architectures are series hybrid, parallel hybrid and power-split hybrid. As illustrated in reference [15], there are many basic hybrid architectures, under each category, compatible with one or multiple electrification levels. With comparison to parallel hybrid vehicle, series hybrid powertrain has relatively fixed architecture and application; similarly, power-split hybrid powertrain features limited variations and small chance for further innovation due to patent domination of Toyota. Thus, focus has been put on innovation of parallel hybrid powertrain.

1.2.1 Series and Power-split HEV/PHEV

Classification of architectures of hybrid electric vehicle is more complex than PEV because hybrid vehicles refer to ICE, EM(s), coupling device(s), transmission as well as their locations. Theoretically, there are a huge number of architectures for HEVs, PHEV and ER-EV. The mainstream classification method is to categorize those architectures into series, parallel and power-split architectures [7] [16] [17] [18].

1.2.1.1 Series hybrid architectures

A series hybrid, often applied on locomotives, generally consists of a gasoline or diesel engine, an electric generator (EM1) and motor (EM2), energy storage system (ESS) and VCC. Series HEV has different layouts, some of which are illustrated graphically in Figure 1-3. The engine-generator assembly converts chemical energy of petroleum into electric energy that powers traction motor to propel vehicle. More variants of seris hybrid vehicle architectures are summarized in survey [15]

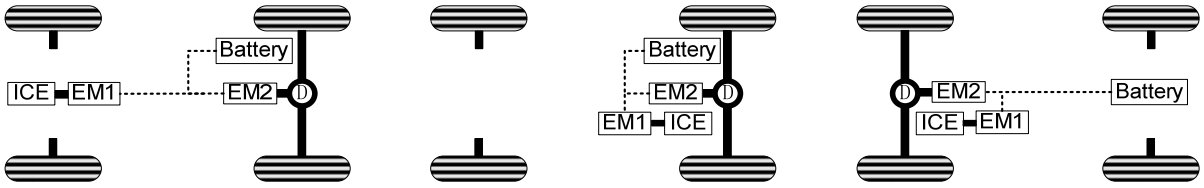

(a) Front-engine rear-drive (b) Rear-engine rear-drive (c) Front-engine front drive

Figure 1-3 Series HEV architectures

Series HEV is advantageous in many aspects over other HEV architectures. For example, since there is no mechanical path between the engine and the wheels, ICE can always operate at peak-efficiency zone and reduce fuel consumption even if during busy traffic time; in deceleration stage, powerful traction motor EM2 switches to a generator, recapturing more kinetic energy via regenerative braking and store it in battery for next vehicle launch; compared with parallel and power-split hybrid vehicles, Series HEV can be well managed using a relatively simple control system. However, a series of shortcomings hinder wide acceptance of series hybrid powertrain: 1) multiple energy conversions reduce overall efficiency of Series, especially when vehicle is at high speed; 2) EM2 is the only direct power source, which means EM2 and electronics should

meet maximum power demand, increasing costs, weight and installation space; 3) The power of engine is unable to provide direct torque while electrical units fails or torque demand is beyond capability of EM2. All these characteristics decide that Series HEV is primarily used on city bus that experiences frequent start-stop, idling, deceleration and acceleration [16]. In 1999 GM launched the series version of EV1, which is powered by a gas turbine engine and a high-speed permanent-magnet AC generator. In 2006, PML Flightlink demonstrated an in-wheel electric motor for cars called the Hi-Pa Drive based on a Mini dubbed the "Mini QED" [19].

1.2.1.2 Power-split hybrid architectures

Power-split hybrid powertrain consists of power-split device (PSD), an ICE, two EMs, ESS and VCC. Power-split architectures is a compromise between series and parallel hybrid [14]. Engine torque is delivered to output shaft via efficient mechanical path and less efficient electric path. PSD has two important features: 1) rotation speeds of three ports (sun gear, ring gear and carrier gear) are governed by equation (1.1), so two degrees of freedom (DOF) enables rotation ration of ICE be controlled to operate within peak-efficiency zone; 2) torques into three ports of PSG should be proportional to each other, as shown in equation (1.2) and (1.3), so EMs should have big output torques and power-split hybrid architectures are not fitting for Micro-HEV and Mild-HEV, unlike parallel hybrid architectures.

A PGS consists of sun gear, ring gear, carrier gear and a set of pinion gears, as shown in Figure 1-4. The relationship among three ports (sun gear, ring gear and carrier gear) of planetary gear set (PGS) is expressed mathematically by equation (1.2) to (1.3), whose linearity can be represented by level diagram [20] [21] [22] [23].

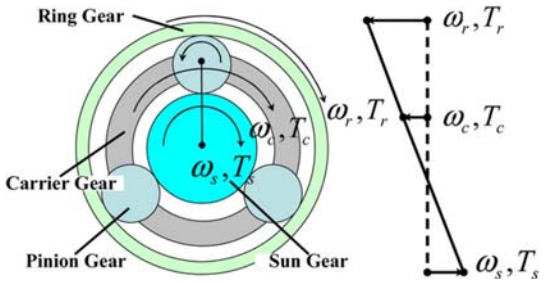

Figure 1-4 PGS and lever diagram

$$\omega_s \frac{R_s}{R_s + R_r} + \omega_r \frac{R_r}{R_s + R_r} = \omega_c \tag{1.2}$$

$$\frac{R_s + R_r}{R_s} T_s = T_c \tag{1.3}$$

$$\frac{R_s + R_r}{R_r} T_r = T_c \tag{1.4}$$

Since ICE can always operate efficiently, power-split xEVs can reach remarkable FE improvement and currently dominate hybrid vehicle sector. However, this type of powertrain

also suffers from limitations of PSG. For example, the ratio of power via two paths relies heavily upon vehicle speed, so power-split hybrid vehicles are efficient only within a certain speed range, otherwise, overall efficiency will be lowered apparently by multiple energy conversion [21] [24] [25]; power-split architectures require ICE and EMs are bonded together by PSD, which limits flexibility of layout; has limited towing capacity and acceleration; compared to parallel hybrid architectures, this unique category has very limited variants and essentially monopolized by AISIN. From a broad perspective, the assembly of PSD and motors connects ICE and differential to explore potential of ICE in efficiency and torque output, so this assembly is also called hybrid transmission [26].

Power-split powertrain architecture can be categorized to input-split, output-split and compound-split architectures [21]. More complicated power-split can be generated from the three fundamental architectures. Input-split architecture requires ICE, EM1 & 2 are connected to three ports of PSD and output shaft is connected with one of EM1 & 2, as shown in Figure 1-5 (a); Output–split architecture requires ICE, one EM and output shaft are connected to three ports of PGS and the second EM is linked to ICE fixedly, as shown in Figure 1-5 (b) [27] [28]; Compound-split architecture is more complex since compound PSD contains two interconnected PGSs, which are bonded by two compound braches inside PSD. The remaining four ports (two single ports and two compound ports) are linked to ICE, EM1 &2 and output shaft, respectively, as shown in Figure 1-5 (c).

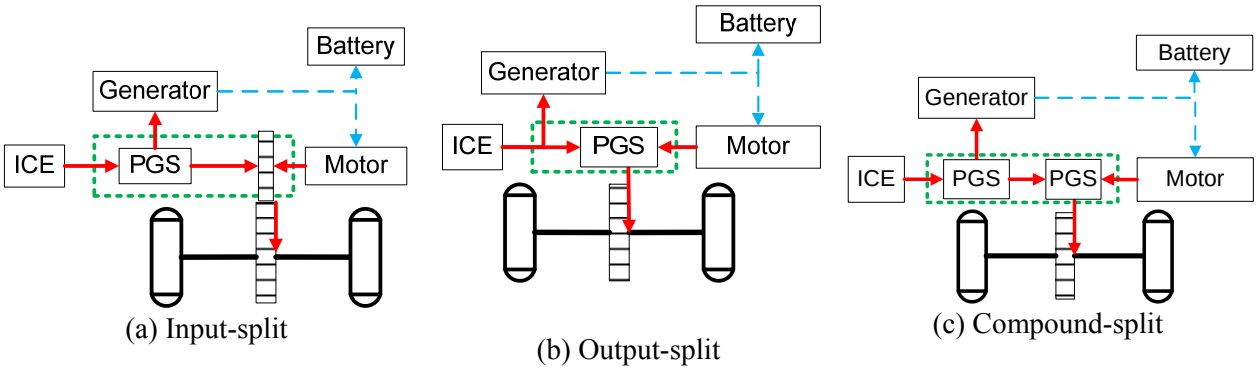

Figure 1-5 Fundamental power-split architectures

Architecture of input-split hybrid is the most popular power-split one since it is the only one suitable for full-range single mode hybrid system within the three basic power-split architectures [21]. Many researchers have conducted related theoretical analysis and simulation about efficiency of power-split hybrid [29] [30]. Toyota Prius and Ford Escape Hybrid are representative passenger car and SUV of this type. Figure 1-6 summarizes architectures of important input-split hybrid vehicle on market. The Toyota hybrid system has experienced three generation, as shown sequentially in Figure 1-6 (a-c). The first generation, also called THS, was initially applied on Prius. The second and third generations, named as Hybrid Synergy Drive (HSD), share basic input-split architecture of THS, but additional PGS as torque multiplier is added to enhance efficiency at high speed. Ford Hybrid System (FHS), shown in Figure 1-6 (d), is quite similar to THS and HSD, but the EM2 torque is sent to wheel via gear pairs, rather PGS-

based torque multiplier. Compound PSD for compound-split hybrid vehicles is also possible to fit for input-split hybrid architectures. Figure 1-6 (e) presents an input-split architecture with compound-split PSD. Although the compound PSD generally contains four ports, one compound port can be left unconnected and other three ports are connected with ICE, two EMs as input-split structure. Other power-split variations include GM 2-mode hybrid system [31] [32] [33].

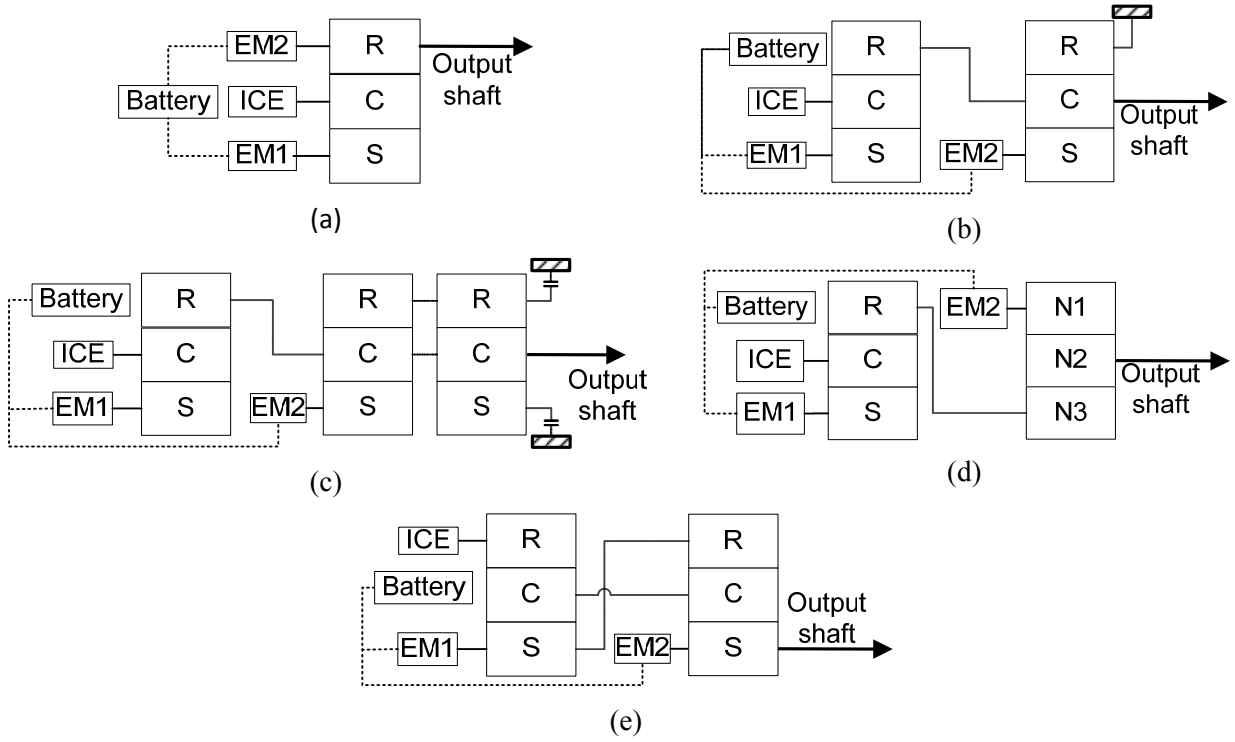

Figure 1-6 Representative input-split architectures

Compared to input-split hybrid architectures, output-split architectures have different efficiency characteristics. Two representative output-split architectures are listed in Figure 1-7. This type of architecture is not suitable for single-mode hybrid vehicle, but it can be used as a sub mode on multiple-mode hybrid vehicles [21].

Figure 1-7 Representative output-split hybrid architectures

Compound-split transmissions have two PSDs, which are connected mutually to reduce 2 DOF. Therefore, compound-split hybrid system has also two DOFs to control. Compound-split transmissions can provide two node points and achieve high efficiency between the two node points. Another advantage of this architecture is that torque demand for EMs can be reduced.

Limitation of this type includes more complicated structure and low system efficiency at low speed. A representative architecture is listed in Figure 1-8 .

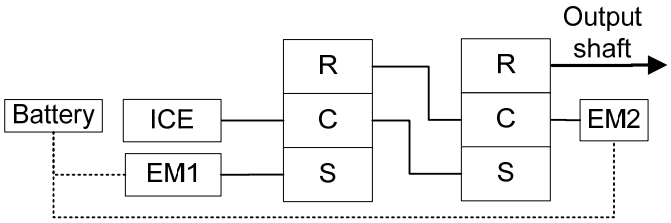

Figure 1-8 Representative compound-split hybrid architecture

1.2.2 Parallel HEV/PHEV Architectures

Parallel hybrid powertrain means that engine and electric motor are coaxially or parallely fixed to provide driving torque to wheel, separately or together. Al low load, ICE can drive EM to generator electric energy to recharge ESS; under heavy load conditions, the load is jointly driven by the engine as well as the motor driven by the electricity of the ESS. Unlike series or power-split hybrid vehicles, parallel hybrid vehicle could be any one of those electrification levels. This advantage, to a certain degree, that parallel hybrid will be mainstream choice of Micro- and Mild-HEV. The drawback of the system is that the engine is rigidly linked by wheel, unable to have the engine run at its optimal speed.

Parallel hybrid architecture typically includes an ICE, an EM, a transmission, one or more coupling device (clutch, torque converter), battery package and VCC. Primary variable of Parallel xEV architectures is location of EM relative to other components. Figure 1-9 depicts a representative powertrain architecture that is adopted in most conventional Front-Wheel-Drive (FD) or Rear-Wheel-Drive (RD) vehicles. C, D and Trans stand for clutch, differential and transmission, respectively. Transmission could be any of manual transmission (MT), AT, dual-clutch transmission (DCT) and continuously variable transmission (CVT). The clutch may be replaced by torque converter if AT or CVT is selected. Those numbers within circles of Figure 1-9 indicate possible positions where EM could be mounted to formulate a Parallel HEV. Therefore, there are total five different parallel architectures derived from the basic architecture, as shown in Figure 1-10 [34]. A summary of relationship among those architectures is shown in Table 1-2. By mixing this summary with Figure 1-10, prospective energy-saving capabilities of each architecture becomes clear. On one hand, each of the five parallel architectures possesses corresponding unique characteristics and limitations; on the other hand, those electrification levels connect different architectures. Type-a and type-b parallel xEVs can only operate in hybrid mode, like a regular parallel HEV; the remaining three types enable vehicle to operate in PEV mode by disengaging clutch and to operate in hybrid mode.

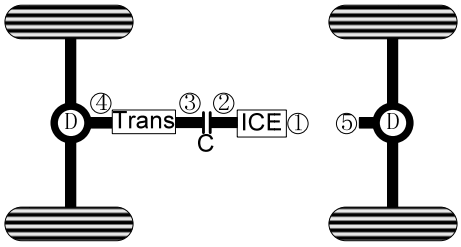

Figure 1-9 Possible location for EM in parallel architectures

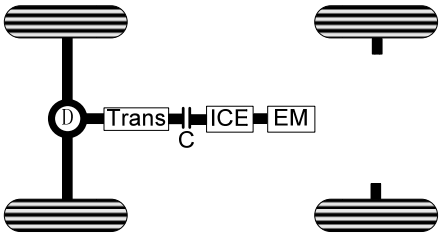

(a) type-a parallel architecture

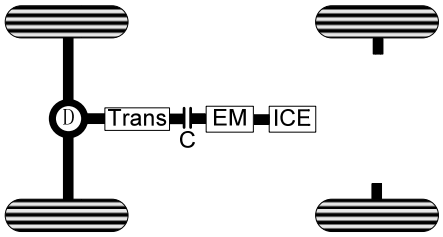

(b) type-b parallel architecture

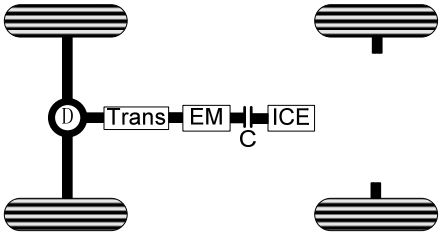

(c) type-c parallel architecture

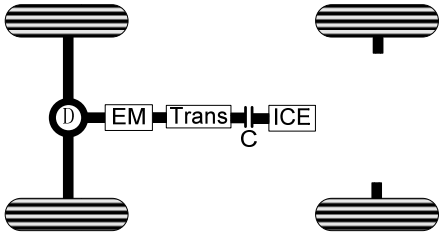

(d) type-d parallel architecture

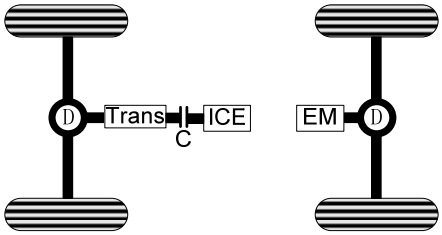

(e) type-e parallel architecture

Figure 1-10 Parallel hybrid architectures

Table 1-2 Comparisons among five parallel architectures

	Micro-HEV	Mild-HEV	Strong-HEV	PHEV	ER-EV
Type-a	◎	◎			
Type-b		◎	◎	◎	◎
Type-c			◎	◎	◎
Type-d			◎	◎	◎
Type-e			◎	◎	◎

I) Type-a parallel architecture

This type is suitable for both Micro-HEV and Mild-HEV. Compared to other architectures, this one is the economic parallel hybrid with limited changes of conventional powertrain platform. For Micro-HEV, regular starter motor will be replaced by an EM with power of 3-5kW; for Mild-HEV, the EM of power typically 7-12 kW can also provide power assist to ICE and modest regenerative braking [27]. Other important changes include modified air conditioner system that can continue to work as engine is off [5]. Micro-HEV of this type becomes more and more common. Belted alternator starter (BAS) of GM is a representative Mild-HEV of this architecture; the more powerful second-generation BAS, eAssist, has been used on 2013 Malibu and 2012 Buick Regal [35]. Since ICE needs to keep rotate with EM all the time, this architecture is not suitable for PEV driving due to undesirable ICE friction torque.

II) Type-b parallel architecture

This architecture requires compact EM to be mounted within narrow space between engine and clutch. Honda Integrated Motor Assist (IMA) is representative of this architecture, with a "pancake" motor flywheel mounted. Details about IMA can be found in related patents [36]. This architecture shares common energy-saving capabilities with type-a parallel architecture and cannot propel vehicle in PEV driving mode with ICE static, either. Since this architecture is more costly than type-a architecture, Honda is the only one major manufacturer commercializing this type until now. According to joint technical support document, this architecture is not listed as promising solution due to its high costs [5].

III) Type-c parallel architecture

This hybrid, often named as pre-transmission (P2) parallel hybrid, is a very promising architecture thanks to its balance in costs, size, energy-saving potential and operation flexibility. Since the EM can be isolated from ICE by a clutch, xEVs of this type can operate like a PEV without rotating engine. In light of evaluation criterion for Mild-HEV and Strong-HEV mentioned in section 2, P2 architecture should be possible for Mild-HEV, Strong-HEV, PHEV and ER-EV. The EM is generally incorporated into transmission case to reduce installation space. When vehicle runs in PEV driving mode with clutch disengaged, the transmission may help to solve conflict between vehicle performance and top speed via variable gear ratios, as discussed in section 3. As power demand is beyond capacity of electric system or battery State of Charge (SOC) drops below pre-defined threshold value, engine will be ignited and clutch engaged gradually. EM may play the roles of traction motor and starter via controlled clutch friction at the same time, depending on whether a separate starter is available [37]. This architecture actually can be further diversified with different type of transmission and coupling device [38] [39] [40]. Representative models include Volkswagen Jetta Hybrid, Touareg Hybrid [41].

IV) Type-d parallel architecture

This post-transmission architecture, often referred as P1 parallel hybrid vehicle, shares many features with P2. For example, P1 parallel architecture should also be possible for up to four

xEVs; PEV driving without rotating ICE is allowed as long as power and energy demands are met. The biggest difference between P1 and P2 is that P1 architecture only allows motor to rotate at a speed proportional to vehicle speed, unlike P2. On the other hand, P1 can output torque to wheel continuously, even if gear shift happens.

V) Type-e parallel architecture

Type-e is the AWD version of P1 parallel vehicle architecture. Compared to P1 and P2 parallel architectures, this type can maintain conventional powertrain architecture except the added traction motor system mounted at rear axle. In addition to more driving modes, this type also allows more installation space for EM and controller [42].

1.2.3 Overview of Hybridized of Transmission

Transmission as critical component in conventional vehicles is also important to increase fuel economy and performance for Series-Parallel PHEV as well as other HEVs and PHEVs. With vehicle hybridization, transmission (from its concept to function) is experiencing fast development and its importance is expanding dramatically [43].

Development of transmission can be generally separated into three stages, as shown in Figure 1-11. Great changes have happened and changed pattern of transmission market during the past thirty years. In stage 1 (before end of 1990s), Manual Transmission (MT) and Automatic Transmission (AT) are the two mainstream transmission options. Stage 2 emerged as new alternative transmissions, including Automated Manual Transmission (AMT), Dual Clutch Transmission (DCT) and Continuously Variable Transmission (CVT), were presented in mass production. As progress in vehicle hybridization, transmission development entered stage 3 around second half of 2000s, marked by conceptualization of Hybridized Transmission (HT). It should be noted that products belonging to any of the three stages are being improved simultaneously.

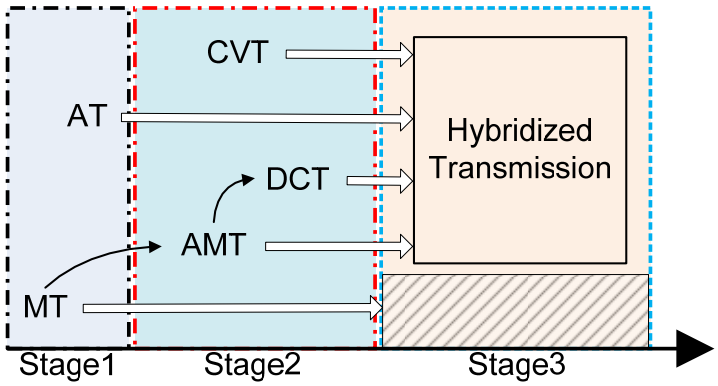

Figure 1-11 Overview of transmission development

All of the five primary transmission choices in stage1 & 2 are compared from four critical directions [44] [34]. Compared to other automated transmission, AMT is of apparent advantage

in cost and weight because it inherits efficiency of MT by imitating actions of driver during gear shifts via added-on hydraulic or electromechanical device and control unit.

Table 1-3 Transmission technology characteristics comparison [based on European market]

Criteria	MT	AMT	AT	DCT	CVT
Shift time (ms)	500-1000	300-500	400-800	150-300	N/A
Fuel savings	Baseline	+2-4%	-5-10%	+3-5%	+3-5%
Weight	Baseline	+5-6%	Up to +50%	+15-30%	+10-15%
Cost ($)	490-840	700-980	1,540-1,960	1,260-2,240	1,820-2,100

AMT had been considered as competent challenger to AT. However, wide acceptation of AMT was curbed by undesirable driveability because of torque interruption during gearshift. Figure 1-12 shows obvious torque gap (solid ellipsoid) and subsequent surging clutch torque (dashed ellipsoid) that appear during 3 gear shifts (neutral to 1st, 1st to 2nd, 2nd to 3rd).

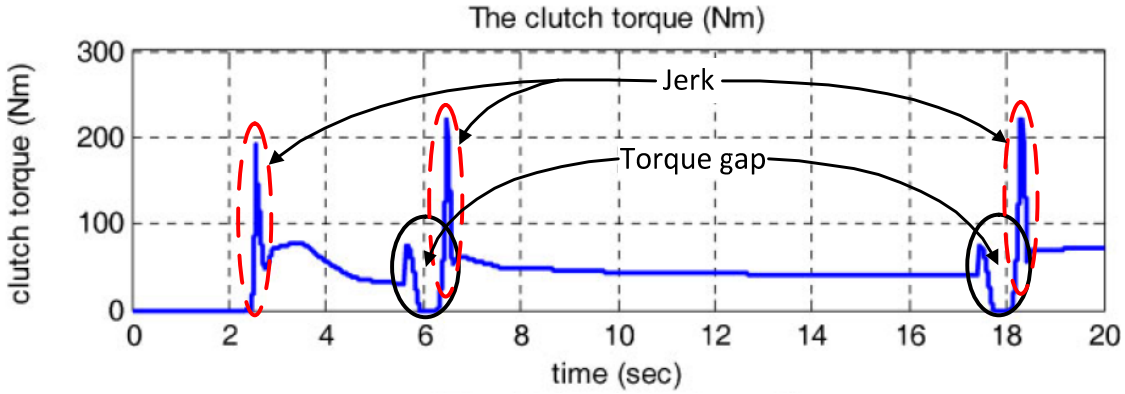

Figure 1-12 AMT gear shift simulations [45]

Stage 3 began in second half of 2000s and was marked by developing Hybridized Transmission (HT), which is now changing definition of transmission. Under the concept of HT, electric motor/generator is no longer a component at the same level of ICE and transmission, but a subsystem of HT. Based on diversification of stage 2, various HTs, like Hybridized AMT (HAMT), Hybridized AT (HAT), Hybridized DCT (HDCT) and Hybridized CVT (HCVT), are realized. Some researchers like Harald Naunheimer with transmission manufacturer ZF prefer to expand domain of HT, dating development of HT back to debut of Toyota Hybrid System (THS) in 1990s and Ford Hybrid System (FHS) later. Still, this classification method is not used here because those power-split architectures do not contain separate transmission units. This transformation is a specific form of vehicle hybridization and is useful for generalization of HEV and PHEV powertrain architecture, shortening development cycle and lowering overall costs. Different manufacturers and suppliers select the best choice for them, depending on technical strength and strategies. For example, HCVT is developed by Nissan and Jatco; HAT is presented by Hyundai and Ford; HDCT is from VW. Among the four mainstream choices of HT, only development of HAMT falls behind.

AMT is dominating transmission in heavy-duty truck due to its outstanding torque capacity and efficiency. However, its wide adoption will not take place in near future. This state can be explained from aspects of commercialization of hybrid powertrain systems and transmission history: 1) AMT has never been mainstream transmission for passenger cars and SUV due to undesirable driveability; 2) hybrid vehicle first appeared on passenger cars and SUV, which has been mainstream platform of hybrid vehicles, so torque demand is limited; 3) the transition among different transmission type is an extremely time-consuming and costly migration. These three reason limits development of HAMT in the past. However, as driveability problem can be solved by new technologies that come with deepening electrification of vehicle powertrain, AMT may be granted a chance to compete with other types of transmissions in segment of passenger cars. As this trend of electrification expands to heavy-duty truck segment, HAMT will be of high potential.

1.3 Development of AMT with Torque-Gap-Filler Feature

Torque Gap Filler (TGF) is the fundamental solution to overcome torque gap of AMT as gear shift happens. That torque-gap-filler concept is explained in Figure 1-13. In order to provide the path 2, various novel ideas were researched and implemented to enable continuous torque output to wheels. According to whether the source of path 2 is engine or a second power unit to realize TGF function, techniques can be classified as active and passive compensation TGFs. Passive compensation TGF transmits torque from ICE to wheels via the second torque path between engine and wheel, when original torque path is cut off during gear shift; Active compensation TFL can absorb power from another power unit, and ICE is disconnected from input shaft of AMT for gear change. This feature makes it possible to replace mainstream transmissions (AT, CVT and DCT) in Parallel-HEV segment with efficient and economic automated manual transmission (AMT). Another advantage of this type is that EM can be mounted more easily.

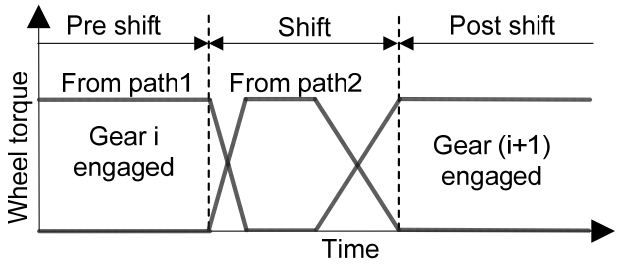

Figure 1-13 Torque gap filler principle

1.3.1 Passive Compensation AMT

1.3.1.1 Torque-assist AMT

In 2004, HITACHI Group presented its torque-assist AMT. The synchronizer for highest gear is replaced by an assist clutch (ACL) to provide torque path. When upshift is required, torque through assist clutch increases by increasing normal force of ACL until torque transmitted from engaged gear approaches zero. After gear is shifted from low gear to high gear, torque through

newly engaged gear increases until gear through ACL drops to zero. Real car tests show that this torque-assist AMT can realize seamless acceleration and high efficiency comparable to MT. Galvagno in [46] presented detailed dynamic analysis of this new AMT and verified TGF function. However, gear shift of this torque-assist AMT depends heavily on precise coordinate control of ACL torque and gear disengagement/engagement. Since absence of a secondary torque path is direct reason of torque interruption during gear shift, some researchers added new torque path to AMT via different methods. [46] [47] [48] [49]

1.3.1.2 Uninterrupted Shift Gearbox

The second important passive compensation AMT was Uninterrupted Shift Gearbox (USG) invented jointly by BMW, Getrag and LUK. It shared the same idea of torque assist clutch (powershift clutch here) of HITACHI design, but the added clutch was moved from highest gear to clutch house, and two clutches are controlled by the same actuator, making it more compact and less expensive. Compared to regular AMT without TGF ability, torque gap can be filled by 40% to 100%, depending on gear and accelerator position [50]. It is noteworthy that partial torque filling can make gear shift undetectable subjectively. Figure 1-14 shows the layout of USG and TGF performance during the shift from 1st to 2nd gear. However, USG as well as torque-assist AMT relies slipping friction torque at high relative speed to transmit ICE torque to wheels, so it is significantly more heavily loaded than regular start-up clutch, which restricts its application on engine torque less than 250 Nm.

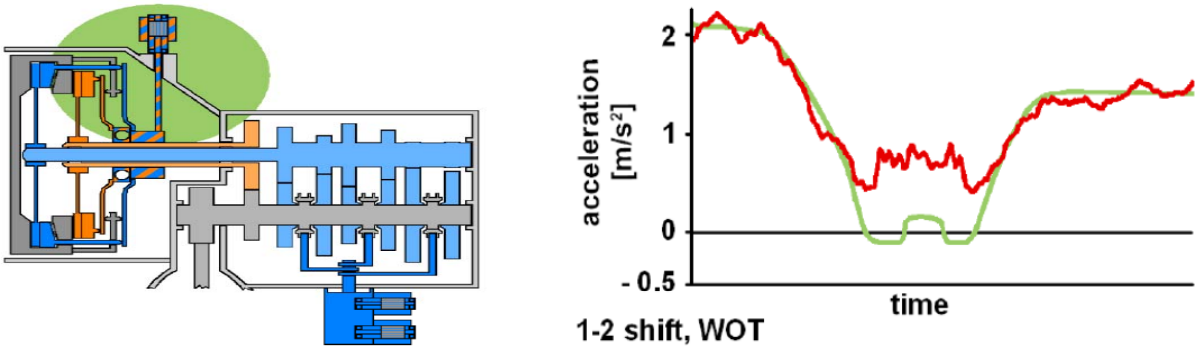

a) Layout of USG b) Acceleration comparison during gear shift

Figure 1-14 Uninterrupted shift gearbox

1.3.1.3 Flywheel-assist AMT

Flywheel-assist AMT (FA-AMT) absorbs much attention from OEMs, transmission suppliers to research community. Representative samples include Powershift AMT (PS-AMT) from Drivetrain Innovations (DTI) and FAT from Polytechnic University of Turin [51] [46]. One planetary gear set is installed between ICE and gearbox output shaft, with ICE and output shaft of gearbox connected to ring gear and sun gear, respectively and gear carrier to inertia flywheel. As gear shift starts, start-up clutch CL is open, ICE and inertial flywheel send torque to output shaft of ATM via gear carrier to maintain original acceleration, at least partly; when gear shift is finished, clutch will be engaged gradually and torque from ICE will be transmitted via new gear

pair. Compared with regular AMT without TFL capacity, this low-cost (DTI claims) AMT variant can help to improve driveability. Still, some drawback also comes with PSG: ICE torque during acceleration is split into PSG and gearbox input shaft, restricting powertrain acceleration performance. Detailed introduction about variants of this kind of FA-AMT can be found in [52].

1.3.2 Active Compensation AMT

1.3.2.1 Automated Shift Manual Transmission

This automated shift manual transmission (ASMT) comes with post-transmission Parallel HEV/PHEV naturally. One representative structure was presented by Ford, as shown in Figure 1-16 [53]. It should be admitted that ASMT reflects essence of TFL and should be a potential option in the trend of hybridization because of a series of advantages. Compared to those passive compensation solutions, its hybrid nature endows much higher potential of increasing fuel efficiency GFs; In addition, fast response and short-term power surge of EM could fill the torque gap faster and fuller. Figure 1-15 shows that this ASMT can provide continuous acceleration with limited fluctuation. Still, in slipping closing phrase, this system with two degrees of freedom in rotational dynamics is governed by three control variables: EM torque, ICE torque and clutch. Therefore, this over-actuated system demands more complicated control to coordinate the three control variables as well as well as gear shift actuator. Relevance between EM torque and acceleration profile shown in Figure 1-15 illustrates how sensitive and important the coordinate control among the four component is. In light of some unpredictable factors, including slope of road and accelerator pedal angle, constantly desirable TFL performance is really a challenging objective. Another drawback of this P2 HEV layout is that EM is connected to differential via a fixed gear. From perspective of efficiency, it ignores energy saving from changing operating points of EM cannot be moved. Similar design was used in Series-Parallel hybrid electric bus by researchers from Shanghai Jiao tong University [54]. Actually, this concept of ASMT can be executed in different powertrain layout as long as P1 HEV is included.

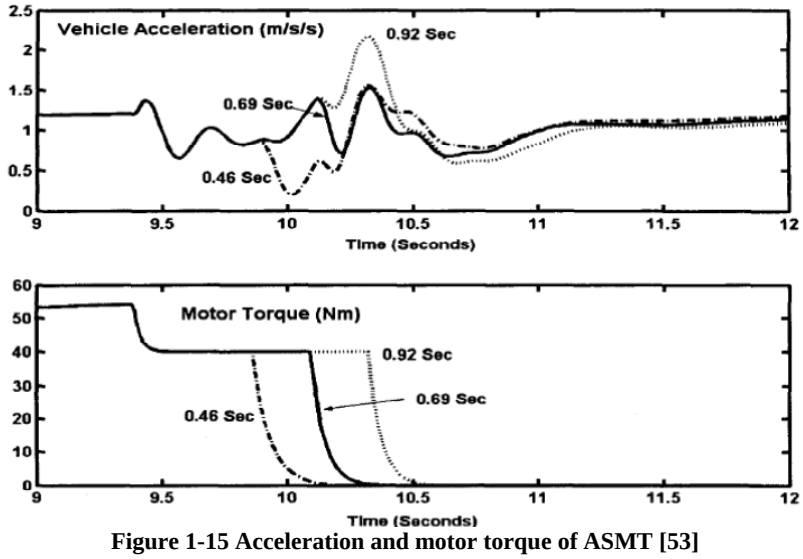

Figure 1-15 Acceleration and motor torque of ASMT [53]

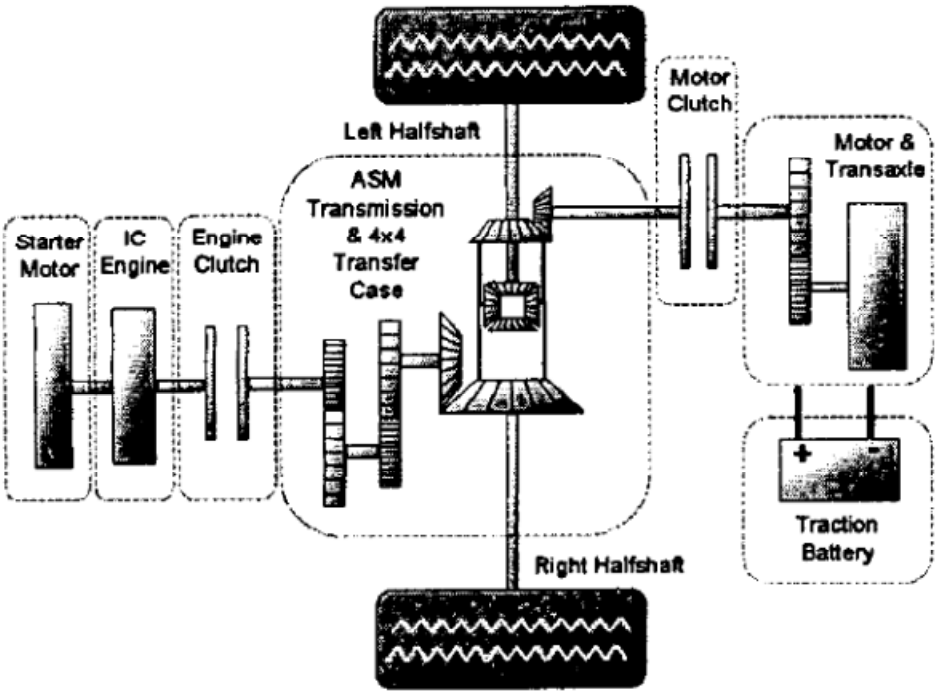

Figure 1-16 Layout of ASMT [53]

1.3.2.2 Hybridized Automated Manual Transmission

As a further step from ASMT, HAMT inherits the principle of TFL from ASMT completely, but it changes relationship between EM and transmission from equality to subordination by integrating EM as a subcomponent into HAMT. With additional change of gearbox structure, HAMT likely solve drawbacks of ASMT or expand its advantages. Amplitude of improvement from ASMT varies with specific design. FEV prototyped a 7-speed HAMT, 7H-AMT, and conducted driving tests on a demonstrator vehicle based on Ford Focus ST [55] [56] [57] [58].

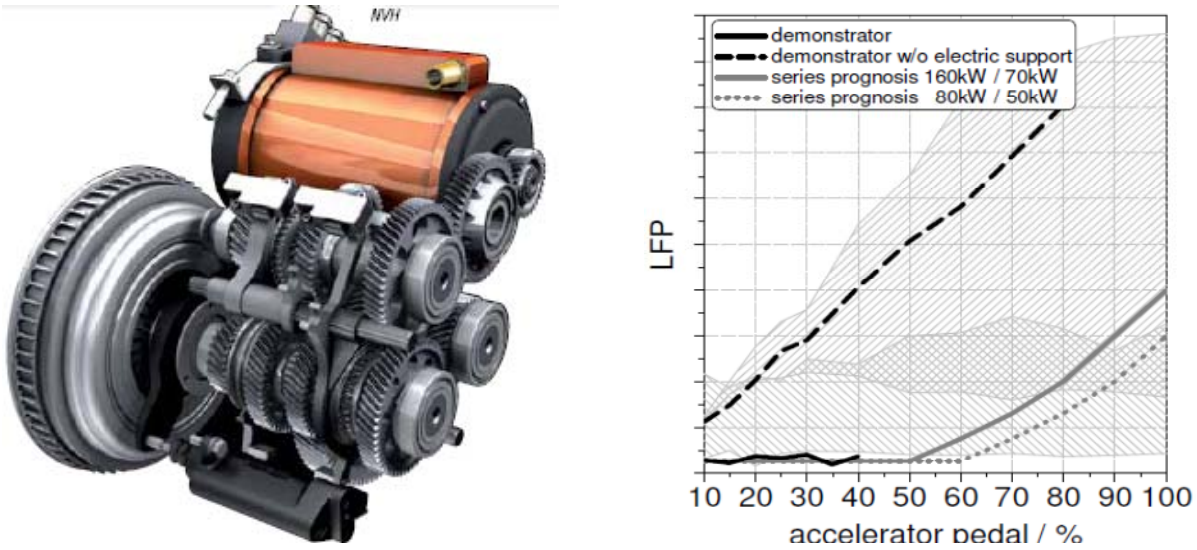

a) Conceptual layout of 7H-AMT b) Shift quality comparison

Figure 1-17 7H-AMT [55] [56]

This 7H-AMT adopted a specially-design gearbox structure, enabling EM linked to both input and output shaft of gearbox. A conceptual layout of 7H-AMT is shown in Figure 1-17(a). This compact structure is important for small cars. Meanwhile, switchability between P1 and P2 HEV by controlling engagement/disengagement of 4 synchronizers can further extend EV drive range. Real-car test results also verified that the TFL function upgrades successfully the smoothness of gear shift from regular AMT level to AT and DCT, as shown in Figure 1-17(b). Prof. Hohn with TUM proposed this kind of HAMT.

1.3.2.3 AMT with Post-transmission Motor

This transmission in Figure 1-18 was introduced by Oerlikon Graziano in March 2013 [59] [60]. It includes a 6-speed gearbox, 2-speed epicyclical gearbox, a water-cooled EM with a maximum of 120kW, shown in Figure 1-18. Essentially, it is also based on post-transmission Parallel HEV/PHEV, like the automated shift manual transmission of Ford, but some apparent differences distinguish this AMT from other similar products. Firstly, this AMT actually includes two gearboxes, 6-speed MT gearbox for ICE and 2-speed epicyclical gearbox for EM; secondly, the two gearboxes are integrated into an entity, and the merging point of output shafts of two gearboxes is inside AMT case; Finally, this AMT employs the concept of HAMT because the EM is embedded into the transmission casting. When gear shift is requested, the EM can fill the torque gap via the 2-speed gearbox, which can be shifted to meet drivers' demand. To further reduce the duration of gear shift process, the dual-shaft gearbox uses Independent Shift Rod system that can minimize time for gear shifts.

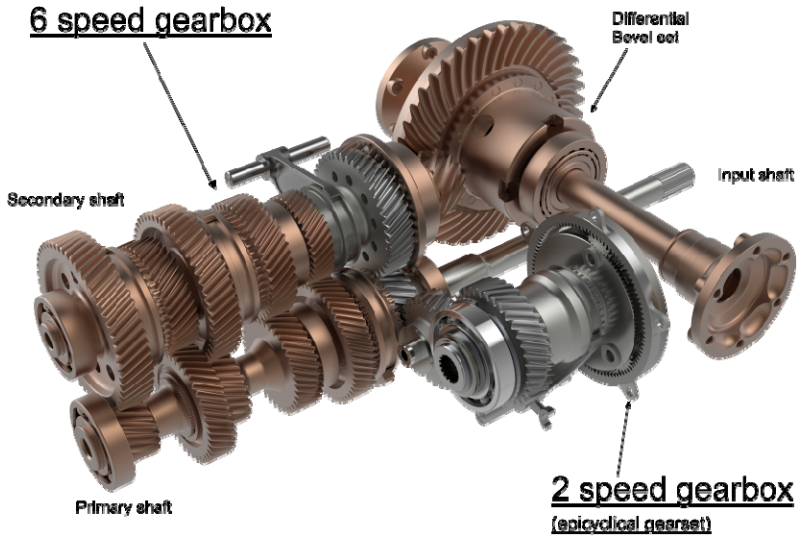

Figure 1-18 Layout of AMT with TGF feature [59]

1.4 Research Objectives and Problem Definition

According to analysis above, enhancing electrification level (strong HEV, PHEV & PEV) of automotive powertrain systems is critical and promising solution to lessen serious environmental

crisis and to meet increasingly stringent rules. Among 3 big categories of hybrid powertrain, parallel hybrid powertrain systems can offer sufficient space and flexibility for research, with comparison to series and power-split hybrid systems. For any parallel hybrid, a transmission unit is almost indispensable element of hybrid powertrain and plays a key role to bond engine and electric system together. Within 4 mainstream automated transmissions, AMT has the least developed on the track of hybridization, due to persistent torque gap during gearshift. However, electrification of powertrain provides unique chance to AMT to overcome that issue and explore its advantages in torque capacity, cost and efficiency. Some pioneering researchers have done some good work to prove survivability of HAMT in this fast-developing area, but full picture and all likelihoods of HAMT are far from explored. Innovative work about HAMT is highly necessary. In addition, basic idea of TGF for improving gearshift quality is revealed, but control strategies and other driveability-related issue, like mode transition, still contain many chances to broaden this technical path.

In order to contribute to solve severe environment crisis and to support sustainability of transportation system, the goal of this research work is to further explore and prove other hybrid powertrain opportunities along this track of parallel hybrid equipped with HAMT. In specific, this whole research contains three objectives:

1) Design novel electrified powertrain systems based on HAMT, including powertrain for PEV and HEV/PHEV;
2) Verify advantages of new systems in driveability, performance, efficiency and costs;
3) Build full vehicle model with necessary details for transmission and full control strategy.

Given the fact that a prototype of a new hybrid system is extremely expensive and requires a huge human resources and financial supports, simulation model is thought to be more containable. In order to achieve these 3 objectives, 4 challenges should be overcome.

1.4.1 Challenge 1: Design Novel Powertrain Architectures

The target hybrid powertrain should meet several requirements to get higher chance to surpass other rivals in this serious competition. Specifically, those requirements are listed below:

a) Target hybrid powertrain should be different from any known hybrid powertrain architectures at best knowledge of author and must be compatible with HAMT.
b) It should be able to operate in PEV mode and parallel hybrid mode.
c) It should support multi-speed operation in EV mode.
d) In hybrid mode, Torque-Gap-Filler function can be implemented to address issue of gearshift quality;
e) Whole powertrain architecture should not be more complex than rival systems from aspects of component amount and compactness;

All the five requirements are extracted from previous analysis, from background to technical paths. Each one is important to success of this research.

1.4.2 Challenge 2: Gear Ratio Design & Vehicle Modeling

Since target hybrid powertrain design should be unique, a prototype is easily accessible. In order to verify advantages of new powertrain systems, it is important to have reasonable simulation model that can mimic normal behavior of vehicle. However, customized simulation model and control strategy are not available.

Considering requirements (b-d) above, the modeling not only supports flexible operation of powertrain in different modes and gears, but also reveals details of powertrain operation, like gearshift. Map-based model without transient process, like gearshift and mode transition, cannot meet the listed requirement. Thus, it is another challenge to build simulation model based on proposed architecture.

As basis of modeling work, especially for gearbox, gear ratio and gearshift schedule are most fundamental work before any progress can be made.

1.4.3 Challenge 3: Powertrain Control for Transient Powertrain Operation

HAMT is advantageous over other transmission types in efficiency, torque capacity and costs. Requirement (d) is of special importance for feasibility of this technical path. In order to demonstrate TGF implementation on new hybrid powertrain system, systematic powertrain control should be able to coordinates ICE, EMs, clutch as well as gearbox. Although gearshift typically lasts no more than a couple of seconds (even less than 1 seconds for conventional stepped transmission), this short process consists of multiple phases, each of which involves complicated interaction of multiple components. Engine and motor dynamics, together with discontinuity of dry clutch, further increase level of difficulty for powertrain control.

Besides gearshift, another important type of transient event is mode transition between PEV mode and hybrid mode, especially from PEV to hybrid mode. Similar to gearshift, mode transition requires researchers to look into details very closely.

1.5 Research Contributions and Thesis Outline

The goal of this research work is to exploit new hybrid powertrain systems and verify the proposal via simulation model, control and optimization. A series of research activities are completed on the track of powertrain electrification and hybridization in order to achieve 3 objectives.

- Introducing a new hybrid powertrain system: a series of HAMT-based hybrid powertrain architectures are invented. Those hybrid powertrain architectures meet all of those requirements listed above. This research work was published in US patent application [61]. As further development of this work, a series of HAMT-based PEV powertrain with variable gear ratios were invented. Compared to those hybrid powertrain systems, PEV

powertrain does not include an engine. In order to maintain smooth gearshift, one extra clutch is added to HAMT gearbox to make the transmission behavior like a DCT.

- Vehicle modeling: one representative hybrid powertrain of patent-pending powertrain architectures is modelled using SIMULINK, SimDriveline and StateFlow, based on one regular parallel PHEV. SIMULINK is used to model basic structure and communication system among components; SimDriveline models HAMT and driveline; StateFlow is primary tool for control. The modeling work is being prepared for a journal paper. In addition, eight gears of this HAMT are assigned gear ratios, and gearshift schedule of transmission is prepared. During the process of gear ratio design, dynamic-programming (DP) method is used to find two critical gear ratios, which becomes base for other gear ratios. The optimization work of gearshift was published on 2013 SAE technical paper.
- Vehicle control: In order to develop basic principle of powertrain control for gearshift and mode transition, one DP-based global optimization method is used to find the optimal powertrain control based on a quasi-static model. This work was published on a 2014 SAE technical paper. Rule-based gearshift and mode-transition control are developed to enable smooth operation, even if during transient events. Detailed control for gearshift and mode transition is split into several phases, and each phase is analyzed in detail to develop control strategy. Some beneficial principles from the optimization results are extracted and implemented on control strategy. This part of work has been prepared as journal article draft.

The thesis contains seven chapters. Chapter 1 introduces development of electrification and classification of primary hybrid vehicle architectures and latest development of hybrid technologies. Advantages of AMT and its driveability shortcoming are discussed in details. HAMT is proposed as a promising candidate to inherit advantages of regular AMT and avoid undesirable driveability. Chapter 2 introduces operating principle of proposed HAMT-based hybrid system, and illustrate torque/power flow paths among different components and insider HAMT. Chapter 3 illustrate clutch combinations for different gears and how optimization method is used to fix two gear ratios for EV mode; Chapter 4 covers system dynamics and details of vehicle modeling principles, including details about gear shift mechanism, controller and main clutch model; a model-based optimization method employing Dynamic Programming helps to find the optimal control trajectories of primary components during mode transition. Four mode transition principles for powertrain are extracted from the optimization results. Chapter 5 describes details of vehicle model configuration, Vehicle Central Controller, sub-system controllers (engine control, gearbox control, motor control and main clutch control) and a lot of details about how the research subject is modeled in Simulink-SimDriveline platform; rule-based control strategy based on global optimization for improving driveability is implemented on simulation model; Chapter 6 provides simulation results of this hybrid system during target driving scenarios, including power-off gearshift, mode transition and power-on gearshift and result discussions. Chapter 7 summarizes the completed work, further discuss the model simulation results, reviews the original contributions, and discusses recommended future work.

2 Architecture and Power Flow of HAMT-Based PHEV Powertrain Systems

2.1 Torque Paths of HAMT Concept

Hybridized AMT (HAMT) offers new approaches to fill torque gap by creating an independent or semi-independent torque path from motor during gearshift. Generally, there are two ways to combine motor with AMT, which are pre-transmission and post-transmission hybrid, shown in subfigure (b) of Figure 2-1. Pre-transmission configuration allows both engine and motor to have variable gear ratio to better balance requirements for motor torque and speed, but motor cannot provide second torque path during gearshift; in comparison, post-transmission configuration supports the second path during gearshift for engine, but motor speed is determined by vehicle speed via a single gear, which inhibits advantages of HAMT in a wide speed range. Ford presented a post-transmission parallel hybrid vehicle equipped with its Automated Shift Manual Transmission (ASMT) [53]. Motor and final drive is connected via a fixed gear. In 2009, FEV released test result of a unique 7-speed HAMT on a demonstrator vehicle based on Ford Focus ST [55] [56] [62]. This special 7H-AMT adopted a merged dual-gearbox structure with 3 parallel shafts, uniquely realizing flexible switch between pre- and post-transmission configurations at different gears. The basic idea is shown in subfigure (c). In March 2013, Oerlikon Graziano unveiled another post-transmission HAMT with dual gearboxes, with a 6-speed gearbox for engine and a 2-speed epicyclical gearbox for a motor of 120kW. Like FEV's concept, it can also support variable gear ratio for motor and smooth gearshift in hybrid mode [60] [59]. Basic concepts from Oerlikon Graziano can be described as subfigure (d) of Figure 2-1.

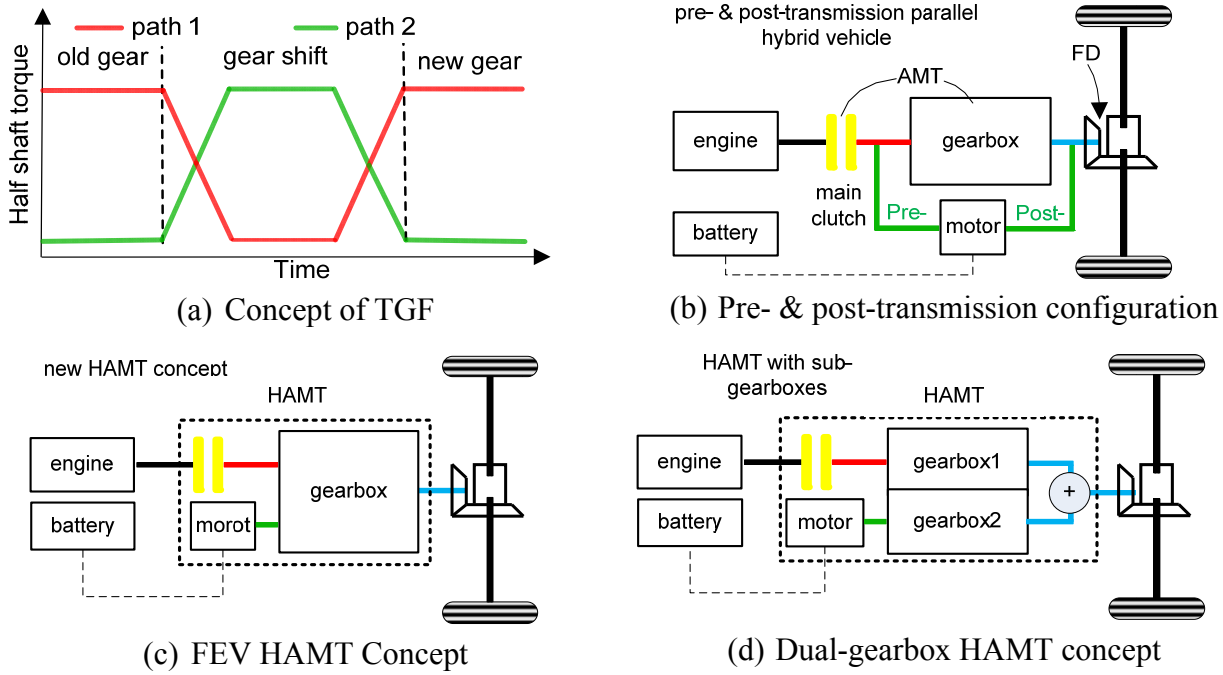

(a) Concept of TGF

(b) Pre- & post-transmission configuration

(c) FEV HAMT Concept

(d) Dual-gearbox HAMT concept

Figure 2-1 TGF concept and HAMT parallel HEV

One representative hybrid powertrain configuration, which belongs to part of a pending patent application, is introduced in detail [61]. The HAMT-based powertrain takes advantage of pre- and post-transmission parallel hybrid configurations, whose basic idea is described in Figure 2-2. This HAMT integrates a motor, main clutch and an 8-speed parallel-shaft gearbox into a unit. The gearbox based on manual gearbox has three connection ports, which are connected to engine via main clutch, motor and final drive, respectively. Directions of three arrows represent primary power flow direction, but reversed directions are also allowed. For example, the arrow between port 2 and 3 represents power flow in normal EV mode, but the arrow direction will be reversed during active braking. Through effective combinations of actuators inside gearbox, this new configuration can support very flexible operation and achieve desirable driveability and fuel economy. The port 1 is linked to port 3 directly via two gear ratios; the port 1 and port 2 are connected through three gear ratios; in addition, two gears exist between port 2 and port 3. As a result, port 1 is linked to port 3 through 8 gear ratios. The HAMT also supports EV driving mode. In EV mode, 8 gear ratios are also available for motor (only partly used). Compared to aforementioned HAMTS, the research subject does not require the 2nd gearbox. In order to illustrate operation principle of this new HAMT concept, one representative 8-speed HAMT variant with 8 gear ratios for engine and up to 8 gear ratios for motor are analyzed in detail.

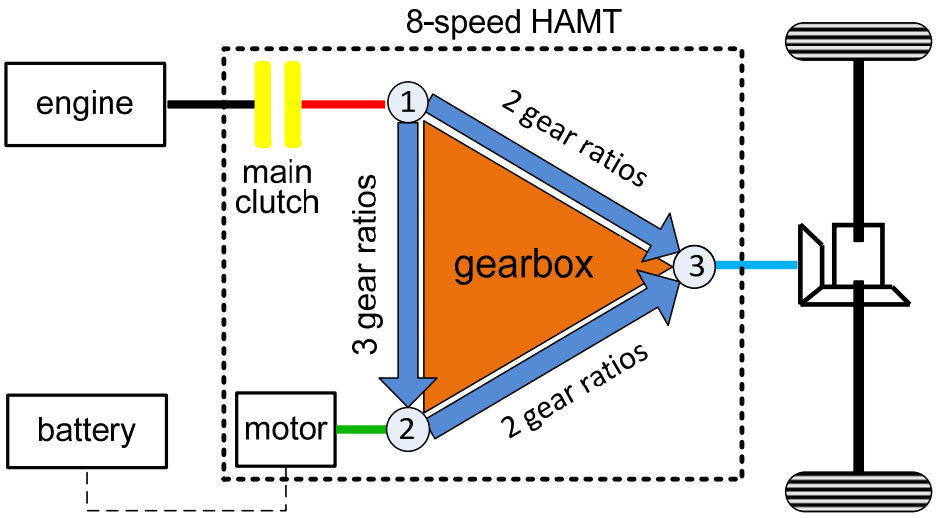

Figure 2-2 Basic concept of new HAMT

2.2 Parallel Powertrain Architecture & HAMT Structure

Several hybrid powertrain architectures based on the concept shown in Figure 2-2, are proposed, with one pending patent application submitted. Depending on number of motors and overall powertrain layout, a variety of parallel hybrid systems and series-parallel hybrid systems are included in the application. One representative parallel hybrid system is selected as representative of new hybrid architectures and detailed analysis is conducted from torque/power flow, gear ratio optimization to modeling and powertrain control. Mechanism of the representative HAMT is shown in Figure 2-3. This HAMT contains one long input shaft (IS1),

one short input shaft (IS2) and one aligned output shaft (OS), four gear selectors and many gear wheels. Each gear selector can move in either left or right, except selector 1 (S1), which can only move to left side. Each side of gear selector consists of a dog clutch and synchronizer. Dog clutch serves to lock gear to shaft; synchronizer serves to eliminate slip speed via friction torque during gearshift. Core part of synchronizer is cone-shape friction. More details about gear selector and synchronizer can be found in reference books and papers [26].

The three shafts correspond to the three ports in Figure 2-2. IS1 is connected to parallel IS2 via three gear pairs that are controlled by gearshift sleeveS1 and S2, which can engage and disengage gearwheels and shaft via dog clutches; OS is connected to parallel IS1 via another two gear pairs controlled by S4; connection of IS2 and aligned OS relies on positions of gearshift sleeve S3. A unique design for this gearbox is the compound gearwheel whose two wheels are bonded together and engaged with a fixed gear wheel on IS2 and a rotating gear wheel on OS. Engine is linked to port IS1 through the main clutch, which could also be replaced by torque converter with by-pass clutch. The gear ratio between input shaft 1 and output shaft is i_{1o}; the ratio between input shaft 2 and output shaft is called i_{2o}. Both i_{1o} and i_{2o} can be selected from multiple gear ratios, which varies with engaged gears. More details will be discussed latter. Motor connects the IS2 through a gear pair, which could be other connection method, like chain gear. The gear ratio of this gear pair, i_m, can serve to change overall gear ratios for motor.

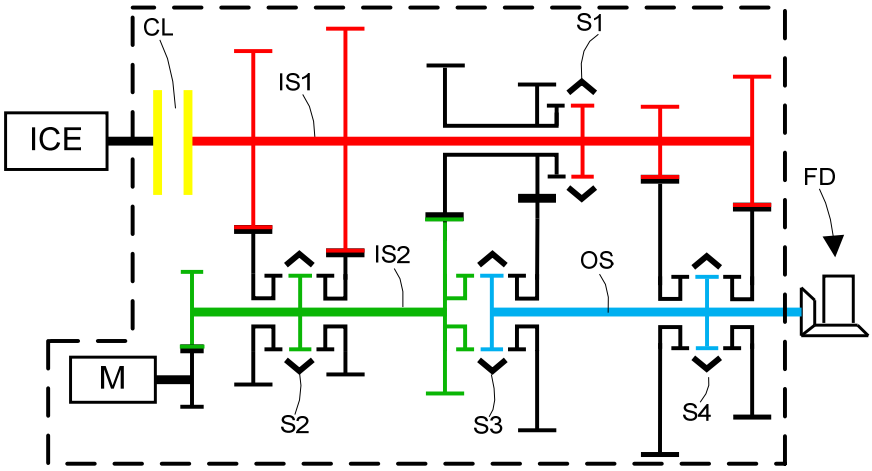

Figure 2-3 Gearbox layout for HAMT and its 8 speeds

This HAMT enables hybrid vehicle to operate in two modes: HEV mode and EV mode. As HEV mode is active, this HAMT-based design, unlike regular parallel hybrid powertrain, allows flexible switch between post-transmission and pre-transmission hybrid architecture to take advantage of two architectures; in EV mode, this design also supports variable gear ratios for motor in EV mode. From driven side of main clutch to output shaft, there are only six pairs of gears. This amount of gears in one vehicle equipped with regular AMT or DCT, can only support five speeds (one reserved for reversing vehicle). However, specially designed HAMT architecture can support not only eight gear ratios for engine but also up to eight gear ratios for

motor, with capacity to implement TGF function. Details about torque paths in each operation mode will be discussed later.

When electric system can meet energy, power or torque demand, engine is off and main clutch disconnected; as electric system is no longer able to propel vehicle individually, engine will be started and torque will be shifted from motor to engine via coordinated powertrain control; during gearshift for hybrid vehicle mode, engine, motor, main clutch and gearbox are controlled to achieve smooth gearshift. No matter which mode is active, its unique mechanism supports 8 gear ratios for hybrid mode and even up to 8 gear ratios (not all used) for electric motor.

2.3 Power Flow of Hybrid Mode

2.3.1 Gearshift Arrangement-HEV Mode

In mechanical engineering, gear generally means wheel with multiple teeth to convey power flow. However, in automotive industry, gear generally means finite power flow paths inside gearbox. Gear 1 is the gear path with highest gear ratio between input shaft and output shaft; top gear is the path with lowest gear ratio [63]. Gear selector serves as mechanical switch to control power flow inside transmission [64]. In Table 2-1, arrangement of gear selectors for the 8 gears in hybrid mode is illustrated. L and R represent locations of gear selector. Each gear has two engaged gear selectors simultaneously and that two neighbour gears share one common engaged gear selector.

Table 2-1 Selector arrangement for hybrid mode

Gear	S1	S2		S3		S4		i_{1o}
		L	R	L	R	L	R	
1					●	●		GR_1
2	●				●			GR_2
3		●			●			$GR_7 \times GR_2/GR_6$
4			●		●			$GR_8 \times GR_2/GR_6$
5				●↔●			●	GR_5
6	●			●				GR_6
7		●		●				GR_7
8			●	●				GR_8

Take 1-2 upshift (gear 1 to gear 2) as example, S4 is moved from left position to neutral position first to release gear 1; S1 will lock corresponding gear and shaft after S1 helps to eliminate slip speed between gear and shaft. Gear selector 3 is the critical one that keeps engaged in all gears. S3 is locked to right side when gear lower than 5th gear is engaged; S3 is locked to left side when

gear above 5th gear is engaged. During 1-2 gearshift process, S3 maintains engaged. At 5th gear, S3 can be shifted to either left or right. The eight available gear ratios between input shaft 1 and output shaft, i_{1o}, contains six independent gear ratios and two generated ratios.

When the dog clutch S3 is shifted to right side, a reduction gear is formed between IS2 and OS via the compound gear on IS1. This position of S3 is used for first four low gears. As dog clutch S3 is engaged with gear on left, IS2 and OS rotate like a rigid shaft. This engagement will render gearbox like a regular two-shaft gearbox with motor linked to output shaft. This direct connection between IS1 and OS is used for three high gears. The fifth gear serves as bridge between high gears and low gears. The eight gears for hybrid mode, indicated in circled numbers in Figure 2-4. This HAMT and the gear selector schedule are designed to achieve eight gears using only six pairs of gears, which include two direct gears from IS1 to OS via S4, three gear pairs via S1 and S2, and two gears between IS2 and OS via S3. More straitforward expression of this layout is shown in Figure 2-2. No separate reverse gear is set in this proposed gearshift arrangement. Vehicle backs as motor drives vehicle in opposite direction via one of forward gears.

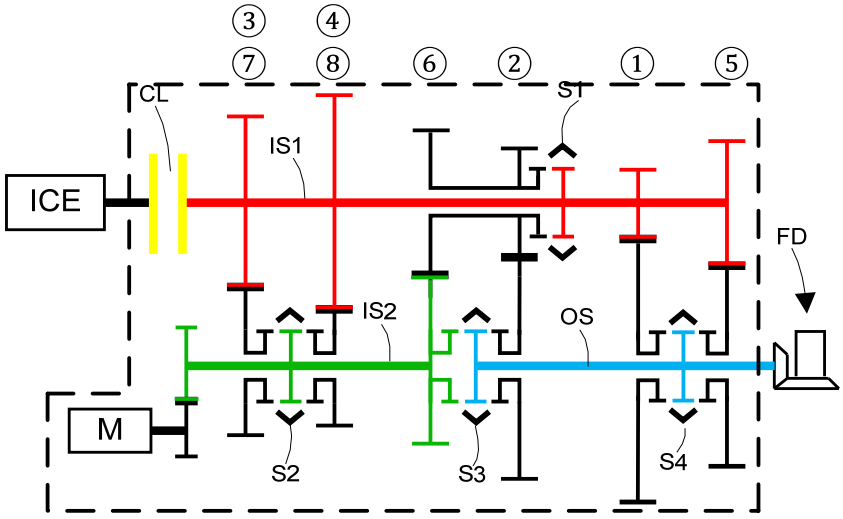

Figure 2-4 Eight speeds of HAMT

2.3.2 Power Flow of 1st and 2nd Gear

Power flow at first gear is shown in Figure 2-5. S4 is engaged with left side to link engine and OS. Engine torque is sent to final drive via main clutch, IS1, gear pair for gear 1, S4 and OS. gearshift sleeve S3 is moved to right side to transmit motor torque to output shaft OS; so, motor can also output torque through IS2, compound gearwheel on IS1, S3 and OS. It can be seen that torque-combining point is the gearshift sleeve S4. Two power sources provide propulsion force in parallel. The power flow paths reveal that HAMT works like a post-transmission gearshift because merging point of two torque paths is on output shaft, although it is not out of gearbox. Depending on power demand, motor can serve as torque balancer by providing positive (motor) torque or negative (generator) torque.

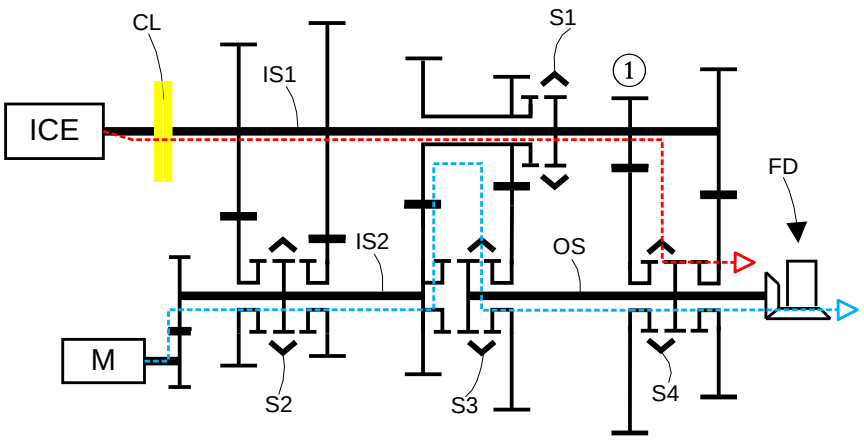

Figure 2-5 Power flow of the 1st gear in hybrid mode

As 1-2 upshift is commanded, TGF feature of HAMT-based hybrid powertrain will be triggered. Engine torque will become smaller gradually, and motor torque increases to compensate torque reduction from engine. Eventually, engine torque will drop to zero and main clutch becomes open, transmitting no torque to output shaft, as shown in Figure 2-6. As 2nd gear for engine is ready, engine torque is increased and motor torque is controlled to exit TGF mode. Since one gearshift lasts only 2-3 seconds, thermal protection for motor and power electronics could be suspended to meet torque demand of motor, aiming to minimize torque gap. At the end, main clutch is reengaged and engine becomes primary torque source.

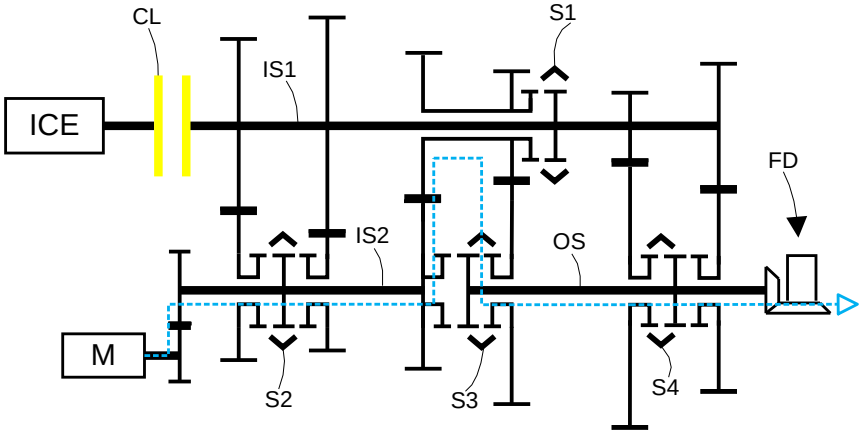

Figure 2-6 TGP of 1-2 upshift

At the 2nd gear, power flow is similar to that in Figure 2-7. At 2nd gear, torque path for motor is not changed, but the torque-merging point is shifted from S4 to S3 through disengaging S4 and engaging S1. At second gear, HAMT works like a merged pre-transmission and post-transmission parallel hybrid system. During this process, main clutch, together with motor, engine as well as selector actuators, should be coordinated well by control algorithm. More details about this TGF process and control algorithm will be discussed in Chapter 5&6.

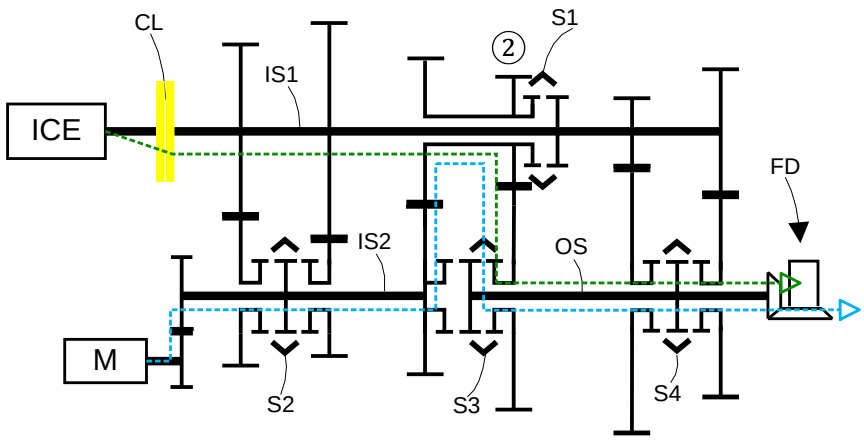

Figure 2-7 Power flow of 2nd gear

2.3.3 Power Flow of the 3rd and 4th Gear

Power flow paths at third and fourth gear are similar to the first and second gear, including the 2-3 and 3-4 upshift/downshift process. It is important that the first four gears are that motor can provides torque via identical path. After selector S3 is put at neutral position and S2 is moved to left position, main clutch is locked and 2-3 gearshift ends. Power flow paths at third gear are shown in Figure 2-8.

Unlike the 1st and 2nd gear, this hybrid system works like a pre-transmission parallel hybrid at third gear because merging point of two torque paths is at one of input port of gearbox. Main clutch links engine to input shaft IS1, which rotates with IS2 via locked selector S2. Engine torque motor torque are merged at S2 and propel vehicle via locked selector S3 and output shaft OS. Two power sources provide propulsion force in parallel. Depending on power demand, motor can serve as torque balancer by providing positive (motor) torque or negative (generator) torque.

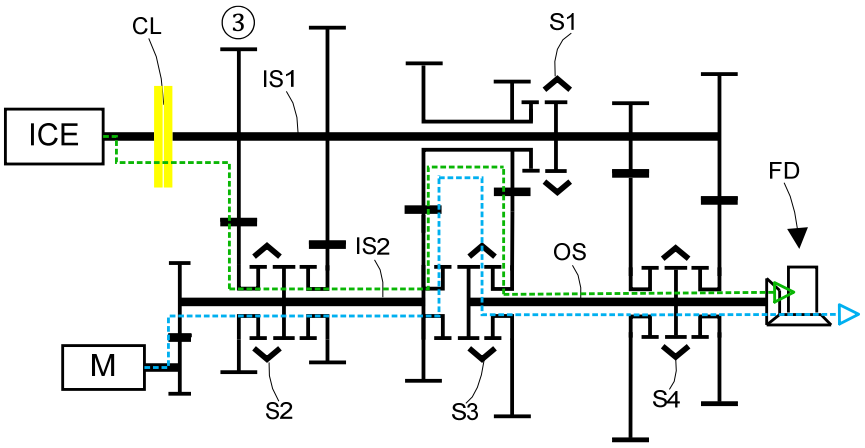

Figure 2-8 Power flow of 3rd gear in hybrid mode

Power path at fourth gear is illustrated in Figure 2-9. A 3-4 upshift changes position of S2 from left to right position. During gearshift, motor M compensates torque reduction from engine. In

comparison to 3rd gear, engine torque is transmitted to input shaft 2 via right side of selector S2, moving the merging point of torques toward inside of gearbox.

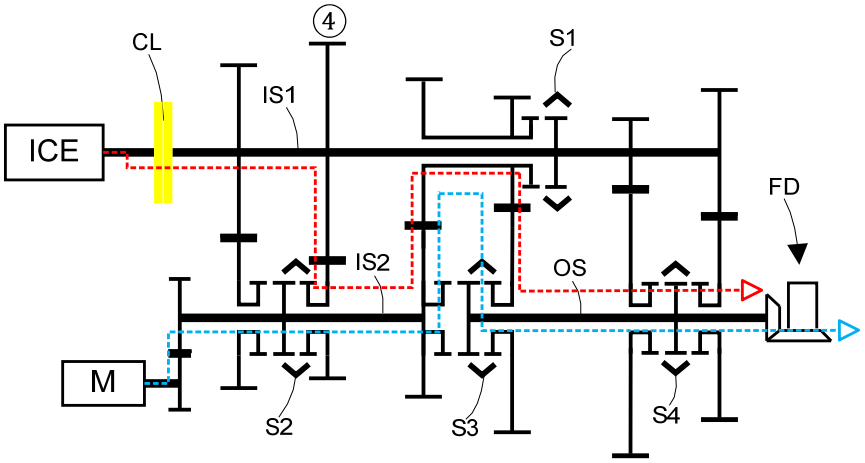

Figure 2-9 Power flow of 4th gear in hybrid mode

2.3.4 Power Flow of 5th Gear

The fifth gear is the connecting gear between low gears (1-4) and high gears (6-8). This gear uniquely has two types of power flow paths. Type 1 is for low gears and upshift from low gears and 5th gear; Type 2 for high gears and downshift from high gears to 5th gear. Type 1 and 2 differs each by power path from motor.

Type 1: After one upshift, e.g. 4-5 upshift, gear selector S2 is put at neutral position, and selector S4 locks OS and 5th gear. As low gears discussed above, motor is connected to output shaft via compound gear and right side of S3. This type of power flow is authentic post-transmission parallel hybrid, with two torque paths merged at the end of output shaft. As engine can provide enough propulsion torque to output shaft, whole system is ready for transition from type 1 and type 2.

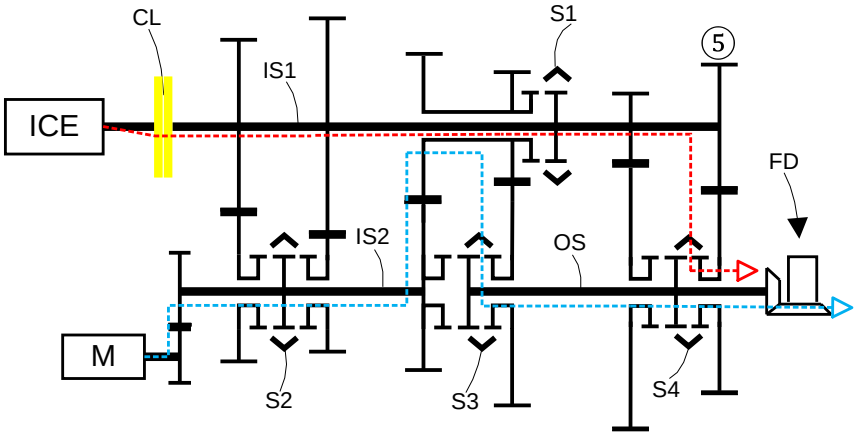

Figure 2-10 Power flow of 5th gear in hybrid mode – type 1

Type 2: Position of S3 is shifted to left side from right side, which combines IS2 and OS as a single shaft. This action makes two shafts rotate synchronously like just one rigid shaft. In addition, gear ratio for motor is also reduced. Actually, this layout is one of typical layouts of conventional manual gearbox. As result, the compound gear will not transit torque, although it rotates with IS2.

One important point is the process of gear ratio change for motor. After S3 is pushed to neutral position by actuator, motor speed is still too fast to be engaged in left dog clutch of S3. Since there is no separate clutch for motor, accurate motor speed control is the key for smooth and fast speed synchronization of IS2 and OS. Until speed gap between IS2 and OS is almost is reduced to zero, actuator for S3 can move it to left and lock the two shafts. During this process, engine serves as second torque source to finish TGF feature. Now, motor and its torque path are ready for upshift from 5th gear to high gears.

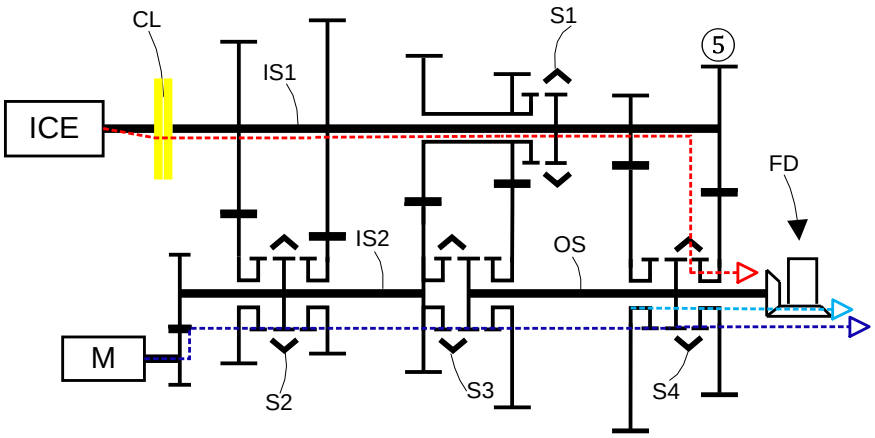

Figure 2-11 Power flow of 5th gear in hybrid mode – type 2

2.3.5 Power Flow of 6th, 7th and 8th Gear

These three high gears share the same torque path from motor, which contributes torque via the IS2-OS shaft. Power flow paths at sixth gear are shown in Figure 2-12.

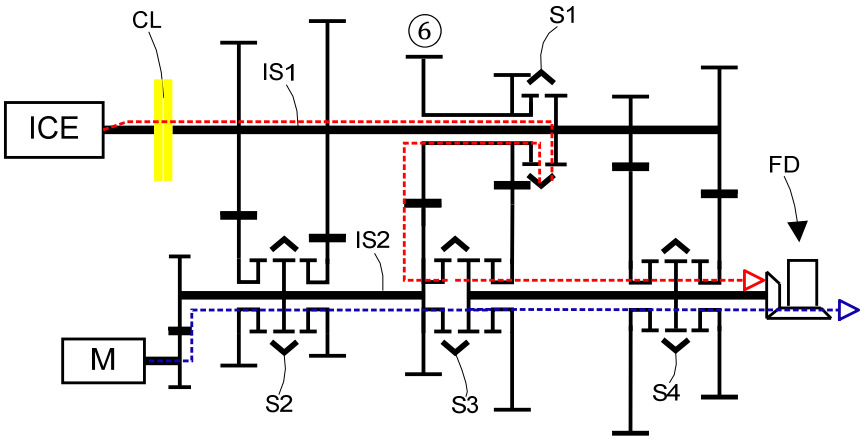

Figure 2-12 Power flow of 6th gear in hybrid mode

Input shaft IS1 is linked to compound gear via engaged selector S1. IS1 and IS2 rotate together via a gear pair on left of S3. Torques from motor and engine are combined at left dog clutch of selector S3. This combined torque is transmitted to OS via left dog clutch of S3. The second torque path for TGF is from motor to OS, shown in Figure 2-13. During all power-on gearshift, including upshift and downshift, among 5th gear and high gears, this identical power path takes effect.

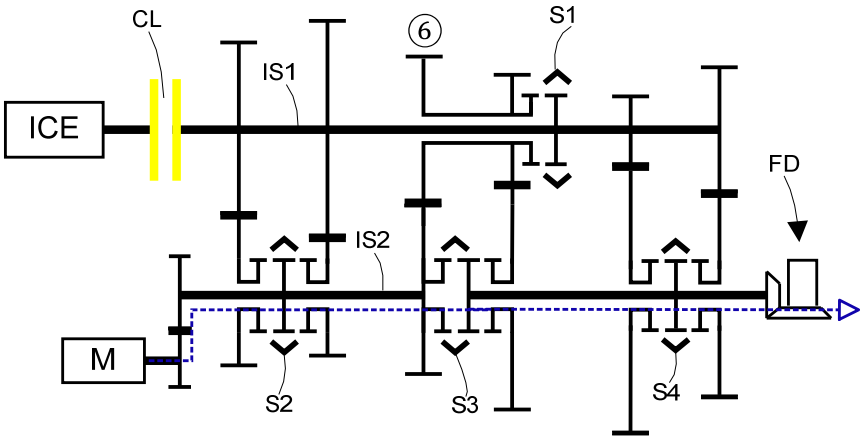

Figure 2-13 TGP of 5-6 upshift

Figure 2-14 shows power flow paths at 7th gear. S2 is reengaged on left side once again (like 3rd gear). Engine torque is combined with motor torque at the input port 2, typical pre-transmission parallel hybrid. Due to gear ratio between IS2 and OS is reduced to zero by shifting S3 from right to left, overall gear ratio for engine is smaller than 3rd gear. Figure 2-15 is for 8th gear. By shifting S3 from left to right, gear ratio between IS1 and IS2 is changed. During this gearshift, motor torque path in Figure 2-13, provides torque compensation to achieve smooth gearshift.

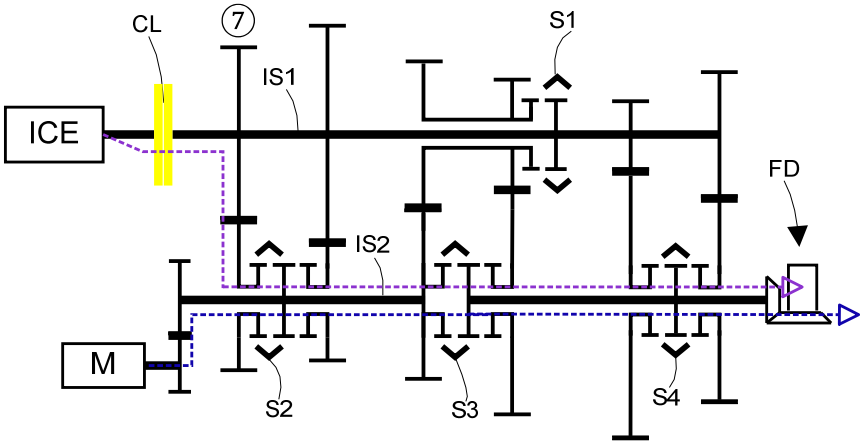

Figure 2-14 Power flow of 7th gear in hybrid mode

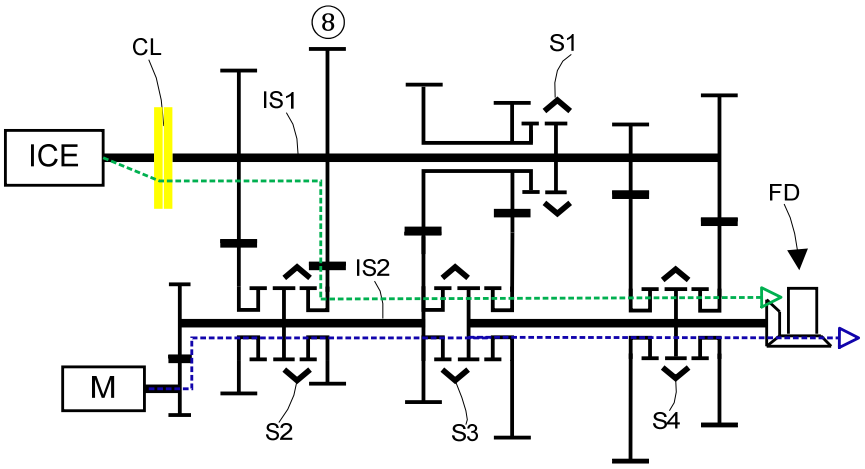

Figure 2-15 Power flow of 8th gear in hybrid mode

2.3.6 Direct Gearshift

The analysis above shows gearshift process of simple gearshift between two neighbouring gears. Actually, this HAMT supports very flexible gearshift in hybrid mode. For example, 2nd gear supports not only simple 2-1 downshift and 2-3 upshift but also two direct upshifts (2-4 and 2-5 upshift). Power flow paths during 2-4 direct upshift is shown in Figure 2-16. As such direct upshift happens, selector S1 for off going and S2 for oncoming gear are disengaged and engaged, separately.

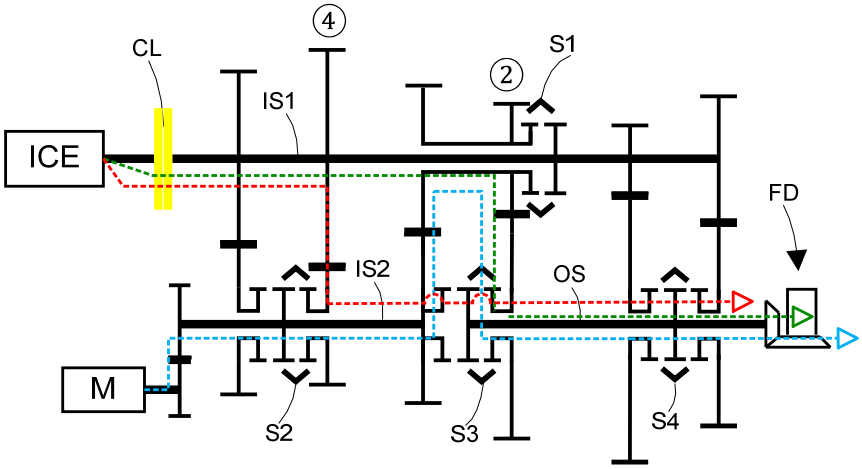

Figure 2-16 Power flow of 2-4 direct upshift in hybrid mode

Table 2-2 includes all possible gearshifts of this HAMT that are compatible with TGF feature. First column and first row are old gears and new (target) gears. Green cells represent current gears, and blue cells are neighbouring gears, whose torque paths are illustrated individually. Direct gearshifts – shift to non-neighbouring gear, are represented in brown. The 5th gear as connecting gear between low gears and high gears is also represented by the narrow channel between upper-left rectangle and bottom-right rectangle. It is not allowed to shift gear from low

gear to high gear without using 5th gear. The 2 big blank cells in the Table 2-2 means gearshifts between any two gears are not allowed.

Table 2-2 Possible gearshifts of HAMT

Old \ New	1	2	3	4	5	6	7	8
1								
2								
3								
4								
5								
6								
7								
8								

2.4 EV Mode Operation

In EV mode, this powertrain will operate like an EV, with engine off and main clutch open. There are different configurations of EV powertrain. For example, electric motor can be mounted inside wheels [65]; electric motor can propel vehicle directly without transmission [66]; a transmission with variable gear ratios can also be added between motor and wheels [67]; As early as 1975, a patent was granted for EV configuration with two electric motors [68]. This proposed powertrain system can work in EV mode as well, but its operation does not like any of those EV configurations. As shown in Figure 2-2, motor torque received at port 2 is sent to port 3 (output shaft) via either 2 direct gears or the 6 indirect gears between the port 2 and 3. Table 2-3 lists 8 potential gear ratios in EV mode and required selector combinations to achieve the gear ratio.

At present, almost all PEVs on the market (passenger car and minivan) adopt a configuration in which electric motor and final drive are connected via a fixed, single-speed gearbox rather than a multi-speed transmission. The configuration is largely due to three major reasons: a) electric motors have much higher efficiency than the ICEs across the board; b) fuel efficiency map of electric motor is flatter and less sensitive to the variation of vehicle speed and needed torque; c) the electric machines can produce much higher torque at low speed than the ICEs to meet the torque requirement for vehicle start up acceleration; d) motor, unlike engine, can deliver torque from zero speed, so no need for clutch.

However, two-speed and multi-speed transmission can still improve the efficiency and performance of PEVs by allowing the electric machine to operate in the high-efficiency zone.

Many researchers have made some attempts based on certain assumptions [69] [70]. Standard driving cycles are generally used in the past research of EVs (HEV, PHEV and PEV) to considerate various driving conditions. Thus, wheel speed and torque demand along with power demand at every moment can be pre-calculated. A less well-studied area is the combination of a low-cost electric machine with smaller peak efficiency zone and the two-speed or multi-speed transmission to assist the operation of the electric machine at its peak efficiency. Operating points of electric machine and/or engine are primarily controlled by two major elements: gear ratios and gearshift map. Considerable research efforts have been devoted to optimize the control of various transmissions [71] [72] [73] [74] [75](update). Figure 2-17 illustrates that two gear ratios for motor not only improve performance at low vehicle speed, but also expand vehicle speed range in EV mode. Two to three gears are believed to be beneficial to achieve advantageous performance and fuel efficiency [76] [31](update). Due to advantage of motor over engine in absence of idle speed and huge torque capacity of motor at low speed, vehicle can be launched at any selected gears, providing extra flexibility of gearshift.

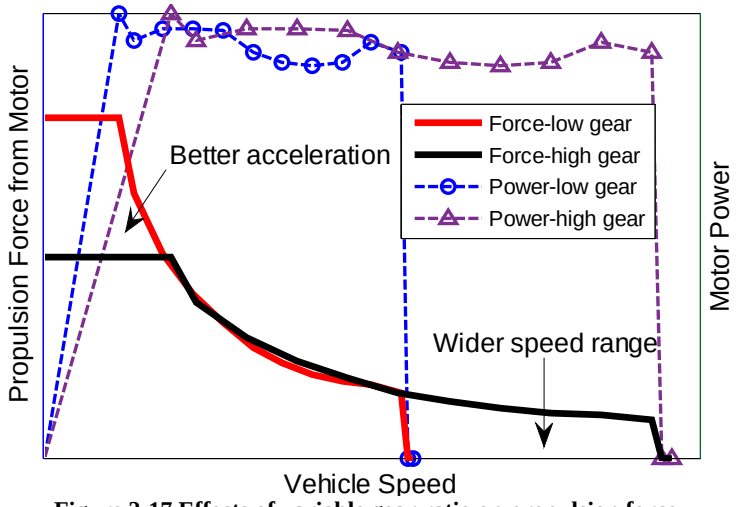

Figure 2-17 Effects of variable gear ratio on propulsion force

For this HAMT-based hybrid system, the same gearbox is used in two operation modes. Gear ratios in EV mode are i_{2o} - gear ratios between input shaft 2 and output shaft. Since i_{2o} is totally pre-determined by gear ratios in hybrid mode, as shown in Table 2-3, gear ratio design discussed in next chapter should take two modes in consideration, although hybrid mode is more important factor because electric motor features flatter efficiency map than engine BSFC map. It is note-worthy that more gear ratios are also possible by engaging S1, S2 and S3. Considering other combinations only requires two engaged dog clutches, these gears are dropped to avoid complicated gearshifts.

Power flow paths for 1st, 2nd and 3rd gear in EV mode are shown in Figure 2-18. The 3 paths transmit torques from motor to output shaft via IS1, which connects to OS via left dog clutch of S4. The 3 paths between IS2 and IS1 are also represented by the 3 gear ratios between port 1 and port 2 in Figure 2-2. The gear pair between IS1 and OS is also one of two gears between port 1 and 3 shown in Figure 2-2.

Table 2-3 Gear ratios and selector combinations for HAMT in EV mode

Gear	S1	S2		S3		S4		i_{2o}
		L	R	L	R	L	R	
1			●			●		GR_1/GR_8
2		●				●		GR_1/GR_7
3	●					●		GR_1/GR_6
❹					●			GR_2/GR_6
5			●				●	GR_5/GR_8
❻		●					●	GR_5/GR_7
7	●						●	GR_5/GR_6
❽				●				1

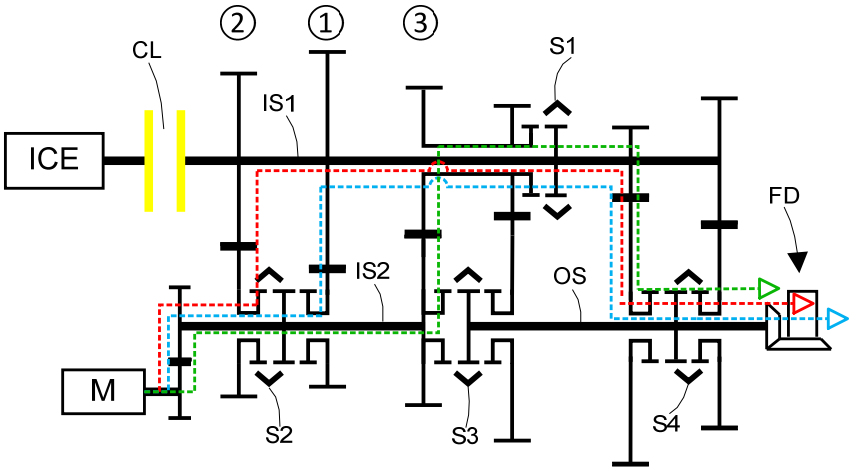

Figure 2-18 Power flow at 1st, 2nd and 3rd gear in EV mode

Power flow paths for 5th, 6th and 7th gear in EV mode are shown in Figure 2-19. The 3 paths are similar to those in 1st, 2nd and 3rd gear. Primary difference is that gear ratio from IS1 to OS is reduced by shifting S4 from left to right side. The gear pair between IS1 and OS is another gear between port 1 and 3 shown in Figure 2-2.

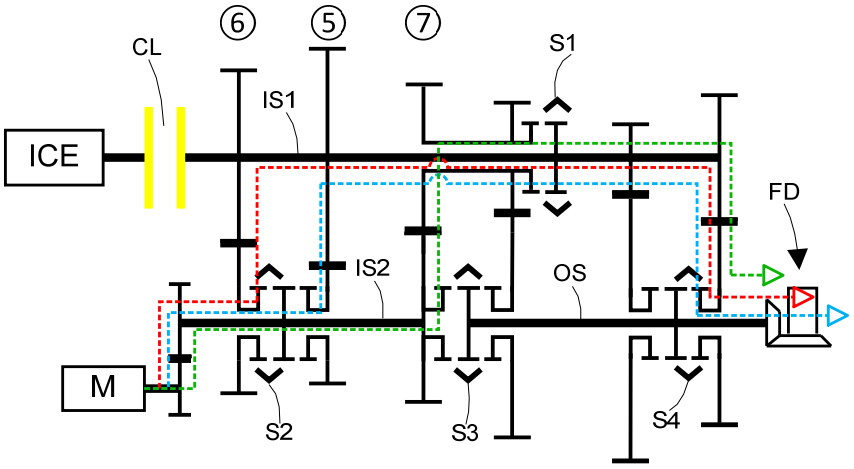

Figure 2-19 Power flow at 5th, 6th and 7th gear in EV mode

Other two gears, 4th gear and 8th gear, are shown in Figure 2-20. These two gears are two direct connections between IS2 and OS, just indicated by the two gears between port 2 and port 3 in Figure 2-20. Like discussed above, 4th gear in EV mode is critical for TGF feature at low gears of hybrid mode; 8th gear in EV mode is key to TGF feature at high gears of hybrid mode.

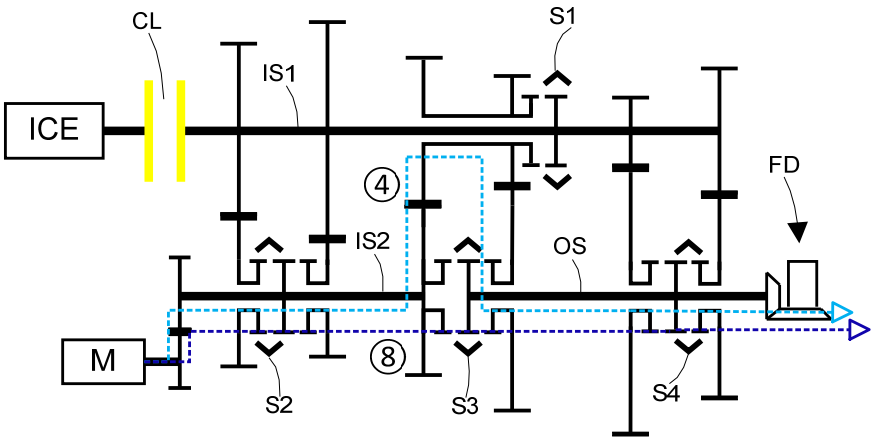

Figure 2-20 Power flow paths of 4th and 8th gear in EV Mode

This HAMT allows so many torque flow paths (primarily for hybrid mode), but there is no need to use all of them in EV mode. Here, the 4th, 6th and 8th gears, marked by black circle in Table 2-3, are selected preliminarily as the potential gears for EV mode. When gearshift in EV mode occurs, there is no secondary torque path to fill torque gap during gearshift in EV mode, control strategy can be set to support one torque path driveability or allow gearshift with torque gap. A no-torque-hole invention for EV is patent-pending [67].

2.5 EV-HEV Mode Transition

EV-HEV mode transition happens as driver input triggers performance mode or electric system cannot meet demand of torque or power or battery SOC is too low. Engine should be ignited and

accelerated to a speed over idle speed. This HAMT supports two ways to start engine. The first way is to use conventional starter to spin up engine to about 200RPM and let engine drives itself to target speed; the second way is to rely on motor that splits some torque to start engine via control of motor and main clutch. Torque control for motor and main clutch is critical to avoid deterioration of driveability. In EV mode, engine speed is zero, while speed of IS1 is determined by vehicle speed (with required selector engaged). Main clutch is controlled to increase torque capacity carefully to start up engine. Motor torque is controlled to increase torque output and compensate torque loss for engine start-up, as shown in Figure 2-21. After engine is turned on, main clutch should be released temporarily to prevent vehicle jerk due to reverse direction of clutch torque near zero-slip moment. Later, torque from engine will be increased gradually, just like torque shift during gearshift in hybrid mode.

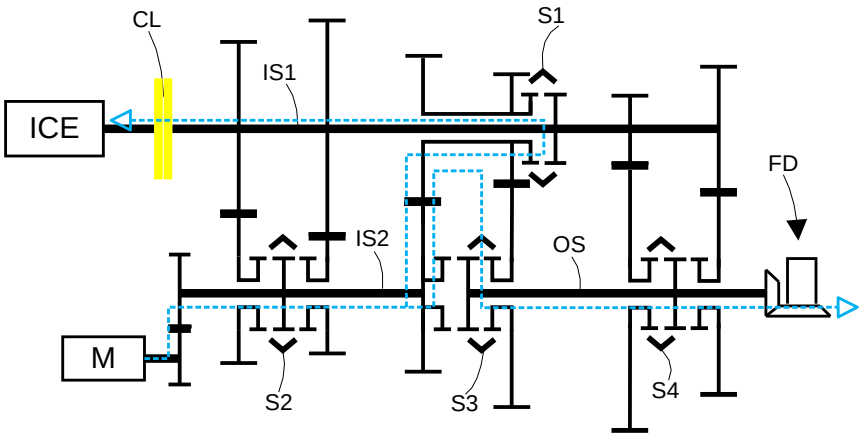

Figure 2-21 Engine start during EV mode

2.6 Summary

This chapter gives a fundamental introduction of one representative HAMT-based parallel hybrid powertrain system, disclosed in one patent application [61]. Firstly, abstract concept of various HAMT is introduced. Essential differences of those listed typical HAMT variations are explained using a special power-flow triangle with 3 ports. Then, operating principle of a novel HAMT is described. Detailed power flow paths in hybrid mode and EV mode are covered, including status of clutch, engaged and disengaged gear selectors. Gear ratios in each mode as well as relationship of gear ratios of two modes are also defined. Mode-transition process between hybrid mode and EV mode is also covered. In this chapter, the first challenge described in 1.4.1 is solved and first objective in 1.5 is achieved. This chapter provides key research subject in following chapters to overcome other 2 challenges and achieve remaining objectives.

3 Optimization of Gear Ratios

Gear ratio design for this 8-speed HAMT is another important task. There are total 8 gear ratios for engine, but those gear ratios are not totally independent. In addition, these gear ratios are shared by two operating modes. Vehicle operation in hybrid mode is the major consideration for gear ratio design because motor has much higher and more consistent efficiency within a wide range of speed and torque.

3.1 Key Problems Related to Gear Ratios

This HAMT features two modes, each of which has eight possible gear ratios. Detailed gear ratios in two modes are listed in Table 3-1. For engine, gear ratio at each gear is equal to i_{1o}, the speed ratio from IS1 to OS. Among the eight gear ratios in hybrid mode, six gear ratios are independent of each other, while the ratios of 3rd and 4th gear are generated gear ratios. As shown in Table 3-1, the 3rd gear is determined by 2nd, 6th and 7th gear; the 4th gear is the result of 2nd, 6th and 8th gear. In this work, gear means power flow path inside gearbox, rather than individual gearwheel. In addition, the gear ratios for EV mode are also determined by the six independent gear ratios. As the six independent gear ratios are finalized, gear ratios for 3rd and 4th gear in hybrid mode and all gear ratios in EV will be determined automatically.

Table 3-1 Summary of all gear ratios in hybrid mode and EV mode

Hybrid Mode	i_{1o}	EV Mode	i_{2o}
1	GR_1	1	GR_1/GR_8
2	GR_2	2	GR_1/GR_7
3	$GR_7 \times GR_2/GR_6$	3	GR_1/GR_6
4	$GR_8 \times GR_2/GR_6$	4	$\boxed{GR_2/GR_6}$
5	GR_5	5	GR_5/GR_8
6	GR_6	6	$\boxed{GR_5/GR_7}$
7	GR_7	7	GR_5/GR_6
8	GR_8	8	1

Hybrid mode should be primary consideration for gear ratio design because of differences between engine and motor, summarized in Table 3-2. Engine efficiency is more sensitive to engine torque and speed, which is controlled by vehicle speed and gear ratio. Wide speed range of motor lowers requirement for count of gears. Another important topic is to select correct gears for EV mode. It is unnecessary to apply all the 8 gear ratios (i_{2o}) in EV mode. Or else, redundant gearshifts will deteriorate driveability.

Table 3-2 Comparison of engine and motor

	Engine	Motor
Idle speed	600~800 RPM	No idle speed
Low-speed torque	Small	Big
Top speed	≈ 6000 RPM	≈ 10000 RPM
Efficiency map	Convex	flat

Two critical questions for gear ratio are:

a) How to select 6 independent gear ratios?
b) Which gear(s) should be selected for EV mode?

3.2 Preliminary Design of Independent Gear Ratios

Gear ratio design is a very complicated analysis work and requires extensive knowledge and experiment/simulation data to finalize gear ratio. Additionally, gear ratios are also adjusted for different powertrain platforms to maximize powertrain system potential. Since focus of this research work is not to invent new methods for gear ratio design, which is one important topic for systematic optimization of HAMT, some design methods used in industry are applied here. The finalized gear ratios are pre-requisites for following powertrain modeling, control and verification of whole HAMT invention.

Gear ratio steps are very important for powertrain performance and fuel economy. One set of baseline gear ratios for HEV mode, shown in Table 3-3, are from gear ZF 8-speed transmission 8HP70. Gear ratio step, which indicates rate of gear ratio change from low gear to high gear, is shown in equation (3.1). By feeding all baseline gear ratios into the equation (3.1), all step ratios are shown in Figure 3-1.

Table 3-3 Baseline gear ratios from ZF 8HP70 transmission [77]

Gear	1	2	3	4	5	6	7	8
Ratio	4.71	3.14	2.10	1.67	1.29	1.00	0.84	0.67

$$\varphi = \frac{i_{1o}(n-1)}{i_{1o}(n)} \tag{3.1}$$

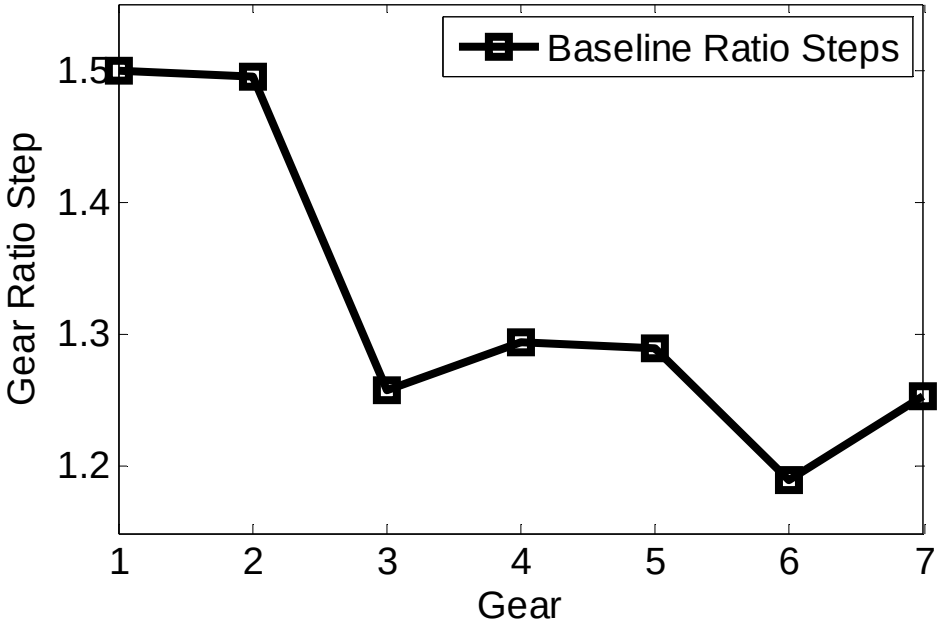

Figure 3-1 Steps of baseline gear ratio

In light of formula of gear ratios for 3rd and 4th gear, the gear ratios should be changed to meet formulas of i_{1o} in Table 3-1. The calculated gear ratios for 3rd and 4th gear in hybrid mode are from equation (3.2) and (3.3).

$$i_{1o\_3} = GR_7 \times GR_2/GR_6 = 2.6376 \approx 2.64 \tag{3.2}$$

$$i_{1o\_4} = GR_8 \times GR_2/GR_6 = 2.1038 \approx 2.1 \tag{3.3}$$

Formulas to calculate ratio steps of HAMT are summarized in Table 3-4, which is converted from gear ratios in Table 3-1 and equation (3.1). With change to the baseline gear ratios, ratio step trajectory along 1st to 7th gear differs from baseline trajectory apparently. Although each data point is above 1.0, which means gear ratio decreases monotonically from low gear to high gear, but the trajectory of generated ratio steps in Figure 3-2 indicates that this version of ratio step fluctuates dramatically. According to theory for gear ratio design, the ratio step for high gear is lower than low gear for transmission of passenger cars [78]. Therefore, the gear ratios should be modified based on baseline gear ratios. One important constrain to gear ratio steps is that $\varphi_{2/3}$ and $\varphi_{3/4}$ are equal to $\varphi_{6/7}$ and $\varphi_{7/8}$, respectively.

Table 3-4 Ratio step formulas of HAMT

Ratio	$\varphi_{1/2}$	$\varphi_{2/3}$	$\varphi_{3/4}$	$\varphi_{4/5}$	$\varphi_{5/6}$	$\varphi_{6/7}$	$\varphi_{7/8}$
Ratio Step	$\frac{GR_1}{GR_2}$	$\frac{GR_6}{GR_7}$	$\frac{GR_7}{GR_8}$	$\frac{GR_8GR_2}{GR_6GR_5}$	$\frac{GR_5}{GR_6}$	$\frac{GR_6}{GR_7}$	$\frac{GR_7}{GR_8}$

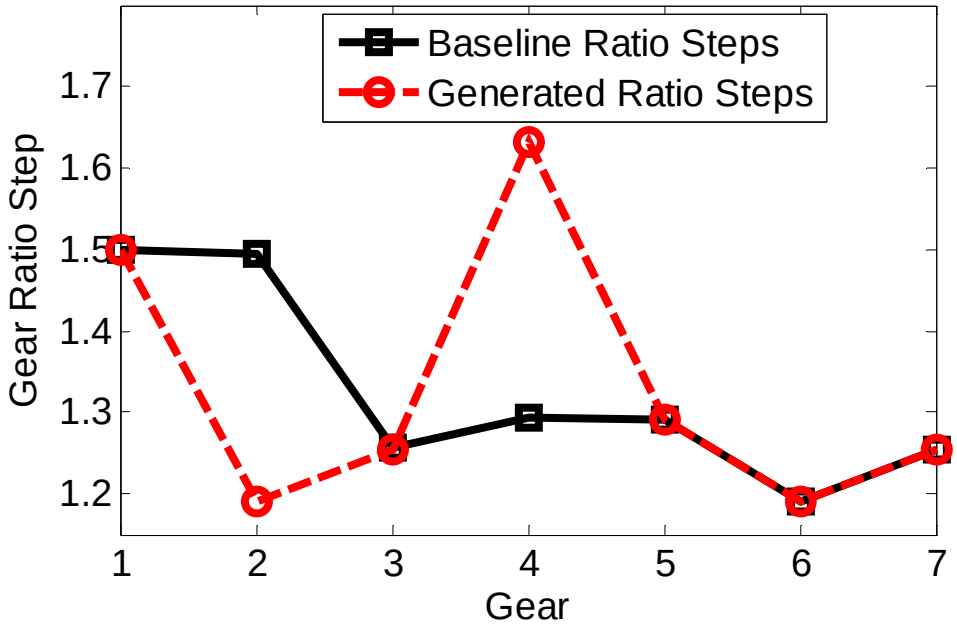

Figure 3-2 Generated ratio steps – 1st version

Two formal formulas for calculation of gear ratios are proved effective, which are geometrical gear steps and progressive gear steps [78]. The geometrical gear steps are used for commercial vehicles; the progressive gear steps are for transmissions of passenger vehicles. Figure 3-3 shows an example of effects of progressive ratio steps on vehicle traction and engine operation. One set of reasonable gear ratios should make traction curves at different gears close to hyperbolic curve enough, as shown in subfigure (a) of Figure 3-3, limiting engine speed change during gearshift. These progressive step ratios will be calculated and applied to this HAMT.

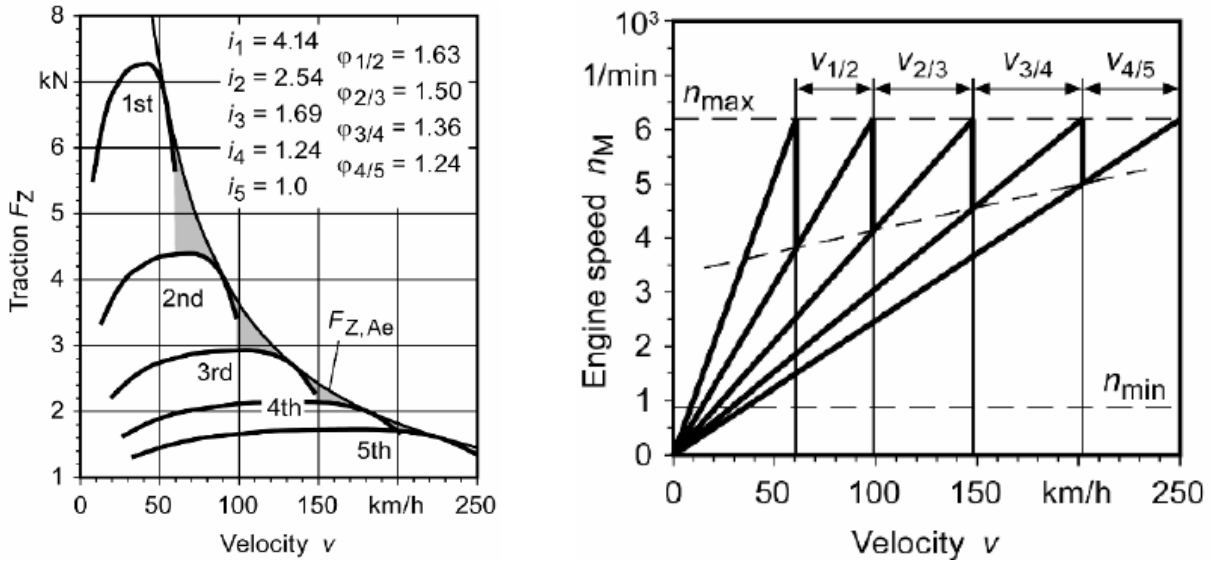

(a) Traction diagram (b) Velocity/ engine-speed diagram

Figure 3-3 Effects of ratio steps on traction diagram and velocity/engine-speed diagram [62]

3.3 Gear Ratio Design – Applying Progressive Ratio Steps

For this research work, whose focus is not to find optimal gear ratios but assign a reasonable gear ratios for each gear in hybrid mode and EV mode, step ratio from baseline gear ratio, is selected. Progressive ratio steps help to calculate ideal value of each gear ratio, as long as lowest gear and highest gear are assigned one value. The lowest gear ratio (1st gear ratio) is generally determined by gradeability; the highest gear (8th gear ratio) is determined by maximum vehicle speed. More details can be found in various books and research papers.

Formula of progressive step ratios is like equation (3.4), where φ_1 is basic step ratio and φ_2 is modification factor. Typically, φ_1 is between 1.1 and 1.7; φ_2 is between 1.0 and 1.2 [78]. Using equation (3.4), one set of progressive ratio steps (except $\varphi_{2/3}$, $\varphi_{3/4}$ and $\varphi_{4/5}$) are calculated, shown in Table 3-5. The $\varphi_{2/3}$, $\varphi_{3/4}$ and $\varphi_{4/5}$ are calculated using formulas in Table 3-4.

$$i_{1o}(n) = i_{1o}(8)\varphi_1^{(8-n)}\varphi_2^{[0.5(8-n)(7-n)]} \tag{3.4}$$

$$\varphi_1 = i_{1o}(7)/i_{1o}(8) \tag{3.5}$$

$$\varphi_2 = \sqrt[0.5(8-1)(7-1)]{\frac{1}{\varphi_1^{(8-1)}} \times \frac{i_{1o}(1)}{i_{1o}(8)}} \approx 1.0162 \tag{3.6}$$

Trajectory of progressive step ratios, together with other two trajectories, is included in Figure 3-4. Generated gear ratios are summarized in Table 3-5.Compared to generated step ratios, fluctuation of this new trajectory is less, but it is still apparently different from baseline trajectory. The essential reason for this fluctuation is two constraints of 3rd and 4th gear ratio, which are exactly reason why 8 gear ratios can be generated from only 6 gear pairs. In other words, that is cost of more gear ratios.

Table 3-5 Gear ratios from method of progressive ratio steps

Gear	1	2	3	4	5	6	7	8
Ratio	4.71	3.4	**2.49**	**1.86**	**1.41**	1.08	0.84	0.67

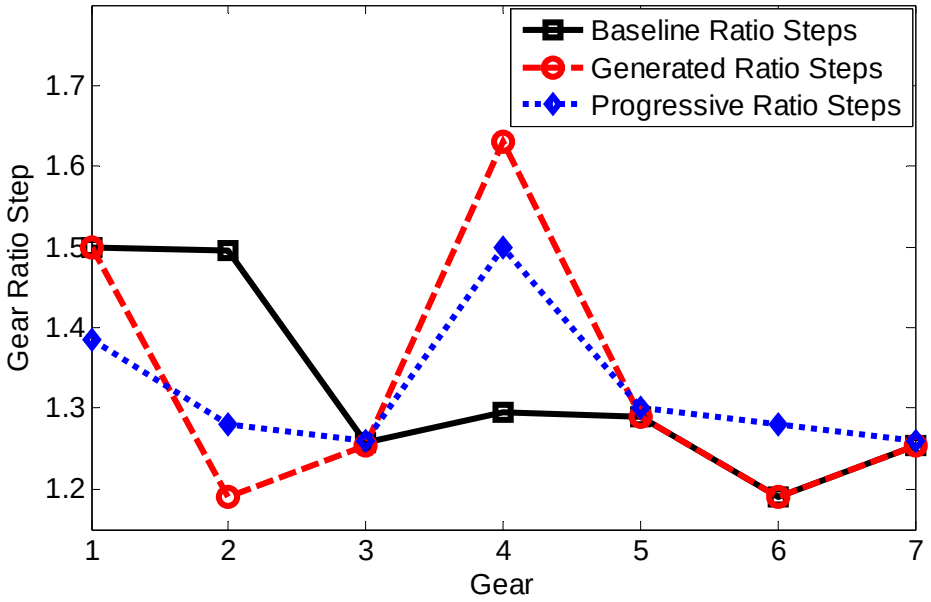

Figure 3-4 Progressive ratio steps

Through analyzing formulas of ratio steps in Table 3-4, it is found that decreasing 2nd gear ratio not only increases $\varphi_{1/2}$ but also lower $\varphi_{4/5}$. After several trials, the 2nd gear ratio is changed from 3.14 to 3, as shown in Table 3-6. Consequently, 3rd and 4th gear ratios are changed according to equations in Table 3-1.This final step ratios can are smoother apparently, with almost all ratio steps slightly vary around 1.3.

Table 3-6 Final step ratio

Gear	1	2	3	4	5	6	7	8
Ratio	4.71	**3.0**	2.34	1.86	1.41	1.08	0.84	0.67

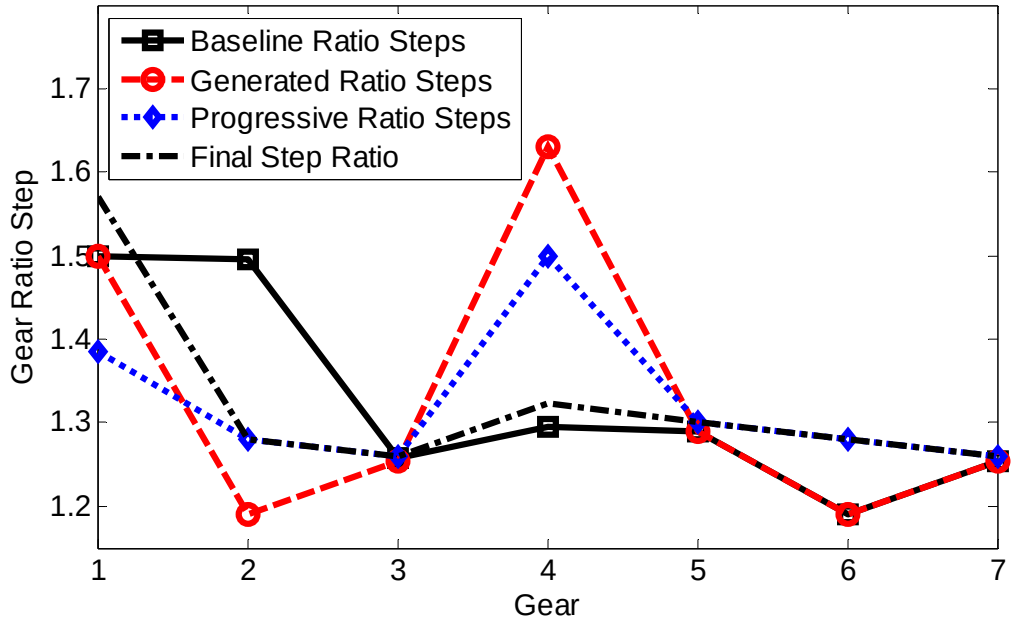

Figure 3-5 Final step ratio

All possible gear ratios between engine/motor and output shaft are listed in
Table 3-7. Since motor features flat efficiency map, big speed range and high torque at low speed. As EV mode does not need so many variable gear ratios to connect motor and transmission output shaft, the second part of this chapter is to select the 'optimal' gears needed for EV mode. The major objective is to maximize fuel economy, but frequent gearshifts should be avoided.

Table 3-7 Gear ratios for hybrid and EV mode

Hybrid Mode	i_{1o}	EV Mode	i_{2o}
1	4.71	1	$GR_1/GR_8 = 7.03$
2	3.0	2	$GR_1/GR_7 = 5.54$
3	2.34	3	$GR_1/GR_6 = 4.36$
4	1.86	4	$GR_2/GR_6 = 2.78$
5	1.41	5	$GR_5/GR_8 = 2.10$
6	1.08	6	$GR_5/GR_7 = 1.66$
7	0.85	7	$GR_5/GR_6 = 1.31$
8	0.67	8	1

3.4 Introduction of Variable Gear Ratio in EV Mode

Selection of gear ratios in EV mode from
Table 3-7 involves three related questions:

a) How many gears are needed for EV mode?
b) What are desirable gear ratios available?
c) How to determine gearshift?

These three questions are related to each other and can have unlimited possibilities. Here, the first question is answered first, and remaining two questions are answered using optimization method.

At present, almost all PEVs on the market (passenger car and minivan) adopt a configuration in which electric motor and final drive are connected via a fixed, single-speed gearbox rather than a multi-speed transmission. The configuration is largely due to three major reasons: a) electric motors generally have much higher efficiency than the ICEs across the board; b) fuel efficiency map of electric motor is flatter and less sensitive to the variation of vehicle speed and needed torque; c) the electric machines can produce much higher torque at low speed than the ICEs to meet the torque requirement for vehicle start up acceleration. However, two-speed and multi-speed transmission can still improve the efficiency and performance of PEVs by allowing the electric machine to operate in the high-efficiency zone. Many researchers have made some attempts based on certain assumptions [69] [70]. In 1993, one patent was issued for two-speed transmission used on EV, shown in subfigure (a) of Figure 3-6 [79]. One 2-speed transmission based on AT, described in plot (b) of Figure 3-6 was patented in 2003 [80]; another 2-speed AT-based transmission, whose basic stick diagram is like in plot(c) of Figure 3-6, are researched as one mode of GM's 4ET50 multi-mode electric transaxle [81]. One 4-speed clutchless transmission with two coupling motors were presented by Oerlikon Graziano [82].According to

previous research, the added gear ratio could increase FE by 2-5%, depending on driving cycles and vehicles [76] [81] [83]. In light of increased costs and driveability concern, number of this gearbox does not exceed four. Here, only two of multiple gear ratios in EV mode will be selected.

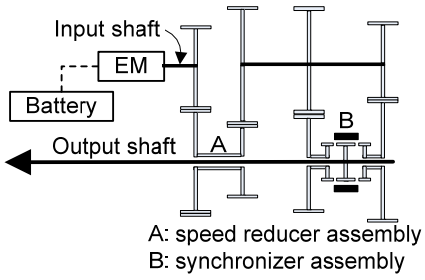

a) Parallel-shaft gearbox [79]

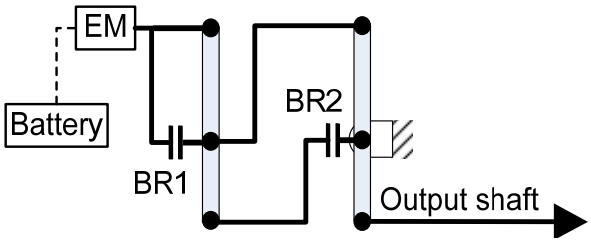

c) Planetary gearbox 2 [80]

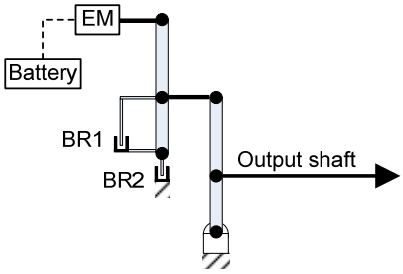

b) Planetary gearbox 1 [81]

Figure 3-6 Representative architectures PEV with two-speed gearbox

After question (a) is answered, gear ratios in EV mode should be selected from Table 3-7. To find the maximum potential of the addition of a transmission to a given EV, the two aspects need to be considered systematically due to their interdependence and interactions. How to effectively handle these two interdependent parts of the problem and find the optimal gear ratios and corresponding gearshift schedule is the focus of this chapter. In this work, gear ratio selection for EV mode emphasizes improvement of fuel economy, with performance as secondary objective. In this analysis, HAMT is simplified as a two-speed AMT before full powertrain model and control logic is ready. One EV model with a two-speed automated manual transmission is extracted from AUTOMONIE as baseline model and some changes are made to reach purpose of optimization using MATLAB and SIMULINK. In recent years, many researchers have integrated different optimization methods/tools into the model based design and control system development of HEVs and PEVs. Dynamic Programming (DP) has been widely used to find the optimal control strategy or the maximum fuel economy that the powertrain can achieve to serve as the benchmark of different control methods over the past 10 years [84] [85] [86] [87]. In this work, DP is used to find the optimal gear ratios and figure out optimal gear-shift schedule. The optimal gear ratios will be used as baseline to find the best gear combinations in 8 possible gears of EV mode.

3.5 Model Description for Gear Ratio Selection

AUTONOMIE is a MATLAB SIMULINK-based tool introduced by the US Argonne National Research Lab [88]. With a module-based structure, various HEV and PEV templates could be

used to form the performance model of mature hybrid powertrain architectures with additional adjustments of design parameters [89]. Since engine is totally off during this analysis, one simple EV model with two-speed transmission is first used, as shown in Figure 3-7. To obtain additional flexibility, the model from AUTONOMIE was modified to support the needed analyses and optimization in MATLAB SIMULINK environment after initial analysis was completed within AUTONOMIE.

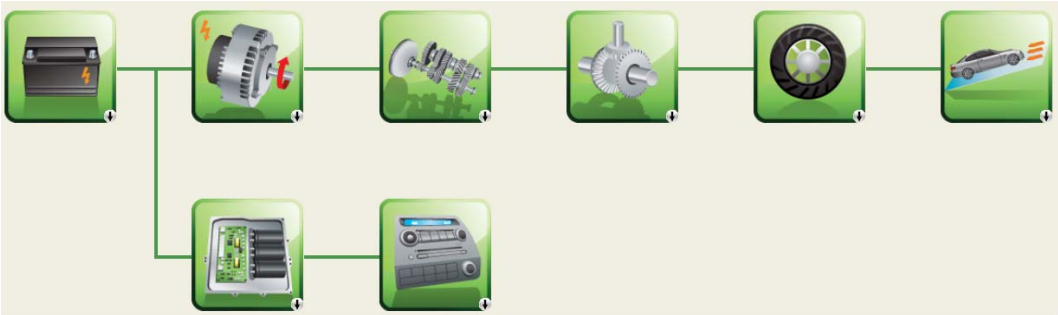

Figure 3-7 Powertrain configuration of Transit Connect Electric

The introduced forward PEV model consists of a driver model, a vehicle propulsion controller, and a powertrain primarily. The driver model is essentially a PID controller, regulating power input to meet driver's demand. The powertrain configuration of the PEV is shown in Figure 3-7 with a battery (ESS), a converter, an induction electric motor, a gearbox, a differential, wheels and chassis. Primary parameters are set according to the Ford Transit Connect made by AZURE DYNAMICS, as shown in Table 1.

Table 3-8 Vehicle model characters

Parameter	Value
Battery Energy	28kWh
Motor power	100Kw (Peak) ,65Kw(Const);
Motor torque	314Nm (Peak), 158Nm (Const)
Max Motor speed	10,000RPM
Overall gear ratio	8.28:1
Cd (air drag coefficient)	0.359
A (Frontal area)	3.12m^2
Curb Weight	1807Kg

In order to offer a fair comparison between the single-speed reduction gearbox and the two-speed transmission, the overall gear ratio needs to be optimized because the efficiency map used in this model is different from the one used originally in developing the Transit Connect Electric, so the original gear ratio is no longer optimal. Taking top speed, acceleration and energy consumption

in city and highway driving cycles, the overall gear ratio is selected to be 9.3 according to the efficiency map used in this work, rather than original gear ratio of 8.29.

3.5.1 Battery and Electric Motor

The Li-ion battery based onboard energy storage system (ESS), forms an extremely complex time-varying and nonlinear system. Several battery models are used to model its electrochemical behavior. Since battery behaviors and cycle life are not the focus of this work, thermal issues are ignored in this model and a static equivalent circuit is used, like equation (3.7).

$$V_{ter} = Voc - i(t) * R_{int} - i(t) * R_{pol} \tag{3.7}$$

where, V_{ter}, Voc, $i(t)$, R_{int} and R_{pol} are battery terminal voltage, open circuit voltage, instantaneous current, internal resistance and polarization resistance of battery. The internal and polarization resistances of battery, whose relationships with SOC are shown in Figure 3-8, have noticeable influence on battery efficiency.

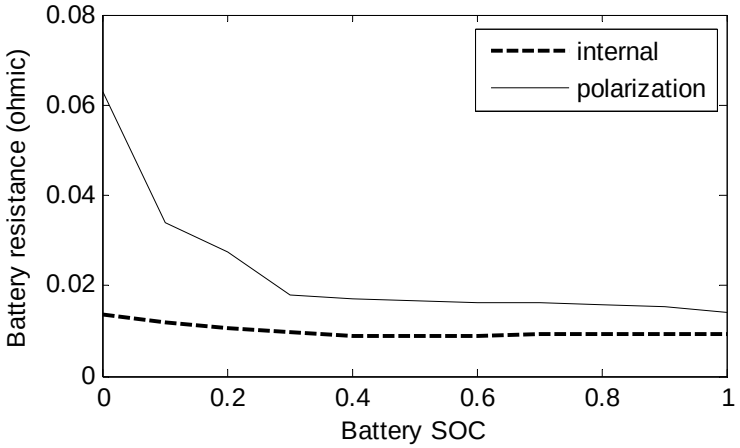

Figure 3-8 Battery characteristics

The power and maximum/continuous torque curves of the induction motor used in the vehicle were modified from the induction motor model in the AUTONOMIE powertrain component database. It is assumed that the motor operates at its static, post warm-up state under constant temperature. The efficiency map of this induction motor is from AUTONOMIE's default efficiency table under different motor speed and output torque.

3.5.2 Transmission

Electric motor has higher and flatter efficiency map, so it is reasonable to consider only two-speed transmission for lower cost in this work. The transmission in original model is a fixed-ratio gearbox with efficiency around 98%, which is substituted by an Automated Manual Transmission (AMT) with two fixed gear ratios. AMT has advantage of lower weight and higher efficiency than other types of automatic transmissions (AT). In addition, AMT can be transformed from MT by adding actuators and sensors so the cost is lower than other types of

automatic transmission [90]. Efficiency of an AMT is influenced by its input torque, input speed and selected gear. In this work, the efficiency of the 2-speed AMT is around 95% [91].

Operating points of electric machine and/or engine are primarily controlled by two major elements: gear ratios and gearshift map. Optimization of the gear ratios is the first goal in this work. The second goal is to find a desirable gearshift map. The required gear ratios and its gearshift map are interdependent, leading to a complex modeling and analysis problem. The traditional trial-and-error design method, drawing heavily upon engineers' experience and intuition, is time-consuming and unable to produce the optimal solution. A neutral gear ratio is set when the car is not moving. AUTONOMIE offers a two-speed transmission model, whose gear-shift schedule depends upon vehicle speed and percentage of accelerator pedal position, as shown in Figure 3-9. Direction of acceleration determines which criterion would be used. For example, when vehicle accelerates from 5 *m/s* to 15 *m/s*, the gearbox will be shifted to the second gear as the state point transgresses the right line; when it experiences one reverse process, the first gear will be used as state point crosses the left line. When vehicle speed is beyond 15 *m/s*, Gear ratio 2 will also be chosen. The zone between two lines can serve as a filter to prevent unnecessarily busy gearshifts. Optimization on the schedule lines is the second major focus of this work. The dynamics of the gearshift process and its influence on performance are ignored to simplify model.

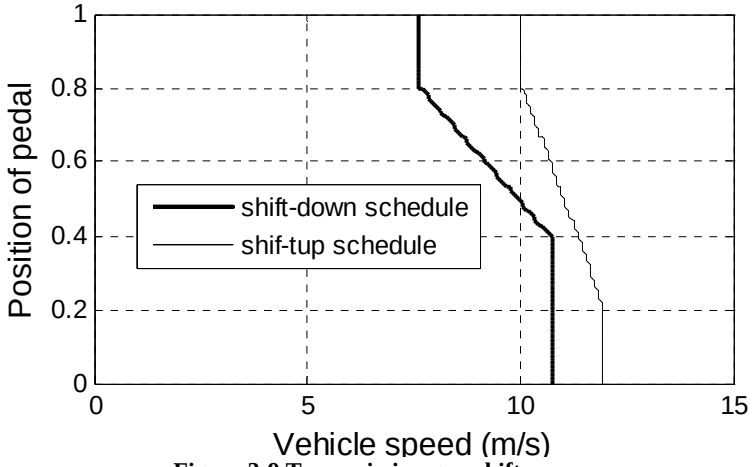

Figure 3-9 Transmission gearshift map

3.5.3 Chassis

The PEV is considered as moving mass only along its longitudinal direction. Thus, lateral and vertical as well as other dynamics elements whose frequencies are higher than 1Hz are ignored [86]; Wheel radius is assumed a constant; inertias of wheels and motor are transferred to mass and other rotational components are ignored. The elementary equation governing vehicle's movement is illustrated in equation (3.8) [92].

$$M_{eff}\frac{dV(t)}{dt} = F_v - \left(F_{air} + F_f + F_g\right) - F_d) \tag{3.8}$$

where M_{eff} is equivalent mass (sum of static mass and dynamic mass), V is vehicle velocity, F_v is the driving force, F_{air} aerodrag force, F_f is the rolling friction between wheels and ground surface, F_g the force caused by slope, and F_d the disturbance force like braking force and others. In this work, ground slope is set as 0, F_{air} and F_f are represented by a polynomial function, which are widely used in automotive industry. The formula is changed to an alternative form, shown in equation (3.9).

$$\frac{dV(t)}{dt} = \frac{[F_v - (F_0 + F_1 V + F_2 V^2) - F_d]}{M_v + (I_w + I_m g_i^2)/R_w^2} \tag{3.9}$$

where F_0, F_1 and F_2 are three dynamic parameters tested from dynamometer, M_v is vehicle testing weight (sum of curb weight and cargo of 136Kg), α is slope angel, I_w and I_m are inertias of 4 wheels and electric motor, g_i is overall gear ratio including the first/second gear ratio and final drive gear ratio, R_w is radius of wheels. Primary chassis parameters are listed in Table 3-9.

Table 3-9 Vehicle parameters

parameters	value
F_0	162.23 (N)
F_1	6.06 (N/(m/s))
F_2	0.49 (N/(m/s)^2)
I_w	1*4 (Kg.m^2)
I_m	0.4 (Kg.m^2)
R_w	0.316 (m)

In this work, we follow standard of automotive industry to use fuel economy as index that indicates miles per gallon (mpg) of fuel can propel. Simulation results from AUTONOMIE show that city/highway fuel economy is equivalent fuel economy around 107 *mpg* and 78 *mpg*. The discrepancy between this fuel economy and tested results of EPA (city/highway 60 *mile/L*) can be attributed several reasons. For example, EPA employs a five-cycle test using varying driving conditions and climate control, while in this work the city/highway fuel economies are tested only using city and highway driving cycles; accuracy of the model is limited by that of components, like battery and motor. In spite of the discrepancy, fuel economy and efficiencies of each component are generally acceptable to support the relative comparison of simulation results.

3.6 Dynamic Programming Problem

Dynamic programming can provide the optimal control input sequence that produces the least energy consumption a vehicle can possibility achieve for a given driving cycle. One important condition for the DP-based target search is the availability of a known driving cycle. Although real driving depart from the ideal driving cycle associated with the DP search, improvements of the rule-based controller following the target set by results of DP are still beneficial in most cases.

3.6.1 Problem Formulation

Representative city and highway driving cycles are assumed as driving conditions for the design optimization and optimal control target setting. The US federal test procedure (FTP-75, also called EPA75) and highway fuel economy driving schedule test (HWFET) are selected to compare various designs and controllers. The EPA75 driving cycle represents typical city driving pattern that features frequent start & stop and relative low average speed, and HWFET that is composed of cold start phase of the first 505 seconds, 864-second transient phase and the hot start phase of last 505 seconds, is characterized by higher vehicle speed, no intermediate stop and limited acceleration and deceleration [3]. In this work, the efficiency fluctuation caused by temperature variance of components and environment are ignored. In forward model, acceleration is not evaluated directly by differentiating two continuous speeds of driving cycles like in backward model, but by using one driver model that calculates acceleration demand using a PID controller according to difference between practical vehicle speed and desired speed. It is shown in Figure 3-10 to Figure 3-13 that actual acceleration and speed of the vehicle match the desired very well. Tier slide effect and deformation of tiers are ignored to relate vehicle speed V_v and driving force F_v with motor speed ω_m and motor torque output T_m approximately via Equations (3.10)-(3.11). T_{frc}, imposed friction torque by intermediate components between motor and wheel, is a function of V_v and F_v in the PEV model. The transmission's gearshift command, as the only control input, $u(k)$, directly determines the operating points of the motor with the given efficiency map.

$$\omega_m = \frac{V_v}{R_w} g_i \tag{3.10}$$

$$T_m = \frac{F_v}{g_i} R_w + T_{frc} \tag{3.11}$$

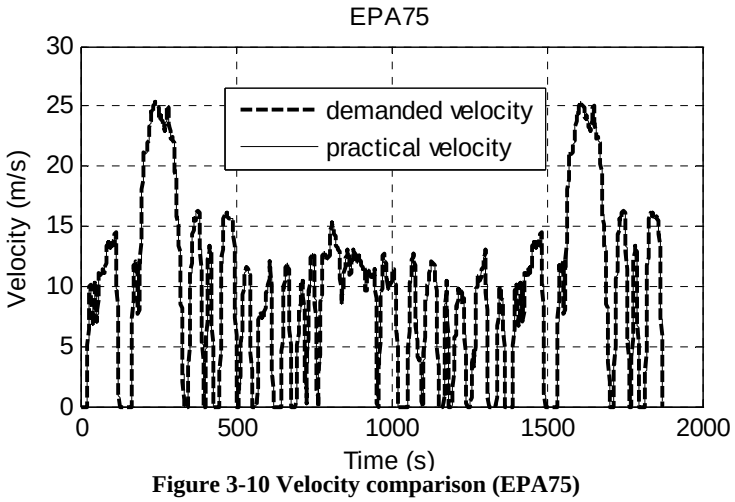

Figure 3-10 Velocity comparison (EPA75)

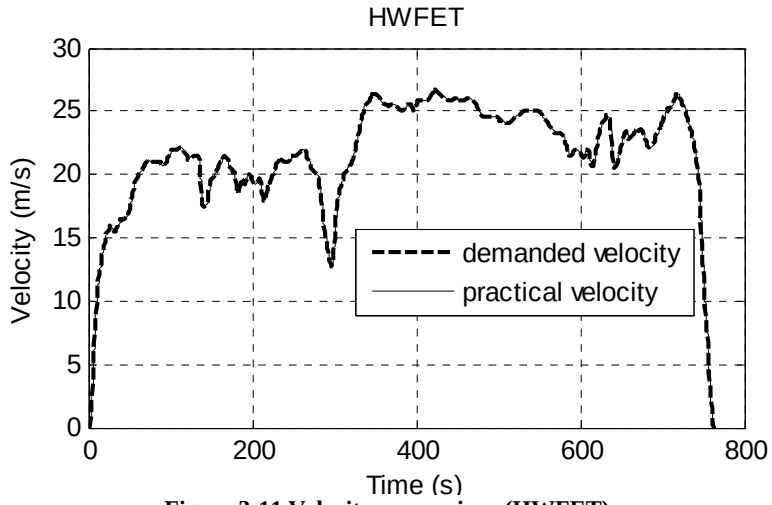

Figure 3-11 Velocity comparison (HWFET)

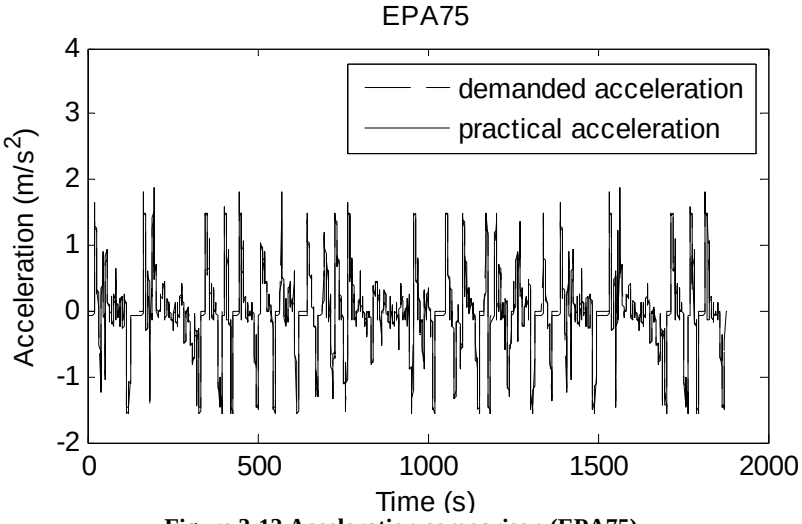

Figure 3-12 Acceleration comparison (EPA75)

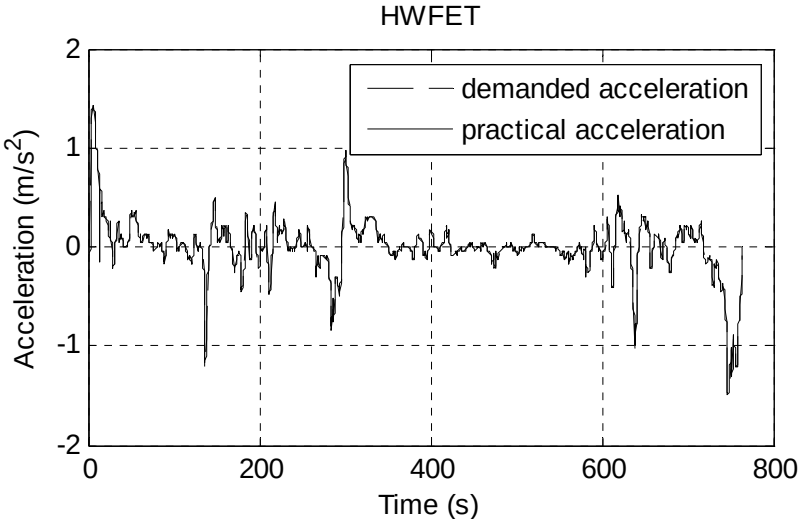

Figure 3-13 Acceleration comparison (HWFET)

This problem, essentially a shortest-path problem, is to find the optimal gearshift sequence that minimizes overall energy consumption defined by the objective function. Figure 3-14 provides a conceptual view of the problem. The horizontal axis is separated into N stages, and every stage has duration of one second. According to author's engineering experience, the duration of one second is believed to appropriate because minimum interval between two gearshifts is about two seconds. The vertical axis is discrete transmission gears, $u(k)$, gear one or gear two. To be consistent with conventional powertrain, the transmission is set to the neutral gear compulsively when vehicle speed reaches zero. Those horizontal arrow lines, $EC(k,11)$ and $EC(k,22)$, represent ESS's energy consumption without gearshift during a time interval, and the diagonal lines, $EC(k,12)$ and $EC(k,21)$, represent the energy consumption with an upshift or downshift action within 1 *s*. In order to reduce computation load, driving cycles are split into multiple segments by zero vehicle speed. Therefore, the whole DP problem is then separated into several minor DP problems. Since the model includes only two-level state operations, the required computation effort is still manageable.

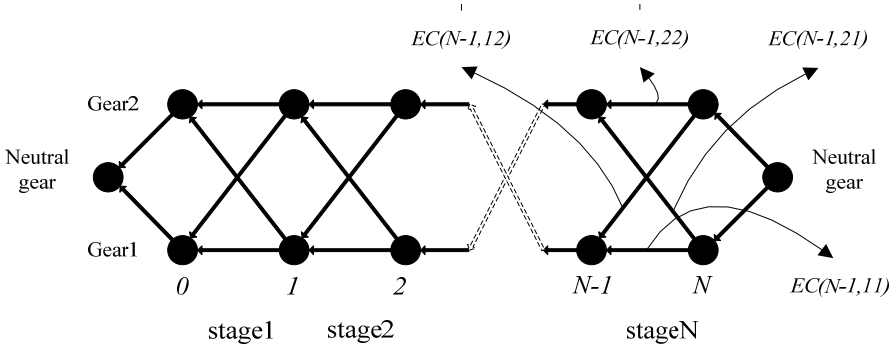

Figure 3-14 Description of gear selection process

The total energy consumption in combined EPA75 and HWFET forms the objective function of the DP, and the energy consumption is calculated using EPA75 and HWFET driving cycles. For a given driving cycle, the objective function takes the following form.

$$EC_t = \sum_{k=0}^{N-1} \Delta T * EC(k, ij) \tag{3.12}$$

where EC_t is total energy consumption, N is total samples during driving cycle, ΔT is the time interval, EC is energy consumption rate, k is current step, i and j are selected gears at beginning and end of one interval.

A weighting factor, α, was added to the gearshift term in the objective function to prevent unnecessarily frequent and undesired gearshifts. The modified objective function is shown in Equation (3.13). The value of, α, can be adjusted to tune the business of gearshift. Gear shift is only modeled and simulated in city cycle EPA75 since gear shift is not frequently needed during highway driving represented in HWFET. The increase of α value from 0 to 1400 led to gearshift number fall from 120 to less than 10. The obtained gearshift sequences are then used in the

simulation to verify energy consumption calculation of DP. Comparisons show that the energy consumption discrepancy between DP results and simulation results is reduced from 12% to 2%, negligibly small. This small resulting discrepancy is because this quasi-static model is more accurate when less gearshifts happen. The weighting factor α of 600 was used because it can reduce gearshift number from 120 to about 10, keep energy consumption close to minimum, and lead to very small difference between the DP-based result and simulation result. The gearshifts between neutral and first or second gear are ignored.

$$\overline{EC_t} = min \sum_{k=0}^{N-1} \{\Delta T \times EC(k, ij) + \alpha |g(k+1) - g(k)|\} \tag{3.13}$$

$$\text{Subject to} \begin{cases} \text{SOC}_{\min} \leq \text{SOC} \leq \text{SOC}_{\max} \\ T_{m_{min}}(k) \leq T_{m\_dmd}(k) \leq T_{m_{max}}(k) \\ 0 \leq \omega_{m\_dmd} \leq \omega_{max} \end{cases}$$

where $T_{m_{min}}(k)$ and $T_{m_{max}}(k)$ are minimum and maximum torques provided by the motor at the state $x(k)$, $T_{m\_dmd}(k)$ is torque demand from input shaft of transmission, ω_{m_dmd} is demanded motor speed, which is nonnegative because vehicle does not drive reversely in driving cycles. Compared to torque and speed, SOC of the battery is more complex to handle because it is not only influenced by the current control input but also by the past values. Therefore, the SOC is often separated as one item of objective function in HEV research. For PEV the constraint of SOC can be eliminated through trial simulations ahead of time since battery is the only energy source, different from the HEV.

3.6.2 Solution Method

Dynamic Programming (DP) is a method of breaking a complex optimization problem into many simpler sub-problems that seeks the optimal solution by reiterative usage of principle of optimality [93] [94]. Separability of the problem or process is critical for the effective and efficient implementation of DP. The implementation in this work consists of the following steps:

Algorithm:

Step N-1

$$\overline{EC_{t_{N-1}}}\,(x(N-1)) = \Delta T \times EC(k, ij) + \alpha |g(k) - g(k+1)| \tag{3.14}$$

Step k, for $0 \leq k < N-1$

$$\overline{EC_{t_k}}\left(x(k)\right) = \min_{u(k)} \{\Delta T \times EC(k, ij) + \alpha |g(k) - g(k+1)| + \bar{J}_{k+1}\,(x(k+1))\} \tag{3.15}$$

End

where k is the stage number, x(k) is selected gear, u(k) is vector of possible gears at step k, $\overline{EC_{t_k}}$ is the minimum cost of from stage *k* to terminal stage. DP is a powerful tool to solve this type of complex problems because its computation needs only increase linearly with the number of stages, compared to exponentially in direct enumeration. However, DP may not be the general solution to all complex problems since curse of dimensionality (called by Bellman) would make computation efforts of DP increase exponentially with dimension of system. Ignoring the dynamic processes and the reducing number of states simplify the solution of the optimal control input and optimization search using DP.

3.6.3 Problem Simplification

To reduce computation efforts prior to the identification of the optimal gearshift sequence, several approaches are used:

1) It is assumed that *EC(k,11)* is equal to *EC(k,12)* and *EC(k,22)* equal to *EC(k,21)*. This assumption is introduced since the duration between two continuous gearshifts during practical driving is at the order of 10 to 100 *s*, much larger than the simulation time interval of 1 *s*. In addition, high-frequency gearshift sequence from DP with $\alpha = 0$ can be filtered by large parameter α [86].

2) The feasible region of gear ratios is confined in a rectangular region by trials. The feasible region is circumvented by boards, which are determined by top velocity, acceleration and fuel consumption. This step is important to eliminate those infeasible gear ratios at certain step. The first gear ratio,g_1, is evaluated by running model in EPA75 and second gear ratio, g_2, in HWFET. The trials are based on the assumption that g_1 is primarily used in city driving and g_2 in highway driving. After repeated trials, the feasible ranges of gear ratios for first and second gear are set as g_1 from 10 to 22 and g_2 from 2 to 12. This feasible region forms a rectangle and can be split into smaller areas using grid. Finer grid leads to higher precision and quadratically increased computation burden, while gross grid sacrifices precision for efficiency [84]. In this work, the step for both g_1 and g_2 is set as one. Therefore, the maximum number of possible gear pairs is 143.

3) The look-up tables of energy consumption ratios were pre-calculated. This static method used widely in early research can produce precise result if the state space is split densely. The EPA75 and HWFET driving cycles are analyzed and their speed-acceleration maps are shown in Figure 3-15 and Figure 3-16, which defines the range of the look-up table variables (0 to 28 m/s for speed and -2 to 2 m/s^2 for acceleration). The state space (vehicle acceleration, vehicle speed and transmission gear) is discretized into a 3-D grid and values of look-up tables, energy consumption at every grid point from simulating model with fixed speed, acceleration and gear, are all obtained to form cost-to-go functions. In this work, vehicle speed is split by an interval of 1 *m/s*, acceleration is split from -2 m/s^2 to 2 m/s^2 by 0.1 m/s^2. Consequently, for a pair of gear ratios, calculation of such a look-up table costs about 7,600 *s* and 3,400 *s* for EPA75 and HWFET, respectively. Considering the number of possible gear pairs, the total

computation time would exceed 400 hours on workstation with 24G memory and 2.59GHz (8 cores), so a more efficient way to produce these tables is needed.

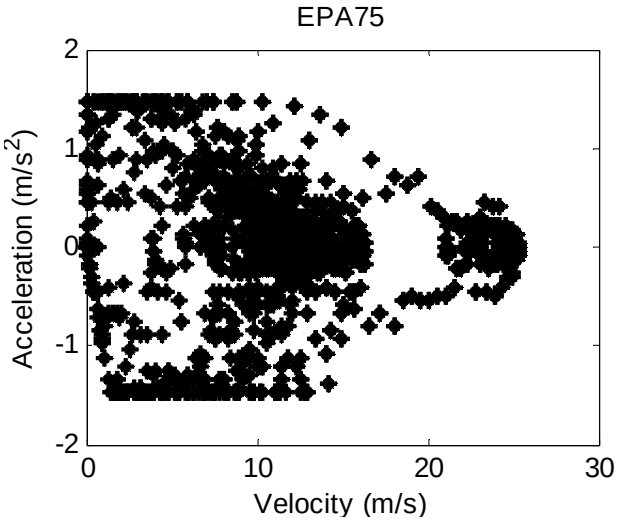

Figure 3-15 Velocity -acceleration distribution (EPA75)

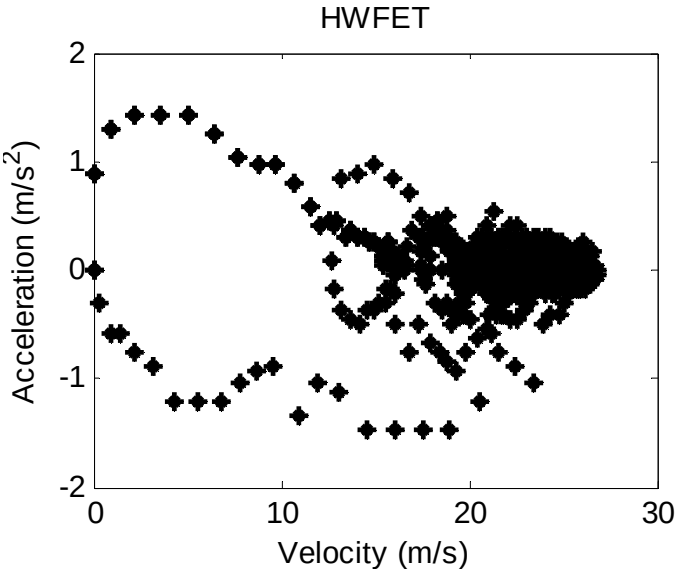

Figure 3-16 Velocity -acceleration distribution (HWFET)

The alternative approach is to run the simulation using an arbitrary driving cycle without gearshift, which means the gear is fixed at the first or second gear during each driving cycle. Compared to the first method, this approach only calculates the needed state space (vehicle acceleration, vehicle speed and transmission gear) and totally ignores the operating points not included in the two driving cycles (blank area). For a pair of gear ratios, the calculation time for EPA75 and HWFET using this method is reduced to about 200 *s* and 40 *s*. The total computation time to establish all simplified look-up tables is about 10 hours, only accounting for 2.5% of the first approach.

4) A penalty factor is added to scale the energy consumption if the inequalities do not prevail (for instance, vehicle in the first gear may not be able to reach the maximum speed of either of

the two driving cycles). The computed energy consumption and corresponding gear number will be eliminated eventually in the DP search, so all of the three constraints are satisfied.

3.7 Results and Discussion

The whole search process is transformed into a dual-loop optimization problem. The outer loop is to search the gear ratio pair from feasible region. For reduction computation efforts, the feasible region of *GR* is split into small squares. DP is used in the inner loop to find the "optimal" gearshift sequence and minimum energy consumption for center point (gear ratio pair) of every square. Energy consumption is simulated using EPA75 and HWFET cycles repeatedly with different gear ratios inside the feasible region. As a result, two 2-D cost-to-go tables are established, each element of which represents the potential minimum energy consumption of the PEV related to one pair of gear ratios in EPA75 and HWFET, respectively. Those potential gear pairs correspond to small objective function values in both EPA75 and HWFET. In this work, $gr1$ is 17 and $gr2$ is set as 9 based on the energy consumption involving both driving cycles.

3.7.1 Energy Consumption

After the energy consumption objective function and gear ratios are determined, the vehicle performance model and driving cycles are used once again. Figure 3-17 and 3-18 show the optimal gearshift during HWFET and EPA75 driving cycles. It is clear that Gear 1 is primarily used in EPA75 and Gear2 in HWFET, which is consistent with Assumption 2. During EPA75 driving cycle, the operating points of the electric motor with a single-speed gearbox often operate in the less efficient region, while the motor with a two-speed transmission operate closer to high-efficiency zone, as shown in Figure 3-19 and 3-20. However, change from a single-speed gearbox to a two-speed transmission does not significantly influence the operating points of the motor in HWFET, as shown in Figure 3-21 and 3-22, because Gear2 is primarily used. Meanwhile, addition of a two-speed transmission also lowers the overall powertrain efficiency due to the added weight and the lower transmission efficiency. In this work, the two-speed transmission is set to be $20kg$ heavier than single-speed gearbox, adding around 0.5% of energy consumption. The less efficient two-speed AMT also increases another 1.5% of additional energy consumption. As a result, the two-speed AMT helps to increase fuel economy by about 4.5 % in EPA75 defined city driving, and only 1.2% improvement is achieved by adding this transmission that allows additional operation speed. Fuel economy improvements are illustrated in Table 3-10. The results are consistent with distribution of operating points of the motor. It should be emphasized that the benefits of two-speed transmission for city and highway vary with how peaky efficiency map of the electric motor is, and the type and efficiency of the transmission. For a low-cost electric motor that is more efficient at low speed than at high speed, the benefits of energy consumption will be more apparent in highway than in city driving.

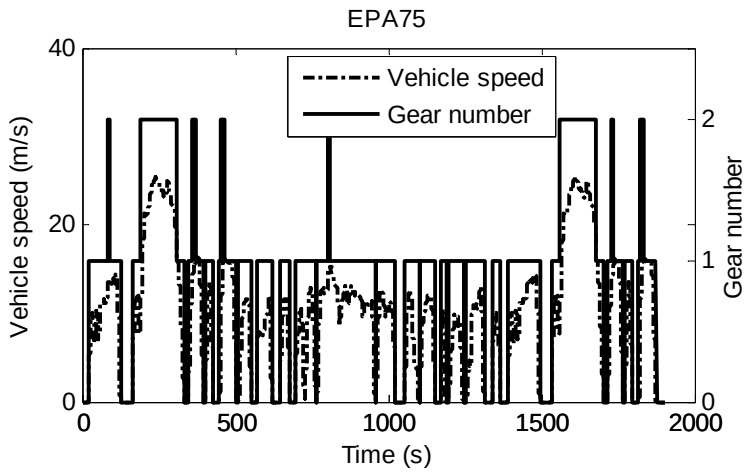

Figure 3-17 Selected gear and velocity (EPA75)

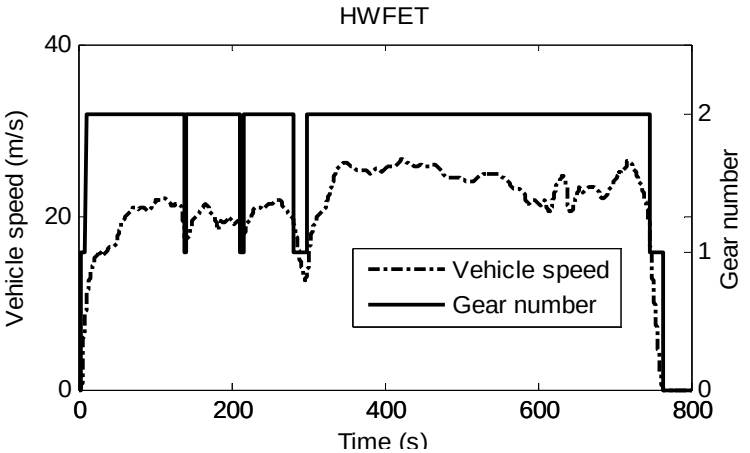

Figure 3-18 Selected gear and velocity (HWFET)

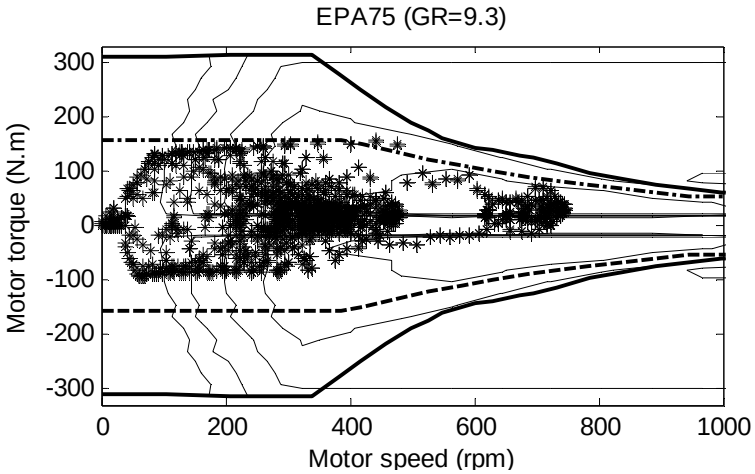

Figure 3-19 Operating points of motor with 1-speed gearbox (EPA75)

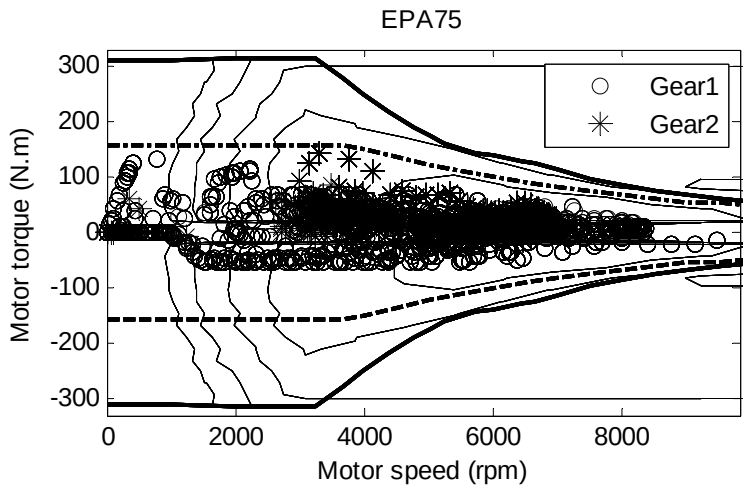

Figure 3-20 Operating points of motor with 2-speed gearbox (EPA75)

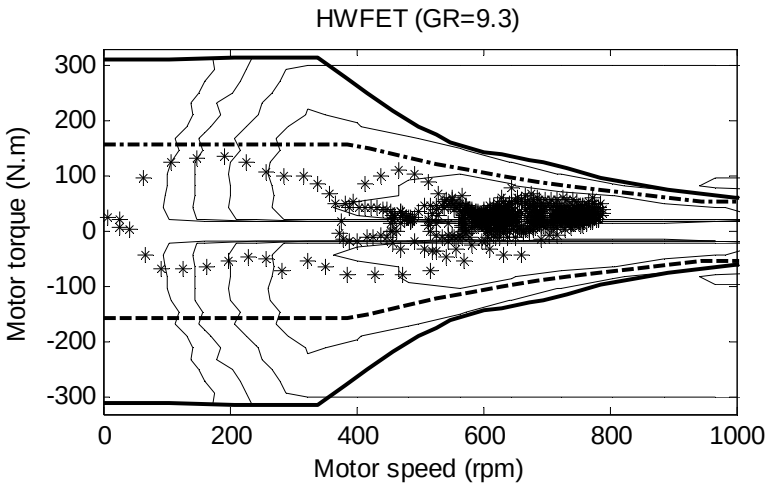

Figure 3-21 Operating points of motor with 1-speed gearbox (HWFET)

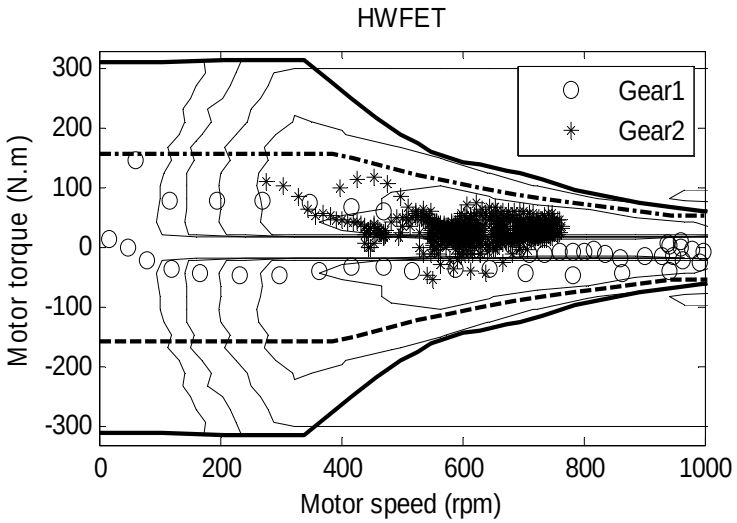

Figure 3-22 Operating points of motor with 2-speed gearbox (HWFET)

Table 3-10 Fuel consumption improvement

Fuel Consumption (mpg)	HWFET	EPA75
One-speed Gearbox	99.5	118.8
Two-speed Transmission	100.7	124.1
Efficiency Improvement	1.2%	4.5%

3.7.2 Gearshift Map

The effects of the two-speed transmission are not exclusively determined by the gear ratio selection. A well-designed transmission controller plays a key role to reach the full potential of transmission. The rule-based transmission controller in AUTONOMIE accepts vehicle speed and driver's pedal position as two inputs. Since the driver model presents certain level of uncertainty and does not exist in the DP model, the driver's pedal signals are replaced by driving force inputs. The Figure 3-23 and 3-24 illustrate the gears distributions in velocity-driving force map during two driving cycles, respectively. Considering the fact that EPA75 cycle requires more gearshifts than the HWFET cycle, EPA75 is thus the main consideration to extract the gearshift schedule. It can be seen that the signs of two gears for EPA75 are almost separated into two parts with no overlap, and those for HWFET are also separated with a tiny twilight zone.

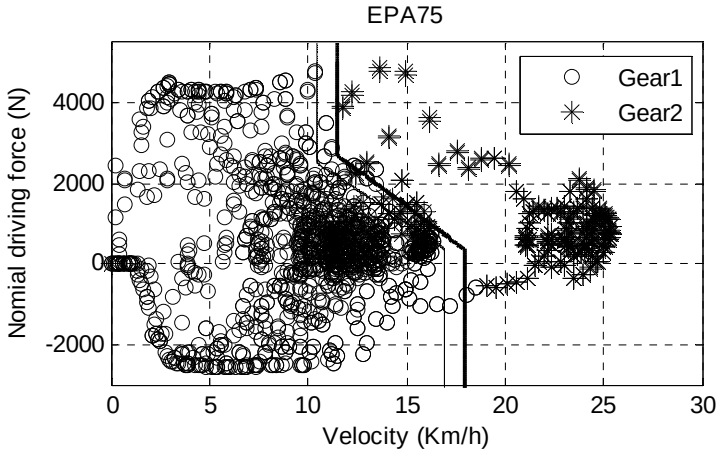

Figure 3-23 Gear operating points of DP (EPA75)

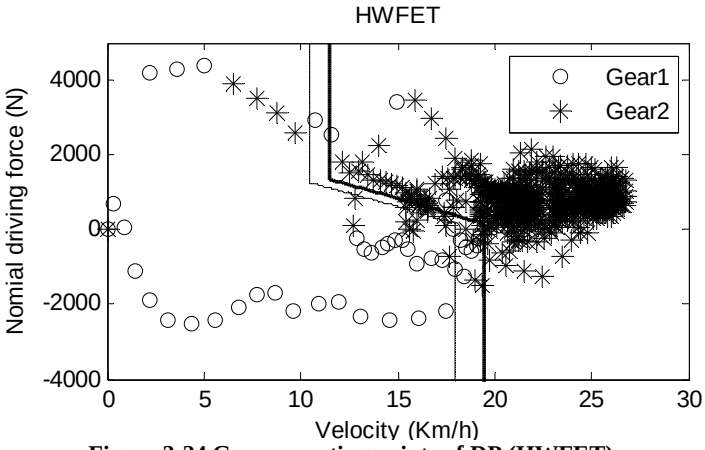

Figure 3-24 Gear operating points of DP (HWFET)

The optimized gearshift map is used to replace the original one and its energy consumption benefit is shown in Table 3-11 through reduced overall energy consumption. Two-speed transmission improved energy consumption over the one fixed-speed gearbox, especially for the EPA75 driving cycle. DP is able to identify the lowest possible energy consumption of the two-speed transmission. The actual improvement is also constrained by the controller. Compared to original controller, the DP-improved new controller led to better results.

Table 3-11 Overall energy consumption (mpg)

Gear Ratio	9.3	[17; 9] - old map	[17; 9] - new map	DP-Best Possible
EPA75	118.8	121.3	123.3	124.1
HWFET	99.5	100.1	100.3	100.7

3.7.3 Power Performance

Added two-speed transmission with an optimized controller can improve the power performance of vehicle as well. Vehicle performance of the modeled vehicle with the single-speed gearbox and the two-speed transmission controlled by the old and optimized controllers are compared by a series of simulations using the standard testing methods [95]. The comparison consists of five aspects, from acceleration and gradeability to top speed at even road and slope, as shown in Table 3-12.

Table 3-12 Results over vehicle performance

Measures	Criterion	1-speed	2-speed
Acceleration (m/s^2)	13.5	9	8.3
Top speed (m/s)	31.3	37	37
Gradeability limit	⩾25%	40.6	70
Top speed (3%)	⩾24.6	32.9	32.8
Top speed (6%) slope)	⩾20.1	29.4	29.4

Figure 3-25 and 3-26 show that the added large gear ratio increases the maximum output torque of transmission that leads to larger gradeability limit and acceleration, especially at low speed range. Larger gradeability limit that stands for better acceleration is generally not reachable because friction force between wheels and road surface limits the maximum acceleration. The top speed of the vehicle is constrained by the maximum power; therefore, top speed is not changed by the new transmission. Top speeds at slope of 3% and 6% are maintained because the added first gear exerts no influence on it and the original gear ratio is quite close to the second gear ratio of new transmission. The torque hole during gearshift in EV mode, which is indicated by zero acceleration at around 3.5 seconds, is an issue for transmission in EV mode. However, engine can help to achieve the TGF feature, just like Figure 2-10 and 2-11. In addition, dual-clutch version of this HAMT can also overcome this issue in EV mode, without turning on engine. Several 3-speed transmission versions specifically for EV are patent-pending [67].

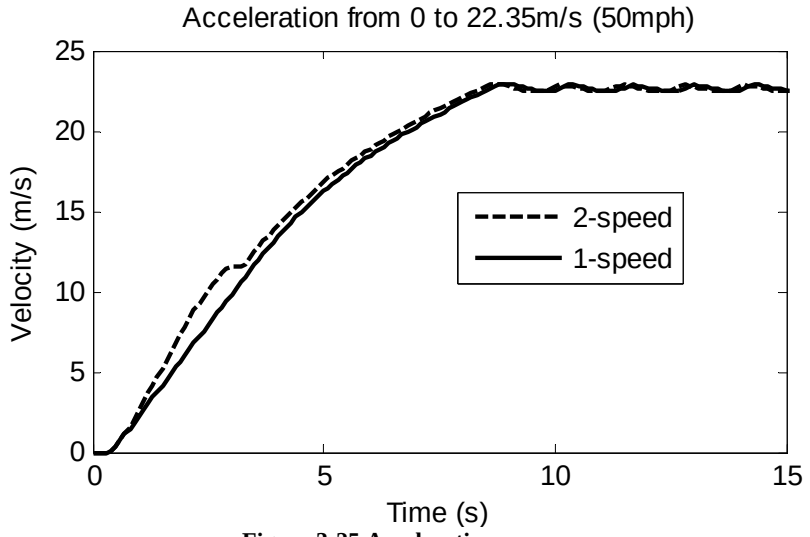

Figure 3-25 Acceleration curves

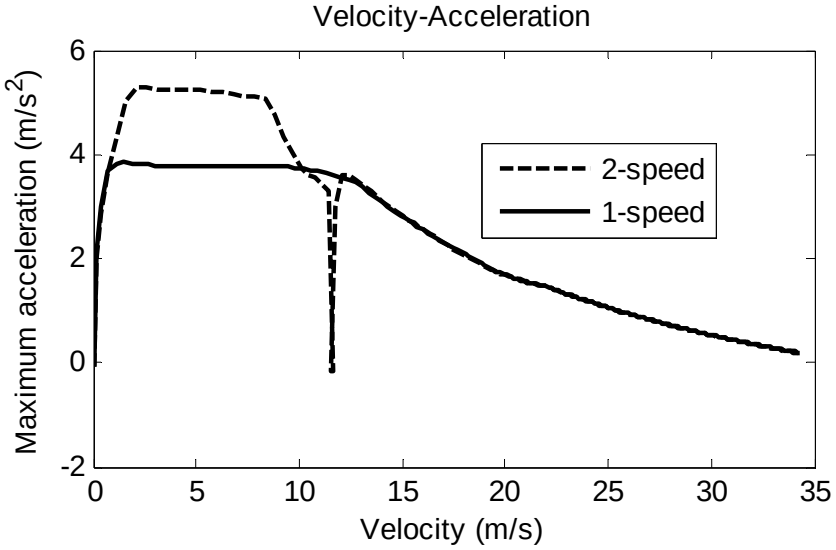

Figure 3-26 Maximum acceleration

From model-based design and optimization above, it is found that an ideal gear ratio step between two gears in EV mode is 1.89, which is ratio of 17 over 9. Considering extremely importance of gear selector 3, which is discussed in detail in Chapter 2.3.1 and Table 2-2, the 4th possible gear (gear ratio equals 2.78) in EV mode (Table 3-1) should be selected as gear 1. Therefore, this HAMT is always ready to enter one of first five gears in hybrid mode. Another selected gear is gear 6, whose gear ratio in EV mode is 1.66. Therefore, the ratio step would be 1.67, quite close to the optimal number 1.89.

3.8 Summary

This hybrid system supports EV mode and hybrid mode. In the process of designing gear ratios, hybrid mode is major consideration. Gear ratios for hybrid mode are determined based on classical method: aggressive gear ratios. Considering extra constraints for gear 3 and gear 4, gear ratios are adjusted to achieve stable ratio steps. The same set of gear ratios is also used in EV mode. Since there is no need to use the up to 8 gear ratios, 3 fundamental questions are answered: 1) How many gears are needed? 2) What are optimal gear ratios? 3) What is gearshift schedule for selected gears? At first, two speeds are accepted as good choice based on past research work. Then, one model-based optimization method, based on Dynamic Programming, is used to generate optimal gear ratios and optimal gearshift schedule. Key model parameters are based on Transit Electric presented by Ford and Azure Dynamics. This optimization of gear ratio and gearshift schedule helps to find optimal ratio step is 1.89. This ratio step provides a good reference to answer the second question: selecting gear ratios from available ratios. Considering importance of selector 3 and this optimal ratio step, eventually 4th and 6th possible gear are selected for EV mode. The third question is also answered by the optimization method. Although eventual ratio step, 1.67, in EV mode is a little different from optimal ratio step, the gearshift schedule is inherited because two ratios steps are quite close.

4 Steady and Transient Dynamics Analysis

This chapter primarily covers powertrain dynamics analysis in steady and transient states. The steady state means constant driver command, locked main clutch and absence of gearshift. Although this steady-state operation is relatively simple, it is extremely important for more complicated transient dynamics and vehicle development. In automotive industry, a variety of specially designed tests and different control methods are necessary to deliver desirable driveability. Some important driveability-related topics include backlash, tip-in/tip-out response vibration, mode transition and gearshift [96] [97] [98] [99] [100] [101] [102] [103] [104] [105] [106] [107] [108] [109]. Other research considers trade-off between efficiency and driveability [110] [111] [112]. In this research work, this proposed powertrain system based on HAMT could generate higher efficiency naturally. Only mode transition and gearshift are investigated in depth from driveability aspect.

With different states of engine and main clutch as well as dog clutches, whole powertrain has very flexible operation behavior. During complicated powertrain events, like gearshift or mode transition, often one or more clutches need to change states. Based on steady-state analysis, transient dynamics analysis is conducted. The most important transient events for this hybrid powertrain are power-on gearshift and EV-hybrid transition. So, these two events will be analyzed separately and in depth. As precondition of dynamics analysis, one lumped-mass model (LMM) is built to describe fundamental physics of driveline system.

4.1 Driveline Model and Assumptions

4.1.1 Lumped-mass Model

A lumped-mass model is illustrated in the Figure 4-1. LMM is widely used to analyze driveline dynamics [46] [113] [114] [115] [116]. This model is composed of four types of elements:

a) Moment of inertia: engine and motor are described as two moments of inertia (J_e and J_m) with imposed torques; rotational parts inside gearbox are converted to 4 moments of inertia (3 shafts and main clutch);
b) Zero-mass shaft: six shafts are engine crankshaft, motor shaft, two HAMT input shafts, one HAMT output shaft and a representative half shaft; all moments of inertia are attached to three shafts;
c) Gear pairs: overall gear ratios from input shaft1 (IS_1) to output shaft (OS) is simplified as i_{1o}, no matter how the gear ratio is generated; similarly, the gear ratio from input shaft2 (IS_2) to output shaft is represented by a gear ratio i_{2o}; i_{1o} and i_{2o} in different modes are summarized in Table 2-1and 2-3; the gear ratio from motor to IS_2 is i_m;
d) Clutch: main clutch can connect or disconnect engine to HAMT IS_1; two gear selectors CL_1 and CL_2 consist primarily of dog clutch and frictional cone clutch; dog clutch is engaged consistently except during gearshift, which requires one of two dog clutches to be disengaged temporarily to change gear ratio i_{1o} or i_{2o}.

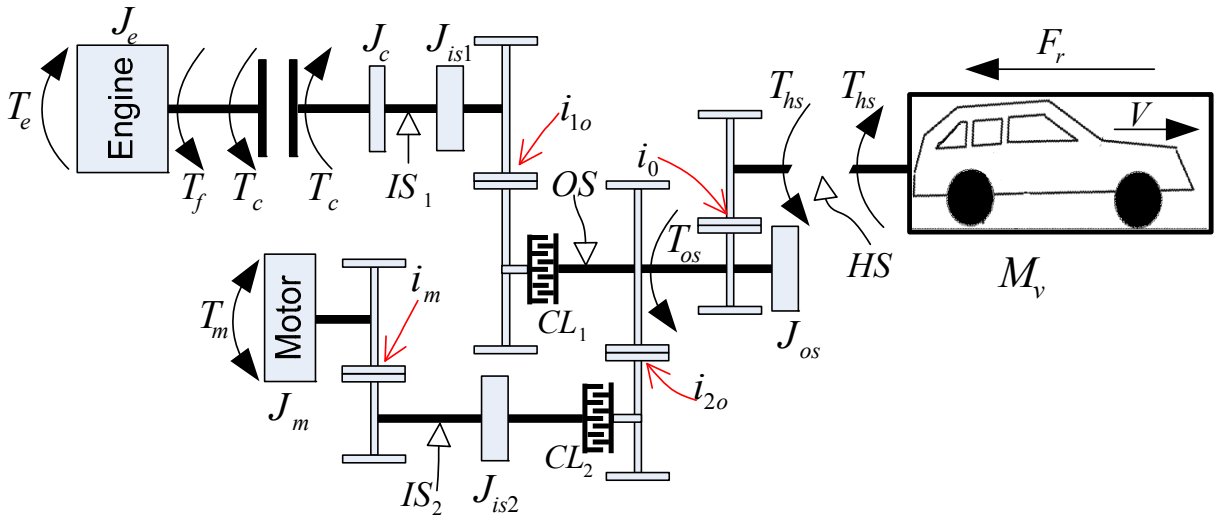

Figure 4-1 LMM model for vehicle with HAMT

Torques from engine and motor is combined at OS and further amplified by main reduction gear i_0 (differential not considered here); finally, output torque is sent to half shafts (HF) to propel vehicle. For purpose of focusing on operation principle of HAMT, some aspects of powertrain dynamics are ignored. For example, it is assumed that the vehicle runs longitudinally; suspension system is not considered; air speed is 0; both wheels and half shafts are assumed rigid.

External retarding force F_r , shown in equation (4.1), is estimated using road load coefficients (F_0, F_1 and F_2), which can be obtained from repeated vehicle coastdown tests at neutral gear.

$$F_r = F_0 + F_1.V + F_2.V^2 \tag{4.1}$$

Sum of half shaft Torque, T_{hs}, overcomes retarding force and accelerates inertia mass of vehicle and all rotational moments of inertias, primarily 4 wheels, as shown in equation (4.2) and (4.3).

$$M_{eff}.a_v = \frac{T_{hs}}{R_w} - F_r - F_d = \frac{T_{os}.i_0}{R_w} - F_r - F_d \tag{4.2}$$

$$M_{eff} = M_v + 4\frac{J_w}{R_w^2} \tag{4.3}$$

An equivalent version of the LMM model in Figure 4-1 is shown in Figure 4-2. Whole model is split into 4 rotational moments of inertias by main clutch and two dog clutches. Engine and all connected accessories are represented by J_e; motor and connected shafts are merged to input shaft2 as $\overline{J_{is2}}$; vehicle weight and all other rotational moments of inertia are equivalent to moment of inertia $\overline{J_{ext}}$, which is linked to output shaft.

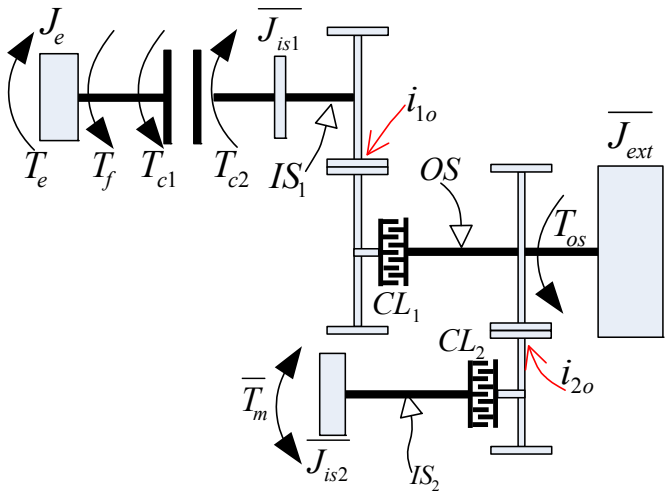

Figure 4-2 Simplified LMM model of vehicle

$$\overline{J_{is1}} = J_c + J_{is1} \tag{4.4}$$

$$\overline{T_m} = T_m . i_m \tag{4.5}$$

$$\overline{J_{is2}} = J_{is2} + J_m . i_m^2 \tag{4.6}$$

$$\overline{J_{ext}} = (M_v R_w^2 + 4J_w)/i_o^2 + J_{os} \approx (M_v R_w^2 + 4J_w)/i_o^2 \tag{4.7}$$

4.1.2 Modeling Principle of Main Clutch

Main Clutch is a frictional component used to connect and disconnect engine with transmission and plays a critical role in gear shift and some mode transitions. Its primary parts include clutch disc(s) and clutch mechanism that is driven by an electro-hydraulic or electro-mechanical actuator, as shown in Figure 4-3. When clutch is engaged, static friction between flywheel disc and clutch disc transmit torque from ICE to transmission; as throw-out bearing driven by mechanical or electromechanical elements pushes diaphragm spring to separate clutch disc from flywheel, torque path is cut. Compared to disengagement of clutch, the reverse process is more critical and more complex.

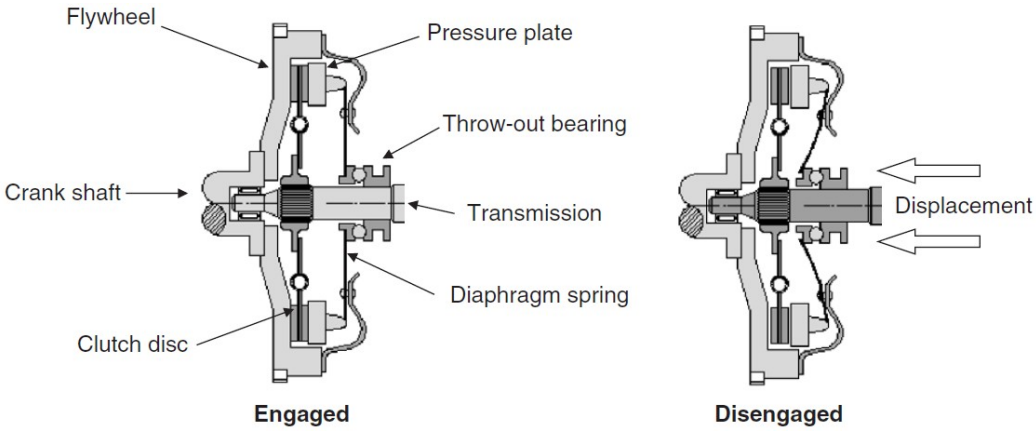

Figure 4-3 Schematic overview of a dry clutch [117]

There exist two sequential phases during clutch engagement: slipping phase and sticking phase. When relative speed (ICE to input shaft of transmission) is nonzero (slipping phase), clutch transmits torque via kinetic friction that is determined by normal force; when the rotation speeds are equal and clutch is locked up (sticking phase), static friction that is controlled by engine torque could be any value between extreme frictional torques. In order to describe friction-action relationship and discontinuous stick-slip phenomenon, several mathematic models have been proposed to meet different purposes from macroscopic and microscopic aspect [118] [119] [120] [118] [121] [122] [123]. Amstrong-Helouvry *et al* presented a comprehensive survey about different friction models and control methods [118]. Among different friction models, classical (discontinuous) Coulomb friction model is widely used in modeling and control of powertrain system for its simple but close expression in a macroscopic sense, in spite of less accurate description of stick-slip transition that is a source of driveline vibration. For example, Zhang combined vehicle jerk and shift duration together to formulate a comprehensive objective function and employed Hamilton optimal control method to obtain 'optimal' clutch engagement process [124]; Chen *el al* focused on control of slip-stick transition during gear shift, using model reference adaptive controller (MRAC) to compensate discontinuity of friction torque [125]. Gaillard investigated driveline dynamics and clutch damping effects [126].

The Coulomb friction model is used to describe sliding-phase friction action, which is described as Equation (4.8).

$$T_c = \begin{cases} \mu_s . N . R_{eff} . F_c . sign\big(\omega_1(t) - \omega_2(t)\big) & , \| \ \omega_1(t) - \omega_2(t) \ \| > \omega_{thre} \\ [-\mu_l . N . R_{eff} . F_C \ , \mu_l . N . R_{eff} . F_C] & , \| \ \omega_1(t) - \omega_2(t) \ \| \leq \omega_{thre} \end{cases} \tag{4.8}$$

where T_{clutch} is clutch torque, N is number of friction plates, R_{eff} is effective radius, F_c is the applied clutch force, μ_s is friction coefficient as clutch slides and μ_l is friction coefficient as clutch is locked. ω_{thre} is a threshold slipping speed that is used to judge which phase is active. The ω_{thre} is set as very small positive value for purpose of avoiding numerical issue.

Dynamic property and response delay of actuators have ineligible influence on control and results, but these aspects will not be focus of this research and not discussed.

4.1.3 Modeling Principle of Gear Selector

During gearshift in HEV mode, main clutch is open, engine is totally isolated by open clutch, and input shaft together with connected gears are isolated from both engine and output shaft if virtual clutch CL1 is open. Gear selector can be considered as a combination of dog clutch and frictional cone clutch. One side of dog clutch is linked to shaft, and another side to hub. The dog clutch transmits all torque when it is engaged; the cone clutch is a frictional device to eliminate relative speed between two sides of gear selector. Only after the cone clutch reduces relative speed to a very low value, dog clutch can be locked by actuator smoothly. Or else, noticeable noise and vibration can be detected, deteriorating driveability and component life span. Gear selector is important for gearshift.

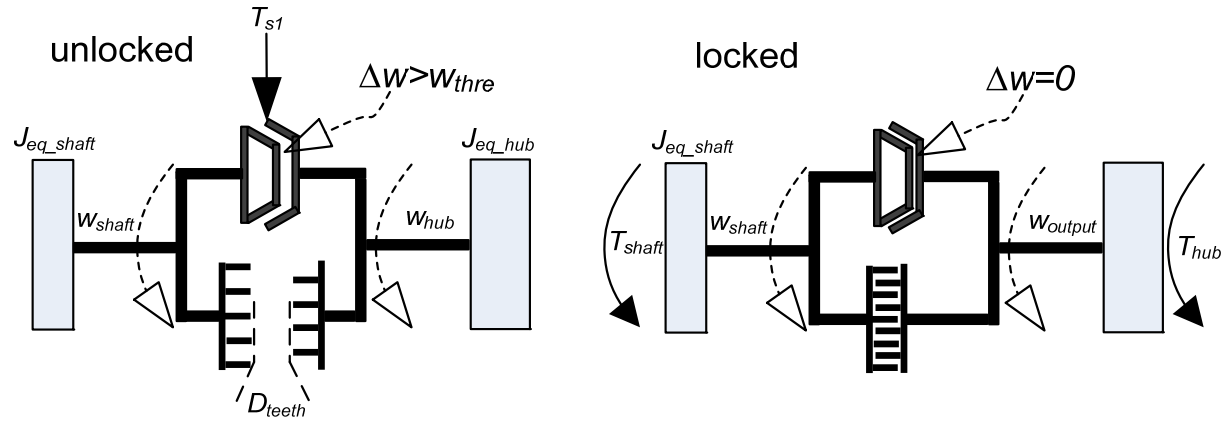

Figure 4-4 Scheme of gear selector

Figure 4-4 shows a typical diagram of gear selector. All inertias on two sides of dog clutch are reduced to two lump masses. Engagement and disengagement of selector are two different events and should be analyzed separately.

Engagement: Initially, this dog clutch is unlocked (slipping or open) with slip speed of cone clutch Δ_ω above a threshold value, like 5rpm. In this state, actuator has no acting force and maintains D_{teeth} at D_{max}, the maximum teeth distance of dog clutch. When command for engaging new gear is executed, the actuator will have positive acting force to reduce D_{teeth} to D_{thre}, the threshold distance for locking dog clutch (while D_{teeth} is over D_{thre}, only cone clutch can transmit torque between two sides of gear selector; while D_{teeth} falls below D_{thre}, only dog clutch can transmit torque between two sides of gear selector). As long as slip speed drops below threshold value, actuator will push gear selector to enter locked state. The force on cone clutch of gear selector will generate friction torque between two slipping surface and eliminate speed difference to lock each other. Now, dog clutch enters locked state. In unlocked state, friction torque T_s can only affect rotation speed of shaft ω_{shaft} and has no effect on hub side because moment of inertia J_{eq_hub} is much larger than J_{eq_shaft}. J_{eq_hub} is equivalent moment of inertia on the wheel side. When dog clutch is in locked state, locked dog clutch reduces one degree of freedom and transmits torque from input shaft side to output side. J_{eq_shaft} is equivalent moment of inertia on the engine side. J_{eq_hub} can be calculated from vehicle mass, wheel radius, final drive ratio and actual gear ratios from output side of gear selector to transmission output shaft. J_{eq_hub} can be calculated from inertias between input shaft and dog clutch. Considering flexible operation of this hybrid system, there is no universal formula to calculate equivalent inertias, but this barrier can be easily overcome by simulation model, which will be discussed in detail in Chapter 5. Similarly, rotation speeds of cone clutch.

The change rate of relative slip speed Δ_ω is controlled by frictional torque of cone clutch T_{sf}. The cone clutch is specially designed to eliminate slip speed fast and shorten gearshift length. Basic physical principle of this cone clutch is shown in equation (4.9).

$$T_{sf} = \frac{\mu_{syc} F_{syc} R_{syc}}{\sin \alpha} \tag{4.9}$$

Disengagement: Initial state is locked state. Two sides of dog clutches rotate at the same speed because dog clutch rigidly synchronizes two sides. As command for disengaging gear selector is implemented, unlocking gear selector will be realized by negative acting force on gear. This negative force overcomes friction force between dog clutch teeth to increase D_{teeth} until it is over D_{thre}. As long as the dog clutch of gear selector is disengaged, the friction force between teeth will disappear instantaneously and negative force will push gear selector to the position D_{max}, entering unlocked state.

Table 4-1 provides a concise summary of the two processes, starting from unlocked state and returning the unlocked state after an engagement and disengagement.

Table 4-1 Gear selector states

	$\Delta\omega$	D_{teeth}	T_{sf}
Unlocked state	$\Delta\omega > \omega_{thre}$	$D_{teeth} = D_{max}$	$T_{sf} = 0$
Locking in process	$\Delta\omega > \omega_{thre}$	$D_{max} > D_{teeth} > D_{thre}$	$T_{sf} > 0$
Locked state	$\Delta\omega = 0$	$D_{teeth} = D_{min}$	$T_{sf} = 0$
Unlocking in process	$\Delta\omega = 0$	$D_{thre} > D_{teeth} > D_{min}$	$T_{sf} < 0$

4.2 Basic Operating Modes

A powertrain system needs to work in various conditions. With change of vehicle states (speed and acceleration) and driver inputs (brake pedal, accelerator pedal and steering wheel), powertrain needs to smoothly transmit torque to wheels. In order to analyze powertrain dynamics systematically, 6 basic operating modes – including 2 steady modes and 4 transition modes – are summarized in Table 4-2. Detailed analysis is followed sequentially. Almost all operation conditions are combinations of these basic operating modes. Various research papers cover this topic via different aspects [90].

Table 4-2 Summary of basic operating modes

	CL	CL2	Engine
Steady 1 – EV	Open	Locked	Off
Steady 2 – Hybrid	Locked	Locked	On
Transition 1	Open	Locked	On
Transition 2	Open	Locked	On
Transition 3	Slipping	Locked	On
Transition 4	Locked	Unlocked	On

4.2.1 Steady Operating Modes

The steady-state operation is that driver command is constant, main clutch is locked and there is no gearshift.

4.2.1.1 Steady EV Mode – Main Clutch Open and Engine Off

Vehicle is driven exclusively by motor (or driving motor during deceleration) as motor/battery can meet torque/power demand and state of charge (SOC) is not too low. All gears and shafts rotate with transmission output shaft rigidly. Engine speed maintains zero and main clutch is open.

$$\begin{cases} (\overline{J_{ext}} + \overline{J_{is1}}.i_{1o}^2 + \overline{J_{is2}}.i_{2o}^2).\dot{\omega_{os}} = \overline{T_m}.i_{2o} - F_r \times R_w \\ \omega_{is1} = \omega_{os}.i_{1o} \\ \omega_{is2} = \omega_{os}.i_{2o} \\ \omega_e = 0 \\ T_c = 0 \end{cases} \tag{4.10}$$

4.2.1.2 Steady Hybrid Mode – Main Clutch and CL1&2 Locked and Engine On

Engine is primary power contributor to drive vehicle, and motor serves as balancer to enable engine operate within high-efficiency zone. Whole powertrain is simplified as a 1-DoF mass lump model, with rotational components linked to transmission output shaft rigidly. Transmitted torque via main clutch does not exceed torque capacity.

$$\begin{cases} (\overline{J_{ext}} + (\overline{J_{is1}} + J_e).i_{1o}^2 + \overline{J_{is2}}.i_{2o}^2).\dot{\omega_{os}} = T_e.i_{1o} + \overline{T_m}.i_{2o} - F_r \times R_w/i_0 \\ \omega_{is1} = \omega_{os}.i_{1o} \\ \omega_{is2} = \omega_{os}.i_{2o} \\ \omega_e = \omega_{is1} \\ T_c = T_e - J_e.\dot{\omega_{os}}.i_{1o} \\ -\mu.N.F_c.R_{eff} < T_c < \mu.N.F_c.R_{eff} \end{cases} \tag{4.11}$$

4.2.2 Transient Operating Modes

4.2.2.1 Transition 1 – Main Clutch Open and Engine On

This transition mode often occurs during transition from EV to hybrid mode. Since engine speed is zero in EV mode, engine torque is used to overcome engine inertia torque and pumping loss and match speed of input shaft 1 before main clutch become engaged, avoiding apparent vehicle jerk. Although engine is on, vehicle is still driven exclusively by motor. Another possible scenario that this mode is activated is during gearshift. Function of transition 1 is to synchronize two speeds of main clutch through engine torque control without engaging main clutch.

$$\begin{cases} (\overline{J_{ext}} + \overline{J_{is1}}.i_{1o}^2 + \overline{J_{is2}}.i_{2o}^2).\dot{\omega_{os}} = \overline{T_m}.i_{2o} - F_r \times R_w \\ \omega_{is1} = \omega_{os}.i_{1o} \\ \omega_{is2} = \omega_{os}.i_{2o} \\ J_e\dot{\omega_e} = T_e - T_c \\ T_c = 0 \end{cases} \quad (4.12)$$

4.2.2.2 Transition 2 – Main Clutch and CL1 Open and Engine On

This transition mode often occurs when dog clutch for current gear is disengaged and dog clutch for new gear has not been engaged during gearshift. Although engine is on, vehicle is still driven exclusively by motor. Synchronizer for new gear is pushed toward gear to eliminate speed gap between synchronizer and target gear. Synchronizer is a combination of cone friction and dog clutch. Cone friction serves to synchronize speeds and dog clutch serves to lock new gear to shaft as speed gap is eliminated. Compared to transition 1, transition 2 involves neither engine torque nor main clutch in speed synchronization.

$$\begin{cases} (\overline{J_{ext}} + \overline{J_{is2}}.i_{2o}^2).\dot{\omega_{os}} = \overline{T_m}.i_{2o} - F_r \times R_w \\ \overline{J_{is1}}.\dot{\omega_{is1}} = T_{sync1}/i_{1o} \\ \omega_{is2} = \omega_{os} \times i_{2o} \\ J_e.\dot{\omega_e} = T_e \\ T_c = 0 \end{cases} \quad (4.13)$$

4.2.2.3 Transition 3 – Main Clutch Slipping and Engine On

This mode is typically used for inertia phase of vehicle launch on conventional vehicle. In addition, the kinetic friction of main clutch also helps to drive vehicle during inertia phase of gearshift. In this type of hybrid vehicle, motor can drive vehicle and make this mode less important. Motor is rigidly linked to vehicle via locked CL2. Engine drives or drags vehicle via friction torque of main clutch that slips.

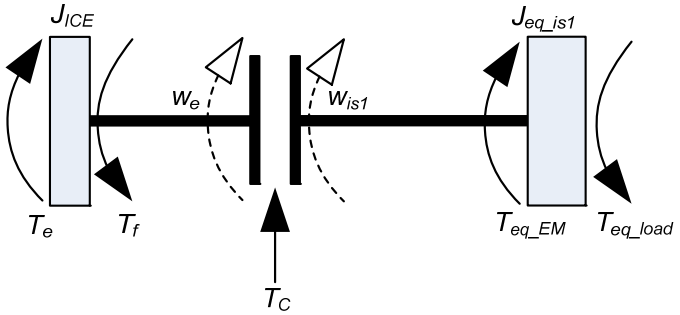

Figure 4-5 Scheme of dynamics relationship in TGF – main clutch open

$$\begin{cases} (\overline{J_{ext}} + \overline{J_{is1}}.i_{1o}^2 + \overline{J_{is2}}.i_{2o}^2).\dot{\omega_{os}} = T_c.i_{1o} + \overline{T_m}.i_{2o} - F_r \times R_w \\ \omega_{is1} = \omega_{os}.i_{1o} \\ \omega_{is2} = \omega_{os}.i_{2o} \\ J_e.\dot{\omega_e} = T_e - T_c \\ T_c = \mu.N.F_c.R_{eff}.sign(\omega_e - \omega_{is1}) \end{cases} \quad (4.14)$$

4.2.2.4 Transition 4 – CL2 Unlocked

This transition mode is used during gearshift for motor. Engine drives vehicle via locked main clutch and CL1. Speed of input shaft 1 is proportional to output speed; engine and input shaft share rotation speed via locked main clutch. Motor speed control enables this speed-synchronization process quite fast and smooth, even without friction clutch helping eliminating speed gap. Transmitted torque via main clutch does not exceed torque capacity.

$$\begin{cases} (\overline{J_{ext}} + (\overline{J_{is1}} + J_e).i_{1o}^2).\dot{\omega_{os}} = T_e.i_{1o} - F_r \times R_w/i_0 \\ \omega_{is1} = \omega_{os}.i_{1o} \\ \overline{J_{is2}}.\dot{\omega_{is2}} = \overline{T_m} \\ \omega_e = \omega_{is1} \\ T_c = T_e - J_e.\dot{\omega_{os}}.i_{1o} \\ -\mu.N.F_c.R_{eff} < T_c < \mu.N.F_c.R_{eff} \end{cases} \quad (4.15)$$

These two steady modes and four transition modes are combined in various driving scenario to achieve good fuel economy, driveability and performance. Specifically, two steady modes are critical to fuel economy; four transition modes determine driveability; performance, primarily vehicle acceleration, relies on both steady modes and transition modes (fast and smooth gearshifts and mode transition).

4.3 Powertrain Dynamics during EV-HEV Transition

EV-HEV mode transition is another important transient event that has obvious impact against driveability. This transition occurs when one of multiple trigger conditions is met. For example, SOC of battery falls below threshold value or torque/power demand exceeds capacity of electric system. Powertrain dynamics during this mode transition is simplified as the scheme in Figure 4-6.

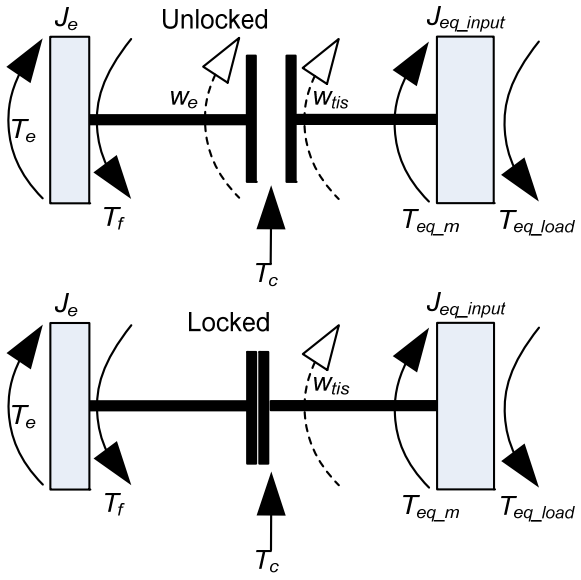

Figure 4-6 Scheme of dynamics relationship during EV-HEV mode transition

During this mode transition, any gearshift is prohibited by control strategy, so all rotational inertias as well as vehicle mass in Figure 4-1 are reduced to input shaft of transmission as a single moment of inertia J_{eq_input}, whose calculation formula is in equation (4.16).

$$J_{eq\_input} = \frac{\frac{M_v R_w^2 + 4J_w}{i_o^2} + J_{os} + (J_m i_m^2 + J_{is2}) i_{2o}^2}{i_{1o}^2} + J_c + J_{is1} \tag{4.16}$$

$$T_{eq\_load} = \frac{F_r . R_w}{i_0 i_{1o}} \tag{4.17}$$

$$T_{eq\_em} = \frac{T_m . i_{\mathrm{m}} . i_{1o}}{i_{1\mathrm{o}}} \tag{4.18}$$

$$\omega_{tis} = \frac{V}{R_W} i_{1o} . i_0 \tag{4.19}$$

Depending on active clutch state, the dynamic system described in Figure 4-6 can have 2 DOFs or 1DOF. As main clutch is open or slipping, the dynamic system can be expressed in equation (4.20). When main clutch is locked, torques from engine and motor drive vehicle together, like shown in equation (4.21)

$$\begin{cases} T_{\mathrm{e}} - T_C - T_f = J_e \dot{\omega}_e \\ T_C + T_{eq\_em} - T_{eq\_load} = J_2 \dot{\omega_{tis}} \end{cases} \tag{4.20}$$

$$T_e + T_{eq\_em} - T_f - T_{eq\_load} = (J_{eq\_input} + J_e) \dot{\omega_{tis}} \tag{4.21}$$

4.4 Post-Trans PHEV Model for Optimal Control of Mode Transition

Both TGF and EV-HEV mode transition refers to coordinated control of engine, motor, main clutch and gearbox as well as several actuators for gear selector. There are unlimited possibilities for this hybrid system. In addition, EV-HEV mode transition and TGF shares 3 identical phases. Therefore, a systematic analysis for mode transition is not only beneficial for powertrain control during mode transition, but also helpful for TGF feature during gearshift in HEV mode. Different research methods were proposed [127] [128]. Here, an optimization algorithm based on one simplified hybrid model is used to systematically analyze mode transition. Since other phases except for the last 3 are not part of mode transition, one post-transmission PHEV is modeled to reveal essence of mode transition.

4.4.1 Overview of Post-Trans PHEV Model

The powertrain layout of post-trans PHEV is shown in Figure 4-7. Compared to conventional two-wheel-drive (2WD) vehicle, this powertrain is added an extra traction motor EM and bigger battery package (second row). Torques from engine and EM are merged at point behind transmission to propel vehicle cooperatively or separately. Initially engine state is off and clutch

disengaged, and the EM can extract electric energy stored in battery package to propel vehicle in EV driving mode. Engine can be launched by EM via careful control of clutch pressure and EM as EM continues to output torque to wheels [37]. Since engine start-up is not within research scope of this work, engine is turned on by a regular starter. Vehicle propulsion controller (VPC) will send demands to engine, EM and clutch to implement mode transition. This model assumes environment temperature is 298K, lateral and vertical vehicle dynamics are not included. Since there is no real PHEV powertrain, parameters are from different sources. Parameters of vehicle and electric motor are from the series-parallel PHEV based on Chevrolet Malibu developed by University of Victoria ECOCAR team, shown in Table 4-3. Engine parameters, including moment of inertia and response time, are from ASM model of dSPACE; Characteristic curve of the engine, transmission gear ratios and clutch parameters are from built-in model of AUTONOMIE.

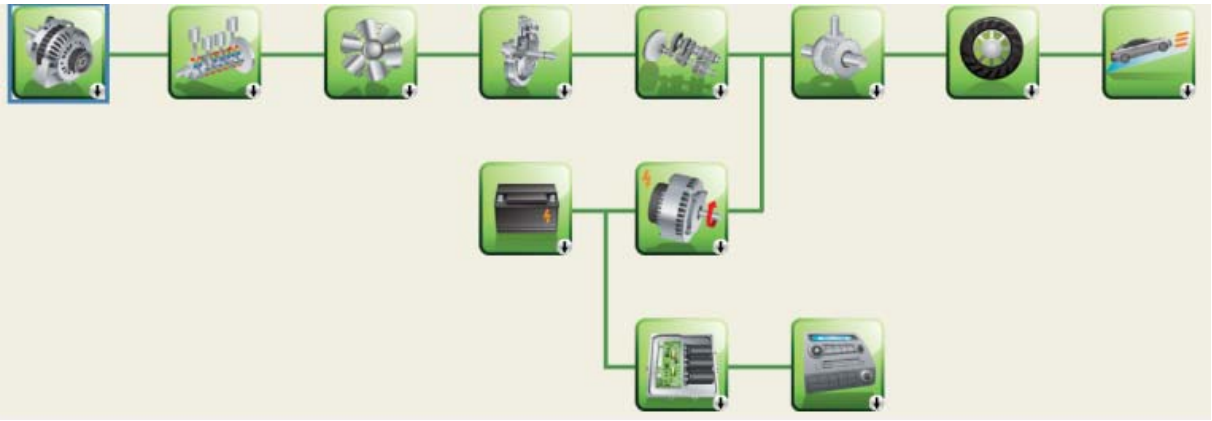

Figure 4-7 Architecture of Post-transmission PHEV

Table 4-3 Primary vehicle parameters of post-trans model

M (Curb weight)	1,564KG
C_d (Air drag coefficient)	0.295
A (frontal area)	$2m^2$
R_w (wheel radius)	0.336m
f_w (wheel friction coefficient)	0.01
GR_d (differential gear ratio)	2.89

This powertrain consist of ICE, traction motor, AMT with one dry clutch, differential and wheels. Here engine and clutch models are paid more attention because these two components feature nonlinearity and/or discontinuity, while EM dynamics is ignored due to its fast response.

Engine model accuracy is one of key factors for this model-based research. Considering that mode transition generally takes place within a couple of second and that fuel consumption map, emissions as well as thermal dynamics modules are not directly relevant to this research, the engine model is reduced to a dynamics block represented by a first-order system. The response

time of this engine model, τ_e, is set as 0.3 second, according to another detailed built-in gasoline engine model of dSPACE and above-mentioned series-parallel PHEV. Meanwhile, engine is assumed warm, so both maximum torque $T_{ICE_{max}}(\omega)$ and friction torque T_f are determined by rotational speed, as shown in Figure 4-8.

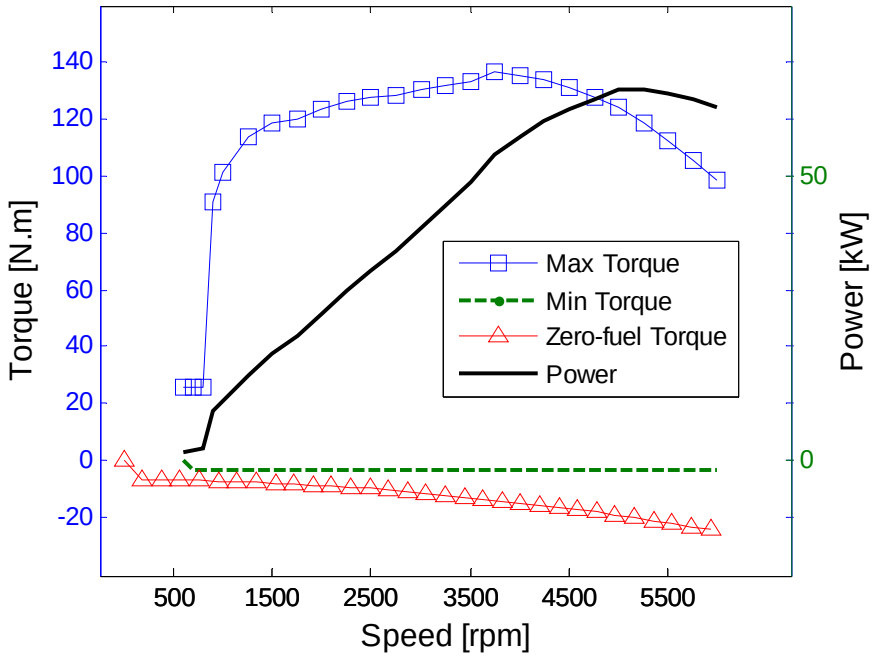

Figure 4-8 Engine characteristics

Although this powertrain model will be different from HAMT-based hybrid system that will be illustrated in detail in following chapter, the essence about mode transition as well as control principle are shared with our research subject. In addition, the optimal control of powertrain system will also help to verify analysis covered in section 4.3

4.5 Methodology of Optimization

This section will introduce how to optimize inputs of engine, clutch and motor to achieve 'optimal' driveability. Generally speaking, this process includes three steps: model discretization, formulation of objective function and implementation of Dynamic Programming. However, this regular procedure needs to be modified to solve this optimization problem here.

4.5.1 Model Discretization

Model discretization, including state space discretization and control space discretization, is a critical step to convert a continuous problem into a discrete problem. Many researchers have presented this process for under-actuated and fully actuated system [37] [86] [129]. These two types of systems have no less state variables than control variables, meaning corresponding control variables for two state points are uniquely determined. However, there would be unlimited combination of control inputs to realize the same change of states in over-actuated system, like this powertrain model during mode transition.

One more state variable influenced by control inputs is needed to construct determined relationship between control inputs and states. Due to engine has apparently longer response time than EM, engine torque is additional variable. Now the system has three control inputs (T_{e_cmd}, T_c and T_m) and three state variables (ω_e, ω_{tis} and T_e), as equation (4.22). In order to unify expressions in both slipping and sticking status, the clutch torque T_c, rather than clutch command φ_c, is chosen as one of control variables.

$$\begin{cases} X = [\omega_e \quad \omega_{tis} \quad T_e] \\ U = [T_{e\_cmd} \quad T_c \quad T_m] \\ \dot{X} = F(X, U) \end{cases} \tag{4.22}$$

By combining equations (4.16) to (4.20) and first-order formula for ICE, state-space equation of powertrain during mode transition is summarized as linear equation (4.23). The locked state expressed in equation (4.21) is covered as a special case, whose φ_c represents the minimum clutch command to lock clutch. Therefore, powertrain system in both slipping and sticking status is a linear system. It should be noted that this formula does not reflect the discontinuity of slip-stick process or sign change of relative speed.

$$\begin{aligned} \dot{X} = &\begin{bmatrix} 0 & -1/J_e & 0 \\ 0 & 1/J_{eq\_input} & \dfrac{i_1}{i_2 . J_{eq\_input}} \\ 1/\tau_e & 0 & 0 \end{bmatrix} U \\ &+ \begin{bmatrix} 0 & 0 & 1/J_e \\ 0 & 0 & 0 \\ 0 & 0 & -1/\tau_e \end{bmatrix} X + \begin{bmatrix} 0 & -1/J_e \\ -1/J_{eq\_input} & 0 \\ 0 & 0 \end{bmatrix} \begin{bmatrix} T_{eq\_load} \\ T_f \end{bmatrix} \end{aligned} \tag{4.23}$$

4.5.2 Linear Discretization

Direct discretization of state and control spaces is not an efficient approach in dealing with this problem. Firstly, there are total six continuous variables for discretization here. According to curse of dimensionality, computation efforts of DP increase exponentially with dimension of system. In addition, it is very hard to harmonize 6 variables to guarantee that each calculated new state point would rest at grid point precisely, which consequently produces huge number of interpolations and further increases computation efforts.

Linearity in slipping and sticking states guarantees that control inputs can be uniquely calculated from two sequential states as long as time step is small enough. In real vehicle and dyno tests, sampling interval of 0.1 second is qualified for most signals, except some fast-changing signals like engine cylinder pressure. Here we also use 0.1 second as interval for linear discretization. The derivative of state is substituted by difference, as shown in equation (4.24), where Δt is 0.1 second. The original state-space equation is converted to equation (4.25). This new algorithm can bring several benefits: (a) eliminating the need to grid control space; (b) ensuring each state is right at grid point and avoid interpolation; (c) precluding unqualified state grid points to further reduce calculation efforts; (d) introducing matrix expression of state and control variables greatly

accelerates calculation process in MATLAB. Model discretization also brings one new problem: engine speed and transmission input shaft speed might not be equal absolutely at any moment. Thus, a narrow 'sticking' region is assumed to exist where tiny relative rotation is ignored. As $\Delta\omega$ maintains within the range at two consecutive points, clutch is seen as in sticking state during the interval; otherwise, clutch is regarded as in slipping state during the whole time step. Another advantage of this method is to extend equation (4.25) to stick-slip process, which only happens at beginning/end of a time interval.

$$\dot{X} = \frac{X_{k+1} - X_k}{\Delta t} \tag{4.24}$$

$$\begin{aligned} U = & \begin{bmatrix} 0 & 0 & 1 - \tau_e/\Delta t \\ J_e/\Delta t & 0 & 1 \\ -J_e i_1/(i_2 \Delta t) & -J_{eq\_input} \cdot i_1/(i_2 \Delta t) & -i_1/i_2 \end{bmatrix} X_k \\ & + \begin{bmatrix} 0 & 0 & \tau_e/\Delta t \\ -J_e/\Delta t & 0 & 0 \\ J_e i_1/(i_2 \Delta t) & J_{eq\_input} \cdot i_1/(i_2 \Delta t) & 0 \end{bmatrix} X_{k+1} \\ & + \begin{bmatrix} 0 & 0 \\ 0 & -1 \\ i_1/i_2 & i_1/i_2 \end{bmatrix} \begin{bmatrix} T_{eq\_load} \\ T_f \end{bmatrix} \end{aligned} \tag{4.25}$$

Since clutch torque is related to both current relative speed $\Delta\omega_{\mathrm{k}}$ and following one $\Delta\omega_{\mathrm{k+1}}$, 9 cases are summarized in Table 4-4. Equation (4.25) is applicable in all of the 9 cases, except the 8th and 6th cases, in which sign of relative speed of clutch changes between two state points and conflicts with prerequisite of Equation (4.25). So, the two cases should be analyzed separately.

Table 4-4 Classification of clutch torque calculation

	$\mathrm{abs}(\Delta\omega_{\mathrm{k+1}}) < \omega_{thre}$	$\Delta\omega_{\mathrm{k+1}} < -\omega_{thre}$	$\Delta\omega_{\mathrm{k+1}} > \omega_{thre}$
$\mathrm{abs}(\Delta\omega_{\mathrm{k}}) < \omega_{thre}$	①	②	③
$\Delta\omega_{\mathrm{k}} < -\omega_{thre}$	④	⑤	⑥
$\Delta\omega_{\mathrm{k}} > \omega_{thre}$	⑦	⑧	⑨

The process of case 6 & 8 can be illustrated by Figure 4-9. As speed difference between engine flywheel and clutch disc is from positive (negative) infinitesimal to negative (positive) infinitesimal, clutch torque is reversed in direction but keeps magnitude. Detailed mathematical expression is given in equations 4.26-4.28, which eventually produces a quadratic equation. Detailed results are not listed here due to its length. It should be noted that the narrow 'sticking' region is ignored here.

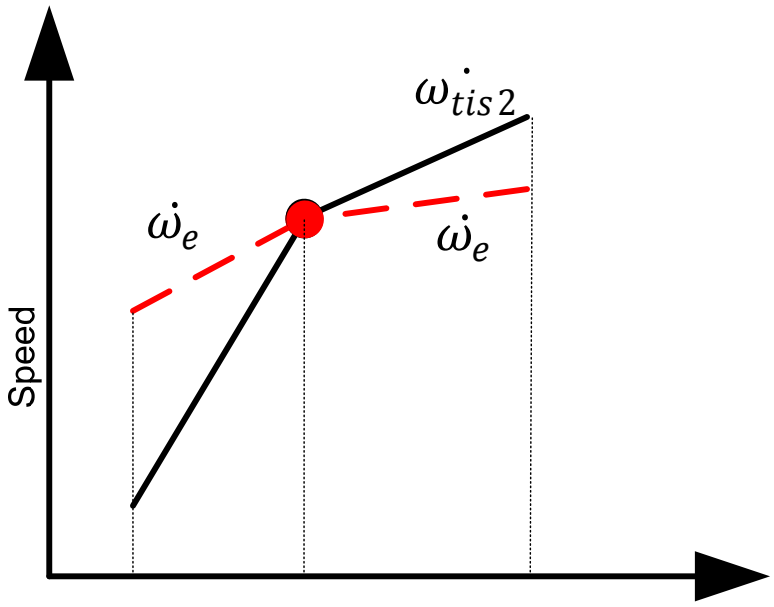

Figure 4-9 Process of sign change of clutch slipping speed

$$\begin{cases} T_e - T_c - T_f = J_e\dot{\omega}_e \\ T_c + T_{eq\_em} - T_{eq\_load} = J_2\dot{\omega}_{tis1} \\ \omega_e(k) - \omega_{tis}(k) = -(\dot{\omega}_e - \dot{\omega}_{tis1}).\Delta t1 \end{cases} \tag{4.26}$$

$$\begin{cases} T_{e1} + T_c - T_f = J_e\dot{\omega}_e \\ -T_c + T_{eq\_em} - T_{eq\_load} = J_2\dot{\omega}_{tis2} \\ \omega_e(k+1) - \omega_{tis}(k+1) = (\dot{\omega}_{e2} - \dot{\omega}_{tis2}).\Delta t2 \end{cases} \tag{4.27}$$

$$\begin{cases} \dot{\omega}_{e1}\Delta t1 + \dot{\omega}_{e2}\Delta t2 = \omega_e(k+1) - \omega_e(k) \\ \Delta t1 + \Delta t2 = \Delta t \end{cases} \tag{4.28}$$

4.5.3 Problem Formulation and Optimization Algorithm

Driveability during mode transition is a comprehensive and subjective index for driver. The key element of driveability metrics should be change of acceleration, which can be transferred to a value according to different transfer function. For example, FEV Group developed software 'FEVos' to evaluate shift quality that converts sequential accelerations into indexes via two functions [57]. Other direct transfer functions include vehicle jerk (derivative of vehicle acceleration) and maximum acceleration fluctuation ($a_{max} - a_{min}$) [130] [53]. In addition to acceleration change, mode transition should also be subject to some constraints, like duration and generated heat by clutch friction. Heat is an important killer of dry clutch.

The objective function can be in different forms, single-objective or multiple-objective optimization under constraints. One proposed objective function is as equation (4.29). The first item stands for total duration for speed synchronization. When relative speed is still out of 'sticking' region of clutch, sum will be added 1, otherwise, sum will be the same with previous value; the second item means weighted torque synchronization. When motor torque T_m drops

forward target motor torque T_{m_tgt}, the penalty will be decreased; the third item represents acceleration fluctuation. Since only average acceleration within current interval can be calculated from vehicle speed, absolute difference between acceleration and the target value is used as an index of acceleration change. Ideally, vehicle acceleration will be equal to reference acceleration; the fourth item is weighted friction loss of clutch during the whole process. Since control inputs can be calculated directly using Equations (4.25) – (4.28) and acceleration is also easy to obtain. Therefore, the objective is a function of current state X_k and next state X_{k+1}, as shown in equation (4.29). $\omega_e(t)$ is engine speed, $\omega_{tis}(t)$ is transmission input shaft speed, ω_{thre} is threshold slip speed (smaller than ω_{thre} is considered as locked), T_m is motor torque, T_{m_tgt} is target motor torque, $a(t)$ is vehicle acceleration, a_{tgt} is target acceleration that is calculated from pedal. The item 1 of objective function is duration of clutch slip, item2 is used to force motor torque drop and penalize motor torque fluctuation, item 3 is to penalize vehicle acceleration fluctuation, item 4 is totally heat loss during mode transition that serves to protect clutch.

$$\begin{aligned}\text{Minimize } \mathcal{H} = \sum_{k=1}^{N} h(X_k, X_{k+1}) = \sum_{k=1}^{N} \{1 \times (|\omega_e(t) - \omega_{tis}(t)| > \omega_{thre}) + \alpha \\ \times |T_m - T_{m\_tgt}| + \beta \times |a(t) - a_{tgt}| + \gamma \\ \times (\omega_e(t) - \omega_{tis}(t)).T_c\}\end{aligned} \tag{4.29}$$

$$\textit{Subject to: } \begin{cases} 0 \le T_e(\omega) \le T_{e_{max}}(\omega) \\ T_e(t_0) - T_f = 0 \\ \omega_e(t_0) = 800\ rpm \\ T_{m_{min}}(\omega) \le T_m(\omega) \le T_{m_{max}}(\omega) \\ T_c(t_0) = 0 \\ 0 \le \varphi_c \le 1 \end{cases}$$

Dynamic Programming is adopted to solve this optimization since DP a method of breaking a complex optimization problem into many simpler sub-problems that seeks the optimal solution by reiterative usage of principle of optimality. It can easily deal with different nonlinear problems with multiple constraints. Since control vector U is a result of X_k and X_{k+1}, computation of this optimization problem follows an algorithm without any control inputs [114].

Algorithm:

Step N-1

For $1 \le p \le L$

$$\bar{\mathcal{H}}_{N-1}(X(p)) = \min\{h(X(p), X_{k+1})\} \tag{4.30}$$

End

Step k, for $0 \le k < N - 1$

For $1 \leq p \leq L$

$$\bar{\mathcal{H}}_k\,(\mathrm{X(p)}) = \min\{\mathrm{h(X(p)}\,, \mathrm{X_{k+1}}) + \bar{\mathcal{H}}_{k+1}\,(\mathrm{X_{k+1}})\} \tag{4.31}$$

End

End

Where $\boldsymbol{p}$ is index of state point, $\boldsymbol{L}$ is number of all state points in state space, X(p) is current state, X_{k+1} is a vector of all possible state at (k+1)th stage, $\bar{\mathcal{H}}_k\,(X(p))$ is the minimum cost from current $X(p)$ to terminal point.

Computation efforts of DP are proportional to number of time steps and square of number of state points. Since this problem has three state variables, it is quite necessary to apply all possible means to reduce computation efforts and avoid out of memory. One of important method is to construct cost table prior to implement to DP, rather than compute the table at every step. As long as the cost table includes all possible state point, the table will be reusable at each time step; another important measure is to use matrix to accelerate computation; other measures includes saving intermediate results, refreshing memory and judging components constraints in order and sparse matrixes.

4.6 Simulation & Results

4.6.1 Simulation

Simulation starts with SIMULINK model that runs in a UDDS cycle. The first mode transition occurs at the time of vehicle velocity equals to 11.38 m/s and acceleration to 1.25 m/s^2. So, initial vehicle speed and acceleration as mode transition happens are determined. This acceleration is also reference acceleration a_r during the whole process, which means that driver should not notice mode transition. After repeated simulation at different speeds and acceleration, various parameters and range of each state variable are determined, part of which are listed in Table 4-5. Total length of 2 seconds are considered to be sufficient to complete mode transition when initial speed of ICE is 84 rad/s (around 800 rpm); maximum engine torque is not feasible at low speed, but this range guarantees one cost table suits each stage of the duration; $\Delta\dot{\delta}$ is set as 2.5 rad/s; In order to avoid excessive torque synchronization, the target motor torque is assigned an value of 50 $N.m$.

Table 4-5 State variables and grid points

Stage (k)	Time	[0:0.1:2]s
Stage *(X)*	ω_{fw}	[84: 2.5: 166.5] rad/s
	ω_{tis}	[129: 0. 34: 164.6]
	T_{ICE}	[0: 2: 120] $N.m$

The most critical portion of this optimization is to establish cost table. Total state points in the 3-D space reach up to over 200,000, which means maximum number of X_k and X_{k+1} combinations will be over 40 billion (square of 200,000). As optimization proceeds, the cost table will keep expanding. It is extremely important to manage computer memory. Or else, the program will crash due to out of memory. The error can occur even if physical memory is still available because those memories are too scattered to save the big and expanding cost table. In order to overcome this issue, count of variables should be minimized; furthermore, it is necessary to keep monitoring memory usage (MATLAB provides such feature). Furthermore, calculation results in MATLAB workspace should be saved and cleaned as long as memory warning shows up. This step helps to fresh memory. Finally, saved calculation results need to be reloaded into workspace. After cost table is established, DP can easily establish optimal trajectory of each state variable and corresponding control inputs at each step.

It should be particularly emphasized that optimal control trajectories at each state point are stored in matrix format. As a result, as long as starting point is determined, following state point will be reached via the optimal control inputs. The procedure is repeated. This is extremely important advantage of this DP algorithm since the cost table can also be used to search optimal state and control trajectories as long as starting point and terminal are inside the state space.

4.6.2 Results of Optimal Mode Transition

Figure 4-10 – 4.15 show four items of objective function; Figure 4-14 and Figure 4-15 present trajectories of three state variables; Figure 4-16 - Figure 4-18 are three control signals. By analyzing there trajectories, some important information can be sorted out. Coefficients of weight for four items of objective function is selected as [1 10, 0.1, 0.1] after many trials. Various simulations reveal some command features.

1) This method can find control inputs that enable vehicle acceleration almost identical with target acceleration, as shown in both Figure and Figure 4-14.

2) EM provides almost all torque before inertia phase ends, as shown in Figure 4-11 and Figure 4-17; so ICE just keep accelerating by itself to reduce duration of time interval; clutch almost keeps open since it does not transmit torque from one side to another, as shown in Figure 4-13.

3) As inertia phase is finished, clutch is engaged fast, as shown in Figure 4-18; meanwhile, apparent overshoot of engine speed and sign change of clutch torque are avoided, as show in Figure 4-10 and Figure 4-14.

4) Torque phase starts after clutch is locked faster. Figure 4-11 and Figure 4-17 prove that clutch and motor torques are controlled to guarantee almost constant torque output. This perfect torque cancellation method is used by previous research as an assumption without proof [37]. The fundamental reason allowing perfect torque cancellation is fast and precise response of clutch and motor.

These 4 points extracted from optimal powertrain control are aligned with the control principle introduced in section 4.3. This control principle is also shared by TGF feature. A rule-based control algorithm using this control principle will be introduced in detail.

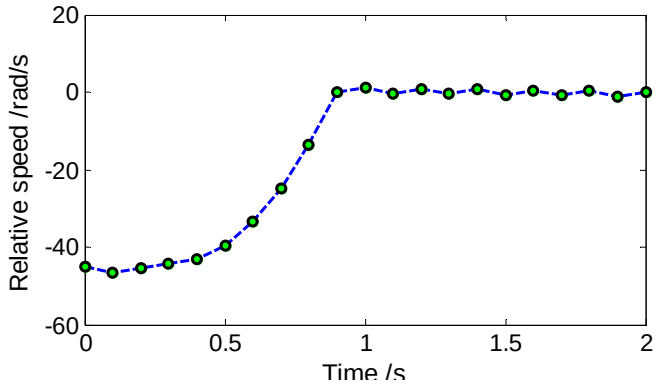

Figure 4-10 Speed synchronization

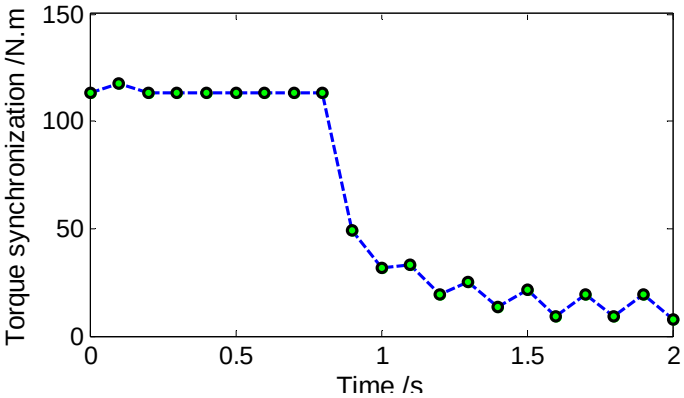

Figure 4-11 Motor torque

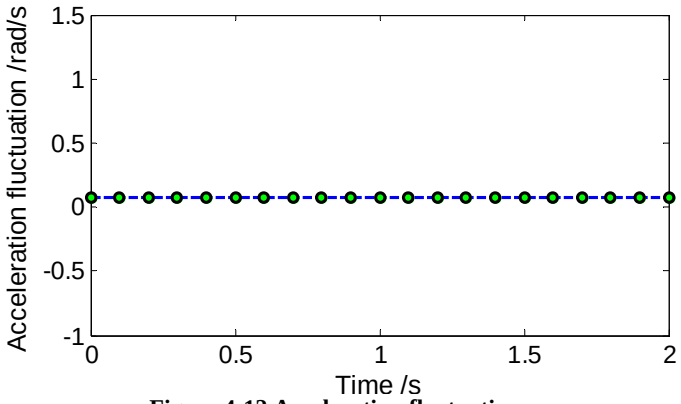

Figure 4-12 Acceleration fluctuation

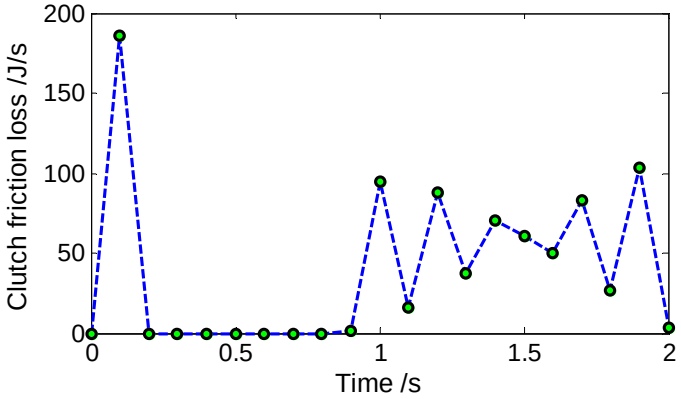

Figure 4-13 Friction loss of clutch

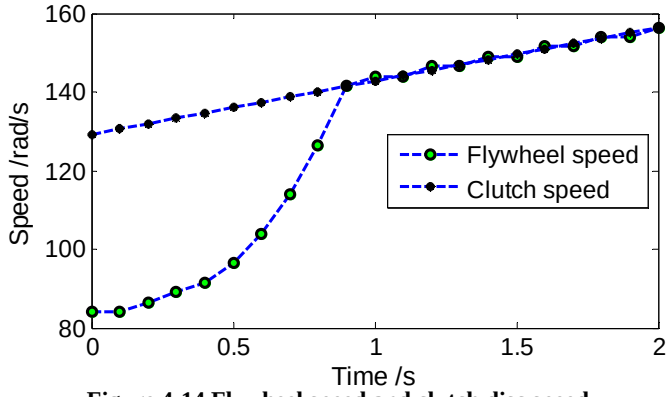

Figure 4-14 Flywheel speed and clutch disc speed

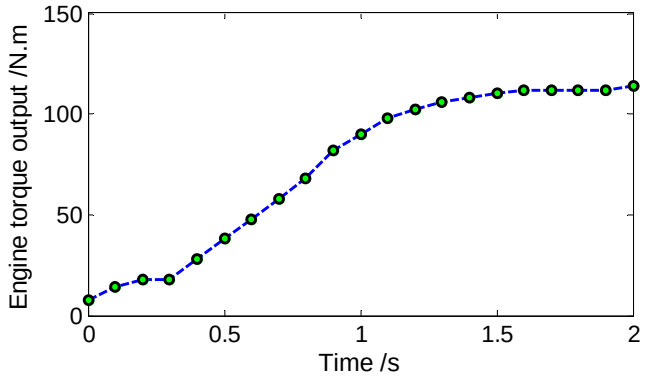

Figure 4-15 Engine torque output

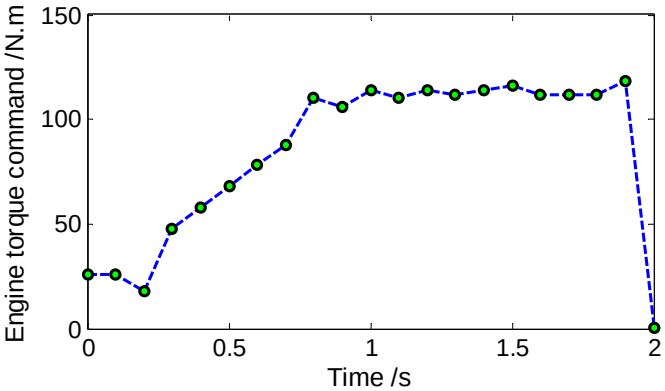

Figure 4-16 Engine torque command

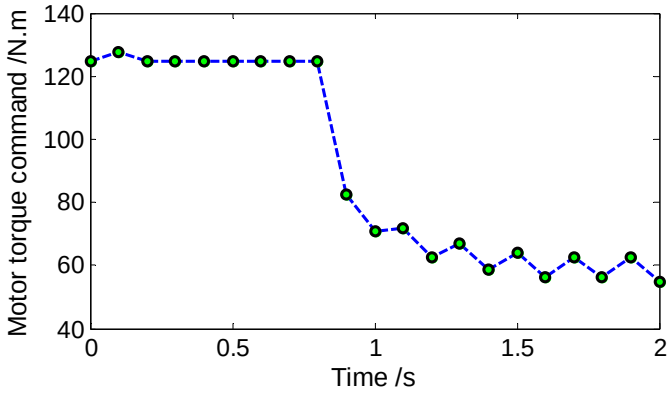

Figure 4-17 Motor torque command

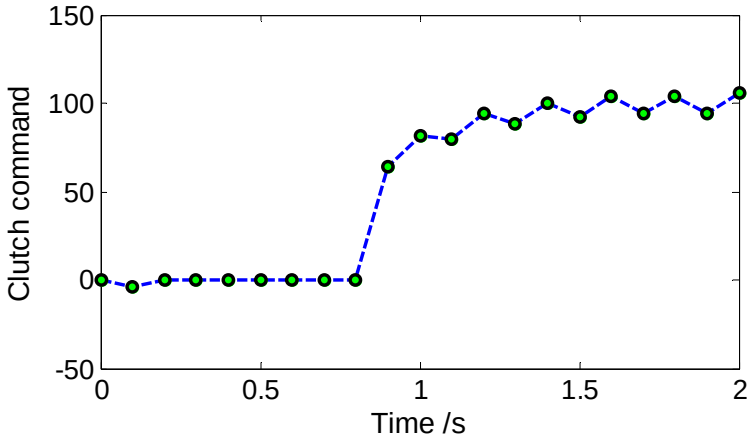

Figure 4-18 Clutch torque command

4.7 Rule-Based EV-HEV Mode Transition Control

Based on the results of DP-based global optimization of EV-HEV mode transition, a rule-based mode transition control strategy is extracted. Figure 4-19 shows fundamental principle of EV-HEV mode transition. This mode transition is split into 2 phases: inertia phase and torque phase. Before EV-HEV mode transition really takes effect, engine should be started and even warmed up for controlling exhaust emission. Since engine start-up prior to mode transition is not among research topics, it is assumed engine maintains idle speed. Motor exclusively propels vehicle with main clutch open.

a. Inertia phase: engine speed is controlled to overcome moment of inertia to reach target speed, which is actually rotation speed of input shaft. According to selected Coulomb friction model in equation (4.8), negative slip speed (engine speed lower input shaft speed) in inertia phase will generate negative torque, which will accelerate engine speed and reduces torque output of transmission. So, normal force on main clutch is controlled to be zero, so clutch does not transmit torque. At the end of inertia phase, slip speed is totally removed.
b. As speed gap of is eliminated, engine will undertake more load gradually. Simultaneously, torque from motor is reduced. As engine becomes primary contributor to propel vehicle, mode transition is finished. With increase of engine torque, torque capacity of main clutch is

increased correspondingly to maintain locked status. During the transient point between inertia phase and torque phase, inertia torque to accelerate engine should be reduced apparently to avoid overshoot of engine speed (main clutch unable to catch engine speed). To avoid this undesirable overshoot, engine torque should be controlled by controlling sparking time. More details will be covered in following chapters.

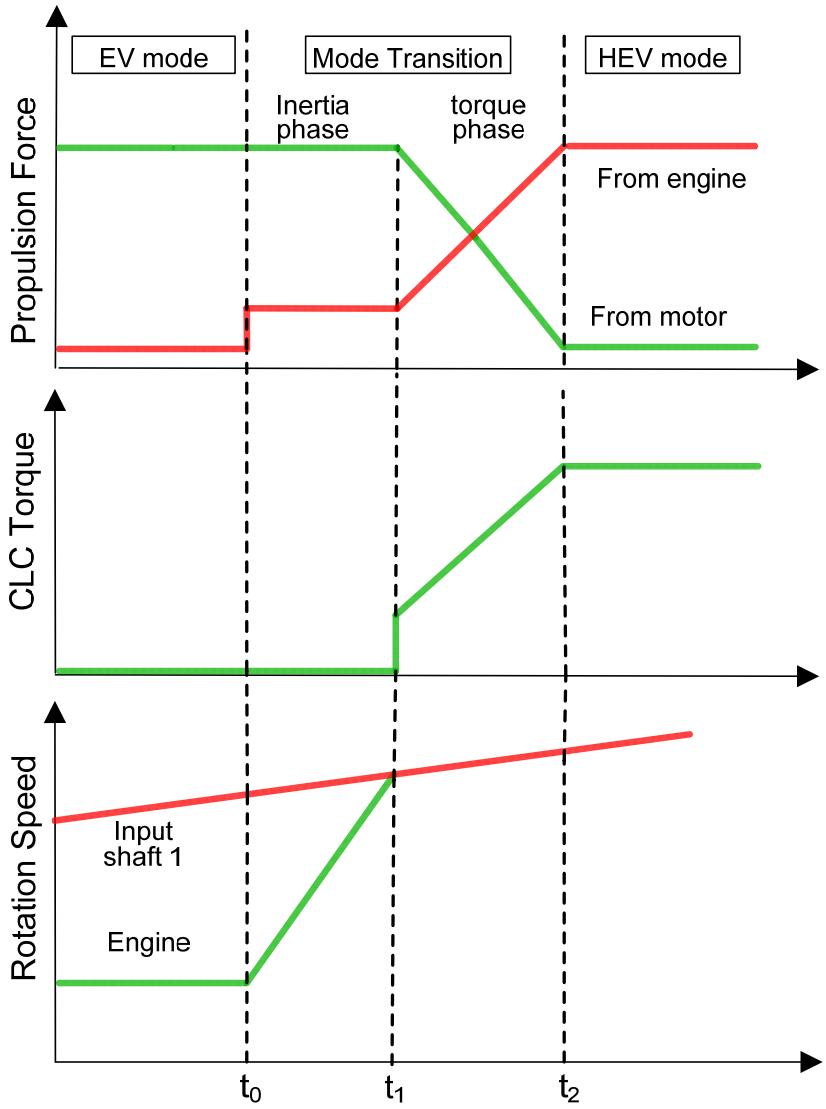

Figure 4-19 EV-HEV mode transition

The basic principle of mode transition process in Figure 4-19 is also summarized in Table 4-6 from aspect of fundamental operating modes. It can be seen that the 3 segments below are identical to the last 3 phases of Table 5-3 for TGF control.

Table 4-6 Decomposition of an EV-HEV mode transition

Time	Function	Operating mode
t_0 - t_1	Adjust engine speed to engage main clutch	Transition 1 or 3

t_1 - t_2	Reduce motor torque and increase engine torque	Steady 2
t_2 - t_3	Mode transition finished	Steady 2

4.8 Summary

This chapter starts with a lumped-mass model to describe driveline dynamics. As key elements of this hybrid system based on invented HAMT, clutch principle, selected clutch model as well as model of gear selector are described specifically. Driveline dynamics in two steady states and four transient states are analyzed using the LMM model. Each state is analyzed independently, according to states of main clutch as well as gear selectors. These operating modes in steady and transient states comprises of fundamental phases of both Torque-Gap-Filler feature and EV-HEV mode transition. Operating principle of TGF is first studied and decomposed into 7 sequential phases, which belong to the 4 transient operating modes and 2 steady operating modes. Each phase of TGF is explained. Then, another important driveability-related event, EV-HEV mode transition, is decomposed to study control principle. This mode transition is further split as 2 primary phases: inertia phase and torque phase, which are commonly used in automotive industry for analysis of conventional automatic transmission. In light of great importance of mode transition as well as its connection to TGF via common phases, a model-based optimization method is proposed to verify correctness of two control principles in session 5.3.2 and 4.3. This research work selects post-transmission parallel PHEV as subject to develop understanding of mode transition that is unique and significant for hybrid vehicles. The powertrain model was initially established based on AUTONOMIE and SIMULINK, and primary parameters are from real platform or ASM model of dSPACE. A state-space equation is built up first and model discretization is the key of whole method since it not only eliminates necessity of split control variables but also relates control inputs to system states in a matrix format, which greatly simplifies calculation of DP latter. Results of optimal control show 4 principles for clutch control, inertia phase and torque phase.

5 Powertrain Model and Control Logic

Simulation model can not only prove conceptual proposal with strong proof, but also help to look into details [131] [132]. As a step to verify this concept of HAMT, it is important to build a vehicle simulation focusing on gearshift and mode transition. This model consists of a driver model, VCC and powertrain model. Driver model is responsible to drive vehicle to follow target speed file or complete specific virtual tests; vehicle central controller (VCC) serves to distribute power between engine and motor according to driver demand and vehicle status; powertrain model is core of whole model in this research and includes whole HAMT-based hybrid system. Since this research subject is a new hybrid system with unique HAMT gearbox, no simulation software contains a built-in model to reach this verification and demonstration purpose. In order to focus on control and modeling of HAMT-based hybrid system, especially unique gearbox, a parallel post-transmission PHEV model from AUTONOMIE is selected as baseline vehicle model. This baseline vehicle model contains comprehensive and necessary components, providing an important base for this work. Due to gearbox uniqueness and higher requirement for powertrain-coordinated control, whole drivetrain system is replaced with new model to model the research subject; in addition, extensive modifications are made on control modular for clutch, engine and gearbox. This rule-based control strategy can help to enable model function fast, although there are varieties of control strategies [133] [134] [135] [136] [137]. The ultimate goal is to achieve smooth EV-HEV mode transition and Torque-Gap-Filler feature.

5.1 Introduction of Baseline Vehicle Model

The baseline model is a parallel post-transmission PHEV equipped with regular AMT. The model consists of a driver, VCC, environment and full powertrain including a simple gearbox.

5.1.1 Driver Model

The driver model in baseline model is a controller with feed-forward and feedback (PID) components. The feed-forward control consists of estimation of road load and inertia force. Road load is calculated based on target vehicle speed v_{tgt}. Although actual speed v_{act} is mostly different from target speed v_{tgt}, sufficient closeness makes the speed difference neglectible. Inertia force estimation is determined by target acceleration, which is calculated using target speed. How to estimate target acceleration is an important topic for driver, but it is not discussed in detail because driver model is not focus of this research. Feedback control is based on speed error. Sum of target inertia force, road load as well as feedback is sent to a first-order transfer function $G(s)$ that represents driver response and outputs force demand F_{dmd}. The F_{dmd} will be translated to pedal positions. If F_{dmd} is positive, accelerator pedal α_{accel}will be commanded and brake pedal; if F_{dmd} is negative, braking pedal α_{brake} will be commanded. The driver model based on feedforward estimation and feedback is shown in **Error! Reference source not found.**. Target speed and acceleration are converted to inertia force and road load demand; a PID

controller serves to supplement feedforward part. A first-order transfer function G(s) is used to filter upstream command.

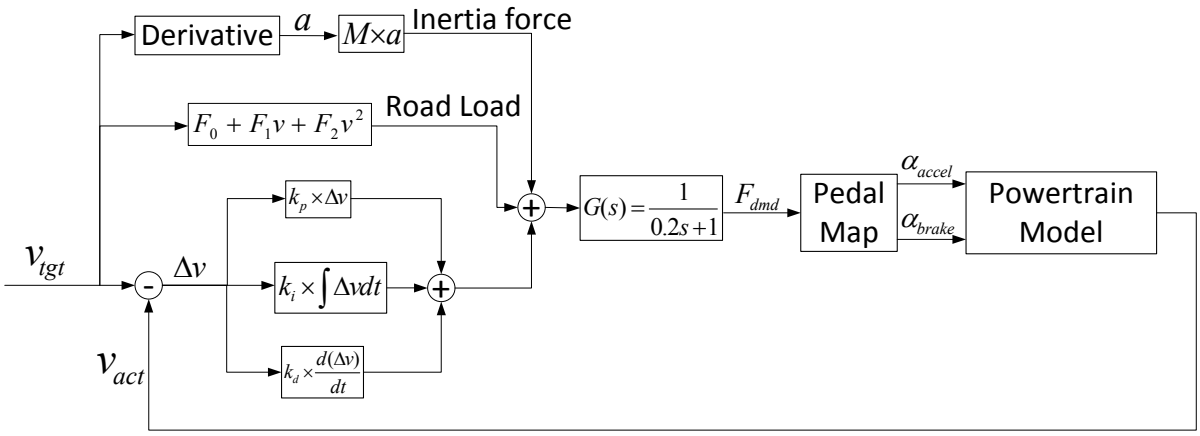

Figure 5-1 Internal algorithm of driver model

This driver can successfully control vehicle to follow target speed profile closely. Figure 5-2 shows comparison between an Urban Dynamometer Driving Schedule (UDDS) and actual vehicle speed achieved by the driver-vehicle combination. The closeness of two curves demonstrates capacity of this driver structure. Of course, how well the driver performs quantitatively and how to evaluate driver behavior are two important but not directly related topics to the research subject here. Therefore, discussion for the driver evaluation is not included.

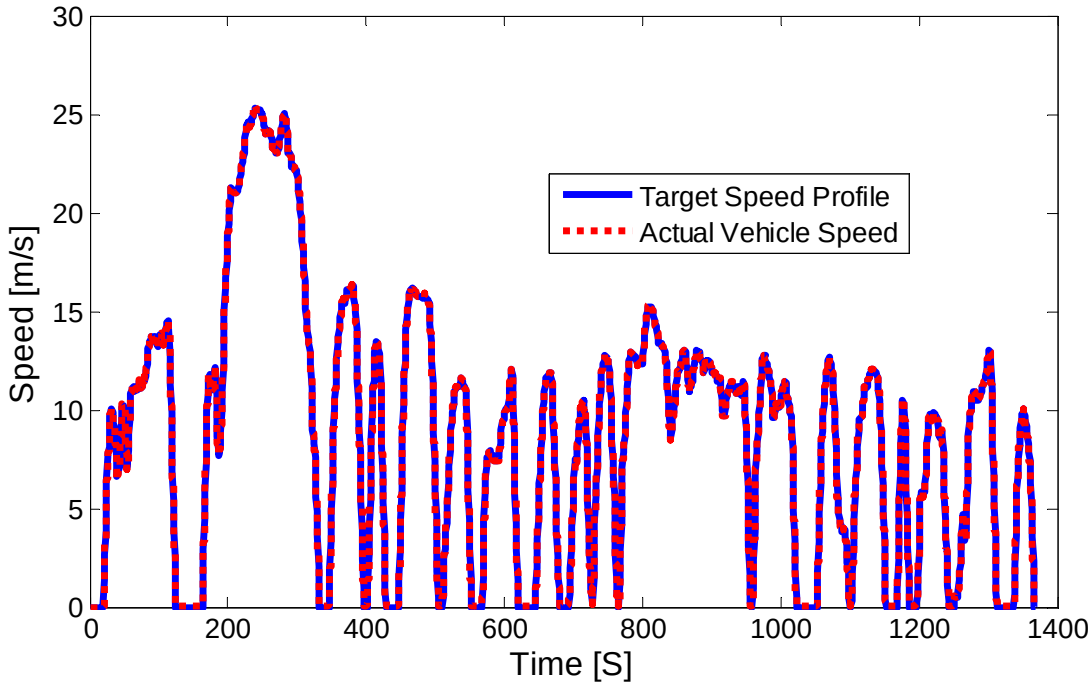

Figure 5-2 Target speed profile VS actual vehicle speed

5.1.2 Baseline Powertrain & Chassis Model

This sub-system model of post-transmission PHEV includes complete powertrain and chassis components, as shown in figure Figure 5-3. This powertrain model can work in either EV mode or HEV mode. As EV mode is active, clutch is open and engine is off. Therefore, motor drives vehicle exclusively or brakes vehicle via regenerative braking. In HEV mode, engine torque is transmitted to final drive via clutch and gearbox, which are often called as transmission as one unit; transmission output shaft combines torque from engine and motor. This combined torque is amplified by final driver and converted to propulsion force via friction between driving wheels and ground. Primary powertrain components (including starter, engine, clutch, gearbox, battery and motor) as shown in Figure 5-3, share the same basic model structure, like Figure 5-4.

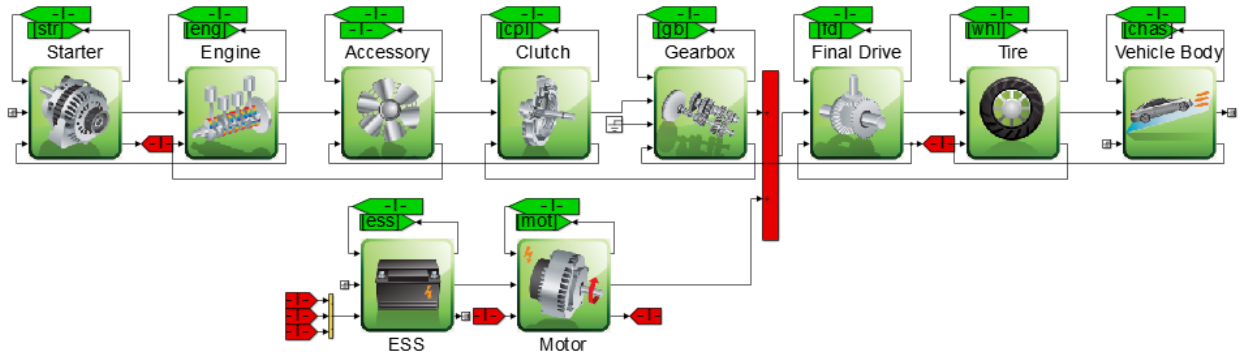

Figure 5-3 Layout of baseline hybrid powertrain

Each of those component models consists of a controller and plant model. The controller model serves to receive vehicle states and command from supervisory vehicle controller, and convert the commands to direct control signals to plant model. The plant model represents a virtual hardware of corresponding component. More details of each component will be introduced in subsection 5.2.

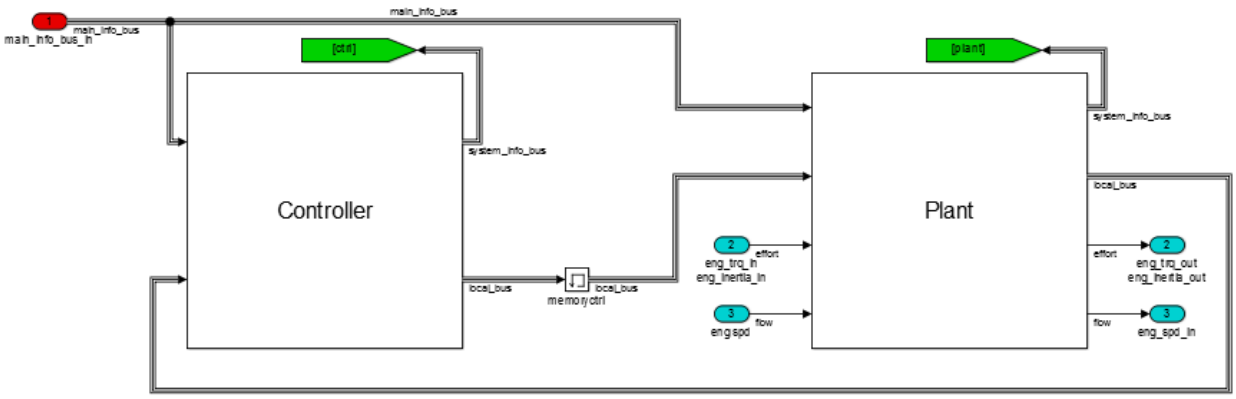

Figure 5-4 Basic model structure of powertrain components

5.1.3 Vehicle Central Controller

Driver commands together with vehicle states, like engine on/off state and battery SOC, are sent to supervisory controller, which determines if following engine/motor torque on/off states as

well as torque demand distribution between the engine and motor. VCC is modeled as finite-state machine using STATEFLOW. Primary blocks of VCC are shown in Figure 5-5. Two exclusive (OR) blocks are Stop_or_Brake block and gb_not_neutral block, which correspond to braking control and vehicle propulsion control. The second one is the key block of whole VCC and consists of two subsidiary blocks, which are responsible for powertrain control in EV mode and HEV mode. The key trigger of EV-HEV mode transition is start of engine as some conditions are met.

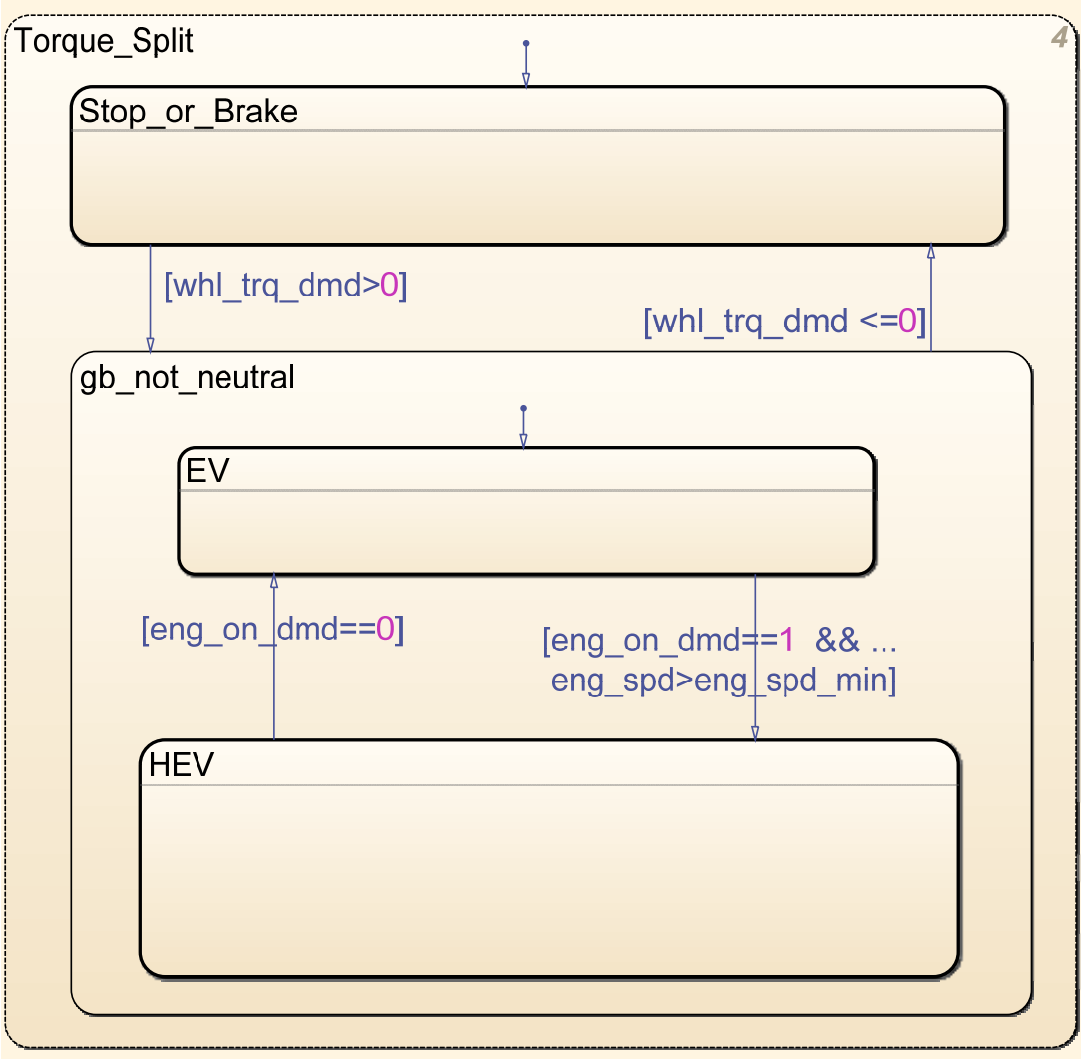

Figure 5-5 Two modes of vehicle central controller

The logic for turning on engine is shown in Figure 5-6. It contains 4 subsidiary states, which are two steady states (on and off) and two transient states (timers for EV-HEV transitions). Conditions for turning on engine include 1) SOC is lower than pre-defined threshold, like 25%; 2) engine power demand is above a threshold power of 25Kw; 3) motor torque demand is beyond torque capacity at the motor speed; and 4) accelerator pedal position is above 90%. As any of these conditions is met and HEV mode is allowed, engine will be turned on and maintained the state for at least a pre-defined period length. After engine is turned on and ECU controls engine

speed to a high speed, mode transition from EV mode and HEV mode will happen. This VCC algorithm pays no attention to driveability-related events, like gearshifts and mode transition. Therefore, many modifications are necessary to achieve feature of smooth mode transition and TGF during gearshift.

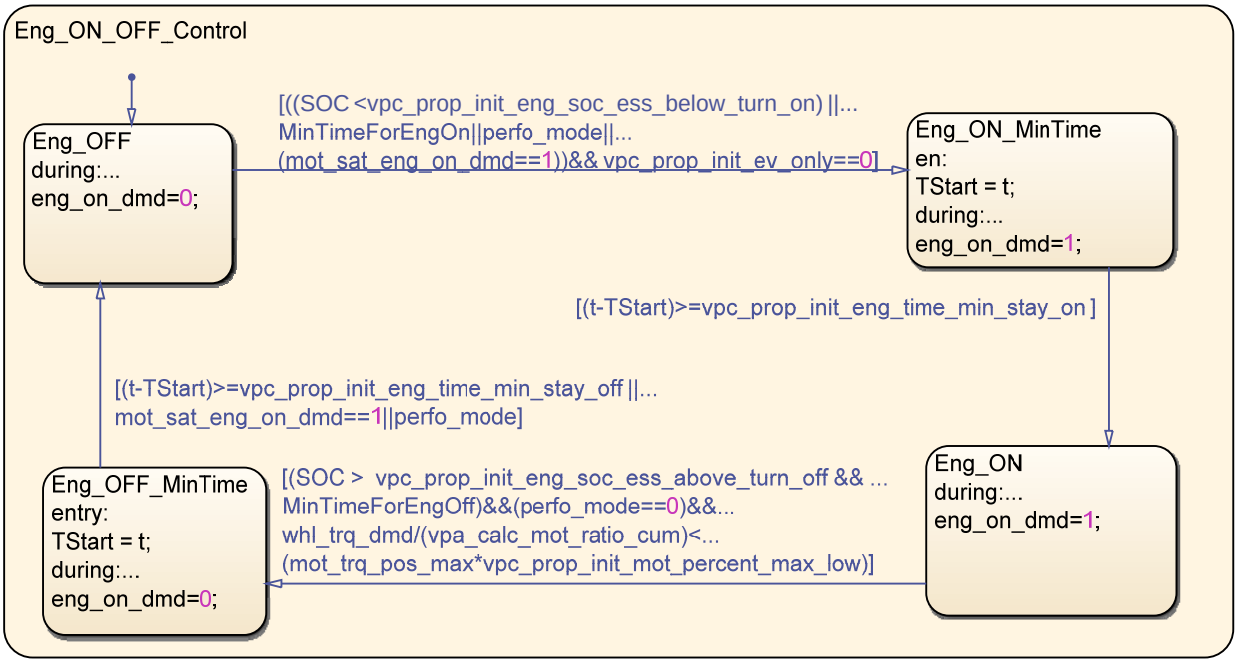

Figure 5-6 Engine on/off state control logic

Details of EV block in Figure 5-5 are shown in Figure 5-7. As other engine-trigger conditions do not prevail and motor can provide enough propulsion torque, EV mode will maintain active. As motor torque demand reaches its limit, engine will be required to take the load. In this logic, warm-up of catalysts for emission control is not considered.

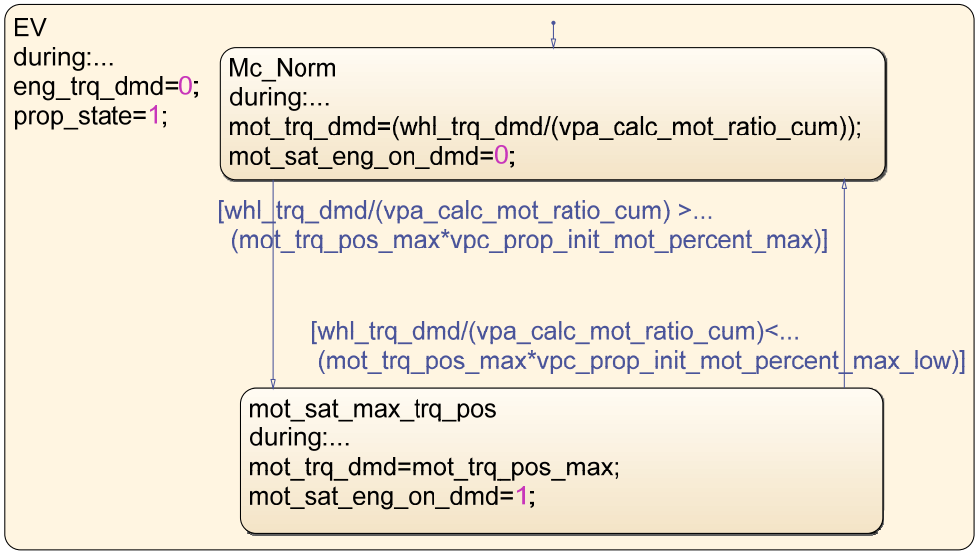

Figure 5-7 State flow for EV mode

In HEV mode, there are two subsidiary modes. The two subsidiary modes are normal driving mode and performance mode, as shown in Figure 5-8. In most of time, normal driving mode is the active one under HEV mode, except when driver depresses accelerator pedal aggressively to above 90% pedal percentage. When engine can provide enough torque to propel vehicle, the VSC will command engine as primary torque source, with motor as complementary torque source.

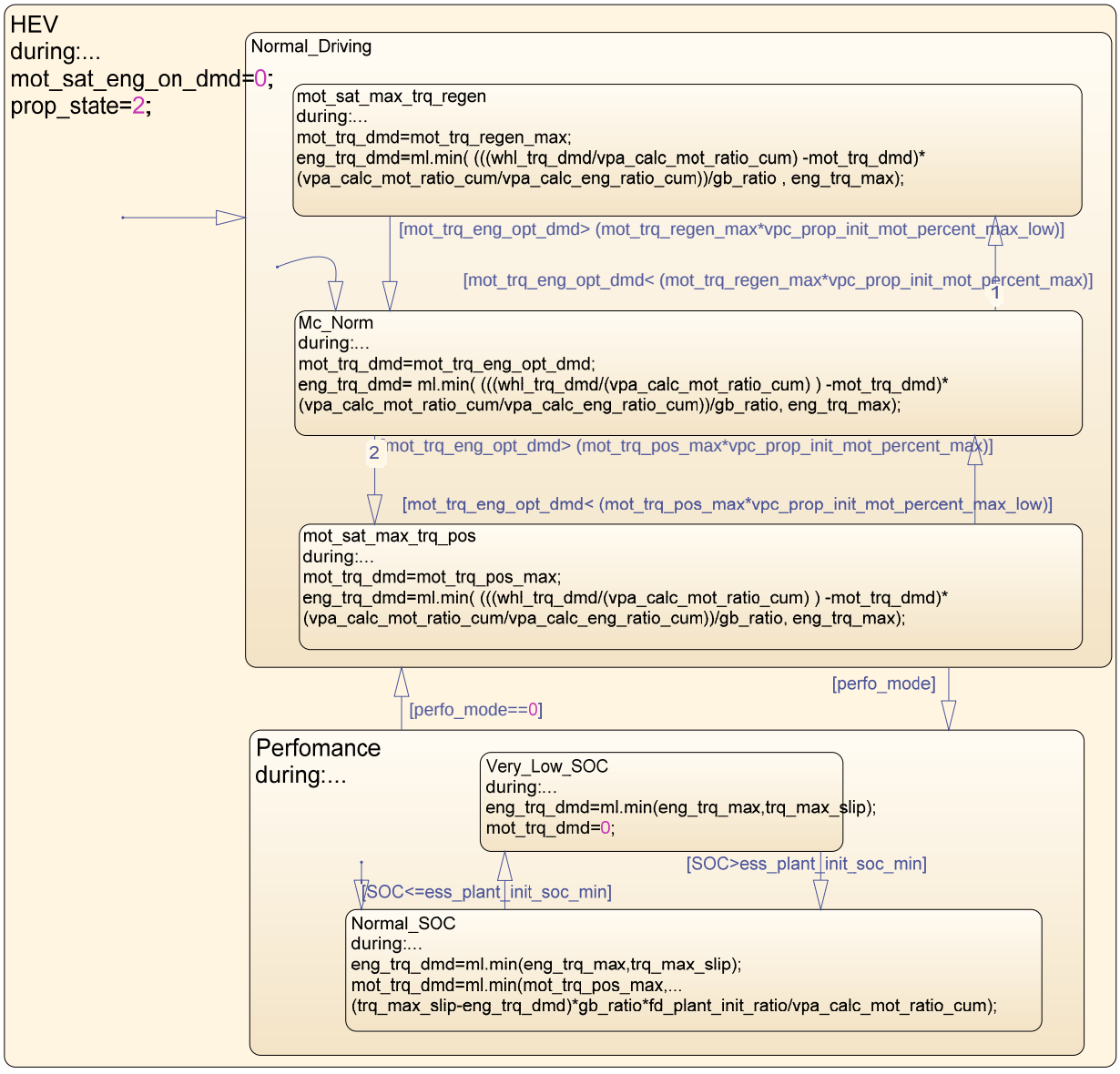

Figure 5-8 State flow in HEV mode

5.2 Modeling of HAMT-based PHEV

Compared to our target hybrid system, shown in Figure 2-3, this baseline model needs to be modified extensively to describe more complicated gearbox and transient behaviors. A parallel

hybrid vehicle featuring the HAMT is modeled using SIMULINK, STATEFLOW and SIMSCAPE, especially SimDriveline. Since this new HAMT-based PHEV does not exist in any commercially available modeling tool, our strategy is to build the simulation model based on baseline parallel PHEV model from AUTONOMIE software. Figure 5-9 shows powertrain overview of target hybrid powertrain model. This SIMULINK-SimDriveline model has many advantages over pure SIMULINK model in terms of simulating this powertrain system with complicated torque flow paths and state changes of clutches in various steady/transition modes.

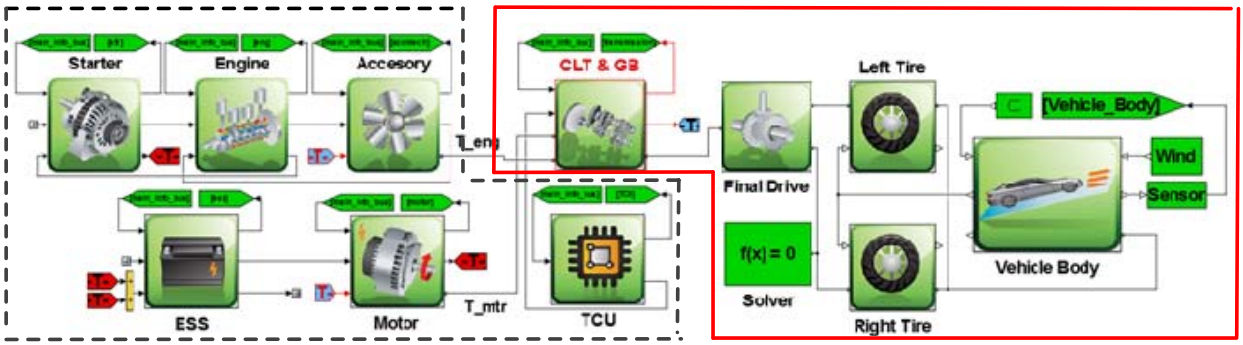

Figure 5-9 Overview of hybrid powertrain and chassis model

Components in left half are inherited from baseline model. Original SIMULINK models of main clutch, gearbox, final drive and vehicle body/weight are replaced with SimDriveline blocks (red box in Figure 5-9. Changes include following aspects:

1) Baseline gearbox model is a look-up table that is used to calculate input shaft speed and output torque, ignoring transient events, which are essential topic for this research. So, original table-based model is replaced with physics-based SimDriveline model that can clearly model each small part of gearbox. Furthermore, gear selector is modeled as well to simulate the gear-change process;
2) Baseline powertrain is a post-transmission parallel hybrid powertrain with motor linked to transmission output shaft. In comparison, target powertrain is novel HAMT-based powertrain with motor linked to one separate input shaft. In addition, gearbox of HAMT has eight gears for HEV mode and up to eight gears for EV mode, more gears than baseline transmission. So, whole gearbox mechanism is changed completely; In addition, gearshift schedule, which determines timing of gearshift as well as target gear, for new HAMT should be totally different from the schedule in baseline model;
3) Controllers for engine, gearbox and main clutch are relatively independent in baseline model. This independency leads to lack of coordination in gearshifts and EV-HEV mode transition. Extensive changes to those baseline controllers are needed to coordinate different powertrain components. For example, a new transmission control unit (TCU) modular is built based on original controllers for main clutch and gearbox to coordinate powertrain components.

5.2.1 HAMT Model – Main Clutch & Gearbox

As key of this simulation model, the modular (CLT&GB in Figure 5-9) with main clutch and gearbox receives commands from VSC and TCU and links to engine, motor and final drive via 3 physical modeling connecting (PMC) ports, as shown in Figure 5-10. This figure is another description of HAMT in Figure 2-3. The actuator commands are generated by TCU to control states of 5 synchronizers; the clutch force command is for controlling main clutch. The three PMC ports are different from the two regular SIMULINK signal in-ports in that PMC ports transmit bi-directional physical signals, including both torque and rotation speed, and two signal in-ports only transmit one unilateral signal.

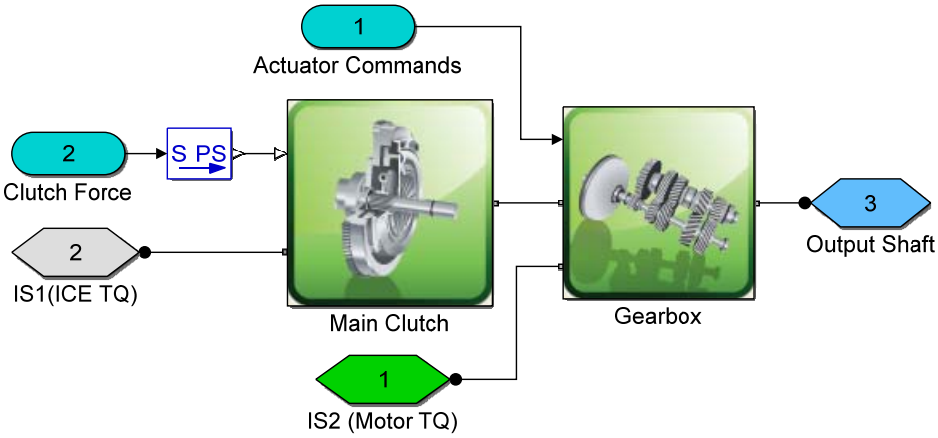

Figure 5-10 Overview of gearbox and clutch model

5.2.1.1 Main Clutch Model and Operating Modes

As main clutch is locked, torque from engine is sent to the first PMC port (2nd port of gearbox model in Figure 5-10) via locked clutch; as main clutch is slipping or totally open, one extra DoF is introduced. Derivative of engine speed is determined by balance between net engine torque and clutch torque (0Nm when clutch is open). Acceleration of first input shaft is determined by balance between clutch torque and torque from gearbox inside. SimDriveline model can greatly solve this issue of changing DoF according to state of clutch.

The main clutch model is one dry clutch model in SimDriveline library. Relationship from pressure to torque is often summarized in Coulomb friction model, as shown in Equation (4.8). The engagement threshold pressure of 10,000Pa is used to describe return spring of main clutch that helps to return to default unlocked state. Only applied pressure surpasses the engagement threshold pressure, return spring can be compressed and clutch can bear some torque. Since main clutch is a dry clutch, viscosity is not modeled. All other parameters are default values or from reasonable estimation.

$$T_C = (P_{app} - P_{thre}) A_{pstn} \mu R_{eff} N \tag{5.1}$$

Where P_{app} is applied normal pressure on clutch surfaces, P_{thre} is a threshold pressure representing resistance of return spring (only when P_{app} is bigger than P_{thre}, clutch starts to

transmit torque), A_{pstn} is area of hydraulic piston of actuator, μ is friction coefficient between friction plates, R_{eff} is effective radius of clutch that is defined by inner and outer radius, N is count of friction disks and is set as one for dry clutch.

Parameter values in equation (5.1) are set in Table 5-1 based on clutch model principle in subsection 4.1.2. The kinetic and static friction coefficients are set equal, although static friction coefficient should be higher than kinetic friction according to principles of tribology [138]. The reason for this assumption is that friction coefficient and measurement of coefficients often include apparent uncertainty. For example, they are not easily measureable and vary in various scenarios, like different temperatures or age of components. In automotive industry, this assumption is commonly accepted for transmission control and modeling work.

Table 5-1 Main clutch parameters

Parameter name	Value
Kinetic friction coefficient	0.15
Static friction coefficient	0.15
Effective torque radius	100mm
Engagement piston area	$0.01m^2$
Number of friction surfaces	1
Engagement threshold	1bar
Viscous drag	0
Initial condition	Unlocked

The main clutch controller enables the clutch to work in five different modes, each of which corresponds to one type of driving scenarios. As clutch features discontinuity during lock-slip transition and clutch determines how much torque can be transmitted between engine and driveline, each mode in this model should be calibrated separately. In this research, TGF and EV-HEV mode transition are primary goals; the control algorithm for the mode 3 & 5 will be emphasized.

Table 5-2 Operation modes of main clutch

	Driving scenario	Clutch action
Mode 1	Vehicle launch	Engaging gradually
Mode 2	Engine shut off as vehicle running	Disengaged gradually
Mode 3	Engine turned on as vehicle running (EV-HEV mode transition)	Engaging (reengaged) gradually
Mode 4	Vehicle stop	Disengaged gradually
Mode 5	Gear shift	Disengaged gradually first; the reengaged gradually after gear change

5.2.1.2 Gear Selector Model & Control

The gear selector model is built as sub-system and reused in whole HAMT model. Part of the target gearbox and corresponding simulation model are shown in Figure 5-11. Input shaft 1 is linked to output shaft via 1st gear and 5th gear, which are engaged by gear selector S4. In order to allow the output shaft to be connected to input shaft 1 via one of two hub gears, two gear selector modules (S4-R and S4-L) are used to describe S4, each side of which contains one cone clutch on each side. As neither left nor right side of S4 is engaged, input shaft 1 in not linked to output shaft via gear selector S4. As either left or right side is engaged, the corresponding gear selector model (S4-R, S4-L) on right side of Figure 5-11 is in locked state. Since actual gear selector can only be engaged with one hub gear at one time, the two gear selector models in SimDriveline model should not be engaged simultaneously.

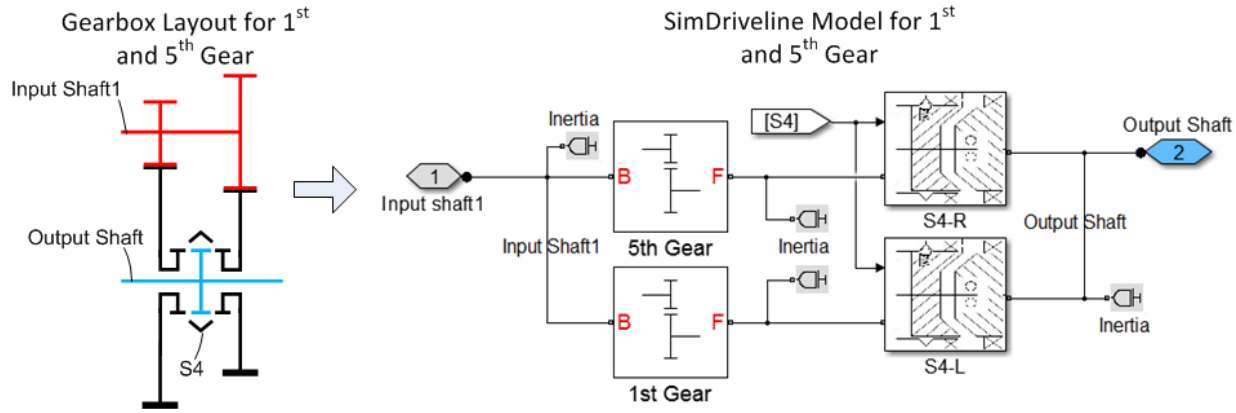

Figure 5-11 Gearbox configuration and SimDriveline model

The gear selector model is a critical part of whole powertrain model to simulate transient events. Gear selector model is built based on physics model, including its assumption, shown in Figure 4-4. A built-in library block called synchronizer, which is a parallel combination of dog clutch and frictional cone clutch, is used directly, as shown in the Figure 5-12. It can be found from the figure that two connectors (port R and H) of gear selector is linked to related hub and shaft. State and transitions among allowable states are controlled by port S, which receives acting force from actuator model that translates force command to acting force.

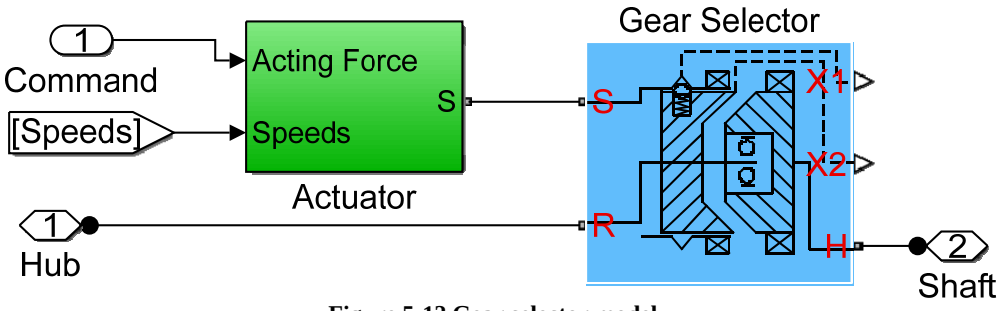

Figure 5-12 Gear selector model

Actuator can be modeled in details [139]. A simple actuator model is shown in Figure 5-13. The command (SIMULINK signal) is converted to acting force (physical signal). Rotation speeds of

hub and shaft, reported by virtual sensors, are used to determine scaling factor of command depending on moving direction of gear selector.

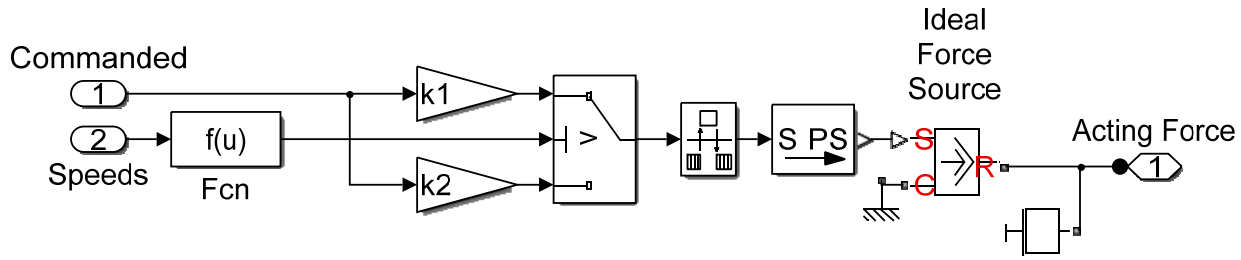

Figure 5-13 Gear synchronizer actuator model

5.2.2 SimDriveline Model for Gearbox and Other Components

Details of gearbox block in Figure 5-10 are shown in Figure 5-14. Three PMC ports linked to main clutch, motor and final drive are connected to input shaft 1, input shaft 2 and output shaft. Shafts and gears in Figure 2-3 are strictly modeled using SimDriveline blocks, and four gear selectors are modeled using 7 gear selector modules (S1 represented by only one module). This physics-based gearbox model supports high flexibility of operation as well as torque/speed signals among 3 PMC ports.

The 3rd PMC port in the Figure 5-14 is linked to final drive that further transmits output torque to wheels to propel vehicle model. The physical model of HAMT downstream is shown in Figure 5-15. The final drive is a built-in differential model from SimDriveline library. Final drive ratio is set as 2.89, identical with the model in Table 4-3. Other friction loss as well as viscosity loss is not covered since advantage of HAMT in driveability is main target. Just like real vehicle, the torque into final drive is split into two for left and right tires. Parameter values in Table 4-3 are used in this model for demonstration. The block solver must be attached one physical connection to start simulation. Here, the solver is set as ODE45 using variable time step. Relative tolerance for error is 0.001.

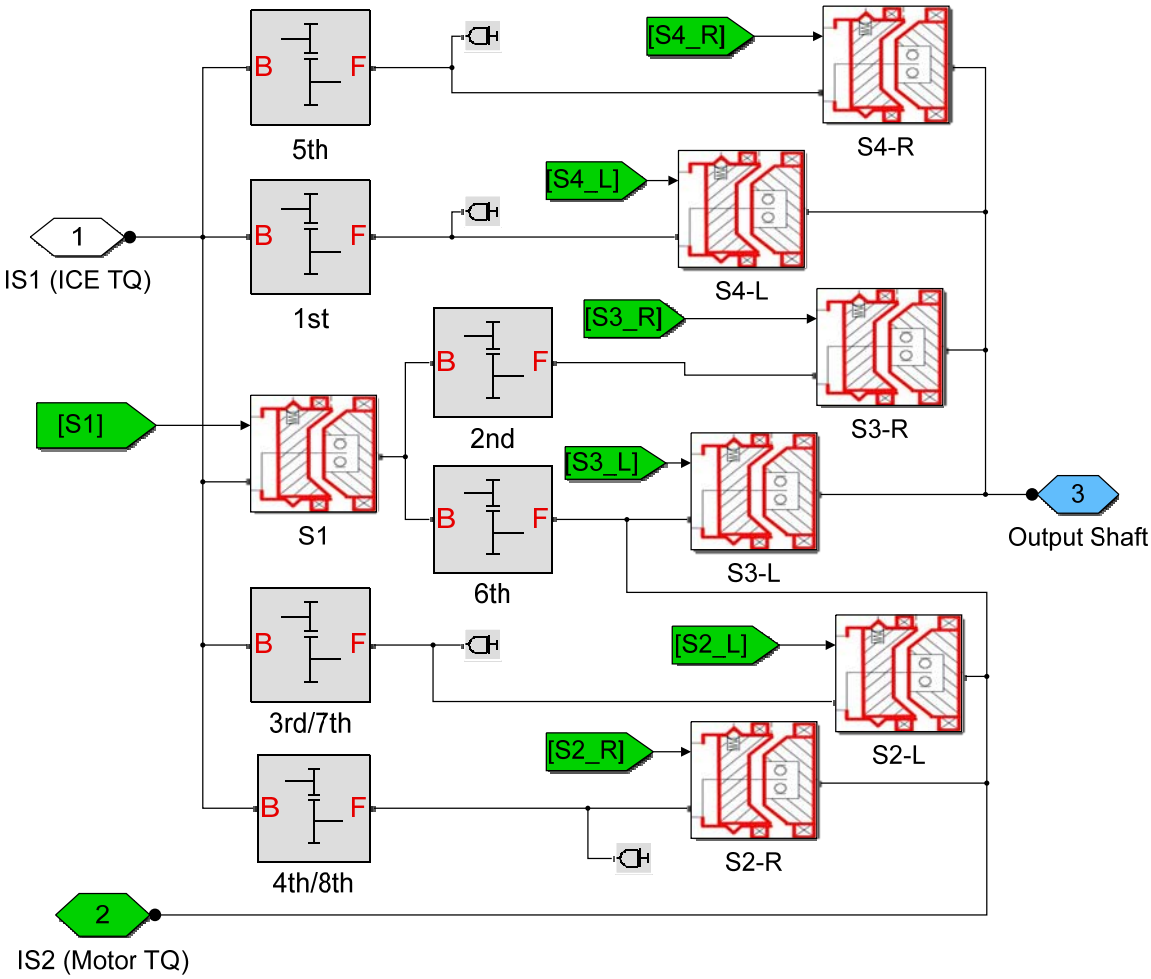

Figure 5-14 SimScape model of HAMT gearbox

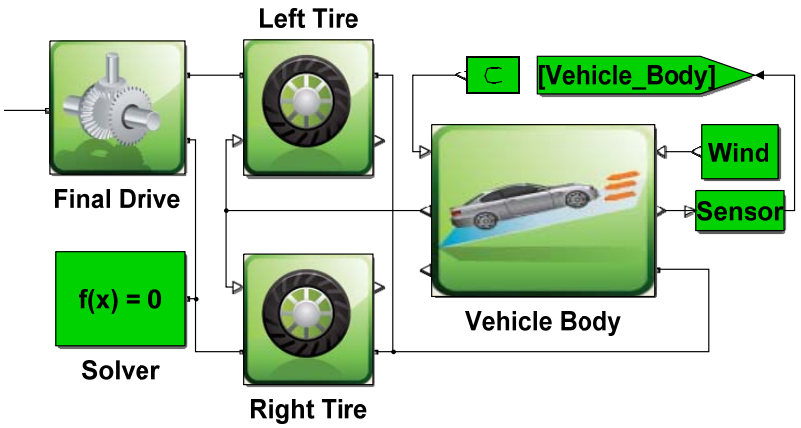

Figure 5-15 HAMT downstream model

c) Control algorithms for VCC, ECU and TCM are overhauled to make powertrain behavior as expected during steady and transient events. As a prerequisite to control newly added synchronizers, control modular and simple actuators for synchronizers are also modeled. In order to reach smooth mode transition and gearshift, it is critical to make sure that engine, motor, main clutch and gearbox are coordinated very well. For example, how to accomplish smooth transition

from inertia phase to torque phase 2 relies on systematic coordination of whole powertrain. All these changes to control system are necessary to achieve desirable driveability and require systematic analysis in depth.

5.3 Gearshift Control

5.3.1 Gearshift Schedule

Gearshift schedule is commonly represented by two maps, one for upshift and another one for downshift. Each map is often a two-parameter look-up table. In automotive industry, the two parameters selected as inputs to gear shift maps are vehicle speed and pedal position. Alternative to the pedal position could be target vehicle acceleration (non-negative). More complicated control strategy will introduce more variables to make gearshift meet driver's expectation better. Since transmission model has only five forward gears, new gearshift maps are needed to command upshifts and downshifts of this new 8-speed HAMT. Figure 5-16 shows a new gearshift schedule, which is built based on baseline gearshift maps in baseline model. The 7 solid thick curves are threshold lines for upshifts (1-2, 2-3 until 7-8); the 7 thin dotted lines with matching colors are lines for downshifts (2-1, 3-2 until 8-7). Since optimization of gearshift map is beyond scope of this research, empirical method is used here. If deeper understanding is needed, some reference papers are available [140] [141] [142].

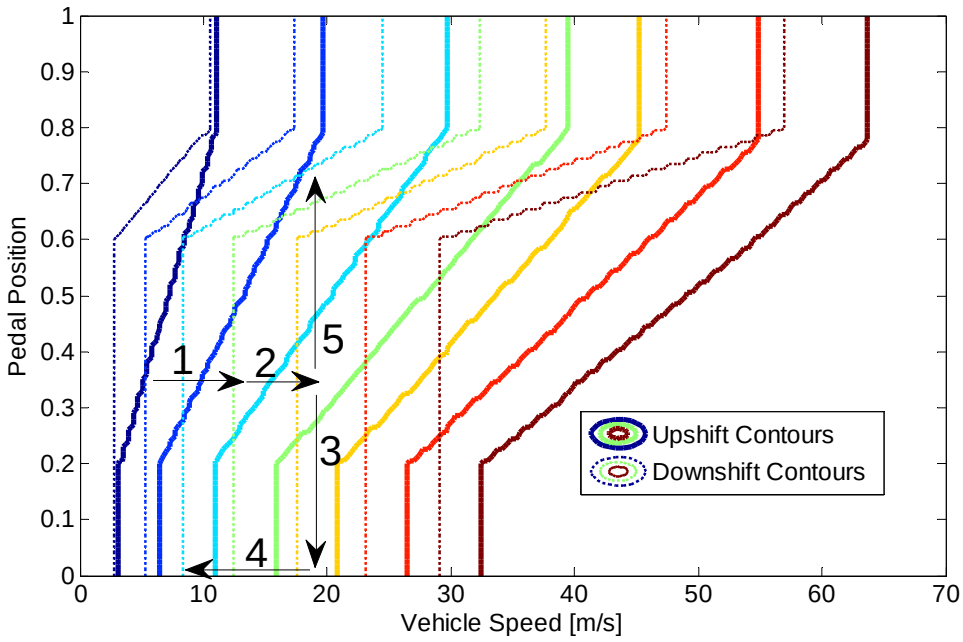

Figure 5-16 New gearshift schedule for HAMT

Between the two input parameters, driver determines target gear by controlling pedal positions. Some typical driver behaviors and gearshift logics are listed here:

1) The arrow 1 and 2 are typical power-on upshifts. Initially, transmission is at 2nd gear. As drive holds accelerator pedal position at certain level and vehicle is being accelerated,

threshold lines for 2-3 upshift (solid blue line) is first crossed. TCU will send command for 2-3 upshift. As vehicle speed increases, the arrow 2 crosses the threshold line for 3-4 upshift (solid light blue line). In reality, driver pedal position keep changing between gearshifts.

2) The arrow 3 represents a typical power-off upshift. Initially, the 4th gear is engaged and pedal is maintained at about 35% (example). With apparent tip-out behavior of driver, which is indicated by the plunging pedal position, the threshold line for 4-5 upshift (solid green line) is crossed immediately. With tip-out of accelerator pedal, power from engine and motor should be cut fast.
3) The arrow 4 is commonly experienced during coastdown from high speed, such as ramping out highway or preparing for far red light. The 5th gear is engaged at the end of arrow 4. With reduced vehicle speed due to road load or engine brake, arrow 4 crosses the 5-4 downshift threshold line (thin dotted green line).
4) The arrow 5 shows another important gearshift type – power-on downshift. This downshift often happens after a tip-in action from driver, which is indicated by the fast increase of pedal position. As the arrow 5 crosses the threshold line for 5-4 downshift (thin dotted green line), the downshift is commanded. With comparison to power-off downshift indicated by arrow 4, this downshift features positive and fast-increasing pedal position. This gearshift often comes from acceleration/torque demand of driver to meet performance expectation.\

The gearshift schedule plays the core role for gearshift command. Two maps are used separately for upshift and downshift with pedal position and vehicle speed as inputs. Figure 5-17 is core part for this module. Since threshold line for an upshift (like 3-4 upshift) is always on the right of corresponding reverse downshift (like 4-3downshift) with some gap between the two lines, simultaneous commands for upshift and downshift can be prohibited.

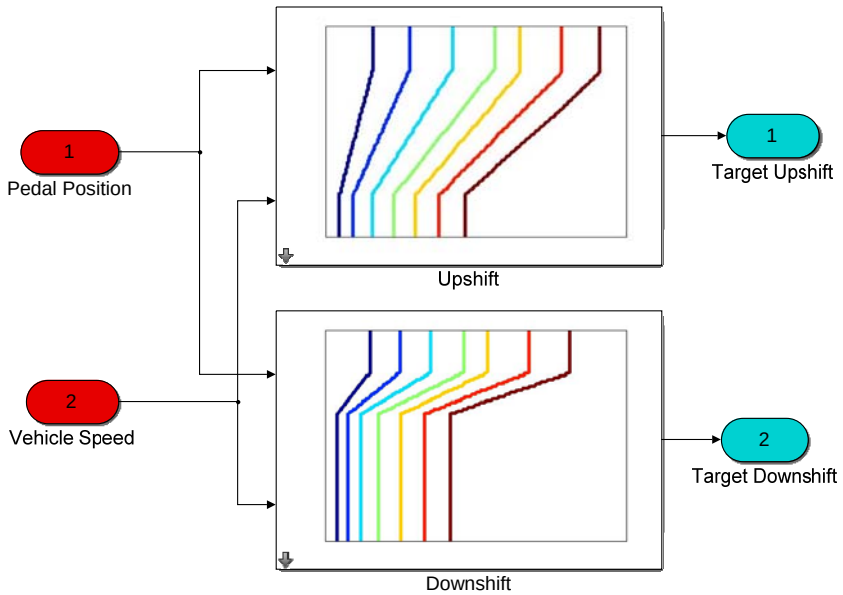

Figure 5-17 Gearshift schedule model

5.3.2 Decomposition of Gearshift

Gearshift control has been key topic for stepped transmission. Various control strategies were proposed and implemented [143] [144] [102] [145] [146] [147] [148]. As gearshift command is generated, how to implement the command refers to coordinate control of powertrain. Based on the rule-based control principle for EV-HEV transition, as shown in Figure 4-19, a rule-based control principle for TGF is also proposed. A complete gearshift involves state changes of almost all powertrain components and internal parts of HAMT, from engine and motor to main clutch and two dog clutches (one oncoming clutch and one off-going clutch). Figure 5-18 contains more detailed information about the TGF process (upshift). As vehicle speed and acceleration pedal input to TCU triggers a power-on gearshift (up or down) at t_0, 7 following phases will happen sequentially to complete gear shift, as shown in Figure 5-18. The relationship between gearshift and basic operating modes is listed in Table 5-3.

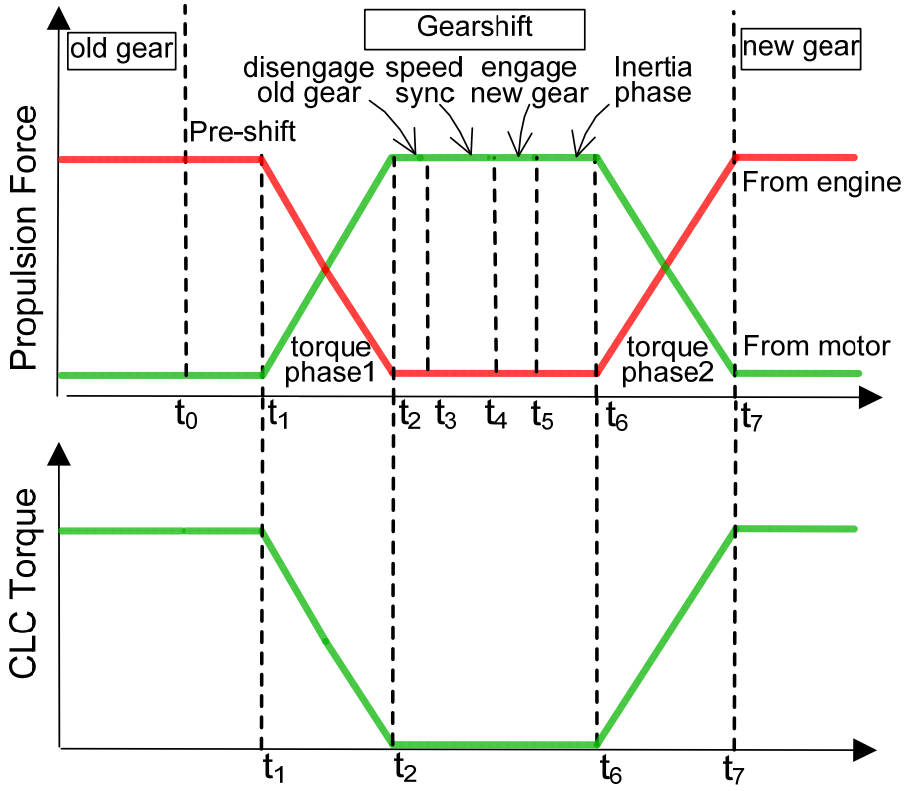

Figure 5-18 TGF function in HAMT

As engine torque and main clutch torque drop to near zero, main clutch is open and transmit no torque (t_1 - t_2); from t_2 to t_3, actuator for sleeve S1 push it to neutral position (powertrain featuring 3 DoFs); at t_3 sleeve S2 starts to be pushed to right side (gear 4) by synchronizer, whose cone-shape friction surface reduces relative speed between S2 and IS2; at the end of this speed synchronization process, actuator will push dog clutch of synchronizer to lock S2 to IS2 (t_4 - t_5); since engine's moment of inertia is much larger than input shaft with linked gears, it takes much longer time for engine to match speed of IS1 (t_5 - t_6). For vehicle equipped with

conventional AMT, main clutch starts to slip with some torque, which helps to drive vehicle and reduce engine speed (inertia phase). However, this new hybrid powertrain could enable engine to be shut off temporarily (cylinders still breathing) to help engine speed down; main clutch can be totally open (transition 1) or slightly engaged (transition 3); When slip speed of main clutch drops below threshold value, normal force of main clutch is increased to lock main clutch; From t_6 to t_7, primary torque source will be shifted from motor to engine, with main clutch torque capacity increasing to peak. The gearshift is finished at t_7. It is clear that, from t_1 to t_7, motor fills the torque hole generated by gearshift and contributes to steady acceleration. This process refers to steady hybrid mode and up to 3 transition modes.

Table 5-3 Decomposition of a gearshift

Time	Function	Operating mode
Phase 1: t_0 - t_1	Prepare for gearshift after gearshift command	Steady 2
Phase 2: t_1 - t_2	Reduce engine torque to open main clutch	Steady 2
Phase 3: t_2 - t_3	Disengage dog clutch for old gear	Transition 1
Phase 4: t_3 - t_4	Eliminate speed gap and prepare for new gear	Transition 2
Phase 5: t_4 - t_5	Lock dog clutch for new gear	Transition 1
Phase 6: t_5 - t_6	Adjust engine speed to reengage main clutch	Transition 1 or 3
Phase 7: t_6 - t_7	Reduce motor torque and increase engine torque	Steady 2
Phase 8: t_7 -	Gearshift finished	Steady 2

When power-on downshift is commanded, almost identical sequence of events will happen, except that engine torque will accelerate engine speed to speed of IS1, rather than dragging it down. Similar analysis can be used to downshift for engine, gearshift for motor, mode transition, vehicle braking.

Comparison between Figure 4-19 and Figure 5-18 further reveals connection between the two transient events. The phase 6-8 for TGF control is very similar to the process described Figure 4-19. Thus, the control algorithm for this part can be shared.

5.4 Structure of TGF Control

Among the 8 phases of TGF, phase 1 and phase 8 don't need specific coordination control because the two phases don't refer to control of any of the three major powertrain components – engine, motor and main clutch. Still, the phase 2 to phase 7 require dedicate control to achieve smooth gearshift.

5.4.1 Engine Control

Although engine model is one simple first-order transfer function, the controller for engine still enables engine model to finish various tasks, depending on power/torque demand for engine. Figure 5-19 shows all the states in ECU, each of which corresponds to a modular of engine

control. Since baseline vehicle model does not have the capacities to finish smooth mode transitions and TGF feature, the engine control strategy is changed to fulfill all requirements of this new HAMT-based hybrid system. In specific, the three states – Torque_phase1, Inertia_phase and Torque_phase2 – are new features of engine controller. The corresponding conditions for Torque_phase1 and Torque_phase2 are linked to two new subsystems to determine if the state should be activated or not.

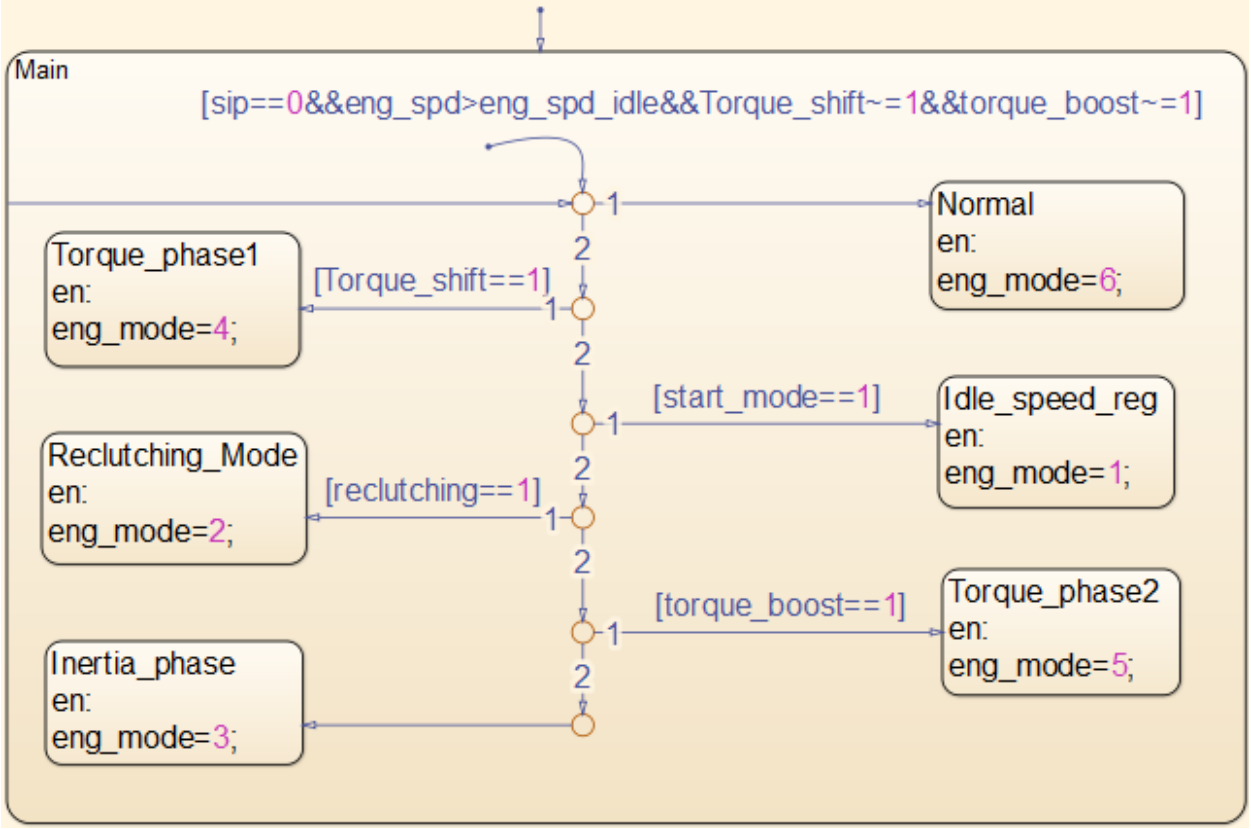

Figure 5-19 Different mode of engine control

5.4.2 Torque Phase 1

A general trend in this phase is that engine torque decreases and motor torque decreases. At the same time, main clutch torque capacity is reduced gradually with decrease of engine torque until it is released at the end of this phase. A simplified linear relationship among engine torque and motor torque as well as transmission output torque is described in equation 5.2. Physical model is described in Figure 4-1.

$$T_{os} = (T_e i_{1o} + T_m i_m i_{2o}) \tag{5.2}$$

Where T_{os} is the output shaft torque, T_e and T_m are engine and motor torques, i_{1o} and i_{2o} are gear ratio from input shafts to output shaft, i_m is speed ratio between motor and input shaft 2. Gear ratios for i_{1o} and i_{2o} are summarized in

Table 3-7.

a) Engine is modeled as a first-order transfer function to simply describe function between T_{e_act} and torque command T_{e_cmd}, shown in equation (5.3).

$$\dot{T_e} = \frac{T_{e\_cmd} - T_e}{\tau_e} \tag{5.3}$$

As control objective during phase 2 is to maintain stable output torque (power), both engine and motor torques can influence final output torque. Therefore, there are unlimited combinations of torque trajectories (one for engine and another one for motor) that enable stable output torque. In comparison to engine, electric motor is much more controllable and selected as coordinator component to compensate change of engine torque. It means ideal motor torque could be determined as long as torque trajectory of engine torque is fixed. For purpose of simplicity, engine torque command is designed to reduce linearly with a time window $\mathrm{t_{dc}}$, which is set as 0.4 second.

$$T_{e\_cmd} = \begin{cases} T_{e\_cmd0} \cdot \left(1 - \dfrac{t}{t_{dc}}\right) & \mathrm{t} < \mathrm{t_{dc}} \\ 0 & \mathrm{t} \geq \mathrm{t_{dc}} \end{cases} \tag{5.4}$$

Where T_{e_cmd} is instantaneous engine torque command, T_{e_cmd0} is initial engine torque command at beginning of this phase, t is elapsed time in phase 2. With linearly decreased engine torque command until it reaches zero, engine torque can be estimated via the first-order transfer function in equation (5.2). According to elapsed time and equation (5.5), two cases for engine torque calculation are analyzed.

a) As elapsed time is less than $\mathrm{t_{dc}}$, trajectory of actual engine torque is calculated by equation (5.5).

$$\dot{T_e} + \frac{T_e}{\tau_e} = \frac{\mathrm{T_{e\_cmd0}}}{\tau_e}\left(1 - \frac{\mathrm{t}}{\mathrm{t_{dc}}}\right) \tag{5.5}$$

General solution for this differential equation is

$$\begin{aligned} T_e &= C e^{-\frac{t}{\tau_e}} + e^{-\frac{t}{\tau_e}} \int \left[\frac{T_{e\_cmd0}}{\tau_e}\left(1 - \frac{t}{t_{dc}}\right) e^{-\frac{t}{\tau_e}}\right] dt \\ &= C_a e^{-\frac{t}{\tau_e}} + T_{e\_cmd0}\left(1 + \frac{\tau_e}{t_{dc}} - \frac{1}{t_{dc}} t\right) \end{aligned} \tag{5.6}$$

where C_a is an unknown constant determined by boundary conditions. The first item on right side of equation (5.6) is general solution of corresponding homogeneous differential equation; the second item is a special solution of nonhomogeneous differential equation.

In order to determine value of C_a, initial engine torque T_{e0} as t is equal to 0 is introduced into equation (5.6). C_a calculation is shown as equation (5.7) and (5.8). The final equation for engine torque estimation is shown equation (5.9).

$$T_{e0} = C_a e^{-\frac{0}{\tau_e}} + T_{e\_cmd0}(1 + \frac{\tau_e}{t_{dc}} - \frac{1}{t_{dc}} \times 0) \tag{5.7}$$

$$C_a = T_{e0} - T_{e\_cmd0}(1 + \frac{\tau_e}{t_{dc}}) \tag{5.8}$$

$$T_{e\_act} = \left(T_{e0} - T_{e\_cmd0}(1 + \frac{\tau_e}{t_{dc}})\right) e^{-\frac{t}{\tau_e}} + T_{e\_cmd0}(1 + \frac{\tau_e}{t_{dc}} - \frac{1}{t_{dc}} t) \tag{5.9}$$

b) Elapsed time is over t_{dc} and engine torque demand T_{e_cmd} stays zero.

Engine torque demand is reduced to zero from beginning of this phase, and governing equation becomes a regular first-order homogeneous equation, shown below. It is clear this part is a special case of analysis above.

$$\dot{T_e} + \frac{T_e}{\tau_e} = 0 \tag{5.10}$$

The general solution for this first-order differential equation is as equation (5.11).

$$T_{e\_act} = C_b e^{-\frac{t}{\tau_e}} \tag{5.11}$$

Similarly, boundary condition is torque as commanded torque reaches 0, which can be calculated from equation (5.9).

$$C_b = \left(T_{e0} - T_{e\_cmd0}(1 + \frac{\tau_e}{t_{dc}})\right) e^{-\frac{t_{dc}}{\tau_e}} + T_{e\_cmd0} \frac{\tau_e}{t_{dc}} \tag{5.12}$$

The analysis above is based on a simple transfer function and a real engine is much more complicated than this model. However, the fundamental goal of this analysis is not to control engine but to prepare for design of powertrain controller that can successfully coordinate engine, motor and clutch. In addition, engine torque estimation for engine in vehicle has been developed quite maturely already.

In light of fast response of motor, transfer function of motor is ignored to simplify analysis here, which means motor torque command is equal to actual motor torque, although a transfer function will be introduced in actual motor model. Based on equation (5.2) and estimated engine torque, motor torque command can be calculated as long as needed output torque is calculated. Then ideal transmission output shaft torque, $\tilde{T}_{os}$, can be calculated using equation (5.13).

$$\tilde{T}_{os} = \left(F_r + M_{eff}\tilde{a}_v\right) R_w i_0 \tag{5.13}$$

where M_{eff} is an equivalent weight of vehicle that is defined in equation (4.3), $\tilde{a}_v$ is required vehicle acceleration, R_w is tire radius and i_0 is transmission final drive ratio. In exception to $\tilde{a}_v$, all other parameters are known constants. In order to determine required output shaft torque, one ideal gearshift process from aspect of vehicle acceleration is figured out as reference of this gearshift process. Ideally, a gearshift should happen without noticeable change of vehicle

acceleration, which can be detected by passengers. Considering short duration of gearshift (at most 1-2 seconds), the filtered acceleration just prior to this torque phase 1 is selected as ideal acceleration. The commanded engine torque can be calculated as equation (5.14). With decrease of engine torque that is estimated in equation (5.9) and (5.11), motor torque command is increased gradually to compensate the lower engine torque.

$$T_{m\_cmd} = \frac{\tilde{T}_{os} - T_e i_{1o}}{i_m i_{20}} = \frac{\left(F_r + M_{eff}\tilde{a}_v\right)R_w . i_0 - T_e i_{1o}}{i_m i_{20}}) \tag{5.14}$$

In this torque phase (t_1 - t_2), torque demand for clutch is also reduced gradually. Here, a linear clutch torque profile is used to describe this process. The maximum pressure as clutch is in default locked state is 140,000 Pas, which is equivalent to 195N.m according to equation (5.1) and Table 5-1. The pressure profile is calibrated to make sure clutch does not slip until end of this process.

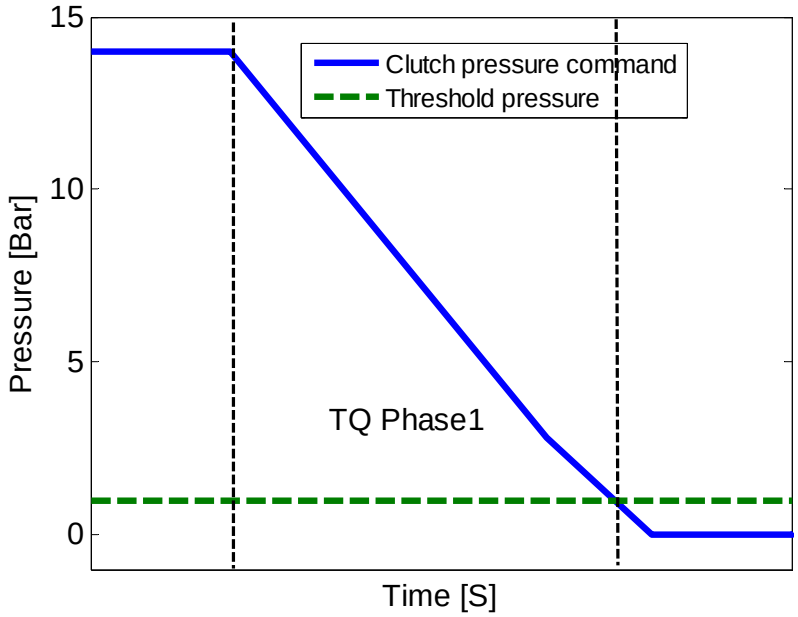

Figure 5-20 Clutch pressure command during torque phase 1

5.4.3 Control Model for Gear Change

This gearshift process consists of three sequential phases in Figure 5-18, which are disengaging old gear, speed synchronization and engaging new gear. As gear command change, according to the outputs from upshift and downshift map shown in Figure 5-17, triggers TGF process, two (sometimes only one) gear selectors for oncoming and off-going clutches will prepare to engage and disengage corresponding gears. A 2-3 upshift is used as example. The 2nd gear is off-going gear, and 3rd gear is oncoming gear. Correspondingly, gear selector S1 and S2-L are off-going and oncoming clutch, described in Table 2-1. Commands for disengaging S1 and engaging S2-L will be generated.

Figure 5-21 shows basic structure of control model for gear selectors in all possible gear shifts, which is described in Table 2-2. Based on gear command (including current gear and target gear), corresponding gear selectors can be identified, which is further sent into a Simulink control model shown in Figure 5-21.

As commanded gear is changed, only two related gear selectors (one oncoming selector and one off-going selector) will be commanded non-zero signals. The gear selector for off-going gear selector will be commanded a negative force to release engaged dog clutch; the gear selector for oncoming gear selector will be commanded a positive force to engage corresponding clutch. For 2-3 upshift, command for gear selector D11 that is from the green block of D11 Engaging will become negative, and command for D12R that is from D12R Engaging will become positive.

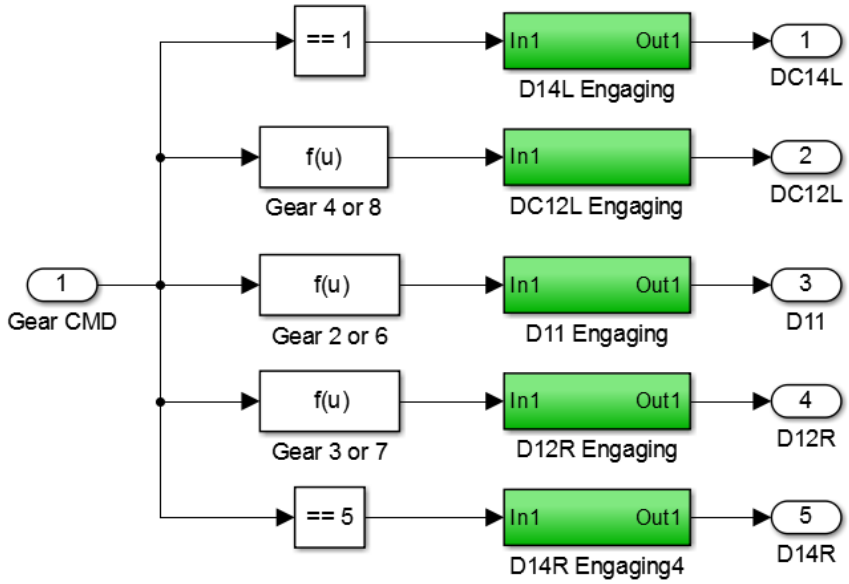

Figure 5-21 Gearshift actuator controller – from gear command to actuator command

Some requirements for each green block in Figure 5-21 should be met, which are 1) disengagement of old gear should happen earlier than disengagement of new gear; 2) there should be a time gap between disengaging old gear and engaging new gear for synchronization of gearshift; 3) the same control model should be applied to all gear selectors; 4) the same control model should function, no matter the controlled gear is oncoming or off-going gear. A Simulink-based model is created in Figure 5-22. The input is a logic signal (0 or 1) from judgement block prior to actuator controller. The same 2-3 upshift is still used to explain this logic. As command is increased from 2nd gear to 3rd gear, the input port of green block D11 in Figure 5-21 will receive a step signal whose value drops from 1 to 0. The change will be used by actuator controller to generate a negative force command for D11. Similarly, the step signal from 0 to 1 is sent to block D12R Engaging, which will generate a positive force command for D12R. By use of delay blocks, all the four requirements described above can be met. Outputs for D11 and D12R will make 2nd gear disengaged and 3rd gear engaged. During this process, gear ratio change from 2nd to 3rd gear makes rotation speed of input shaft 1 decrease fast that becomes

target speed of engine in following inertia phase. Inputs and outputs from this controller will be described in next chapter.

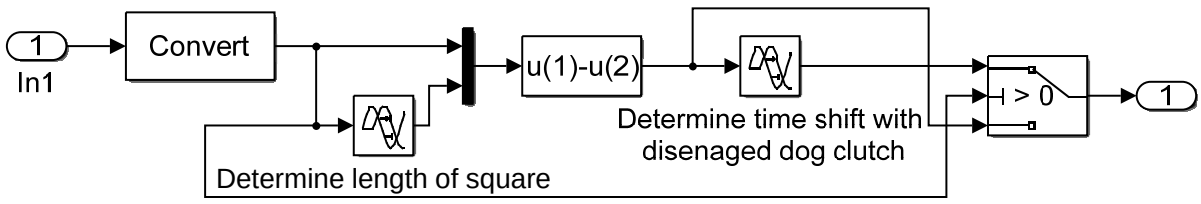

Figure 5-22 Actuator controller

5.4.4 Inertia Phase & Torque Phase 2

Inertia phase is primarily used to overcome inertia of engine to make engine speed equal to target speed w_{tis}, which is rotation speed of transmission input shaft 1. The 1-D physical model for this phase is shown in Figure 5-23. More detailed dynamics analysis can be found in Chapter 4.

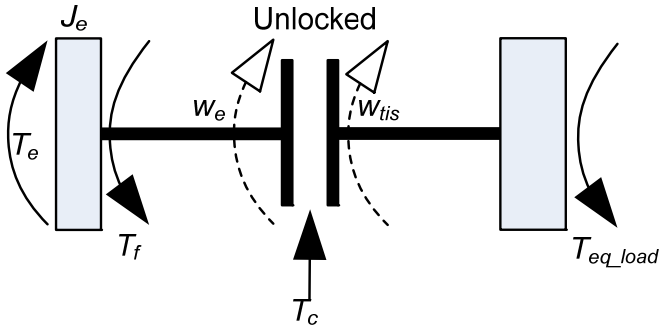

Figure 5-23 Model for engine speed control

Depending on direction of gearshift – upshift or downshift, principle of engine speed control during this inertia phase can be different. Meanwhile, engine speed control during inertia phase of both upshift and downshift consist of two sequential challenges: how to eliminate slip speed and how to complete the transition from inertia phase to torque phase 2.

a) Engine speed and torque control during inertia phase of downshift

For downshift, engine speed is initially lower than target speed during inertia phase. This negative slip speed will lead to negative clutch torque when pressure is applied on clutch. Fundamental principle for engine and main clutch control is described in Figure 5-24. The inertia phase can be split into two segments. As slip speed is far from zero, clutch torque is maintained at zero; engine torque is only used to accelerate engine inertia to eliminate slip speed. As engine speed is quite close to target speed, both engine and main clutch will prepare for the transition from inertia phase to torque phase 2. Details for engine speed control will be will be provided in Chapter 6.

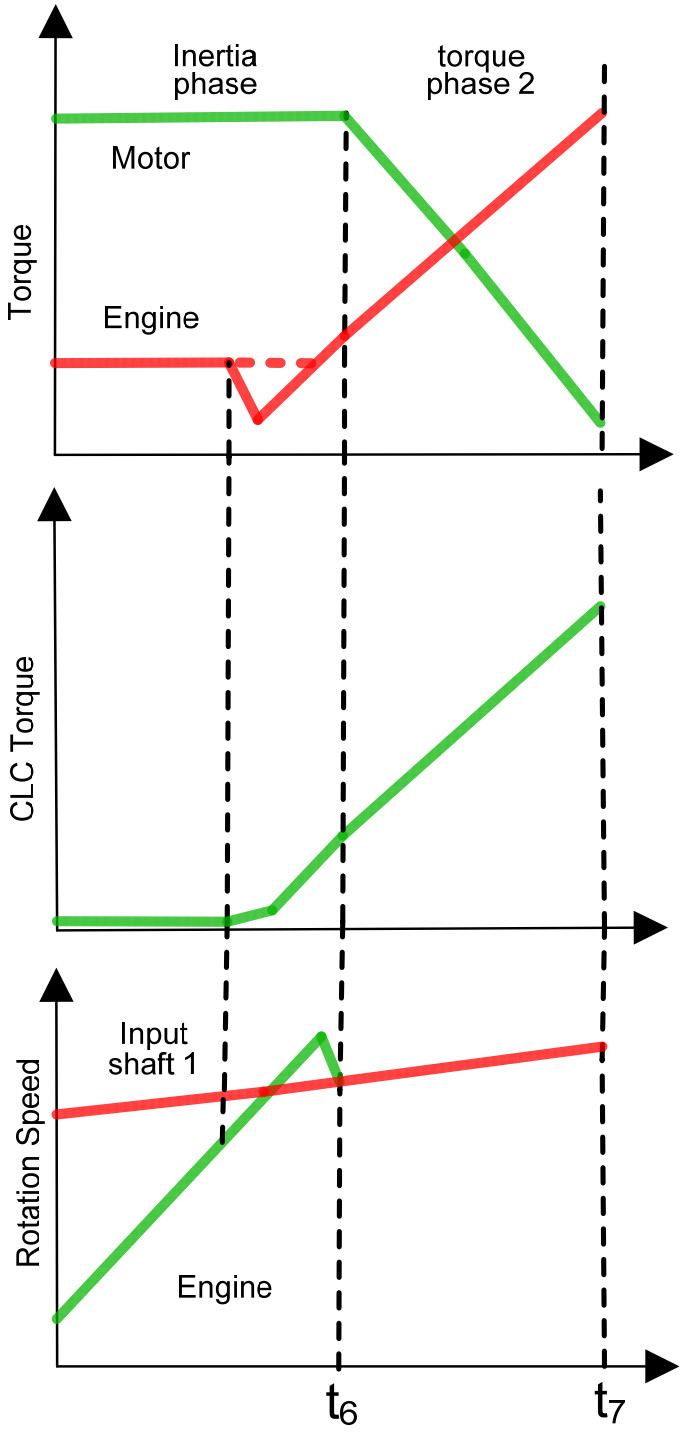

Figure 5-24 Engine speed control for downshift during inertia phase of TGF

Fundamental dynamics equation for whole inertia phase, no matter how big slip speed is, is equation (5.15). As engine speed is lower than target speed apparently, the main clutch should transmit no torque because the negative slip speed will generate negative torque as pressure is applied to main clutch. Although this negative T_c will help to eliminate slip speed, shortening

length of inertia phase, the negative clutch torque will compromise driveability apparently because the negative clutch torque drags down vehicle acceleration and compromise driveability when slip speed is negative, which is due to Coulomb Friction model that is introduced in equation (4.8). Engine speed is governed by equation (5.15), which is extracted from Equation (4.13) and equation (5.3). By adjusting engine torque command T_{e_cmd} to increase or decrease engine torque, the engine acceleration is influenced.

$$\begin{cases} J_e.\dot{\omega}_e = T_e - T_c \\ \dot{T}_e = \dfrac{T_{e\_cmd} - T_e}{\tau_e} \end{cases} \tag{5.15}$$

Engine torque T_e is controlled to accelerate engine to match target speed by adjusting engine torque command, as shown in Figure 5-25. Measured transmission output shaft speed via speed sensor is multiplied with instantaneous gear ratio to calculate rotation speed of input shaft 1, which is target speed ω_{e_tgt}. This target speed will be compared with measured engine speed to determine speed error. Accessory torque loss is also added to the PI controller output. Final engine torque command T_{e_cmd} is clipped to fall within upper and lower limits, which are set as 10 and 40N.m, respectively. The engine torque command will be sent to engine plant model, which is represented by the transfer function introduced above.

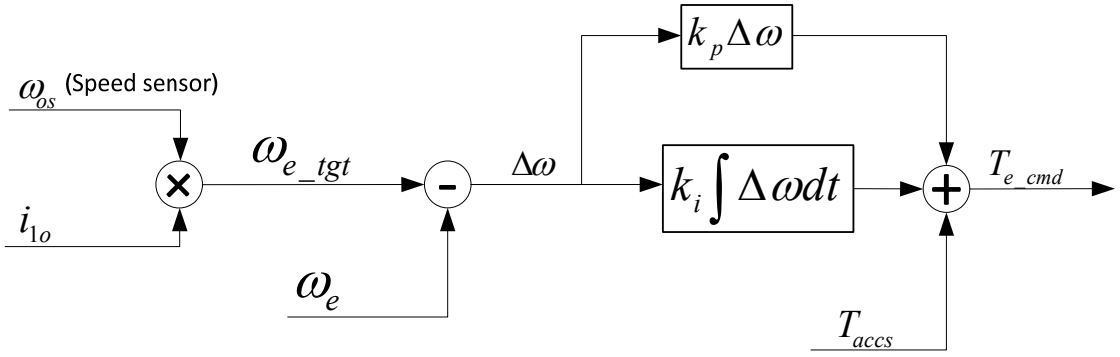

Figure 5-25 Engine speed control (open clutch)

With acceleration of engine speed, the slip speed will be decreased from positive value to zero gradually. As slip speed is below a threshold speed of 100rpm, the 1st part of inertia phase is completed and 2nd part is triggered automatically. It can be seen in Figure 5-24 that engine torque command does not follow the straight dashed line when engine speed becomes only slightly less than target speed. Actually, engine torque drops fast, which is called torque modulation that is critical to avoid engine speed overshoot. Supposing engine speed is equal to target speed and clutch has not built up torque capacity to catch the engine, engine speed will continue to increase, generating an apparent speed overshoot (positive slip speed). This overshoot is beneficial for smooth transition from inertia phase to following torque phase 2 as long as the magnitude of overshoot is acceptable, like less than 50rpm. In order to avoid undesirable engine speed overshoot, engine torque should be reduced fast to help to reduce engine acceleration and lock main clutch, according to equation (5.15). On the other hand, main clutch should build torque

capacity gradually prior to this point. Like the 2nd plot of Figure 5-24, main clutch starts to engage slightly before engine speed reaches target speed to prepare for upcoming engine speed overshoot. From the moment that slip speed becomes positive, main clutch torque capacity will increase faster to lock main clutch. At the same time, engine torque is increased gradually to prepare for torque transfer in torque phase 2. At the end of inertia phase, slip speed between engine and input shaft 1 is totally removed, ideally without apparent fluctuation of acceleration.

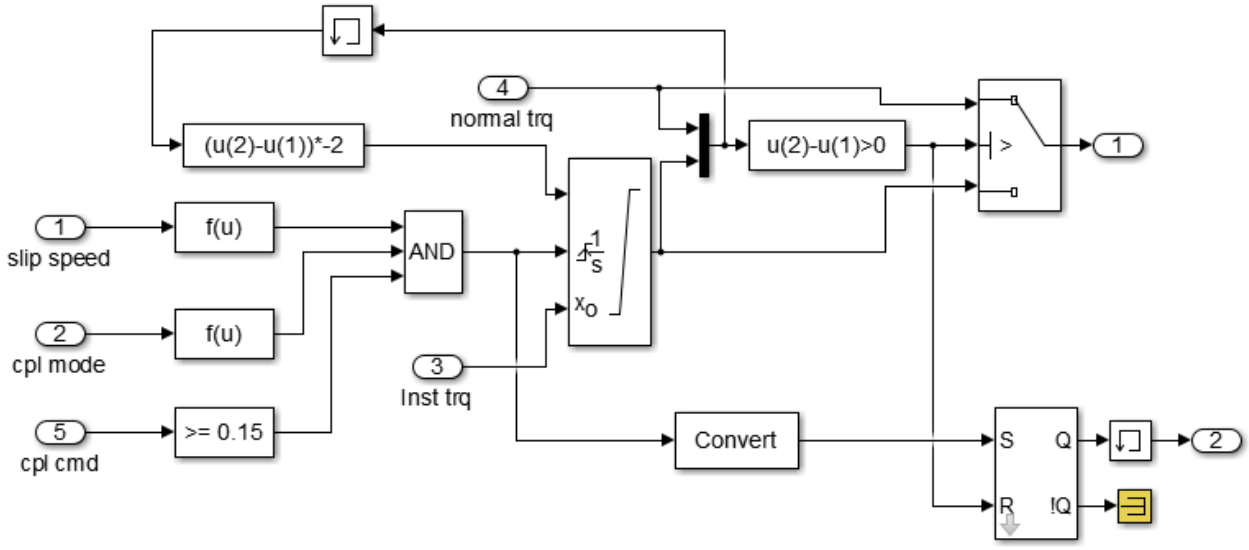

Figure 5-26 Clutch torque during torque phase 2

b) Engine speed control during inertia phase of upshift

For upshift, initial engine speed is above speed of input shaft 1. Therefore, clutch torque during the inertia phase will help to reduce engine speed and accelerate vehicle by transferring some kinetic energy of engine to vehicle, no negative impact on driveability if controlled well. This is a key difference between upshift and downshift. As for how to control clutch torque during inertia phase, there are unlimited possibilities.

Figure 5-27 provides two strategy to control engine and main clutch to complete this inertia phase during downshift smoothly.

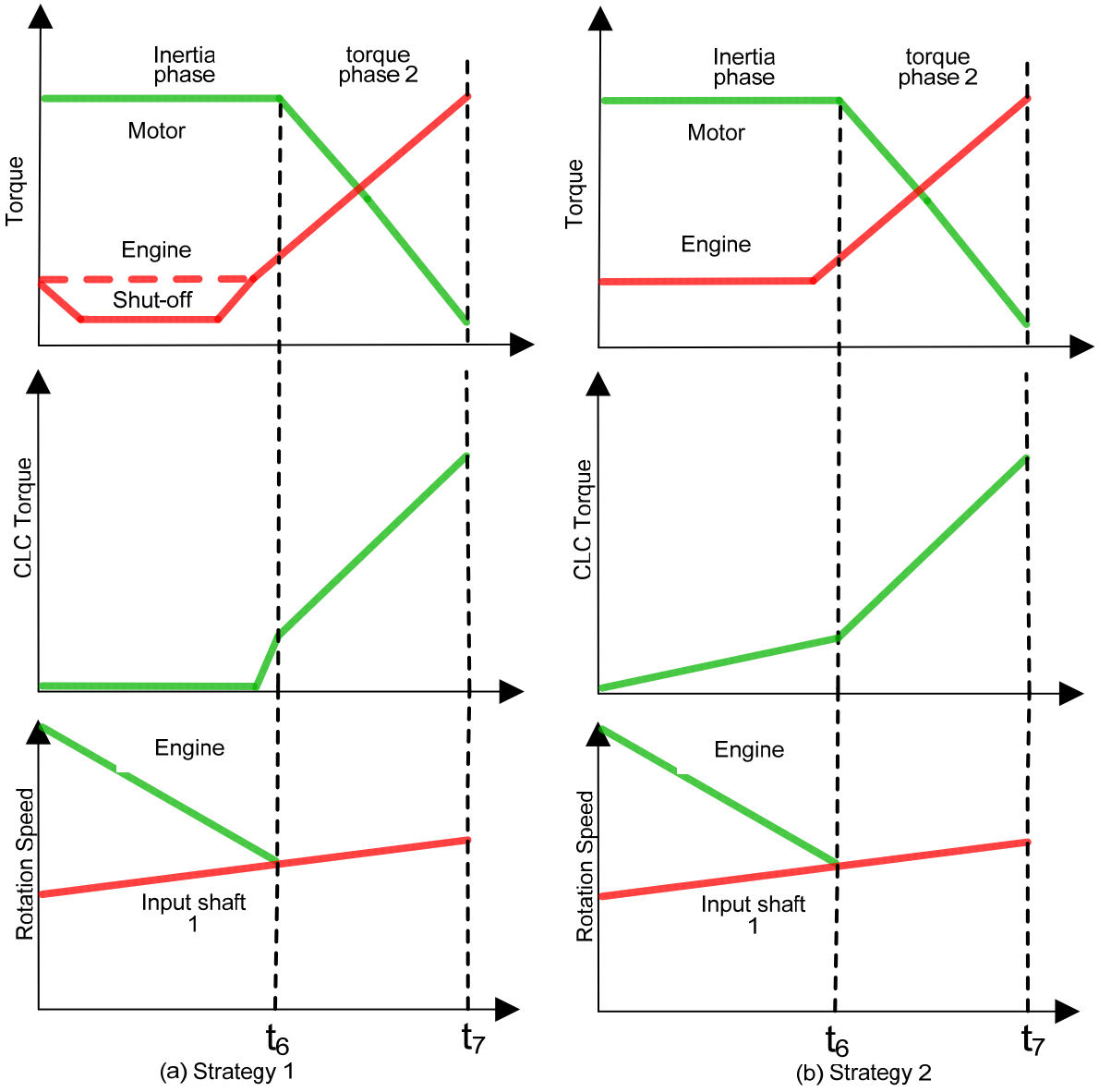

Figure 5-27 Engine speed control for upshift during inertia phase of TGF

Strategy 1: when engine speed is much higher than target speed, main clutch is maintained open to transmit no torque. In addition, engine torque is not controlled based on slip speed, just like the method in Figure 5-25, but maintains a negative torque by cutting off fuel injection. Fuel is shut off temporarily to decelerate engine fast via zero-fuel torque, which is shown in Figure 4-8. The zero-fuel torque is actually from its friction and pumping loss. Dynamics equation is shown in equation (5.16). As slip speed is less than a threshold, like 300rpm, engine will be ignited again to avoid reversed sign of slip speed. The same feedback-based engine speed control method, shown in Figure 5-23, will work to make slip speed drop to zero gradually. At the same time, main clutch torque is built up as engine is turned on again to prepare for the transition from inertia phase to torque phase 2. When slip speed disappears totally, main clutch torque has

enough torque capacity to lock the main clutch. Similar to the method used in Figure 5-24, this method keeps zero clutch torque at the beginning and prepares to lock main clutch as slip speed drops below a threshold.

$$J_e.\dot{\omega}_e = T_f \tag{5.16}$$

Strategy 2: main clutch bears some torque from the beginning of inertia phase to shorten inertia phase. At the same time, engine torque is also controlled to eliminate slip speed fast and smoothly. The dynamics equation for engine speed control in strategy 2 is shown in equation (5.17). With gradual decrease of slip speed, engine torque will gradually increase to prepare for upcoming transition to torque phase 2. With comparison to downshift, torque modulation is not a necessary consideration (based on simulations).

$$J_e.\dot{\omega}_e = T_e - T_c \tag{5.17}$$

In this research work, only strategy 1 is implemented for proving concept.

5.5 EV-HEV Mode Transition

The fundamental principle of EV-HEV mode transition is discussed in detail in Chapter 4. Here, the mode transition is further decomposed into sequential states to implement the principle in simulation model. The EV-HEV mode transition is essentially identical to the control algorithm described in Figure 5-24 because initial engine speed (0rpm) is lower than target speed, which is rotation speed of input shaft 1. The first part of mode transition is engine speed control without any resistance from main clutch. After main clutch starts to bear torque, the main clutch is locked to transmit torque from engine to transmission. More details and results are revealed in next chapter.

The biggest difference is that engine should be ignited at first, rather than following target speed directly. The basic equation to estimate engine acceleration is shown below, where T_s is starter torque. As long as vehicle speed is accumulated beyond a threshold speed, defined as 200rpm, engine model will generate torque and zero-fuel torque T_f will disappear.

$$J_e.\dot{\omega}_e = T_s - T_f \tag{5.18}$$

The starter motor characteristic curve is shown in Figure 5-28. Generally, starter motor can drive engine from static to 200rpm instantaneously. After engine is on, starter motor will be disconnected from engine automatically [149] [150].

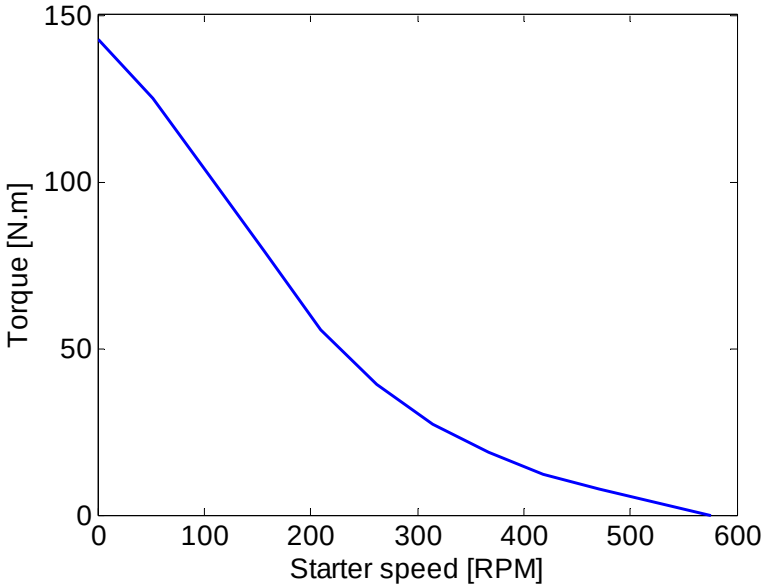

Figure 5-28 Starter motor torque curve

5.6 Summary

This chapter introduces a baseline plug-in parallel hybrid model from AUTONOMIE library at first. Driver model, supervisory powertrain controller and vehicle model are discussed briefly. The baseline simulation model is tailored extensively to build a customized simulation model that shares the same powertrain architecture of research subject. For purpose of avoiding time-consuming modeling work in flexible operation modes and complicated power flows, the whole Simulink model of driveline system in baseline model is completely replaced by SimDriveline model. In addition to replacement, non-existing gearshift actuator model and corresponding controller are also modeled to capture how gearshift process is finished. Meanwhile, remaining parts of baseline model is kept. This Simulink-SimDriveline hybrid powertrain model is used to test proposed control strategy for desirable driveability. In order to achieve smooth gearshift, Torque-Gap-Filler feature is analyzed in detail and further split into 7 phases. Three key phases, which are torque phase 1, inertia phase and torque phase 2, are discussed in detail. In light of difference between upshift and downshift, different control principles are discussed in detail. Finally, EV-HEV mode transition is also discussed, as the mode-transition is very similar to the second half of downshift. This chapter provides some key information about modeling and control. More details of this powertrain model and its behaviors will be described in next Chapter.

6 Simulation Results & Analysis

The simulation model introduced in Chapter 5 is used to evaluate the whole HAMT-based hybrid powertrain system, including mechanism and control strategy. Major efforts are put to enable whole vehicle model operate as expected, especially during EV-HEV mode transition and gearshift with TGF functioning.

Vehicle launch tests with different pedal positions are used to prove if this novel hybrid system with efficient AMT gearbox can also deliver excellent driveability. As shown in Figure 6-1, vehicle is accelerated from standstill under constant but aggressive pedal to observe how smooth the EV-HEV mode transition can be achieved. In addition, smoothness of acceleration during gearshift is another important criterion for this hybrid system.

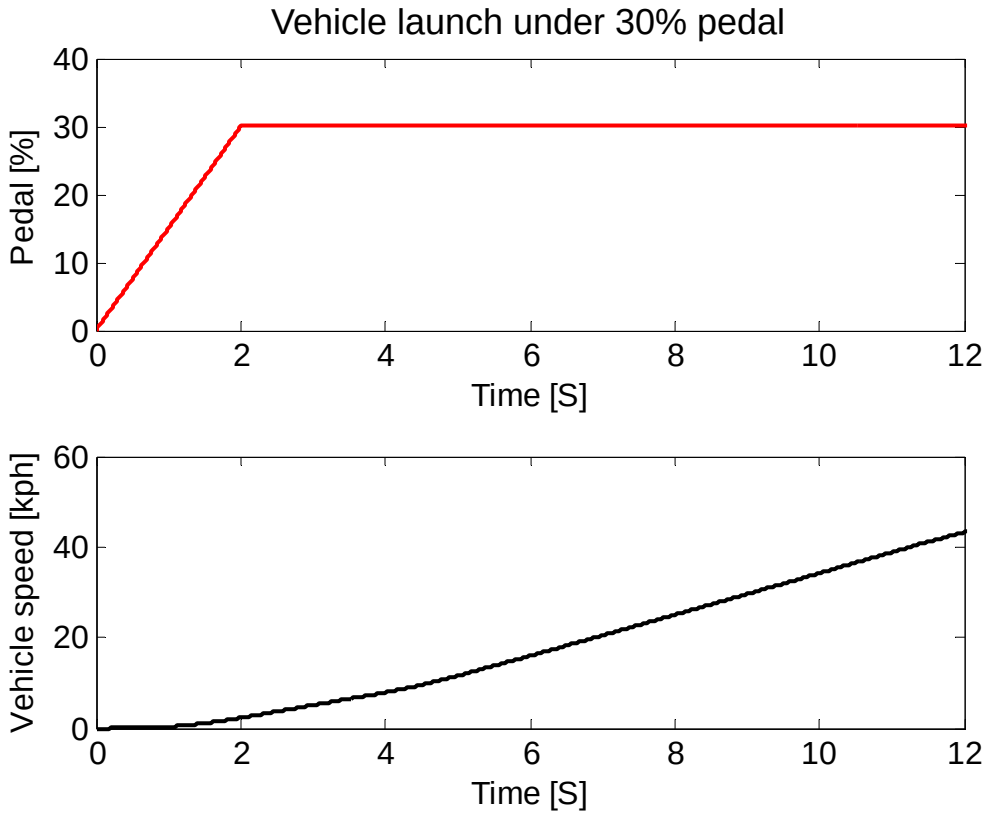

Figure 6-1 Vehicle launch input and vehicle speed

During this short vehicle acceleration process, whole powertrain system experiences EV-HEV mode transition, power-off gearshift as well power-on upshift with active torque-gap filler. Regularly power-on and power-off shifts are judged by whether acceleration pedal is depressed. Due to unique principle of this transmission in this research work, power-off shift means engine is off or acceleration pedal is released; power-on shift means engine is on and acceleration pedal is depressed. The EV-HEV mode transition and power-on upshift are two primary challenges of this HAMT system focused in this work.

6.1 Power-off 1-2 Upshift

This 1-2 upshift occurs as motor can still support vehicle acceleration. The function of this upshift only serves to prepare transmission for engine start and EV-HEV mode transition. As shown in Figure 6-2, 1-2 gearshift command is generated by gearshift controller after 6th second, discussed in 5.3 Gearshift Control. From beginning to this command, engine speed maintains zero, but slip speed of main clutch keeps decreasing because transmission input shaft speed increases with vehicle speed. Since no gearshift nor mode transition is in progress, the generated raw 1-2 upshift command is transferred to actual gear command directly. In contrast, the 2-3 upshift raw command is postponed to avoid gearshift during EV-HEV mode transition (more details in next session).

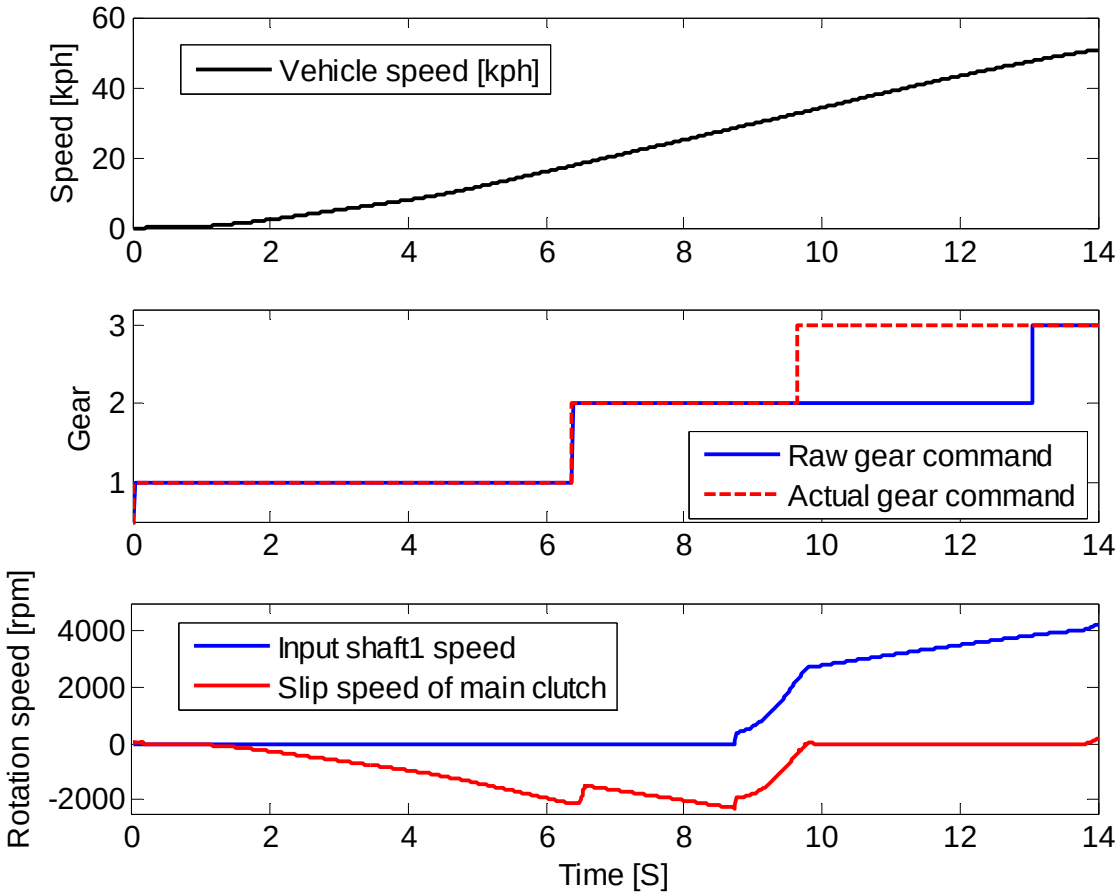

Figure 6-2 Vehicle launch and transmission speeds

The logic how 1-2 upshift command is generated is shown in Figure 6-3. The upshift schedule for engine is included, which is only half of gear shift schedule. Another half is downshift schedule, as shown in Figure 5-17. For this constant-pedal vehicle launch, increasing vehicle speed makes the speed-pedal trajectory move right, crossing different lines, which are boundaries among gears. For example, the 1-2 upshift command is generated as trajectory line cross the first gearshift line. Correspondingly, 2-3 upshift as well as all other power-on upshifts are governed by the same logic.

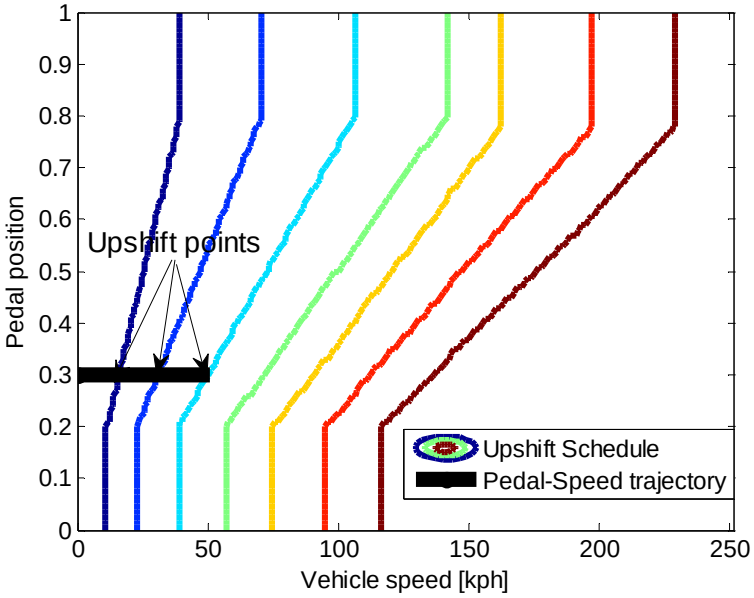

Figure 6-3 Pedal-speed on upshift schedule during launch & EV-HEV mode transition

Figure 6-4 describes how input shaft1 speed changes during this 1-2 power-off upshift in a fan chart. The input shaft1 speed is aligned with target input shaft speed of gear1 because gear1 is engaged. Gearshift happens as input shaft speed jumps from target speed at gear 1 to gear2. The process between the two target lines means inertia phase of this gearshift. The same idea prevails for all upshift, downshift and skip shift (like 1-3 or 3-1 shift).

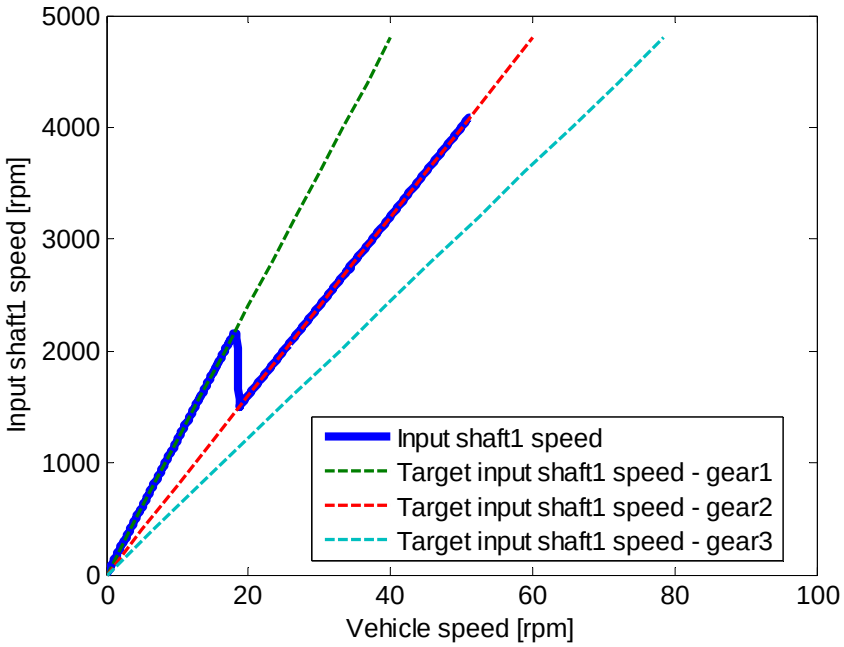

Figure 6-4 Input shaft1 speed and target speeds during launch

A complete power-on shift is decomposed as 6 phases, described in Table 5-3 and Figure 5-18. Compared to power-on shift that will be introduced later, power-off gearshift in this HAMT still

consists of 3 phases – disengaging old gear, speed synchronization of input shaft 1 and engaging new gear. The 3 phases are finished with acting force by actuator that is discussed in detail in subsection 5.2.1.2 Gear Selector Model & Control. The actuator is controlled by actuator controller described in subsection 5.4.3 Control Model for Gear Change.

Figure 6-5 describes how engaged gear (gear1) is disengaged through gear selector actuator and controller. After gear command is sent, controller sends a force command to actuator that is described as a 1st-order function to push synchronizer away from gear 1. To disengage gear, acting force is negative, as shown in subfigure (1) of Figure 6-5. Each side of gear selector is modeled as combination of a dog clutch and cone clutch. Initially, both cone clutch and dog clutch are pushed away until cone clutch rests at 6.4 second. Dog clutch continues to move until it is completely disengaged from gear1. Here, cone clutch moves a short displacement because of structure of gear selector. As dog clutch of gear selector releases gear1 (position of dog clutch less than 3mm), slip speed appears in subfigure (3) of Figure 6-5. Ideally, acting force on gear selector should be zero at this point. However, extra acting force lasts longer to prevent incomplete disengagement during power-on gearshift. After 6.5 seconds, input shaft1 speed is reduced dramatically that indicates another phase of this shift - speed synchronization of input shaft1.

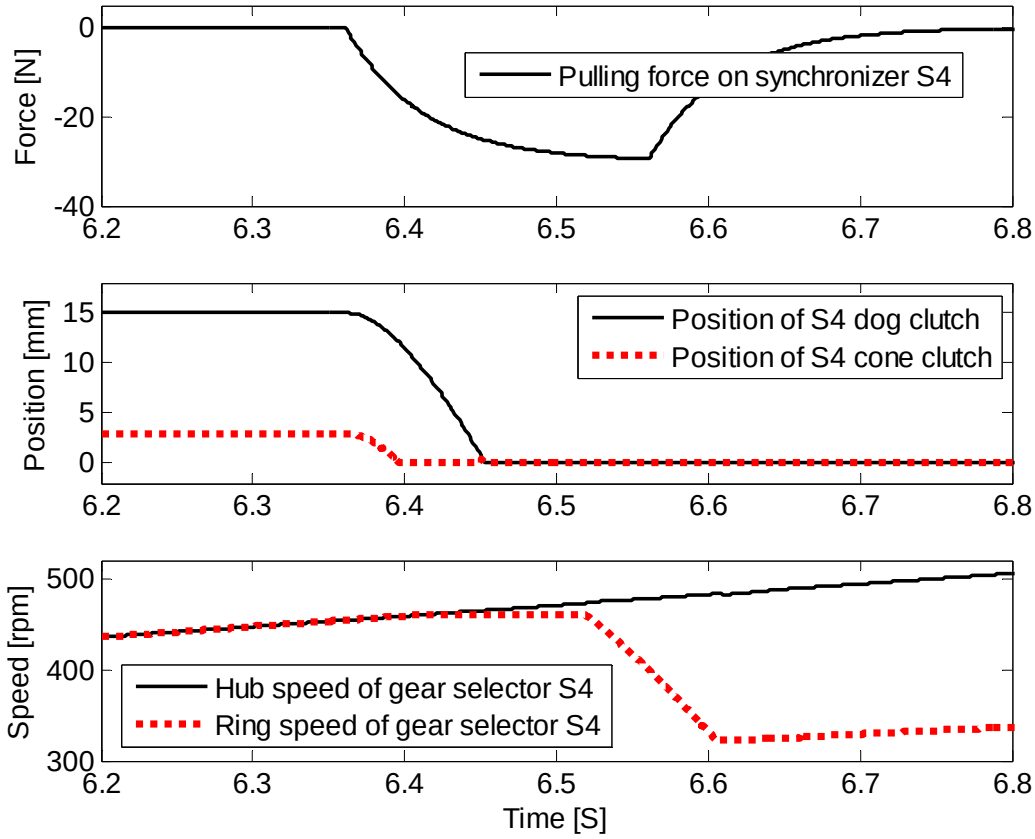

Figure 6-5 Process of disengaging off-going gear selector S4

The speed synchronization is tightly linked to engaging new gear. Synchronizer S1 is commanded a positive acting force by synchronizer controller, as shown in subfigure (1) of

Figure 6-6. With increased acting force, cone clutch and dog clutch of synchronizer S4 starts moving, shown in subfigure(2) until cone clutch moves beyond initial gap (3mm) and generate friction torque between synchronizer and ring gear. The plateau of dog/cone clutch displacement after 6.5 second indicates speed synchronization phase. Friction torque due to acting force of S4 starts to reduce slip speed between hub and ring of S4 until relative speed drops to zero. At the end of speed synchronization, hub and ring of synchronizer S4 share the same speed, which is end of speed synchronization. Since hub speed is directly linked to input shaft1, so transmission input shaft speed drops from about 2200rpm to 1500rpm fast during this speed synchronization phase, as shown in subfigure(3) of Figure 6-2 and Figure 6-4. As a result, two sides of synchronizer S4, described in Figure 5-12, can be locked by moving dog clutch further until maximum displacement. This indicates last phase of power-off gearshift. In order to reduce gearshift time and avoid failed gear engagement as well as overcome friction between moving gear teeth, extra force is added on the acting force to move dog clutch.

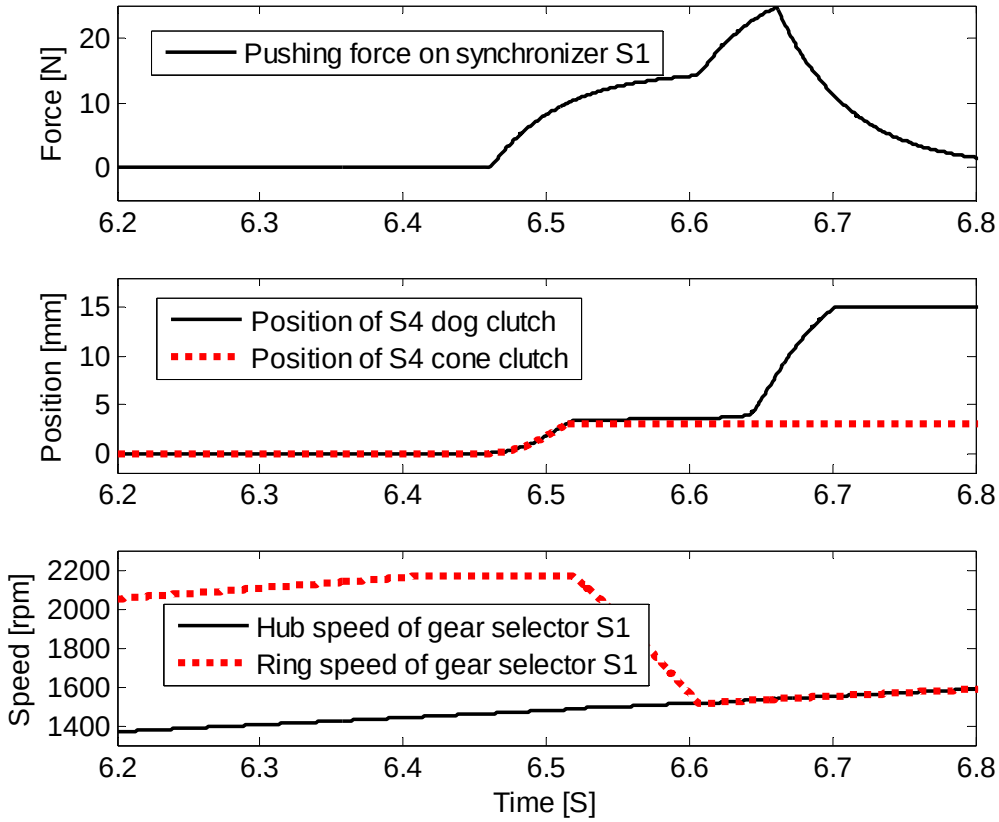

Figure 6-6 Process of engaging oncoming gear selector S1

The friction torque of cone clutch between hub and ring mainly exists during the phase of speed synchronization. Prior to this phase, cone clutch has not touched hub yet; after this phase, there is no relative movement and dog clutch locks hub and ring of synchronizer. Figure 6-7 shows friction torque of synchronizer. The negative sign of friction torque means reduced slip speed; the positive sign after 6.6 second shows static friction torque.

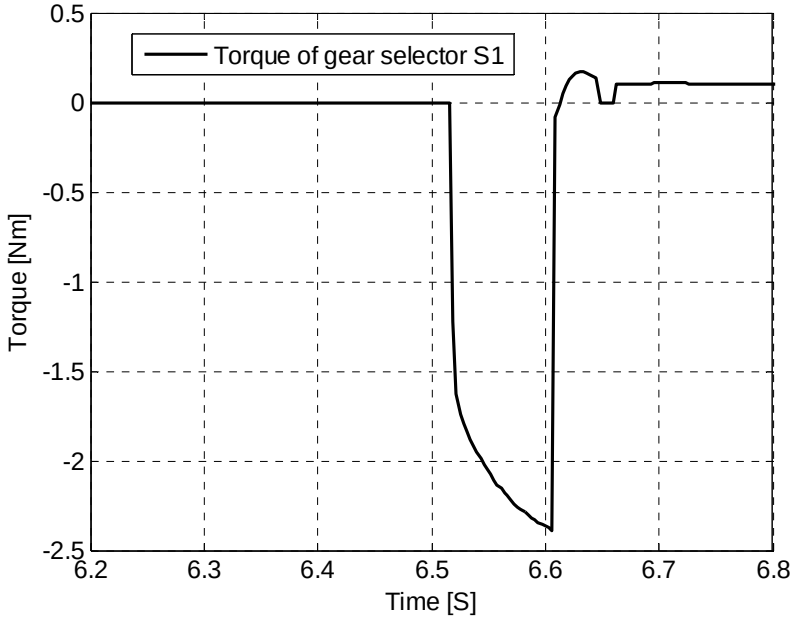

Figure 6-7 Torque of S1 during 1-2 upshift

6.2 EV-HEV Mode Transition

EV-HEV mode transition starts with command for turning on engine. Conditions to turn on engine are summarized in Figure 5-6, including low SOC, high power demand, high torque demand beyond motor capacity and aggressive pedal input. In this simulation, overall power demand is the real trigger. Subfigure (1) of Figure 6-8 shows power threshold and actual power demand prior to and during mode transition. As power demand, which is controlled by pedal position at certain speed, exceeds 25kw, a pre-determined threshold value. A square signal will be sent to engine controller by VCC. In order to avoid wrong command due to signal noise, a filter is needed to calculate power demand. Engine starter, which is introduced in Figure 5-28, will be powered shortly to generate a big torque to accelerate engine fast.

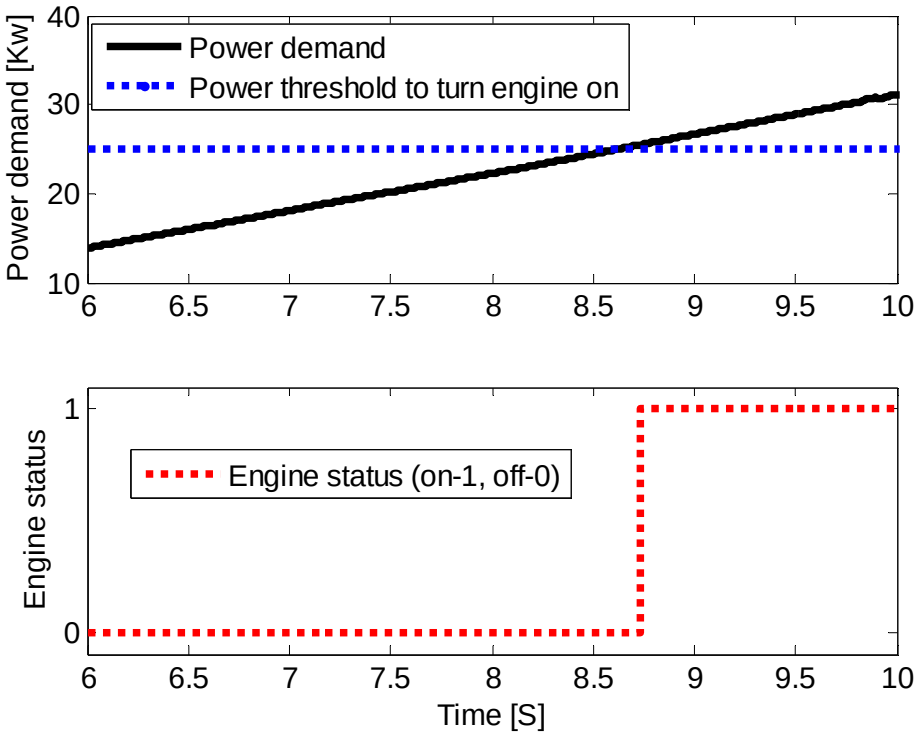

Figure 6-8 Engine starting during EV-HEV mode transition

This EV-HEV mode transition strategy is based on results of optimization using Dynamic Programming. Details of the optimal EV-HEV mode transition is described in Section 4.3 through 4.6. The basic principle of EV-HEV mode transition is extracted from the optimization and summarized in Section 4.7. More detailed analysis on EV-HEV mode transition is discussed in Section 5.5 and Figure 5-24. A complete EV-HEV mode transition includes 4 sequential phases: EV phase, inertia phase, torque phase and HEV phase.

6.2.1 Engine Speed of EV-HEV Mode Transition

Subfigure (1) of Figure 6-9 shows engine speed trajectory in inertia phase after engine ignition. Engine speed increases to 200rpm fast with big starter motor. After that, combustion torque of engine can support the engine acceleration through increased engine power command. Both subfigures (1) and (2) shows engine speed catches up with input shaft speed at second gear without apparent overshoot. After this inertia phase (engine overcoming inertia to adjust speed), engine is rigidly linked to input shaft1 via locked main clutch. Through comparing subfigure (3) of Figure 4-19 and subfigure (1) of Figure 6-9, it can be found easily that our simulation model follows the principle in Figure 4-19 very well during this inertia phase of EV-HEV mode transition.

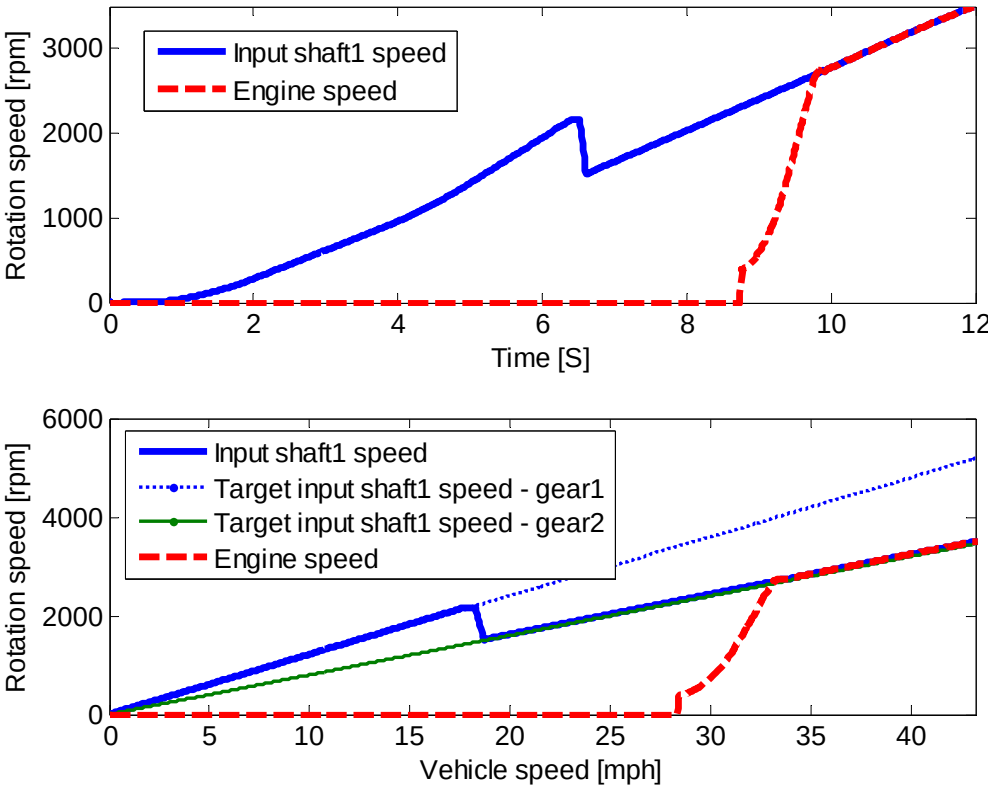

Figure 6-9 Inertia phase of EV-HEV transition

6.2.2 Torques of Engine, Motor and Clutch during EV-HEV Mode Transition

A complete view of engine speed control in inertia phase and torque control in following torque phase, as shown in Figure 6-10 and Figure 6-11, explains clearly how this smooth mode transition is achieved via torque coordination.

The EV phase and inertia phase is separate by engine ignition command. In the first EV phase, although engine mode 3 (speed control mode) is active and engine torque command is above zero in this model, engine is off;

In following inertia phase, engine is turned on due to higher power demand; mode 3 maintains active. A PID controller with upper and lower torque limits, which is summarized in Figure 5-24 (shared with engine speed control during downshift), serves to control engine speed to catch target speed fast and smoothly. As slip speed between engine and input shaft 1 drops, engine torque command drops correspondingly to avoid obvious engine speed overshoot. As engine speed drops to nearly zero and engine torque becomes quite low, main clutch can be locked and engine mode is switched from mode 3 to 4, which is torque control mode. This engine torque is increased gradually, as shown in Figure 6-10.

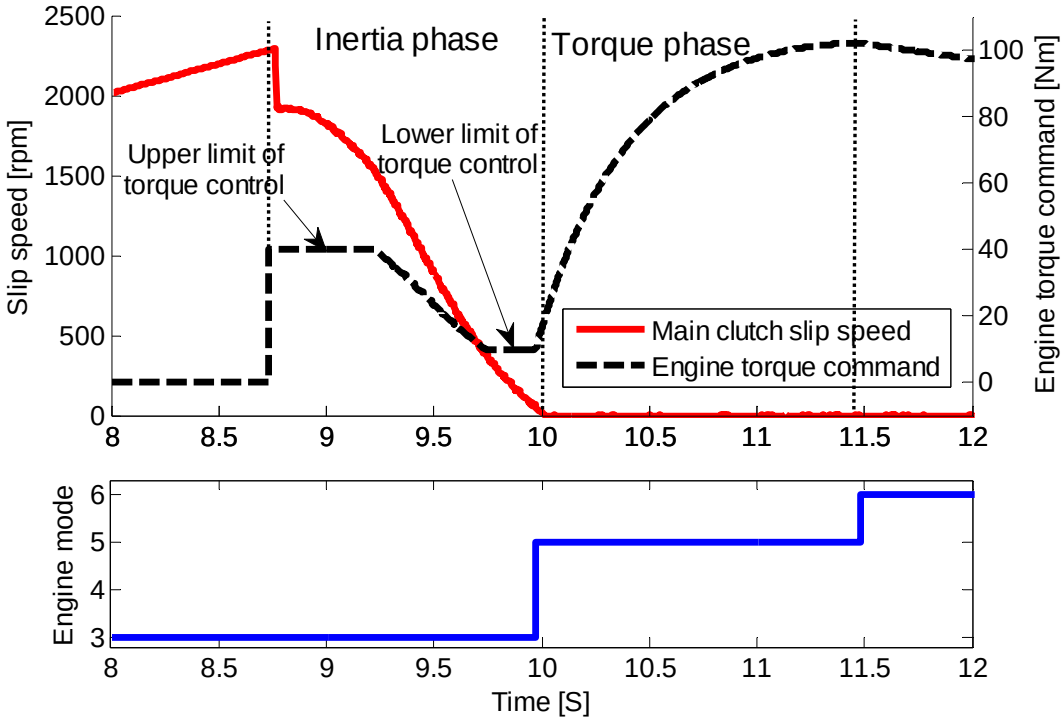

Figure 6-10 Engine speed control during EV-HEV transition

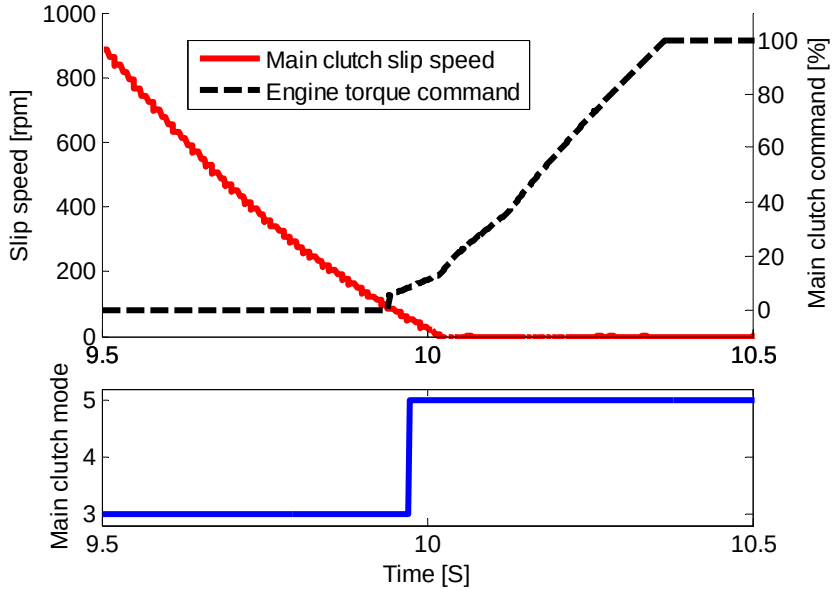

Figure 6-11 Main clutch control during EV-HEV transition

In addition to clutch torque calibration, engine torque control plays a critical role during this phase. As shown in Figure 6-12, the engine torque is controlled to dip to enable low main clutch torque to catch engine shaft easily. Since this torque modulation happens within a very short time, retarding spark timing of each cylinder is a widely used method. Basic principle is to retard timing of ignition from Maximum Brake Torque (MBT) timing to burn gas in a quite inefficient

way. Since this process only lasts for a very short time, fuel economy is not hampered. In this research work, since detailed engine model with combustion system is not modeled, a torque modulation logic modeled by SIMULINK is used to achieve similar effect. Figure 6-12 illustrates the process of engaging main clutch and decrease engine torque right prior to torque phase. Motor serves to coordinate with engine and motor to provide torque compensation. Since mode transition is a simpler version of gearshift with TGF feature, the same formulas explained in 5.4.2 is used for this torque phase. During whole torque phase, main clutch is locked and transfer engine torque via static friction of main clutch. The tiny difference between the engine torque and main clutch torque in Figure 6-12 is inertia loss of engine, including crankshaft, piston, and connecting rod as well as rotating accessories.

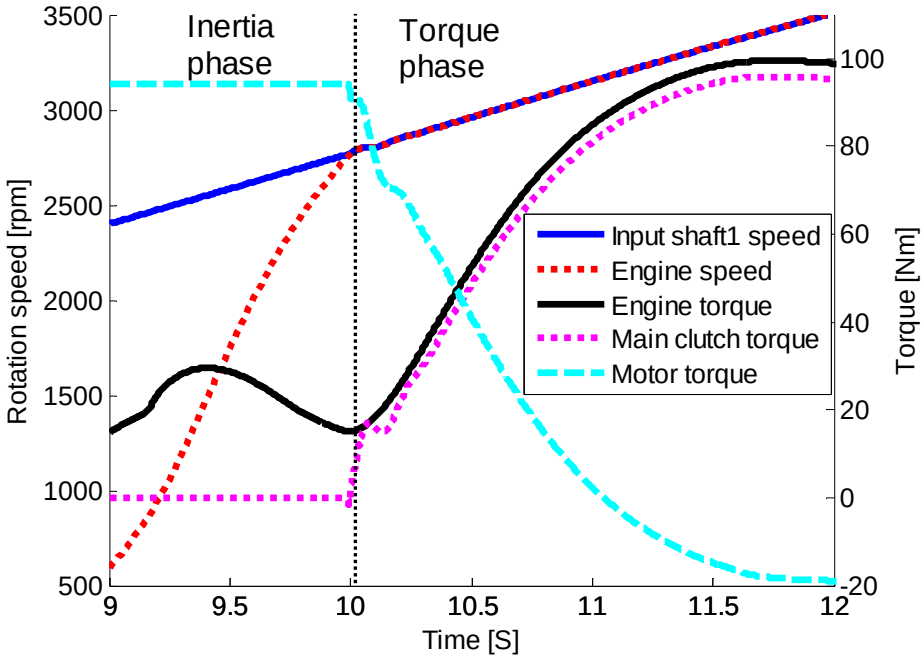

Figure 6-12 Torque inputs to HAMT and main clutch speeds

6.2.3 Vehicle Performance during EV-HEV Mode Transition

Vehicle speed and acceleration during this EV-HEV mode transition is shown in Figure 6-13. Due to well-tuned controller, the vehicle acceleration is stable, which means the EV-HEV mode transition takes place smooth. The short acceleration fluctuation during phase-changing moment from inertia phase and torque phase is still acceptable, based on author's best knowledge in automotive industry and academic filed. The root reason for that acceleration is that non-continuity of main clutch torque due to column friction greatly increases difficulty to coordinate engine, motor as well as main clutch. Main clutch torque changes from a negative torque to positive torque within an extremely short period (about 0.1 second), even if half shaft compliance helps to mitigate the vibration. The trade-off between engine speed overshoot and acceleration smoothness directly leads to this issue.

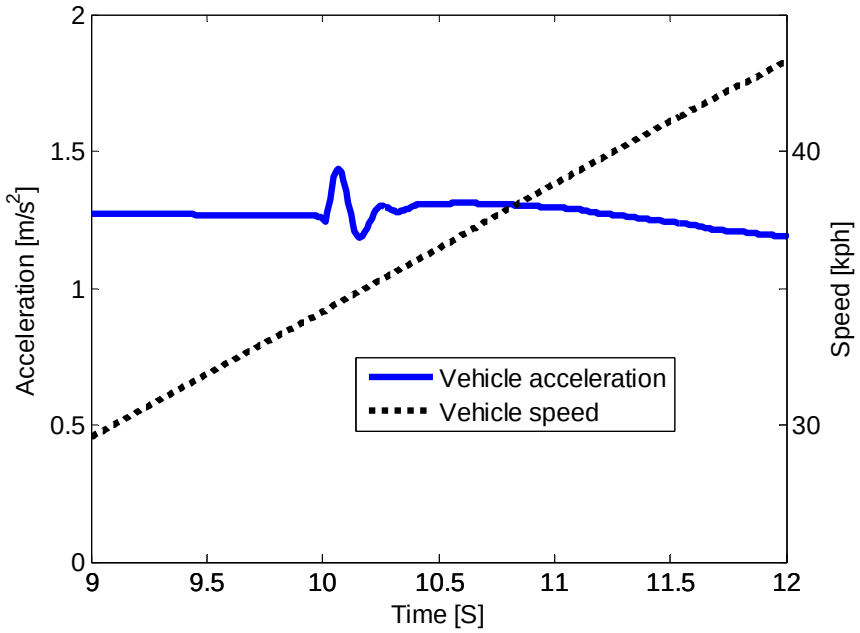

Figure 6-13 Vehicle speed and acceleration during EV-HEV transition

To further improve vehicle driveability during mode transition, motor torque is used as active torque compensator. In order to cancel abrupt increase of main clutch torque that is sent to output shaft directly, motor torque command is modified temporarily in reverse direction, as shown in Figure 6-14. With a slight but fast change of engine torque command, shown in subfigure (2), motor output torque is adjusted to partially cancel abrupt increase of main clutch torque.

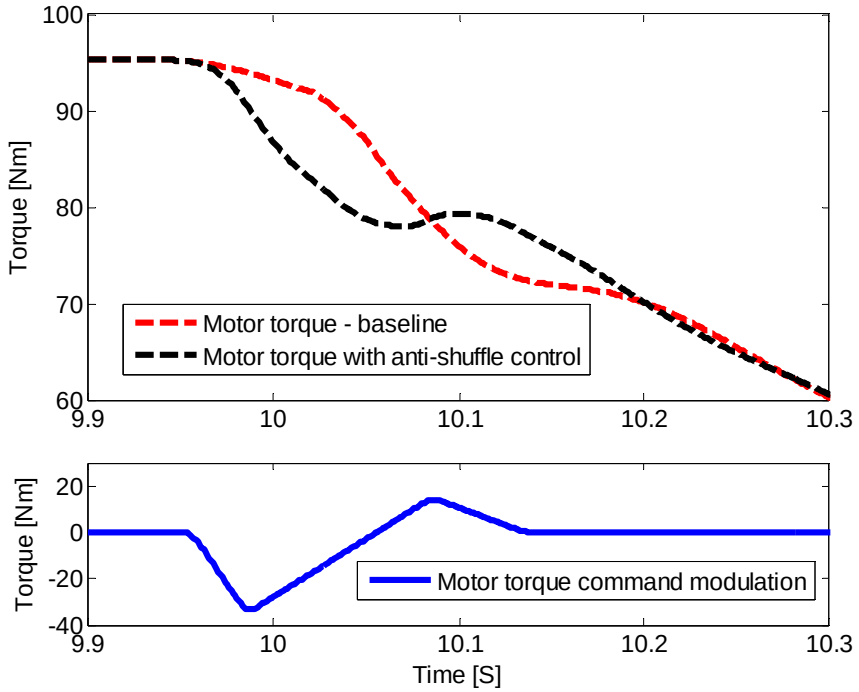

Figure 6-14 Anti-shuffle compensation during mode transition

Simulation results in Figure 6-15 proves this anti-shuffle strategy can further improve vehicle driveability on the base of quite good mode transition. Amplitude of acceleration change is reduced from about 0.25 $m.s^2$ to 0.1 $m.s^2$.

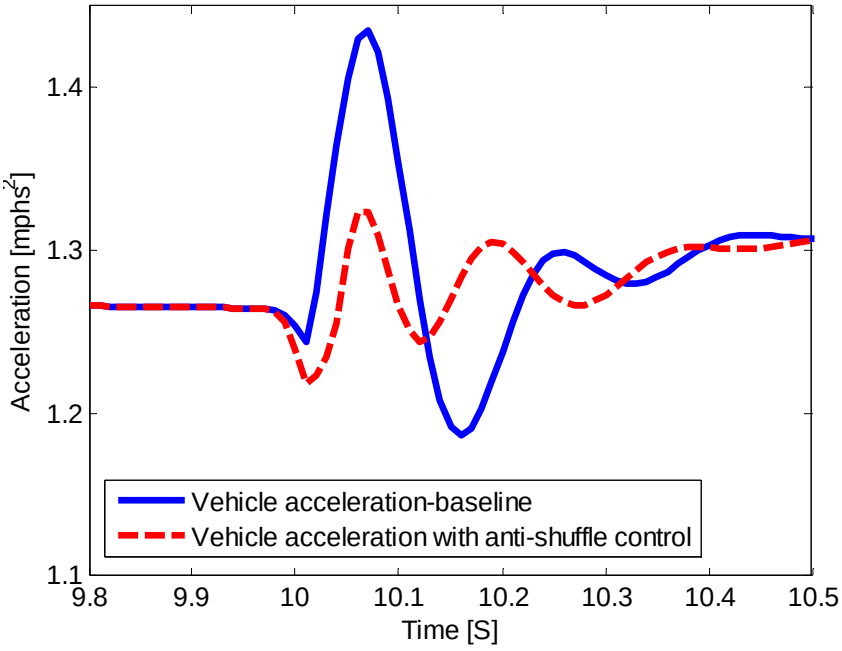

Figure 6-15 Effects of anti-shuffle control on vehicle acceleration

6.3 Power-on Upshift with TGF Feature

Power-on upshift with TGF feature is a comprehensive test for conceptual invention, model and control. Compared to previous power-off upshift, this shift refers to coordination of engine, motor and main clutch; compared to mode transition discussed above, extra torque phase (reducing engine torque and increasing motor torque) and gearshift process makes it more challenging than mode transition. Power-on upshift with TGF feature is even more complicated than combination of power-off gearshift and mode transition.

Figure 6-16 shows first 20 seconds of vehicle acceleration under 30% pedal. With increased vehicle speed, speed-pedal trajectory moves on upshift schedule and cross several upshift schedule lines, as shown in Figure 6-17.

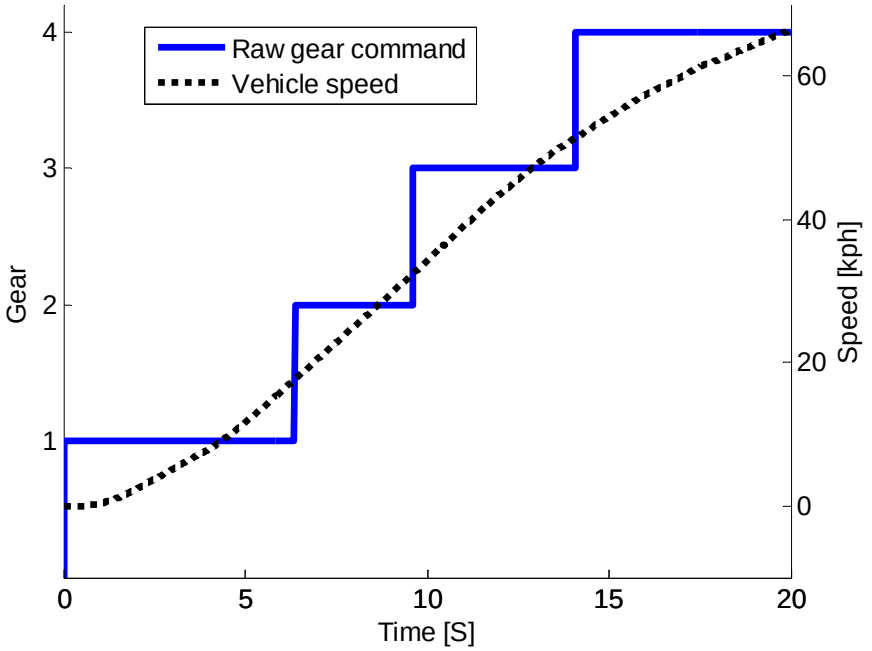

Figure 6-16 Vehicle launch under 30%

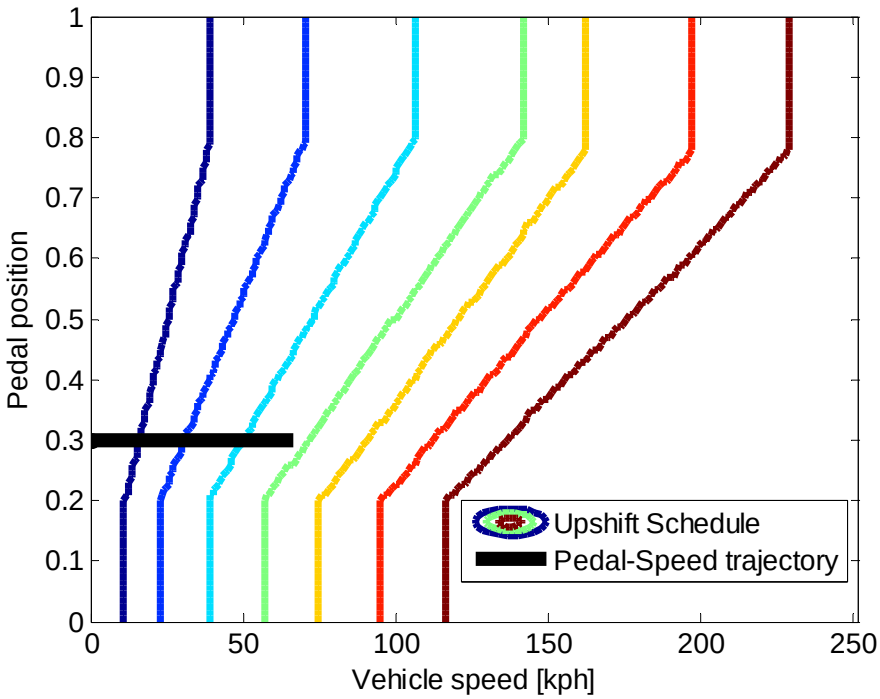

Figure 6-17 Pedal-speed trajectory on upshift schedule during launch

The 1-2 upshift has been discussed in subsection 6.1 Power-off 1-2 Upshift. The 2-3 upshift command is generated at about 10th second, when EV-HEV mode transition is under way. As shown in Figure 6-18, actual 2-3 upshift command is postponed by several seconds until mode transition is fully completed. Correspondingly, 3-4 upshift is postponed until 2-3 upshift is finished.

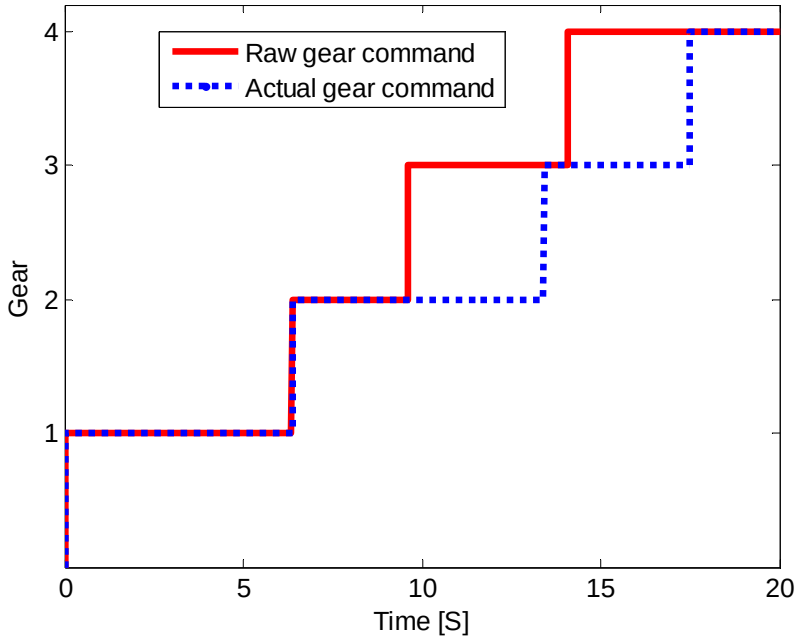

Figure 6-18 Raw gear command and actual gear command

6.3.1 Gearshift Process with TGF

Gearshift principle of this HAMT has been illustrated extensively in section 5.3 Gearshift Control and 5.4 Structure of TGF Control. The 3 primary phases – torque phase 1, inertia phase and torque phase 2 - of HAMT gearshift that is illustrated in Figure 5-18, can be clearly identified from Figure 6-19. From 13.5 to 14.3 second, engine torque together with main clutch torque decreases; meanwhile, motor torque increases to fill the torque gap gradually to reach a relatively stable acceleration. As main clutch torque drops to zero, engine is totally disconnected from transmission. During a short duration of about 200ms, previously engaged gear is disengaged and new gear is engaged. Engagement of new gear is featured by fast change of input shaft speed. From about 14.5 second to 15 second, engine speed is synchronized with input shaft 1 speed through friction torque of main clutch, shown in subfigure (3) of Figure 6-19. Followed is torque phase 2, which features increasing engine and main clutch torque and decreasing motor torque. It is easy to see how similar the torque curves are to the engine and motor torques in Figure 5-18. Therefore, it is safe to claim the proposed TGF concept is successfully implemented in simulation model.

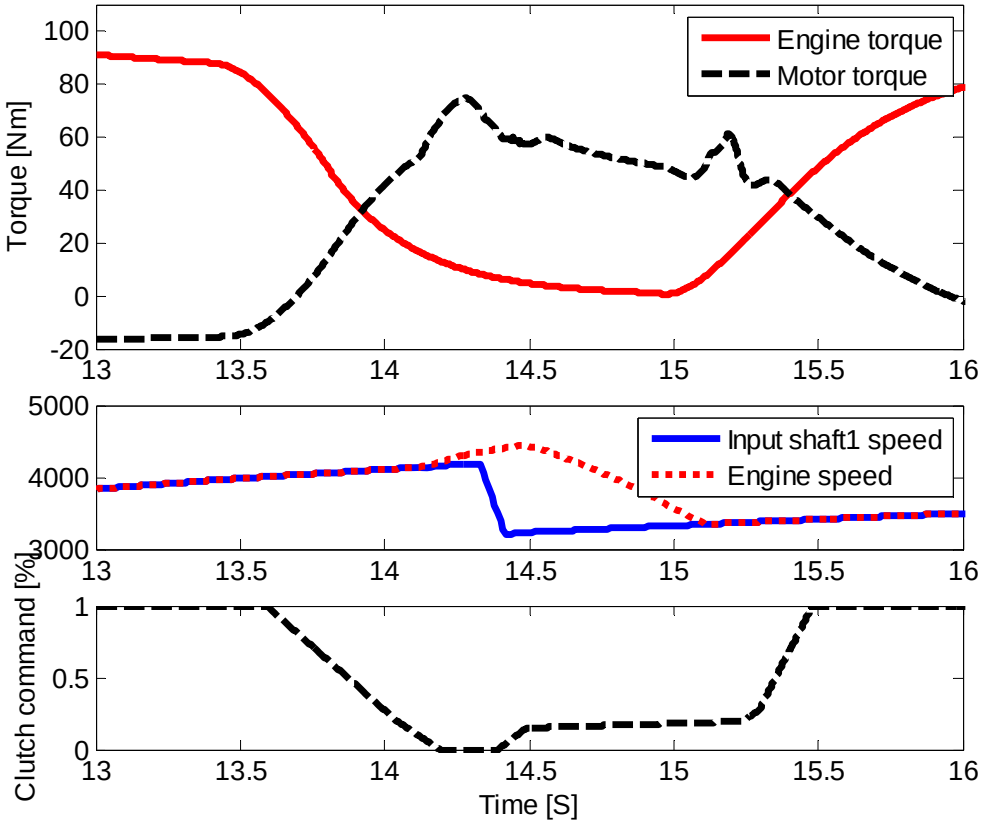

Figure 6-19 Simulation of power-on upshift with TGF feature

The other 3 sequential phases between torque phase 1 and inertia phase in Figure 5-18 are displayed in Figure 6-20 and 6-21. As long as main clutch is open, gearshift controller will send command to actuator to disengage synchronizer S1 that pushes dog clutch and cone clutch away from engaged gear. The gear is completely disengaged as position of dog clutch drops below 3mm. Shortly after full disengagement of S1, actuator of S2 pushes corresponding dog clutch and cone clutch. After consuming initial clearance, the friction torque due to acting force will eliminate slip speed between hub and ring of synchronizer S2. This whole process is discussed elaborately in section 6.1 Power-off 1-2 Upshift.

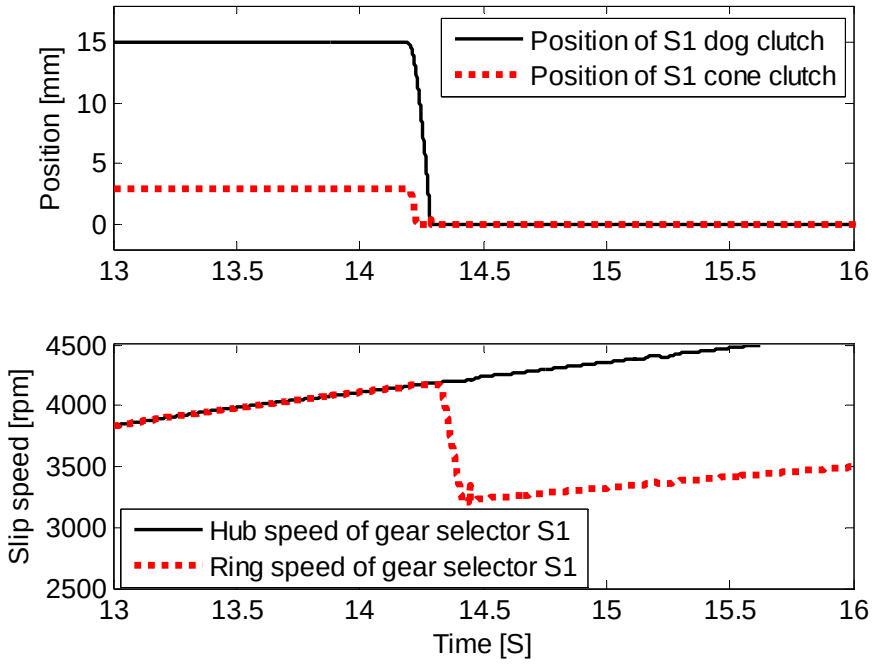

Figure 6-20 Disengagement of old gear during gearshift

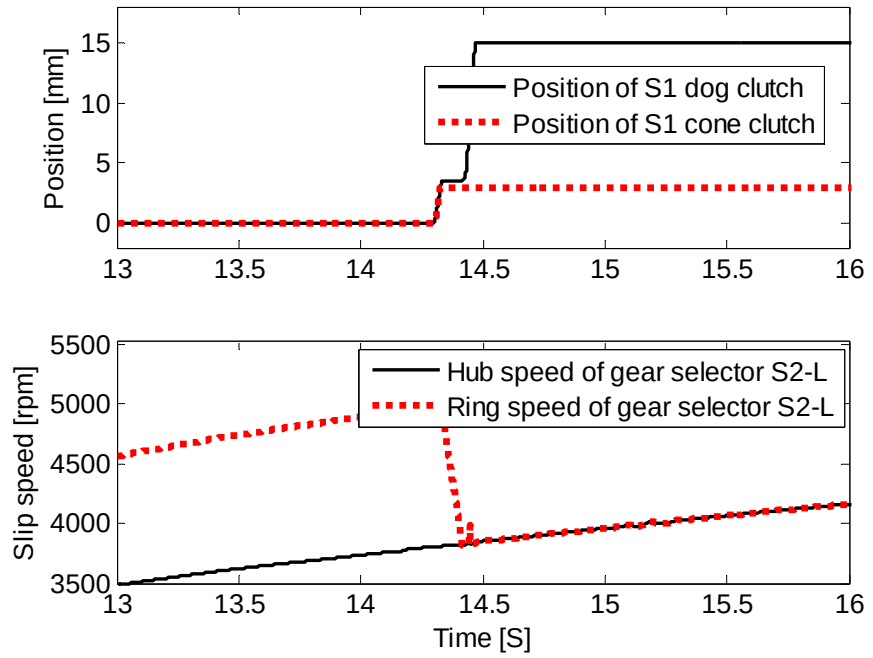

Figure 6-21 Engagement of new gear during gearshift

Figure 6-22 shows slip speed trajectory after torque phase 1 until torque phase 2. The slip speed increases slightly because remaining engine torque drives disconnected engine shortly. As engagement of new gear happens, input shaft 1 is decreased very fast. Compared to input shaft speed, engine speed is relative stable because engine has much bigger moment of inertia and remaining engine torque preventing engine speed drop fast. As a result, slip speed of main clutch

soars during engagement of new gear. As main clutch is re-engaged at about 14.5 second, kinetic friction of main clutch drags engine speed to input shaft 1 speed within 0.5 second. The main clutch torque has two dips, one prior to 14.5 second and another one after 15 second, although gear command in subfigure (3) of Figure 6-19 is quite smooth. This is related to status change of main clutch model – from open clutch to slipping clutch and from slipping clutch (kinetic friction) to locked clutch (static friction).

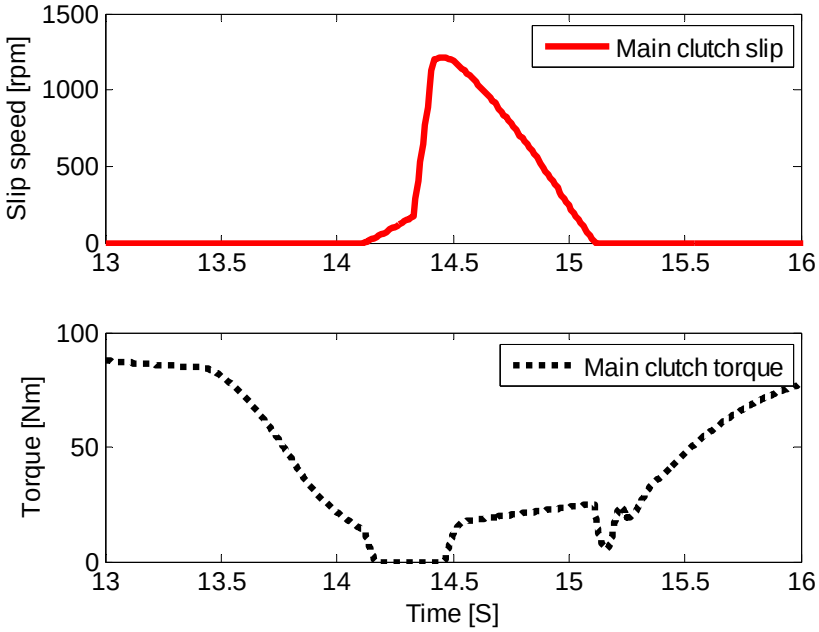

Figure 6-22 Inertia phase of gearshift with TGF

6.3.2 Vehicle Speed and Acceleration

Vehicle response during this 2-3 power-on upshift is shown in Figure 6-23. By turning off the TGF feature during gearshift, the effect of TGF on vehicle performance is shown clearly. The two vehicle deceleration curves with and without TGF show the effect even more clearly. Due to lack of TGF feature, vehicle acceleration drops to slight negative (air drag and rolling resistance); in comparison, the vehicle with active TGF can achieve relatively steady acceleration. The fluctuation of acceleration coincides with clutch torque change between different phases.

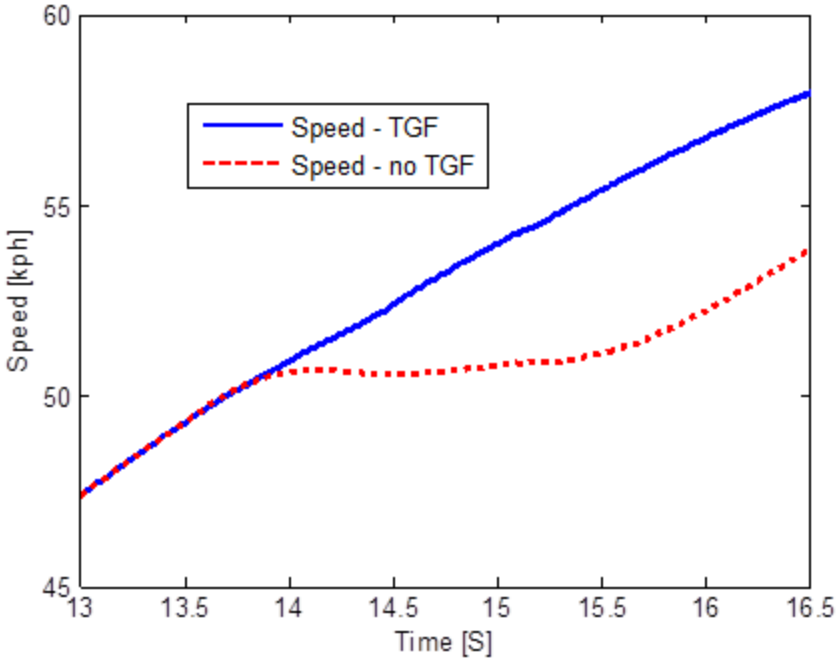

Figure 6-23 Effects of TGF feature on vehicle performance

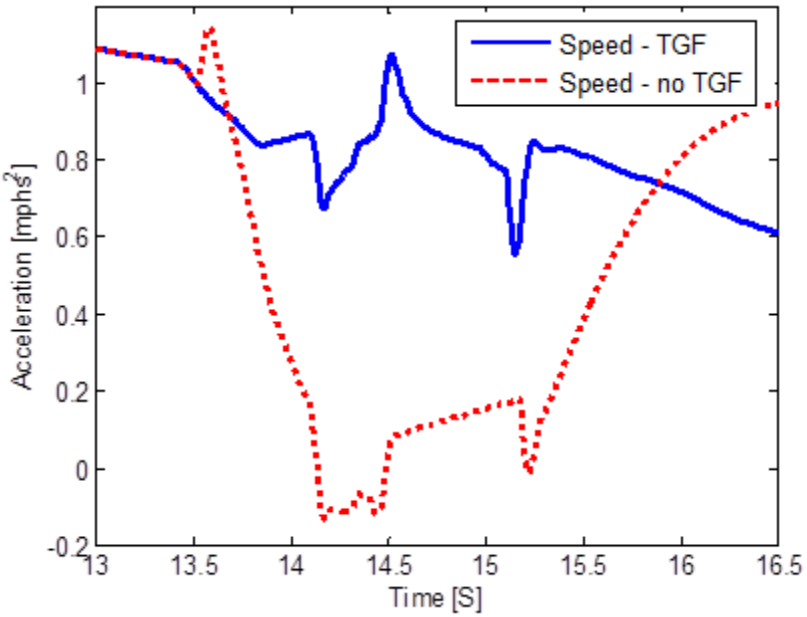

Figure 6-24 Effects of TGF feature on vehicle driveability

The same anti-shuffle compensation method using electric motor torque to mitigate vehicle acceleration change is used. The compensation torque commands at 2 instances are added to normal torque command to smoothen vehicle acceleration. The 1st compensation torque command serves to cancel the clutch torque change during disengagement of main clutch and reengagement; the 2nd compensation torque command serves to fill the torque change as main

clutch slip speed disappears. The anti-shuffle compensation method successfully improves gearshift quality.

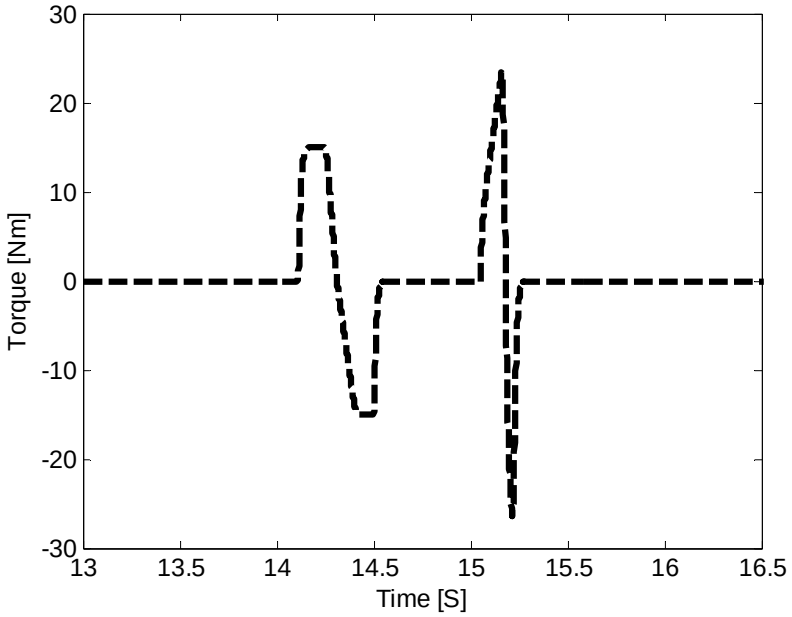

Figure 6-25 Anti-shuffle torque compensation during power-on upshift

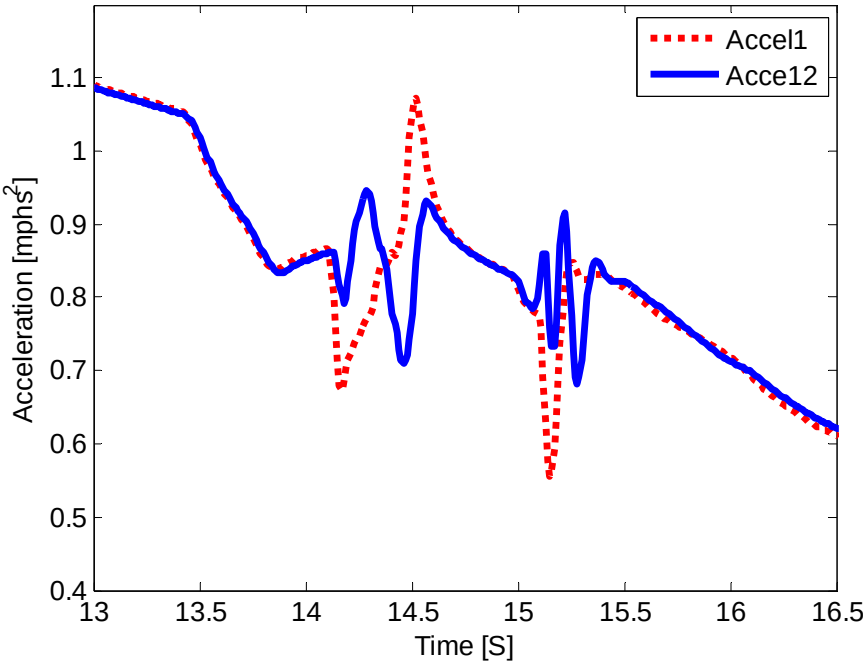

Figure 6-26 Effects of anti-shuffle torque compensation during power-on upshift

6.4 Summary

Simulation of this HAMT-based hybrid vehicle model is completed successfully. Considering complexity of powertrain control, a fixed-pedal vehicle launch is decomposed in detail to demonstrate how this hybrid powertrain system with natural high driveline efficiency can deliver

better performance and avoid persistent driveability issue. This chapter covers 3 typical events to reveal deeply how this hybrid system works. The power-off upshift is a good test to verify the functionality of gearshift mechanism, its controller and the actuator. The EV-HEV mode transition shows that the smooth mode transition can be achieved as long as principle of the mode transition is followed and controller can coordinate engine, motor and main clutch. The 2-3 power-on upshift serves to test the HAMT system with potential driveability advantages and verify simulation model as well as its control logics. In light of non-discontinuity of main clutch torque and its influence on vehicle driveability, motor is assigned a new role as torque compensator. Simulation results prove this idea and further strengthen advantage of this HAMT-based vehicle.

7 Summary

Research work presented in this thesis focuses on a novel type of hybrid system that is based on Hybridized Automated Manuel Transmission. Chapter 1 introduces development of electrification and classification of primary hybrid vehicle architectures and latest development of hybrid technologies. Advantages of AMT and its driveability shortcoming are discussed in detail. HAMT is proposed as a promising candidate to inherit advantages of regular AMT and avoid undesirable driveability. This chapter is summarized in Section 7.1. Chapter 2 introduces operating principle of proposed HAMT-based hybrid system, and illustrate torque/power flow paths among different components and insider HAMT. Chapter 3 illustrate clutch combinations for different gears and how optimization method is used to fix two gear ratios for EV mode; Chapter 2 & 3 is summarized in Section 7.2. Chapter 4 covers system dynamics and details of vehicle modeling principles, including details about gear shift mechanism, controller and main clutch model; a model-based optimization method employing Dynamic Programming helps to find the optimal control trajectories of primary components during mode transition. Four mode transition principles for powertrain are extracted from the optimization results. This chapter is summarized in Section 7.3. Chapter 5 describes details of vehicle model configuration, Vehicle Central Controller, sub-system controllers (engine control, gearbox control, motor control and main clutch control) and a lot of details about how the research subject is modeled in Simulink-SimDriveline platform; rule-based control strategy based on global optimization for improving driveability is implemented on simulation model; This chapter is summarized in Section 7.4. Chapter 6 provides simulation results of this hybrid system during target driving scenarios, including power-off gearshift, mode transition and power-on gearshift. The simulation results clearly show that objectives are achieved successfully. This chapter is summarized in Section 7.5. Original contributions of this work are listed in Section 7.6 and recommended future work is illustrated in Section 7.7.

7.1 Powertrain Electrification Trend and HAMT-Based Hybrid Vehicle

This chapter gives a fundamental introduction of one representative HAMT-based parallel hybrid powertrain system, disclosed in one patent application [61]. Firstly, abstract concept of various HAMT is introduced. Essential differences of those listed typical HAMT variations are explained using a special power-flow triangle with 3 ports. Then, a novel type of HAMT is described. Detailed power flow paths in hybrid mode and EV mode are covered, including status of clutch, engaged and disengaged gear selectors. Gear ratios in each mode as well as relationship of gear ratios of two modes are also defined. Mode-transition process between hybrid mode and EV mode is also covered. In this chapter, the first challenge described in 1.4.1 is solved and first objective in 1.5 is achieved. This chapter provides key research subject in following chapters to overcome other 2 challenges and achieve remaining objectives.

7.2 HAMT System and Its Gear Ratio Design Optimization

This hybrid system supports EV mode and hybrid mode. In the process of designing gear ratios, hybrid mode is major consideration. Gear ratios for hybrid mode are determined based on classical method: progressive step ratios. Considering extra constraints for gear 3 and gear 4, gear ratios are adjusted to achieve stable ratio steps. The same set of gear ratios is also used in EV mode. Since there is no need to use up to 8 gear ratios, three fundamental questions are answered: 1) how many gears are needed? 2) which gears are needed? and, 3) what is gearshift schedule for selected gears? At first, two speeds are accepted as good choice based on past research work. Then, one model-based optimization method, based on Dynamic Programming, is used to generate optimal gear ratios and optimal gearshift schedule. Key model parameters are based on Transit Electric presented by Ford and Azure Dynamics. This optimization of gear ratio and gearshift schedule helps to find optimal ratio step is 1.89. This ratio step provides a good reference to answer the second question: selecting gear ratios from available ratios. Considering importance of selector 3 and this optimal ratio step, eventually 4^{th} and 6^{th} possible gear are selected for EV mode. The third question is also answered by the optimization method. Although eventual ratio step, 1.67, in EV mode is a little different from optimal ratio step, the gearshift schedule is inherited because two ratios steps are quite close.

7.3 Powertrain Dynamics and Optimization of Mode Transition

This chapter starts with a LMM model to describe driveline dynamics. As key elements of this hybrid system based on invented HAMT, clutch principle, selected clutch model as well as model of gear selector are described specifically. Driveline dynamics in two steady states and four transient states are analyzed using the LMM model. Each state is analyzed independently, according to states of main clutch as well as gear selectors. These operating modes in steady and transient states consist of fundamental phases of both Torque-Gap-Filler feature and EV-HEV mode transition. Operating principle of TGF is first studied and decomposed into 7 sequential phases, which belong to the 4 transient operating modes and 2 steady operating modes. Each phase of TGF is explained. Then, another important driveability-related event, EV-HEV mode transition, is decomposed to study control principle. This mode transition is further split as 2 primary phases: inertia phase and torque phase, which are commonly used in automotive industry for analysis of conventional automatic transmission. In light of great importance of mode transition as well as its connection to TGF via common phases, a model-based optimization method is proposed to extract rule of powertrain control via model-based global optimization. This research work selects post-transmission parallel PHEV to develop understanding of mode transition that is unique and significant for hybrid vehicles. The powertrain model was initially established based on AUTONOMIE and SIMULINK, and primary parameters are from real platform or ASM model of dSPACE. A global optimization method using DP is proposed to calculate optimal inputs to powertrain. Results of optimal control show 4 principles for clutch control, inertia phase and torque phase.

7.4 Modeling and Control of HAMT-based HEV

This chapter introduces a baseline plug-in parallel hybrid model from AUTONOMIE library at first. Driver model, supervisory powertrain controller and vehicle model are discussed briefly. The baseline simulation model is tailored extensively to build a customized simulation model that shares the same powertrain architecture of research subject. For purpose of avoiding time-consuming and troublesome modeling work in flexible operation modes and complicated power flows, the whole Simulink model of driveline system in baseline model is completely replaced by SimDriveline model. In addition to replacement, non-existing gearshift actuator model and corresponding controller are also modeled to capture how gearshift process is finished. Meanwhile, remaining parts of baseline model is reserved. This SIMULINK-SimDriveline hybrid powertrain model is used to test proposed control strategy for desirable driveability. In order to achieve smooth gearshift, Torque-Gap-Filler feature is analyzed in detail and further split into 7 phases. Three key phases, which are torque phase 1, inertia phase and torque phase 2, are discussed in detail. In light of difference between upshift and downshift, different control principles are discussed in detail. Finally, EV-HEV mode transition is also discussed, as the mode-transition is very similar to the second half of downshift. This chapter provides some key information about modeling and control.

7.5 Simulation Results

Simulation of this HAMT-based hybrid vehicle model is completed successfully. Considering complexity of powertrain control, a fixed-pedal vehicle launch is decomposed in detail to demonstrate how this hybrid powertrain system with natural high driveline efficiency can deliver better performance and avoid persistent driveability issue. This chapter cover 3 typical events to reveal deeply how this hybrid system works. The power-off upshift is a good test to verify the functionality of gearshift mechanism, its controller and actuator. The EV-HEV mode transition shows that smooth mode transition can be achieved as long as principle of the mode transition is followed to allow the ontroller to coordinate engine, motor and main clutch. The 2-3 power-on upshift serves to test the HAMT system with potential driveability advantage and verify the simulation model as well as control logics. In light of non-discontinuity of main clutch torque and its influence on vehicle driveability, motor is assigned a new role as torque compensator. Simulation results prove this idea and further strengthen advantage of this HAMT-based vehicle.

7.6 Summary of Original Contributions

Original contributions of this research work are summarized as below:

1) A series of novel hybrid powertrain systems based on hybridized automated manual transmission are proposed. These new hybrid systems can more gear ratios in EV and HEV modes using less gear wheels. Compared to other types of hybrid powertrain, it can potentially improve efficiency, expand torque range as well as

avoid driveability issues of regular AMT through TGF. Even if compared to dominating Synergy Drive System of Toyota, this hybrid system is also advantageous in torque capacity, IP and manufacturing;

2) Torque flows, in EV mode and HEV mode at various gears, of a representative 8-speed HAMT system are defined through special gear selector arrangement; gear ratios of each gear HEV mode are designed using progressive gear ratio method; the gear ratios for EV mode are finalized through optimization method;
3) Powertrain dynamics of the representative hybrid vehicle is analyzed thoroughly, including 2 steady modes and 4 transient modes. Gear shifts and mode transition are split in fundamental phases. A model-based global optimization is used to develop optimal control principle for mode transition and gearshift;
4) A full vehicle simulation model, including the proposed HAMT, gearshift schedule, complete gearshift actuator and controller, are built based on a baseline model with extensive change on baseline model; the customized SIMULINK-SimDriveline vehicle model can simulate not only complicated power flow within HAMT but also complicated gear shift and EV-HEV mode transition;
5) A complete control strategy is developed, enabling vehicle to run in EV mode and HEV mode, finish EV-HEV mode transition and complicated TGF operation during gearshift smoothly. For each phase of mode transition and gearshift, engine, motor, main clutch and gearshift actuators in HAMT are controlled to coordinate to achieve desirable driveability. To reduce negative impact on driveability, torque cancellation control during mode transition and gearshifts are used to maintain stable acceleration. Simulation results show that invented hybrid system can overcome persistent driveability issues of regular AMT and take advantage of its benefits in efficiency and torque capacity over other competitors, making it a strong candidate in this trend of vehicle electrification.

7.7 Recommended Future Research

This research work opens new opportunities in this fast-changing period for automotive powertrain research. There are many interesting and promising topics that could be potential from aspects of efficiency, costs, driveability and performance. Here, some of those are listed and discussed briefly.

7.7.1 Optimization of Gearshift for Improved Efficiency and Performance

Gearshift schedule is an extremely important map for vehicle. It can apparently influence fuel economy, performance and driveability. A good shift schedule is based on deep understanding of powertrain components and integral system. Currently, automotive engineers create such schedule via tedious calibration to balance conflicting factors. For different driving scenarios or driver inputs, different gearshift schedules can be selected. Since those calibration work is finished prior to production of vehicles, those gearshift schedule can only suit for a majority of

cases (achieve relatively good efficiency, meet performance target and avoid bad driveability). However, these gearshift schedules relying on calibration is far from optimal solution. Considering unique driving pattern of each driver and climate difference, a systematic tool based on constrained optimization tool is a promising direction. In light of fast increase of transmission speeds over the past 10 years, count of possible gearshifts increases exponentially. In addition, real-time traffic conditions, weather and climate change further dim opportunities of this calibration method. This topic has become a common issue in automotive world. This is always a critical problem for HEV, PHEV or conventional vehicle. As author's best knowledge, there is no groundbreaking progress in this direction, although it has attracted more and more attention. For this proposed 8-speed HAMT system, optimization of gearshift schedule is of high importance as well.

7.7.2 Application of Advanced Control to Powertrain Operation

A rule-based control strategy based on model-based optimization is used in this method. The results strongly prove the conceptual hybrid powertrain system can be free of long-time driveability issue. This rule-based method, including multiple PID controllers, is also widely applied in automotive industry all over the world. From aspects of cutting calibration costs and further releasing driveability potentials, it is beneficial to apply more advanced control method to powertrain control, especially during transient events like mode transition and gearshift. New research work keeps emerging to reach the goal via different paths, like H-infinity control, model predictive control and sliding mode control, but this direction is still far from mature. Ideal state of control strategy should be calibration-free control. Apparently, this is still a realistic at this stage. Still, this further strengthens necessity and urgency of this research direction. Back to research subject, many upshifts and downshifts under different driving pedal levels and vehicle speeds are needed to meet driver demand. It is extremely difficult to calibrate such a hybrid system to achieve mode transitions and gearshifts in all scenarios if only traditional method is used.

7.7.3 High-predictability Model of Vehicle System

Model with high predictability is becoming more and more important in automotive industry and research. Stringent regulations and intense competition are pushing engineers and researchers to look for all possible opportunities to improve product. This requirement heavily relies on high-fidelity model with good predictability. As long as model becomes good enough to replace chassis, powertrain or vehicle tests, many tests can be replaced by simulations. This can help automotive manufacturers cut costs and improve product performance. In addition, high-performance computer makes model more useful for control system design and calibration. From aspect of research, high-predictability model is also critical to reveal some details that are not measureable or hard to measure. For example, twisting angle of driveline during gearshift or mode transition is hard to measure due to small amplitude and fast change. However, it is important to NVH and anti-shuffle control. A good simulation model can help detect this

deformation. Another example is engine friction torque due to mechanical friction between moving parts, like between piston rings and cylinders, valvetrain and valves. These physical variables are extremely difficult to be measured at high accuracy.

For this proposed 8-speed HAMT, more details of the system is no doubt beneficial to future development. For example, a high-fidelity model of main clutch together with damper is useful to improve control system. Good simulation model can help to select most effective control methods; good model and advanced control methods can work together to deliver a realistic and outstanding powertrain control strategy.

7.7.4 Development of AMT-based Transmission for EV

EV is predicted to be another key player in next decade. Currently, top-selling EVs on markets, like Nissan Leaf and Tesla Model S and X, use one motor to propel l vehicle directly, rather than via any transmission with variable gear ratios. This simple configuration depends on following factors: 1) wide speed range of motor; 2) high torque capacity at low speed; 3) flat map efficiency. The factor 1 allows motor to drive at high vehicle speed without changing gear ratio; factor 2 allows motor to launch vehicle at high acceleration without increasing gear ratio; factor 3 enables high efficiency at variable gears without having to adjusting operating points of motor.

However, EV with variable gear ratios has never been out of scope of researcher and engineers, in both industry and academic institutes. It is very possible that more severe market competition will amplify effects of transmission for EV. For example, transmission can increase torque output during vehicle launch and lower motor speed at highway. This can lower requirements for motor. Even if considering motor efficiency only, motor efficiency at margin of efficiency map is apparently lower than peak zone. Previous study also supports this point.

Among various transmission options, AMT-based transmissions hold some unique advantages over AT-based or CVT-based transmissions. This can be an extension of the research subject. It is quite easy to convert the researched HAMT to a clutchless transmission for EV. A separate application is also submitted for US patent.

8 Bibliography

[1] dSPACE, [Online]. Available: http://www.dspace.com/en/pub/start.cfm.

[2] U.S. Energy Information Administration, "Annual energy outlook 2013," www.eia.gov/forcasts/aeo, Washington, DC, 2013.

[3] H. Naunheimer, B. Bertsche, J. Ryborz and W. Novak, "Overview of the Traffic - Vehicle - Transmission System," in *Automotive Transmissions*, Heidberg, Dordrecht, London, New York, Springer, 2011, p. 70.

[4] US EPA, US DOT, *2017 and Later Model Year Light-Duty Vehicle Greenhouse Gas Emissions and Corporate Anverage Fuel Economy Standards; Final Rule,* 2012.

[5] U.S. EPA, NHTSA, "Joint technical support document: final rulemaking for 2017 - 2025 light-duty vehicle greenhouse gas emission stadnards and corporate average fuel economy standards," 2012.

[6] "SAE J1715 information report, hybrid vehicle (HEV) and electric vehicle terminology," 2007.

[7] J. M. Miller, Propulsion Systems for Hybrid Vehicles, London: The Institution of Engineering and Technology, 2004.

[8] X. Wang, Modeling and Experiment of Compressed Air Hybrid Engines, Lost Angeles: University of California, Los Angeles, 2008.

[9] E. Tanaka, T. Narita and H. Maegawa, "Fuel Economy Analysis of Alternator with Kinetic Energy Storage for a Conventional Vehicle," *SAE International Journal of Passenger Cars - Mechanical Systems,* vol. 6, no. 2, 2013.

[10] R. Schnepf and B. D. Yacobucci, "Renewable fuel stadard (RFS): overview and issues," 2013.

[11] S. Davis, R. Boundy and S. Diegel, "2011 Vehicle Technologies Market Report," Oak Ridge National Labrotary, Oak Ridge, TN, US, 2012.

[12] E. D. Tate, M. O. Harpster and P. J. Savagian, "The electrification of the automobile: from conventional hybrid, to plug-in hybrids, to extended-range electric vehicles," in *Proceedings of 2008 world congress*, Detroit, Michigan, 2008.

[13] U.S. Department of Transportation, Federal Highway Adminstration, "Summary of Travel Trends: 2009 National Household Travel Survey," Washington DC, June 2011.

[14] J. Krumm, "How People Use Their Vehicles: Statistics from the 2009 National Household Travel Survey," in *SAE 2012 World Congress & Exhibition*, Detroit, US, 2012.

[15] G. Wu, X. Zhang and Z. Dong, "Powertrain architectures of electrified vehicles: review, classification and comparison," *Journal of Franklin Institute,* vol. 353, no. 2, 2015.

[16] A. Emadi, M. Ehsani and Y. Gao, in *Modern Electric, Hybrid Electric, and Fuel Cell Vehicles: Fundamentals, Theory, and Design*, CRC PRESS, 2005.

[17] K. Bayindir, M. A. Gözüküçük. and A. Teke, "A comprehensive overview of hybrid electric vehicle: powertrain configuration, powertraion control techniques and electronic control units," *Energy Conversion and Management,* pp. 1305-1313, 2011.

[18] C. Chan, A. Bouscayrol and K. Chen, "Electric, hybrid, and fuel-cell vehicles: architectures and modeling," *IEEE Transactions on Vehicular technology,* vol. 59, no. 2, pp. 589-598, 2010.

[19] "Proteanelectric," [Online]. Available: http://www.proteanelectric.com.

[20] H. Benford and M. Leising, "The lever analogy: a new tool in transmission analysis," 1981.

[21] B. Conlon, "Comparative analysis of single and combined hybrid electrically variable transmission," in *SAE 2005 World Congress & Exhibition*, Detroit, 2005.

[22] J. Liu and H. Peng, "Modeling and Control of a Power-Split Hybrid Vehicle," *IEEE Transactions on Control System Technology,* vol. 16, no. 6, pp. 1242-1251, 2008.

[23] J. Kim, J. Kang, Y. Kim, T. Kim, B. Min and H. Kim, "Design of Power Split Transmission: Design of Dual Mode Power Split Transmission," *International Journal of Automotive Technology,* vol. 11, no. 4, pp. 565-571, 2010.

[24] H. Yang, B. Kim, Y. Park, W. Lim and S. Cha, "Analysis of Planetary Gear Hybrid Powertrain System - Part 1: Input Split System," *International Journal of Automotive Technology,* vol. 8, no. 6, pp. 771-780, 2007.

[25] H. Yang, B. Kim, Y. Park, W. Lim and S. Cha, "Analysis of Planetary Gear Hybrid Powertrain System - Part 2: Output Split System," *International Journal of Automotive Technology,* vol. 10, no. 3, pp. 381-390, 2009.

[26] H. Naunheimer, B. Bertsche, J. Ryborz and W. Novak, Automotive transmissions: fundamentals, selectioin, design and application, Springer, 2011.

[27] J. M. Miller, "Hybrid electric vehicle propulsion system architectures of the e-CVT type," *IEEE Transactions on Power Electronics,* vol. 21, no. 3, pp. 756-767, 2006.

[28] B. Conlon, P. Savaglan and A. G. Holmes, "Output split electrically-variable transmission with electric propulsion using one or two motors". Patent US 7867124 B2, 11 Jan. 2011.

[29] J. Wishart, Y. Zhou and Z. Dong, "Review of multi-regime hybrid vehicle powertrain architecture," *International Journal of Electric and Hybrid Vehicles,* vol. 1, no. 3, 2008.

[30] S. Cho, K. Ahn and J. M. Lee, "Efficiency of the planetary gear hybrid powertrain," *Proceedings of Institutde of Mechanical Engineering Part D: Journal of Automobile Engineering,* vol. 220, 2006.

[31] T. M. Grewe, B. M. Conlon and A. G. Holmes, "Defining the general motors 2-mode hybrid transmission," in *2007 SAE World Congress & Exhibition*, Detroit, USA, 2007.

[32] M. R. Schmidt, "Two-mode, compound-split electro-mechanical vehicular transmission". Patent US 5931757, Aug. 1999.

[33] M. R. Schmidt, "Two-mode, split power electro-mechanical transmission". Patent US 5577973, 26 Nov. 1996.

[34] I. Matsuo, S. Nakazawa and E. Inada, "Development of a High-Performance Hybrid Propulsion System Incorporating a CVT," in *SAE 2000 World Congress Technical Papers*, Detroit, MI, US, 2000.

[35] "GM," [Online]. Available: www.gm.com.

[36] M. Kobayashi, T. Maruyama and S. Tanaka, "Hybrid vehicle propulsion apparatus". US Patent US 6729423 B2, May 2004.

[37] D. Kum, H. Peng and N. K. Bucknor, "Control of Engine-Starts for Optimal Drivability of Parallel Hybrid Electric Vehicles," *Journal of Dynamic Systems, Measurement,and Control,* vol. 125, 2013.

[38] A. Phillips, K. E. Bailey and M. Jankovic, "Control system and method for a parallel hybrid electric vehicle". US Patent US 6735502, 11 May 2004.

[39] G. E. Gauthier, "Ford Global Technologies, Inc.". US Patent US 6484831 B1, 26 Nov. 2002.

[40] K. Yamaguchi, A. Obata and A. Masuda, "Hybrid drive". US Patent US 6488608 B2, 3 Dec. 2002.

[41] [Online]. Available: http://www.fueleconomy.gov/.

[42] K. Morisawa and E. Ichioka, "Apparatus for controlling automotive vehicle having a plurality of drive power sources". US Patent US 6484832 B1, 26 Nov. 2002.

[43] M. A. Kluger and D. M. Long, "An Overview of Current Automatic, Manual and Continuously Variable Transmission Efficiencies and Their Projected Furture Improvements," in *Proceedings of SAE 1999 International Congress & Exposition*, Detroit, Michigan, United States, 1999.

[44] T. Lewin, 2010. [Online]. Available: http://www.dctfacts.com/industry-at-a-glance/global-transmission-trends.aspx.

[45] X.-Y. Song, Z.-X. Sun, X.-J. Yang and G.-M. Zhu, "Modelling, Control, and Hardware-in-the-Loop Simulation of an Automated Manual Transmission," *Proceedings of Institution of Mechanical Engineers, Part D: Journal of Automobile Engineering,* vol. 224, pp. 143-160, 2009.

[46] E. Galvagno, M. Velardocchia and A. Vigliani, "Analysis and Simulation of a Torque Assist Automated Manual Transmission," *Mechanical Systems and Signal Processing,* vol. 25, pp. 1877-1886, 2011.

[47] H. Kuroiwa, N. Ozaki, T. Okada and M. Yamasaki, "Next-Generation Fuel-Efficient Automated Manual Transmission," *Hitachi Review,* vol. 53, no. 4, pp. 168-182, 2004.

[48] A. Sorniotti, "Torque Gap Filter for Automated Manual Transmissions: Principles for the Development of Control Algorithm," in *SAE International Congress*, Detroit, 2009.

[49] M. Yamasaki, H. Konno, H. Kuroiwa and N. Ozaki, "Automated Manual Transmission with Torque Assist Mechanism for Reducing Shift Shock," in *Proceedings of SAE 2005 World Congress & Exhibition*, Detroit, 2005.

[50] R. Fischer and G. Schneider, "SCHAEFFLER Media Library," SCHAEFFLER, 2002. [Online]. Available: http://www.luk.com/content.luk.de/en/services/mediathek/mediathek.jsp.

[51] DTI, "http://www.dtinnovations.nl/Image-Library/Documents/0231-DTI_leaflet_psamt_DEF.aspx," [Online].

[52] M. Nievelstein, Design of a PowerShift Module for Long Haulage Trucks, Eindhoven: Eindhoven University of Technology, 2005.

[53] R. Baraszu and S. Cikanek, "Torque Fill-In for an Automated Shift Manual Transmission in a Parallel Hybrid Electric Vehicle," in *Proceedings of the American Control Conference*, Anchorage, AK, 2002.

[54] W. Xiong, Y. Zhang and C. Yin, "Optimal Energy Management for a Series-Parallel Hybrid Electric Bus," *Energy Conversion and Management,* vol. 50, pp. 1730-1738, 2009.

[55] G. Hellenbroich, "Volker Rosenburg," 2007. [Online]. Available: www.fev.com.

[Accessed 2013].

[56] S. Kirschstein, G. Hellenbroich and C. Duindam, "FEV Gmbh," Novenber 2011. [Online]. Available: www.fev.com. [Accessed January 2013].

[57] S. Kirschstein, G. Hellenbroich and C. Duindam, "First driving test results of FEV's 7H-AMT hybrid transmission," FEV, 2011. [Online]. Available: www.fev.com. [Accessed Mar. 2013].

[58] G. Hellenbroich and V. Rosenburg, "FEV's new parallel hybrid transmission with single dry clutch and electric torue support," 2009. [Online]. Available: http://www.fev.com.

[59] C. Torrelli, "Hybrid transmission for a motor vehicle". United States Patent No. 2013/0345008, 26 12 2013.

[60] SAE International, "Graziano's new AMT aims to plug the 'torque-interruption gap'," [Online]. Available: http://articles.sae.org/11944/.

[61] G. Wu and Z. Dong, "Hybrid Drive System With Multiple Driver Machines". US Patent 20150328976, 2015.

[62] G. Hellenbroich, "Method for the operation of a hybrid drive system and hybrid drive system comprising two sub-transmissions". United States Patent US20100311540 A1, 9 12 2010.

[63] Y. Ren, S. Yang and J. Li, "Hybrid power driving system and gear position operation method thereof". Patent US 2011/0160015 A1, 30 Jun. 2011.

[64] Z. Zhong, G. Kong, Z. Yu, X. Chen, X. Chen and X. Xin, "Concept evaluation of a Novel Gear Selector for Automated Manual Transmission," *Mechanical Systems and Signal Processing,* vol. 31, pp. 316-331, 2012.

[65] A. Fraser, "In-wheel electric motors," Protean Electric Ltd, UK, [Online]. Available: http://www.proteanelectric.com/en/white-papers/. [Accessed 2013].

[66] "Karma," [Online]. Available: http://www.fiskerautomotive.com/.

[67] G. Wu and Z. Dong, "Electric Drive System with a Novel Duel-Clutch Transmission". Canada Patent 20160017958, 2014.

[68] T. Abels and S. Puschel, "Vehicle drive with two electric motors". US Patent US 3870935, 11 Mar. 1975.

[69] Q. Ren, D. A. Crolla and A. Morris, "Effects of Transmission Design on Electric Vehicle (EV) Performance," in *Proceedings of Vehicle Power & Propulsion Conference*, Dearborn, Michigan, USA, 2009.

[70] A. Sorniotti, T. Holdstrock, G. L. Pilone and F. Viotto, "Analysis and Simulation of the Gearshift Methodology for a Novel Two-speed Transmission System for Electric Powertrains with a Central Motor," *Proceedings of the Institute of Mechanical Engineers, Part D: Journal of Automobile Engineering,* pp. 915-930, 2012.

[71] S. Delprat, J. Lauber, T. M. Guerra and J. Rimaux, "Control of a Parallel Hybrid Powertrain: Optimal Control," *IEEE Transactions on Vehicular Technology,* pp. 872-881, 2004.

[72] O. Sundstrom, P. Soltic and L. Guzzella, "A transmission-Actuated Energy-Management Strategy," *IEEE Transactions on Vehicular Technology,* vol. 59, no. 1, pp. 84-92, 2010.

[73] B. Mashadi and S. A. M. Emadi, "Dual-Mode Power-Split Transmission for Hybrid Electric Vehicles," *IEEE Transactions on Vehicular Technology,* vol. 59, no. 7, pp. 3223-3232, September 2010.

[74] H. Lee and H. Kim, "Improvement in Fuel Economy for a Parallel Hybrid Electric Vehicle by Continuously Variable Transmission Ratio Control," *Proceedings of the Institution of Mechanical Engineers, Part D: Journal of Automobile Engineering,* vol. 219, pp. 43-51, 2005.

[75] V. Ngo, T. Hofman, M. Steinbuch and A. Serrarens, "Optimal Control of the gear shift command for Hybrid Electric Vehicles," *IEEE Transactions on Vehicular Technology,* 2012.

[76] G. Wu, X. Zhang and Z. Dong, "Impacts of two-speed gearbox on electric vehicle's fuel economy and performance," in *SAE 2013 World Congress & Exhibition*, Detroit, USA, 2013.

[77] Chrysler Group LLC, "ZF 8-Speed Automatic Transmission," 13 June 2012. [Online]. Available: http://www.motor.com/newsletters/20121010/WebFiles/MMM_ZF_8HP_Tranny.pdf. [Accessed 2014].

[78] H. Naunheimer, B. Bertsche, J. Ryborz and W. Novak, Automotive Transmissions: Fundamentals, Selection, Design and Application, Verlag, Berlin, Heidelberg: Springer, 2011.

[79] J. M. Donato and J. C. McCoy, "Two-speed transmission for use with electric powered vehicle". US Patent US 5226339, 13 Jul. 1993.

[80] V. R. Strong and D. J. Hvolka, "Two speed Gearbox". US Patent US 6616567B2, 9 Sep. 2003.

[81] M. A. Miller, A. G. Holmes and B. M. Conlon, "The GM "Voltec" 4ET50 Multi-Mode Electric Transaxle," in *SAE 2011 World Congress & Exhibition*, Detroit, USA, 2011.

[82] SAE International, "Clutchless four-speed EV transmission debuts," 2012. [Online]. Available: http://articles.sae.org/10669/. [Accessed 2013].

[83] X. Zhou, P. Walker, N. Zhang and B. Zhu, "Performance Improvement of a Two Speed EV through Combined Gear Ratio and Shift Schedule Optimization," in *SAE World Congress 2013*, Detroit, 2013.

[84] I. Kolmanovsky, M. v. Nieuwstadt and J. Sun, "Optimization of Complex Powertrain Systems for Fuel Economy and Emissions," in *Proceedings of the 1999 IEEE International Conference on Control Applications*, Island of Hawai'i, Hawai'i, USA, 1999.

[85] J.-M. Kang, I. Kolmanovsky and J. W. Grizzle, "Dynamic Optimization of Lean Burn Engine Aftertreatment," *Journal of Dynamic Systems, Measurement, and Control,* pp. 153-160, 2001.

[86] C.-C. Lin, H. Peng, J. W. Grizzle and J.-M. Kang, "Power Management Strategy for a Parallel Hybrid Electric Truck," *IEEE TRANSACTIONS ON CONTROL SYSTEMS TECHNOLOGY,* pp. 839-849, 2003.

[87] D. Kum, H. Peng and N. K. Bucknor, "Supervisory Control of Parallel Hybrid ELectric Vehicles for Fuel and Emission Reduction," *Journal of Dynamic Systems, Measurement, and Control,* pp. 1-10, 2011.

[88] AUTONOMIE. [Online]. Available: http://www.autonomie.net/. [Accessed 2014].

[89] [Online]. Available: http://www.autonomie.net/.

[90] G. Lucente, M. Montanari and C. Rossi, "Modelling of an Automated Manual Transmission System," *Mechatronics,* vol. 17, pp. 73-91, 2007.

[91] D. F. Opila, X. Wang and R. McGee, "Performance Comparison of Hybrid Vehicle Energy Management Controllers on Real-World Drive Cycle Data," in *Proceedings of 2009 American Control Conference*, St. Louis, MO, USA, 2009.

[92] L. Guzzella and A. Sciarretta, Vehicle Propulsion Systems-Introduction to Modeling and Optimization, 2 ed., Berlin: Springer, 2007, p. 14.

[93] R. D. Robinett, D. G. Wilson, G. R. Eisler and J. E. Hurtado, Applied Dynamic Programming for Optimization of Dynamical Systems, Philadelphia: Society of Industrial and Applied Mathematics, 2005.

[94] L. V. Perez, G. R. Bossio, D. Moitre and G. O. Garcia, "Optimization of Power

Management in an Hybrid Electric Vehicle Using Dynamic Programming," *Mathematics and Computers in Simulation,* pp. 244-254, 2006.

[95] E. T. Applications, "ETA-TP002 Implementation of SAE Standard J1666 May 93 - Electric Vehicle Acceleration, Gradeability, and Deceleration Test Procedure," 01 11 2004. [Online]. Available: www.inl.gov. [Accessed 2012].

[96] P. Couderc, J. Callenaere, J. D. Hagopian and G. Ferraris, "Vehicle Driveline Dynamic Behaviour: Experimentation and Simulation," *Journal of Sound and Vibration,* vol. 218, no. 1, pp. 133-157, 1998.

[97] A. Lagerberg, "Open-loop optimal control of a backlash traverse," Chalmers University of Technology, Chalmers, Sweden, 2004.

[98] A. Lagerberg and B. Egardt, "Model Predictive Control of Automotive Powertrains with Backlash," in *Proceedings of the 16th IFAC World Congress*, Prague, Czech Republic, 2005.

[99] R. A. Krenz, "Vehicle Response to Throttle Tip-in/Tip-Out," 1985.

[100] K. Koprubasi, Modeling and control of a hybrid-electric vehicle for drivability and fuel economy improvement, Columbus: The Ohio State University, 2008.

[101] M. L. Kuang, "An Investigation of Engine Start-Stop NVH in a Power-Split Powertrain Hybrid Electric Vehicle," in *SAE Proceedings, number 2006-01-1500*, 2006.

[102] H. He, Z. Liu, L. Zhu and X. Liu, "Dynamic Coordinated Shifting Control of Automated Mechanical Transmissions without a Clutch in a Plug-In Hybrid Electric Vehicle," *Energies,* no. 5, pp. 3094-3109, 2012.

[103] N. Silva and J. Sodre, "Cold Start and Drivability Characteristics of an Ethanol-Methyl-t-Butyl Ether Blend Fulled Vehicle," *Proceediings of the Institution of Mechanical Engineers, Part D: Journal of Automobile Engineering,* vol. 215, pp. 645-649, 2001.

[104] A. Crowther, R. Singh, N. Zhang and C. Champam, "Impulsive Response of an Automatic Transmission System with Multiple Clearances: Formulation, Simulation and Experiment," *Journal of Sound and Vibration,* pp. 444-466, 2007.

[105] J. S. Gurm and A. R. Crowther, "Transient Clunk Reponse of a Driveline System: Laboratory Experiment and Analytical Studies," in *SAE 2007 Noise and Vibration Conference and Exhibition*, St. Charles, Illinois, USA, 2007.

[106] N. Amann, J. Bocher and F. Prenner, "Active Damping of Drive Train Oscillations for an Electrically Driven Vehicle," *IEEE/ASME Transactions on Mechatronics,* vol. 9, no. 4, pp. 697-970, 2004.

[107] F. U. Syed, M. L. Kuang and H. Ying, "Active Damping Wheel-Torque Control System to Reduce Driveline Oscillations in a Power-Split Hybrid Electric Vehicle," *IEEE Transactions on Vehicular Technology,* vol. 58, no. 9, p. 4769, 2009.

[108] D. Lefebvre, P. Chevrel and S. Richard, "An H-Infinity-based Control Design Methodology Dedicated to the Active Control of Vehicle Longitudinal Oscinations," *IEEE Transactions on Control Systems Technology,* vol. 11, no. 6, pp. 948-956, 2003.

[109] B. Powell, K. E. Bailey and S. R. Cikanek, "Dynamic Modeling and Control of Hybrid Electric Vehicle Powertrain Systems," *IEEE Control System Magazine,* vol. 18, no. 5, pp. 17-33, 1998.

[110] D. F. Opila, X. Wang and R. McGee, "An Energy Management Controller to Optimally Trade Off Fuel Economy and Drivability for Hybrid Vehicles," *IEEE Transactions on Control System Technology,* vol. 20, no. 6, pp. 1490-1505, 2012.

[111] D. F. Opila, D. Aswan, R. McGee, J. A. Cook and J. Grizzle, "Incorporating Drivability Metrics into Optimal Energy Management Strategies for Hybrid Vehicles," in *Proceediings of the 47th IEEE Conference on Decision and Control*, Cancun, Mexico, 2008.

[112] P. Pisu, K. Koprubasi and G. Rizzoni, "Energy Management and Drivability Control Problems for Hybrid Electric Vehicles," in *Proceedings of IEEE Conference on Decision and Control*, Seville, Spain, 2005.

[113] L. Chen, G. Xi and J. Sun, "Torque Coordination Control During Mode Transition," *IEEE Transactions on Vehicular Technologies,* vol. 61, no. 7, pp. 2936-2949, 2012.

[114] G. Wu, X. Zhang and Z. Dong, "Optimal Control for Ensured Drivability of Paralell HEVs/PHEVs during Mode Transition," in *SAE Technical Paper*, Detroit, 2014.

[115] D. Centra, H. Rahnejat and M. T. Menday, "Non-linear Multi-Body Dynamic Analysis for the Study of Clutch Torsional Vibraion," *Applied Mathmatical Modelling,* vol. 25, pp. 177-192, 2001.

[116] C. Duan and R. Singh, "Dynamics of a 3dof Torsional System with a Dry Friction Controlled Path," *Journal of Sound and Vibration,* pp. 657-688, 2006.

[117] A. C. V. D. Heijden, A. F. A. Serrarens, M. K. Camlibel and H. Nijmeijer, "Hybrid Optimal Control of Dry Clutch Engagement," *International Journal of Control,* vol. 80, no. 11, pp. 1717-1728, 2007.

[118] B. Armstrong-Helouvry, P. Dupont and C. Canudas De Wit, "A Survey of Models, Analysis Tools and Compensation Methods for the Control of Machines with Friction,"

Automatica, vol. 30, no. 7, pp. 1083-1138, 1994.

[119] F. Tariku, Simulation of Dynamic Mechanical System with Stick-Slip Friction, New Brunswick: University of NewBrunswick, 1992.

[120] D. Zardecki, "Piecewise Linear Modeling of Friction and Stick-Slip Phenomenon in Discrete Dynamical Systems," *Journal of Theoretical and Applied Mechanics,* vol. 44, no. 2, pp. 255-277, 2006.

[121] D. Karnopp, "Computer Simulation of Stick-Slip Friction in Mechanical Dynamic System," *Journal of Dynamic Systems, Measurement, and Control,* vol. 107, 1985.

[122] P. J. Dolcini, C. Canudas de Wit and H. Bechart, Dry Clutch Control for Automotive Applications, London: Springer, 2010.

[123] P.-A. Bliman and M. Sorine, "Easy-to-Use Realistic Dry Friction Models for Automatic Control," in *Proceedings of the 3rd European Control Conference*, Roma, Italy, 1995.

[124] J. Zhang, L. Chen and G. Xi, "System Dynamic Modelling and Adaptive Optimal Control for Automatic Clutch Engagement of Vehicles," *Proceedings of Institution of Mechanical Engineers, Part D: Journal of Automobile Engineering,* vol. 216, pp. 983-991, 2002.

[125] L. Chen, G. Xi and C. Yin, "Model Referenced Adaptive Control to Compensate Slip-Stick Transition During Clutch Engagement," *International Journal of Automotive Technology,* vol. 12, no. 6, pp. 913-920, 2011.

[126] C. Gaillard and R. Singh, "Dynamic Analysis of Automotive Clutch Dampers," *Applied Acoustics,* vol. 60, pp. 399-424, 2000.

[127] L. Glielmo and F. Vasca, "Optimal Control of Dry Clutch Engagement," in *SAE 2000 World Congress*, Detroit, Michigan, US, 2000.

[128] F. Garofalo, L. Glielmo, L. Iannelli and F. Vasca, "Smooth Engagement for Automotive Dry Clutch," in *Proc. 40th IEEE Conf. Decision and Control*, Orlando, FL, USA, 2001.

[129] G. Wu, X. Zhang and Z. Dong, "Impact of Two-speed Gearbox on Electric Vehicle's Fuel Economy and Performance," in *SAE 2013 World Congress*, Detroit, USA, 2013.

[130] L. Chen, G. Xi and J. Sun, "Torque Coordination Control During Mode Transition for a Series-Parallel Hybrid Electric Vehicle," *IEEE Transactions on Vehicular Technology,* vol. 61, no. 7, pp. 2936-2949, 2012.

[131] X. Wei, "Dynamic Modeling of a Hybrid Electric Drivetrain for Fuel Economy, Performance and Drivability Evaluations," *ASME, Dynamic System,* vol. 72, no. 1, pp. 443-450, 2003.

[132] Weiqing Li, "Shifting Process Study on AMT of a Parallel Hybrid Electric Vehicle," in *Proccedings of 2011 4th International Conference on Power Electronics Systems and Applications (PESA)*, Beijing, China, 2011.

[133] A. E. Sanjaka G. Wirasingha, "Classification and Review of Control Strategies for Plug-in Hybrid Electric Vehicles," *IEEE Transactions On Vehicular Technology,* vol. 60, no. 1, pp. 111-122, 2011.

[134] F. R. Salmasi, "Control Strategies for Hybrid Electric Vehicles: Evolution, Classification, Comparison, and Future Trends," *IEEE Transactions On Vehicular Technology,* vol. 56, no. 5, pp. 2393-2404, 2007.

[135] Z. Sun and K. Hebbale, "Challenges and Opportunities in Automotive Transmission Control," in *Proceediings of 2005 American Control Conference*, Portland, OR, USA, 2005.

[136] D. Kim, H. Peng, S. Bai and J. M. Maguire, "Control of Integrated Powertrain with Electronic Throttle and Automatic Transmission," *IEEE Transactions on Control Systems Technology,* vol. 15, no. 3, pp. 474-482, 2007.

[137] R. Beck, F. Richert and A. Bollig, "Model Predictive Control of a Parallel Hybrid Vehicle Drivetrain," in *Proceedings of the IEEE International Conference on Decision and Control/ European Control Conference*, 2005.

[138] R. Moore, Principles and Applications of Tribology, Oxford: Pergamon press, 1975.

[139] M. Montanar, F. Ronchi and C. Rossi, "Control and Performance Evaluation of a Clutch Servo System with Hydraulic Actuation," *Control Engineering Practice,* vol. 12, pp. 1369-1379, 2004.

[140] K. Kim, H. Peng, S. Bai and J. Maguire, "Control of Integrated Powertrain with Electronic Throttle and Automatic Transmission," *IEEE Transactions on Control System Technology,* vol. 15, no. 3, pp. 474-482, 2007.

[141] V. D. Ngo, T. Hofman, M. Steinbuch and A. Serrarens, "Gear Shift Map Design Methodology for Automotive Transmission," *Institution of Mechanical Engineers: Proc IMechE Part D: J Automobile Engineering,* vol. 228, pp. 50-72, 2014.

[142] V. D. Ngo, Gear Shift Strategies for Automotive Transmission, Eindhoven: Eindhoven University of Technology, 2012.

[143] M. Pettersson and L. Nielsem, "Gear Shifting by Engine Control," *IEEE Transactions on Control System Technology,* vol. 8, no. 3, pp. 495-507, 2000.

[144] H.-D. Lee, S.-K. Sul, H.-S. Cho and J.-M. Lee, "Advanced Gear-Shifting and Clutching

Strategy for a Parallel-Hybrid Vehicle," *IEEE Industry Applications Magazine,* pp. 26-32, 2000.

[145] J. Qu and Y. Zhang, "Control of Clutch Engagement for AMT Based on Fuzzy Logic," in *3rd International Symposium on Information Science and Engineering*, Shanghai, 2010.

[146] D. Cieslar, M. Hancock and F. Assadian, "Modelling of Hybrid Electric Vehicle All Wheel Drive Driveline System Incorporating Clutch models," in *19th International Conference on Systems Engineering*, Las Vegas, Nevada, US, 2008.

[147] L. Glielmo, L. Iannelli, V. Vaccca and F. Vasca, "Gearshift Control for Automated Manual Transmissions," *IEEE/ASME Transactions on Mechatronics,* vol. 11, no. 1, pp. 17-26, 2006.

[148] H. Tanaka and H. Wada, "Fuzzy Control of Clutch Engagement for Automated Manual Transmission," *Veh. Syst. Dyn.,* vol. 24, no. 4, pp. 365-376, 1995.

[149] M. Canova, K. Sevel, Y. Guezennec and S. Yurkovich, "Control of the Start/Stop of a Diesel Engine in a Parallel HEV: Modeling and Experiments," in *Proceedings of the IMECE*, 2006.

[150] Y. Lei, M. Niu and A. Ge, "A Research on Starting Control Strategy of Vehicle with AMT," in *Proc. FISITA World Automotive Congress*, Seoul, Korea, 2000.